INEL-96/0400 (NON-PROPRIETARY VERSION)

April 1997

Adequacy Evaluation of RELAP5/MOD3, Version 3.2.1.2 for Simulating AP600 Small Break Loss-of-Coolant Accidents

C. D. Fletcher, P. D. Bayless, C. B. Davis,
M. G. Ortiz, S. M. Sloan, R. A. Shaw,
R. R. Schultz, C. E. Slater, G. W. Johnsen,
J. P. Adams, L. S. Ghan

D. E. Bessette, USNRC

INEL-96/0400 (NON-PROPRIETARY VERSION)

ADEQUACY EVALUATION OF RELAP5/MOD3, VERSION 3.2.1.2 FOR SIMULATING AP600 SMALL BREAK LOSS-OF-COOLANT ACCIDENTS

C. D. Fletcher, P. D. Bayless, C. B. Davis, M. G. Ortiz
S. M. Sloan, R. A. Shaw, R. R. Schultz, C. E. Slater
G. W. Johnsen, J. P. Adams, and L. S. Ghan
Idaho National Engineering and Environmental Laboratory

D. E. Bessette
U. S. Nuclear Regulatory Commission

April 1997

Prepared for the
Division of Systems Technology
Office of Nuclear Regulatory Research
U.S. Nuclear Regulatory Commission
Washington, D.C. 20555

by
Idaho National Engineering and Environmental Laboratory
Nuclear Systems Analysis Technologies Department
Lockheed Martin Idaho Technologies Company
Idaho Falls, Idaho 83415

under
DOE Contract No. DE-AC07-94ID13223
NRC FIN J6008

ABSTRACT

The adequacy of the RELAP5/MOD3, Version 3.2.1.2, computer code for performing confirmatory analysis of design-basis small break loss-of-coolant accidents (SBLOCAs) in the Westinghouse AP600 reactor is evaluated in this report. The findings of code reviews and assessment evaluations presented here are combined to demonstrate code adequacy for this application. A phenomena identification and ranking table activity was used to structure these reviews and evaluations on the phenomena, processes, components and systems in a manner appropriate for their relative importance to the prediction of AP600 SBLOCAs. The code governing equations and numerics were reviewed for applicability to AP600 SBLOCA analysis. These reviews identified few major limiting assumptions pertinent for this application and none was seen to invalidate the proposed use of the code. Evaluations were made regarding the applicability of important code models and correlations; these showed the models and correlations to be applicable. Evaluations also were made of integrated code performance for predicting important AP600 behavior as observed in both component separate effects experiments and integral systems effects experiments. The assessments of the code against the integral systems effects test data represent the largest part of the code adequacy demonstration case. These integral effects assessments were performed using data from three experimental facilities representing AP600 at different scales and using tests representing three different SBLOCA scenarios. The assessments evaluated code capabilities for representing the phenomena important for AP600 accident behavior. These assessments showed that the code is capable of acceptably simulating both the overall system behavior and the important phenomena as observed in the experiments. Scaling analyses were performed to demonstrate that the set of experiments is both relevant and sufficient for representing the behavior to be expected during the corresponding accidents in AP600. The investigations presented in this report demonstrate that the RELAP5/MOD3 computer code is adequate for performing confirmatory AP600 SBLOCA analyses.

EXECUTIVE SUMMARY

This report evaluates the adequacy of the RELAP5/MOD3, Version 3.2.1.2, computer code for performing confirmatory analysis of design-basis small break loss-of-coolant accidents (SBLOCAs). The findings of this evaluation are summarized in Table E-1; a check mark indicates a favorable outcome regarding code adequacy while a "Not Applicable" entry indicates that it is not appropriate to evaluate the phenomenon identified with the table row using the evaluation method identified with the table column. The table shows that the code is adequate for predicting all of the important phenomena, demonstrating that RELAP5/MOD3, Version 3.2.1.2, is adequate for performing confirmatory AP600 SBLOCA analysis.

Background

AP600 is a new pressurized water reactor design that has been submitted by Westinghouse Electric Corporation to the U. S. Nuclear Regulatory Commission (USNRC) for design certification. For safety during postulated design-basis accidents, the AP600 reactor relies on passive systems.

The RELAP5/MOD3 thermal-hydraulic systems analysis computer code has been developed by the USNRC to provide a capability for independently auditing the analyses submitted by reactor manufacturers and utilities. The USNRC will use RELAP5/MOD3 to perform calculations for the purpose of independently confirming Westinghouse Electric Corporation analyses submitted in support of AP600 design certification. The development of this code has benefitted from extensive assessments against experimental data representing the behavior of existing reactors. The work reported here features extension of the code assessment base to include behavior important for simulating certain postulated accidents in AP600. In particular, the new assessments address the capabilities of RELAP5/MOD3 for predicting AP600 behavior during design-basis SBLOCAs. This document demonstrates the adequacy of the RELAP5/MOD3, Version 3.2.1.2, computer code for performing these analyses. The purpose of this demonstration is to ensure that the computer code and its related facility input models can reasonably represent AP600 SBLOCA behavior and that the USNRC, in its analysis, will reach the correct conclusions regarding that behavior.

Method

Adequacy is demonstrated through code reviews and assessments against experimental data using a process described as follows. Work is focused upon code capabilities for predicting important phenomena and processes as defined by the AP600 SBLOCA phenomena identification and ranking table (PIRT). Adequacy standards are developed and consistently applied to assess the code. These criteria define four levels of agreement: excellent, reasonable, minimal, and insufficient. Judgments are made based on comparisons of the magnitudes and trends of the calculated and measured data in the context of the uncertainty in the experimental data. Excellent or reasonable agreement is considered acceptable. Preliminary judgments were made by the Idaho National Engineering and Environmental Laboratory (INEEL) analyst responsible for each assessment and these were reviewed and approved by the group of INEEL analysts performing all such assessments. The code governing equations and numerics are reviewed for their underlying assumptions and whether those assumptions are appropriate for the AP600 SBLOCA application. Additionally, important code constitutive or closure models and correlations are reviewed for their applicability. The integrated performance of the code is assessed against integral effects tests in three scaled experimental facilities that represent AP600. To maximize the usefulness of the assessments, input models for all facilities were developed using a consistent approach to nodalization and option selection. A scaling applications analysis is performed to demonstrate the relevancy and sufficiency of the integral effects experimental data base for representing AP600. This demonstration allows extension of the code assessment results to the AP600 application. Additional code assessments are performed using separate effects experiments to study code capabilities for predicting local behavior within unique AP600 components. The collective findings of these reviews and assessments demonstrate the adequacy of the code. The methods, results and conclusions presented in this report have been independently reviewed by the USNRC Thermal-Hydraulic Consultants Committee. The membership of this committee is given in the acknowledgments section.

Table E-1. Summary of RELAP5 code adequacy evaluation results.

AP600 PIRT High-Ranked Phenomenon	RELAP5		Experimental Data	
	Closure Relation Applicability	Integrated Code Assessment	Sufficiency	Relevancy
SBLOCA SHORT-TERM PHASE				
Accumulator flow	✓	✓	✓	✓
ADS energy release	✓	✓	✓	✓
ADS mass flow	✓	✓	✓	✓
Break mass flow	✓	✓	✓	✓
Cold leg-to-PBL tee phase separation	✓	✓	✓	✓
Core flashing	✓	✓	✓	✓
Core subcooling margin	Not Applicable	✓	✓	✓
Core two-phase mixture level	✓	✓	✓	✓
CMT flow resistance	✓	✓	✓	✓
CMT level	Not Applicable	✓	✓	✓
Fuel rod core power/decay heat	✓	Not Applicable	Not Applicable	Not Applicable
Hot leg phase separation in tees	✓	✓	✓	✓
IRWST flow resistance	✓	✓	✓	✓
Pressurizer level	Not Applicable	✓	✓	✓
SBLOCA LONG-TERM PHASE				
ADS energy release	✓	✓	✓	✓
ADS mass flow	✓	✓	✓	✓
Core two-phase mixture level	✓	✓	✓	✓
Downcomer level	Not Applicable	✓	✓	✓
Fuel rod core power/decay heat	✓	Not Applicable	Not Applicable	Not Applicable
IRWST flow resistance	✓	✓	✓	✓
IRWST pool level	Not Applicable	✓	✓	✓
IRWST pool thermal stratification	Not Applicable	✓	✓	✓
Sump fluid temperature	Not Applicable	✓	✓	✓
Sump level	Not Applicable	✓	✓	✓
Upper plenum two-phase level	Not Applicable	✓	✓	✓

Reviews of Code Governing Equations and Numerics

The review of the assumptions underlying the code governing equations and numerics uncovered only three limiting assumptions significant for the AP600 SBLOCA application. First, behavior is assumed to be homogeneous within the vapor and liquid phases. As a result of this assumption, the code does not have a capability for predicting thermal stratification effects within the AP600 cold legs and a limited capability for predicting core makeup tank (CMT) thermal stratification behavior. The code assessments described below, under "Integrated Code Performance," address the effects of this code assumption on simulations of AP600 SBLOCAs. Second, a defect in the momentum flux formulation was identified. This code limitation can cause non-physical circulations in model regions represented with quasi-multidimensional nodalization techniques. The effects of this limitation are addressed by avoiding this modeling technique wherever possible; this is done in all regions except for the reactor vessel downcomer and, there, momentum flux is disabled. The assessments described below show that this method eliminates excessive recirculations and represents a satisfactory work-around for this code limitation. Correction of the RELAP5/MOD3, Version 3.2.1.2, momentum flux formulation defect is being pursued for implementation in subsequent code versions. Third, the code has a tendency to overpredict condensation. The two main factors in the overprediction are the assumption of a homogeneous liquid phase and abrupt changes in interphase heat transfer area as flow regimes change. The integral assessments showed that the minimum reactor vessel coolant inventory was not affected by high condensation rates.

Reviews of Code Model and Correlation Applicability

Code models and correlations are evaluated for their applicability to AP600 SBLOCAs. Only models and correlations needed to calculate the AP600 SBLOCA PIRT high-ranked phenomena are evaluated. For applicability of the other models, we rely upon the assessments of integrated code performance against AP600-related experiments as discussed below and upon prior assessments using RELAP5/MOD3. The evaluations reported here address model pedigree; the parameter ranges for which it was originally developed, applied in RELAP5/MOD3 and required for the AP600 application; the fidelity with which it can replicate appropriate experimental data; and the scalability of the model to AP600 plant geometry and dimensions. It was not practical to evaluate all code models and correlations for this application. Instead, seven models and correlations that were judged to dominate AP600 SBLOCA behavior were evaluated. These models and correlations include the accumulator lumped-parameter component model, the decay heat model, the form friction model, the critical flow model, the bundle interphase drag correlation, the interphase mass and energy transfer model and the horizontal stratification and entrainment model. Through evaluation, all of these models and correlations were judged to be applicable for AP600 SBLOCAs.

Integrated Code Performance

Code capabilities for predicting the important AP600 PIRT SBLOCA short-term phase phenomena are assessed using test data from the ROSA, SPES, and OSU integral effects experimental facilities. The short-term phase extends from the time the break opens until steady in-containment refueling water storage tank (IRWST) injection flow is established. These capabilities were evaluated for three different AP600 SBLOCA scenarios initiated by: a 1-in. diameter cold leg break, a double-ended direct vessel injection (DVI) line break and a 2-in. diameter pressure balance line (PBL) break. The assessments for the AP600 PIRT SBLOCA long-term phase (the remainder of the IRWST injection period and the sump injection period) use test data from OSU integral effects experiments for the same three accident scenarios. Overall assessment results are compiled by combining the assessment results from among the various accident scenarios, phases and experimental facilities.

The integral effects assessments indicate that the code has the capability to acceptably predict all of the AP600 PIRT SBLOCA high-ranked phenomena as observed in the experiments.

Top-down scaling analyses are performed to evaluate the global system behavior of the experimental data base used for the integral effects code assessments. The top-down scaling analyses have three objectives. First, the analyses are performed to determine the sufficiency of the integral test data base for code assessment. The evaluation criterion for sufficiency is whether the expected AP600 scaling phenomena are bounded by those observed in the test data. The bounding is evaluated through a complex process that compares events and trends. Second, the analyses are performed to determine the relevancy of the data. The evaluation criterion for relevancy is typicality; if the test behavior is typical of AP600, then it is relevant. Third, the analyses are performed to uncover, through comparisons between test data and the corresponding code calculations of the tests, any biases included in the code calculations that may pertain to code calculations of AP600 accident behavior. A top-down scaling methodology to attain these objectives was developed and applied. The results of the top-down scaling analyses indicate that the integral experiment data base is relevant and sufficient to justify extending the experimental code assessment results to AP600. The analyses demonstrate that the experimental data base provided by the integral test data encompasses the important phenomena and ranges expected of AP600 during a SBLOCA as defined by the PIRT. While each of the experimental facilities has known sources of distortions, none of these was found to cause the data from any of the facilities to be irrelevant for AP600. The scaling analysis considered these known distortions and included their effects in the data-collapsing process. An independent top-down scaling study is being performed at Brookhaven National Laboratory; results will be published when that work has been completed.

Bottom-up scaling analyses are performed to address selected issues related to localized behavior. The purposes of the bottom-up scaling analyses are to explain behavior differences observed among tests in the different experimental facilities by linking facility behavior to facility scaling distortions and to use these explanations to infer the expected AP600 behavior and determine whether the experimental data provide sufficient representation of AP600.

Additional assessments are performed using test data from separate effects experimental facilities representing two unique AP600 components: the CMT and ADS-123. Assessments related to the CMT used data from a scaled experimental facility. Assessments related to ADS-123 used data from a full-scale experimental facility. These assessments indicated no significant deficiencies in code capabilities for representing the behavior of the important phenomena associated with these components. Assessments for a third component, the passive residual heat removal (PRHR) system, remain in progress because of delays in receipt of documentation for the pertinent tests.

Conclusion

The overall picture of RELAP5/MOD3, Version 3.2.1.2, adequacy for AP600 SBLOCA confirmatory analysis is presented in Table E-1. This table lists the AP600 PIRT high-ranked phenomena for the SBLOCA short and long-term phases and shows the outcomes of the evaluations of code capabilities from the reviews and assessments summarized in this report. A box with a check mark indicates a direct or indirect evaluation that resulted in a favorable outcome regarding the acceptability of the code. A box with a "Not Applicable" entry indicates that it is not appropriate to evaluate the phenomenon identified with the table row using the evaluation method identified with the table column. The table shows that the code is acceptable for predicting all of the AP600 SBLOCA PIRT high-ranked phenomena. The assessments have shown that the code is an effective tool for simulating design basis

SBLOCA scenarios covering a variety of break sizes and locations. This investigation therefore demonstrates that the RELAP5/MOD3, Version 3.2.1.2, computer code, when used with the recommended AP600 modeling approach and user guidance described in this report, is adequate for performing confirmatory AP600 SBLOCA analysis.

ACKNOWLEDGMENTS

The authors wish to thank the following Idaho National Engineering and Environmental Laboratory (INEEL) personnel for their supporting contributions to this report:

R. H. Averill, J. D. Burtt, J. M. Cozzuol, J. C. Determan, C. A. Dobbe, P. G. Ellison, J. E. Fisher, D. G. Hall, C. H. Heath, C. M. Kullberg, G. E. McCreery, S. M. Modro, S. T. Polkinghorne, D. L. Reeder (independent consultant), P. A. Roth, L. A. Stickler, G. E. Wilson, and J. R. Wolf.

The authors thank B. E. Boyack of Los Alamos National Laboratory for many instrumental contributions to this report. Acting as a consultant to the U. S. Nuclear Regulatory Commission (USNRC), Dr. Boyack provided key assistance in organizing the approach taken to demonstrate code adequacy that was used in this report. This assistance included providing a draft that led to the overview description of the adequacy demonstration process presented in Section 2. Further, Dr. Boyack provided drafts of the code governing equation and numerics descriptive material presented in Appendix A. The authors also thank Dr. Boyack for timely and thorough reviews of other portions of this report.

The authors thank F. Eltawila, G. N. Lauben, J. M. Kelly, T. M. Lee and S. G. Smith of the USNRC, and M. DiMarzo of the University of Maryland, for their support and reviews of this report.

The approach and results presented in this report have been reviewed by the USNRC Thermal-Hydraulic Consultants Committee. In addition, Committee subgroups have on many occasions reviewed various aspects of this work in detail. The authors thank the Committee participants for their reviews and contributions to this effort: S. Banerjee, B. E. Boyack, P. Griffith, Y. Hassan, M. Ishii, B. G. Jones, A. Klein, G. Kojasoy, G. S. Lellouche, D. Liles, J. Mahaffy, M. Podowski, V. H. Ransom, J. N. Reyes, N. Todreas, and G. Wallis.

CONTENTS

FIGURES

TABLES

NOMENCLATURE

ADS	Automatic depressurization system
ALWR	Advanced light-water reactor
AP600	Advanced Passive 600 MWe Reactor
APEX	Advanced Plant Experiment facility at Oregon State University
CLB	Cold leg break
CMT	Core makeup tank
DEGB	Double-ended guillotine break
DVI	Direct vessel injection
DVILB	Direct vessel injection line break
ECCS	Emergency core cooling systems
EPRI	Electric Power Research Institute
IADS	Inadvertent actuation of the automatic depressurization system
INEEL	Idaho National Engineering and Environmental Laboratory
IRWST	In-containment refueling water storage tank
LOCA	Loss-of-coolant accident
LOFT	Loss-of-Fluid Test
LTCM	Long-term cooling model
OSU	Oregon State University, APEX test facility
PBL	Pressure balance line
PBLB	Pressure balance line break
PIRT	Phenomena identification and ranking table
PRHR	Passive residual heat removal
PSIS	Passive safety injection system
PWR	Pressurized water reactor
RCS	Reactor coolant system
ROSA	Rig of Safety Assessment, Japanese ROSA/AP600 test facility
SBLOCA	Small break loss-of-coolant accident
SET	Separate effects test
SG	Steam generator
SIET	Societa Informazioni Esperienze Termoidrauliche
SPES	Simulazione PWR per Esperienze di Sicurezza, Italian SPES-2 test facility
S Signal	Safeguards initiation signal
USNRC	U. S. Nuclear Regulatory Commission

1 INTRODUCTION

AP600 is a new pressurized water reactor design that has been submitted by Westinghouse Electric Corporation to the U.S. Nuclear Regulatory Commission (USNRC) for design certification. The AP600 reactor coolant system is arranged in a two-hot-leg, four-cold-leg configuration; a schematic of the AP600 thermal-hydraulic systems is shown in Figure 1-1. AP600 is equipped with passive emergency core cooling systems (ECCS). The AP600 design calls for coolant lost during an accident to be replenished by reactor coolant system (RCS)-pressure-balanced core makeup tanks (CMTs), gas-pressurized accumulators, and an elevated, gravity-drain, containment-pressure-equalized in-containment refueling water storage tank (IRWST). Once the contents of these tanks have been discharged, the resulting containment liquid level is sufficiently high to cause liquid to be injected back into the RCS via sump valves. Vaporized coolant that is condensed on the interior of the containment shell is collected and returned to the IRWST. An automatic depressurization system (ADS) is provided to ensure viability of the passive ECCS; the RCS blows down through the ADS into the IRWST and containment, equalizing the RCS and containment pressures. A passive residual heat removal (PRHR) system is included to remove decay heat to the IRWST; this is a full-pressure/full-decay-heat system. Passive containment cooling is provided by gravity-driven evaporative cooling external to the containment.

The AP600 design is fully documented in References 1-1 and 1-2. Reference 1-3 provides a general discussion of the thermal-hydraulic functions of the AP600 components. Reference 1-4 provides more detailed thermal-hydraulic information on AP600 components. Reference 1-5 provides a summary of AP600 plant features and their interactions during accident situations.

The RELAP5/MOD3 computer code[1-6] has been developed by the USNRC to provide a capability for independently auditing analyses submitted by reactor manufacturers and utilities. The USNRC will use RELAP5/MOD3 to perform calculations for the purpose of independently confirming Westinghouse Electric Corporation analyses submitted in support of AP600 design certification. RELAP5/MOD3 is a thermal-hydraulic systems analysis code that is based on a non-homogeneous, non-equilibrium, two-phase fluid model that utilizes a six-equation formulation for mass, momentum, and energy conservation for each phase. The development of the code has benefitted from extensive assessments against experimental data representing the behavior of existing reactors (Reference 1-6, Volumes 5 and 7, and Reference 1-7 provide recent examples). The work reported here features extension of the code assessment base to include behavior important for simulating certain postulated accidents in AP600. In particular, the new assessments address the capabilities of RELAP5/MOD3, Version 3.2.1.2, for predicting AP600 thermal-hydraulic response during design-basis small break loss-of-coolant accidents (SBLOCAs).

This report supersedes a detailed, eight-volume compendium of research[1-8] investigating the adequacy of code versions preceding 3.2.1.2 for the AP600 SBLOCA application. This compendium identified deficiencies in prior code versions related to critical flow, core level and core fluid subcooling predictions. These deficiencies have been addressed through improvements in the code and facility input models that have been incorporated in RELAP5/MOD3, Version 3.2.1.2, which is evaluated in this report. Because of its thorough treatment of many aspects of the evaluations, this compendium remains a valuable reference resource for the investigations presented here.

This report demonstrates the adequacy of the code for performing the analyses described above. The purpose of this demonstration is to ensure that RELAP5/MOD3, Version 3.2.1.2, and related facility input models can reasonably represent AP600 SBLOCA behavior and that the USNRC, in its analysis, will reach the correct conclusions regarding that behavior. The case for code adequacy is made by combining the results of various code reviews and assessments. The key assessments relate to code capabilities as

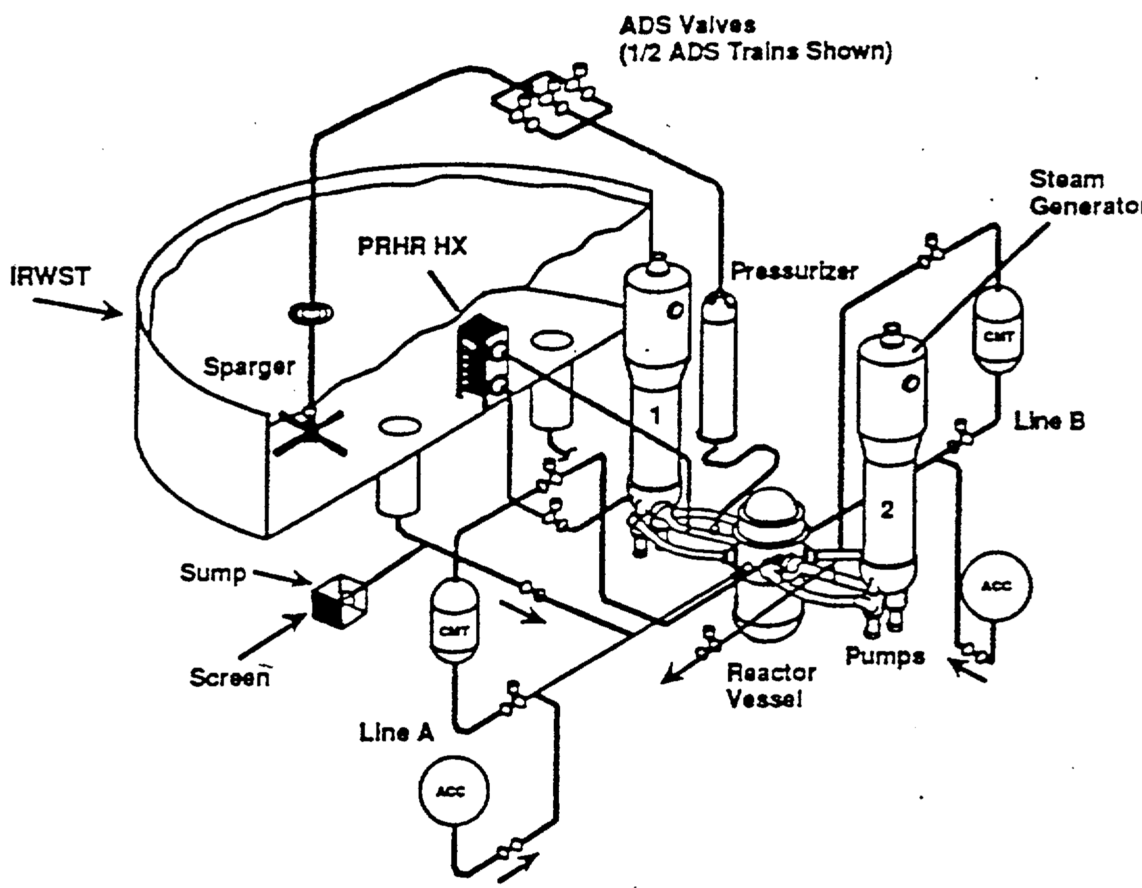

Figure 1-1. Schematic of AP600 thermal-hydraulic systems.

indicated through comparisons between code calculations and tests performed in experimental facilities designed to represent the AP600 systems. Complete assessment analyses were performed for three different SBLOCA scenarios. This set of scenarios was selected because it presents challenges for the AP600 passive safety systems and includes a range of break sizes and locations. These analyses include assessments of code performance against data from comparable experiments in three integral facilities that represent AP600 at different scales.

This report is organized as follows. An overview of the process used for demonstrating code adequacy is described in Section 2. Reviews of the RELAP5/MOD3 governing equations and numerics are discussed in Section 3. The applicability of code models and correlations important for AP600 SBLOCA analysis was evaluated; the approach and results of this evaluation are summarized in Section 4. Code capabilities are best judged by evaluating the performance of the integrated code for predicting experimental behavior. These evaluations are summarized in Section 5, along with scaling analyses that demonstrate the relevancy and sufficiency of the experimental data base for characterizing AP600 SBLOCA behavior. This demonstration allows extension of the judgments regarding code capabilities for predicting experiment behavior to the prediction of AP600 behavior. The findings of the reviews from Sections 3 through 5 are summarized and combined into a judgment of code adequacy in Section 6. This section also provides recommendations, based upon the collective experiences from the assessments, on how to best model the AP600 plant and appropriate user guidance for performing SBLOCA analysis using this code and model. The conclusions regarding code adequacy are stated in Section 7. References are provided at the end of each section. Appendixes are devoted to detailed presentations of the code governing equations and numerics reviews, modeling consistency, code assessments against experimental data for the SBLOCA short-term phase, and experiment uncertainties.

1.1 References

1-1. *AP600 Standard Safety Analysis Report*, Simplified Passive Advanced Light Water Reactor Plant Program, Westinghouse Electric Corporation (Proprietary), June 26, 1992, and revisions.

1-2. *AP600 Design Changes*, Westinghouse Electric Corporation, presentation to U. S. Nuclear Regulatory Commission, (Proprietary), February 22, 1994.

1-3. R. J. Beelman, C. D. Fletcher and S. M. Modro, "Issues Affecting Advanced Passive Light-Water Reactor Safety Analysis," *Nuclear Engineering and Design*, Vol. 146, p. 289, February 1994.

1-4. R. J. Beelman, S. M. Sloan, and J. E. Fisher, P. D. Bayless and S. T. Polkinghorne, *AP600 Quality Assured RELAP5 Input Model Description (Version 3.0)*, Idaho National Engineering Laboratory, EGG-NRE-10824 (Revision 1), (Proprietary), January 31, 1996.

1-5. C. D. Fletcher, G. E. Wilson, C. B. Davis and T. J. Boucher, *Interim Phenomena Identification and Ranking Tables for Westinghouse AP600 Small Break Loss-of-Coolant Accident, Main Steam Line Break, and Steam Generator Tube Rupture Scenarios, Appendix H - Summary of Plant Systems and Automatic Actions (Proprietary)*, Idaho National Engineering Laboratory, INEL-94/0061, Revision 1, July 1995.

1-6. *RELAP5/MOD3 Code Manual*, Idaho National Engineering Laboratory, NUREG/CR-5535, INEL-95/0174, 7 Volumes, August 1995.

1-7. R. R. Schultz, *International Code Assessment and Applications Program: Summary of Code Assessment Studies Concerning RELAP5/MOD2, RELAP5/MOD3, and TRAC-B*, Idaho National Engineering Laboratory, NUREG/IA-0128, EGG-EAST-8719, December 1993.

1-8. *Adequacy Evaluation of RELAP5/MOD3 for Simulating AP600 Small Break Loss-of-Coolant Accidents*, Idaho National Engineering Laboratory, INEL-96/0380, (Proprietary), October 1996.

2 ADEQUACY DEMONSTRATION OVERVIEW

This section provides an overview of the process used in this report for demonstrating adequacy of RELAP5/MOD3 code for the AP600 SBLOCA application.

2.1 Background

The level of current scientific knowledge varies regarding the various thermal-hydraulic processes occurring in nuclear power plants under accident conditions. Some physical processes are well understood, while others are only partially understood.

While governing field equations for single and two-phase flows are well known, mathematical representations for certain parameters in the field equations are not generally well known from first principles. Closure models are developed to represent these parameters and the development may include correlation with experimental data. The adequacy of a closure model is assessed by determining if the model reproduces applicable fundamental and separate effects test data. However, these models are based upon data that usually are limited in some manner (for example, in geometry, orientation or range of thermodynamic state variable). Fortunately, extensive programs of testing in scaled integral facilities have been performed (for example, LOFT,[2-1] MIST,[2-2] 2D/3D,[2-3] and the current AP600 test programs[2-4]). Although the data base supporting some individual code closure or constitutive models may be limited, the integrated capability of the code can be assessed using data from the scaled integral facilities. Therefore, assessment of the code against data from integral facilities assumes an important role in demonstrating code adequacy.

Some systems, components, processes, and phenomena have greater influences than others on the predicted course of an accident and the selected figure of merit. Code models necessary for accurately simulating the most important systems, components, phenomena, and processes must fully satisfy appropriate adequacy standards while code models that have less impact can be held to a lesser standard.

2.2 The Adequacy Demonstration Process

With the background perspectives provided above, we now move to the adequacy demonstration process itself. The process used in this report leads to a decision regarding the adequacy of the code for a specific application. The process, diagramed in Figure 2-1, involves the following key activities:

- The relative importances of systems, components, processes, and phenomena are identified, with particular emphasis on those that are most important,
- standards are established against which code models and performance can be measured,
- code assessments are performed by comparing both the closure/constitutive relationships and the performance of the integrated code against the measurement standards in the context of relative importance of the various systems, components, processes, and phenomena, and
- scaling analyses are performed to ensure that the collective experimental data base employed in the code assessments is both relevant and sufficient for the intended application.

Each of these steps is now addressed individually with regard to the application of RELAP5/MOD3 for AP600 SBLOCAs.

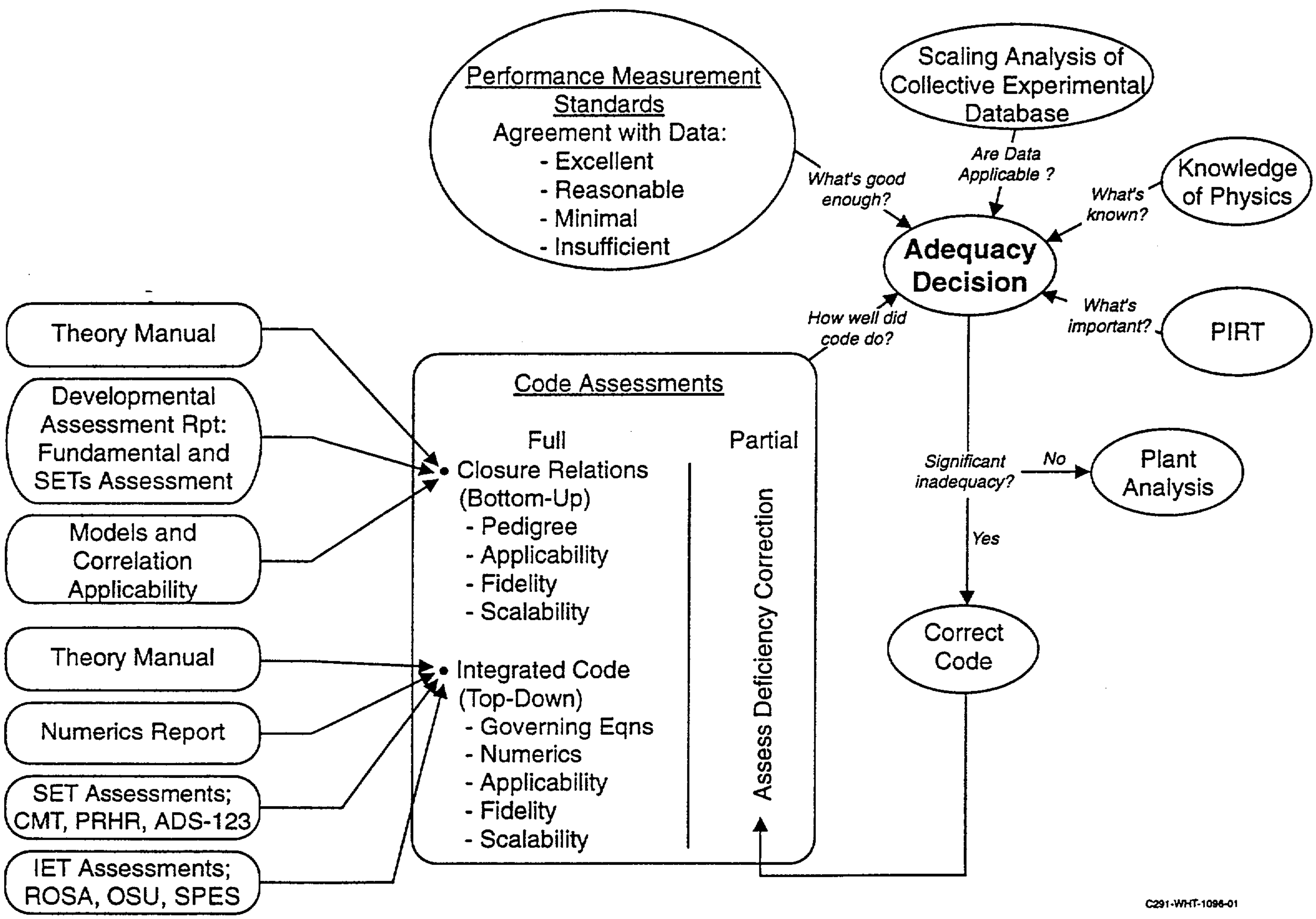

Figure 2-1. The Adequacy Demonstration Process.

2.2.1 Identification of Important Systems, Components, Processes, and Phenomena

A phenomena identification and ranking table (PIRT) lists the phenomena occurring in a specific plant during a specific accident scenario. It also contains a ranking for each phenomenon relative to a key figure of merit that has been selected to characterize the plant accident response. The utility of PIRTs was first demonstrated during the Code Scaling, Applicability, and Uncertainty (CSAU) demonstration effort.[2-5] Subsequently, PIRTs have been used in many elements of USNRC confirmatory research programs. Here, we discuss PIRT usage only as it relates to code adequacy assessment.

The AP600 PIRT[2-6] provides phenomena identification and ranking information for the SBLOCA. The figure of merit used in this PIRT is the minimum reactor vessel inventory. The AP600 PIRT subdivides the SBLOCA scenario into two time periods that are referred to as the "short-term" and "long-term" phases. General AP600 plant response during these SBLOCA phases is described as follows:

> The short-term phase begins at the time that the break in the RCS pressure boundary opens. The resulting RCS depressurization causes reactor and turbine trips and generates a signal that activates the CMT and PRHR systems. The initially-cold water in the CMTs is warmed as RCS water is recirculated through them. As the CMTs are warmed and energy is removed by the PRHR system, the RCS continues to depressurize and lose mass. Eventually, CMT water either flashes or is displaced by steam and the CMTs begin to drain. When CMT level reaches 67.5%, the ADS opens three stages of valves on the top of the pressurizer, allowing the RCS to blow down in a controlled manner into the IRWST. When CMT level falls to 20%, the ADS-4 valves open between the coolant loop hot legs and the containment, allowing the RCS to complete its depressurization. When the differential pressure between the RCS and containment is reduced below the available static head created by the IRWST (which is elevated within the containment), gravity-drain flow of the IRWST water into the RCS begins. The short-term phase ends and the long-term phase begins when stable IRWST injection flow is established.
>
> In the long-term phase, the IRWST drains into the RCS (at the reactor vessel downcomer) and RCS fluid is expelled into the containment (through the ADS-4 valves and break). In the containment, water collects in the sump. Steam is condensed on the interior of the containment shell (through which heat is removed to the atmosphere) and condensate from the shell is returned to the IRWST. When the IRWST has been drained to a specified level, valves are opened allowing equalization of the liquid levels in the sump and IRWST. Thereafter, the sump and IRWST pools provide a combined source of injection to the RCS.

For each phase, the PIRT considers the thermal-hydraulic phenomena, processes, and conditions (for brevity, all of these are referred to as "phenomena" in this report) that affect AP600 SBLOCA response. The phenomena are then ranked as "high", "medium" or "low", according to their influence on the behavior of the figure of merit (as indicated above, the minimum reactor vessel inventory). Phenomena with a controlling influence on that behavior are ranked high; Table 2-1 lists the AP600 SBLOCA PIRT high-ranked phenomena for the short-term and long-term phases.

Table 2-1. SBLOCA PIRT high-ranked phenomena.

Short-Term Phase:	Accumulator Flow ADS Energy Release ADS Mass Flow Break Mass Flow Cold Leg-to-PBL Tee Phase Separation Core Flashing Core Subcooling Margin Core Two-Phase Mixture Level CMT Flow Resistance CMT Level Fuel Rod Core Power/Decay Heat Hot Leg Phase Separation in Tees IRWST Flow Resistance Pressurizer Level
Long-Term Phase:	ADS Energy Release ADS Mass Flow Core Two-Phase Mixture Level Downcomer Level Fuel Rod Core Power/Decay Heat IRWST Flow Resistance IRWST Pool Level IRWST Pool Thermal Stratification Sump Fluid Temperature Sump Level Upper Plenum Two-Phase Level

The PIRT, itself, is not used to decide whether a particular code feature is adequate. Rather, the information in the PIRT is used to guide evaluation of whether the code contains the essential capabilities for modeling phenomena important for the AP600 SBLOCA scenario. Additionally, the information in the PIRT is central in the decision as to whether specific models that are deemed to be inadequate must be corrected before the code can be considered adequate and applied with confidence for confirmatory analysis. As discussed in Section 2.1, some phenomena are more important than others and have dominant influences upon the course of an accident in general and upon the selected figure of merit in particular. The PIRT ranking is used as the indication of the relative importance of phenomena. Code models that are necessary for the accurate simulation of high-ranked PIRT phenomena must fully satisfy the appropriate adequacy standards. However, those code models that are demonstrated to have less impact on the simulation can be held to a lesser standard; for these models, it may be decided that deficiencies need not be corrected.

2.2.2 Performance Measurement Standards

Standards were established by which the capabilities of the code and its models can be judged. These standards are described in this section.

Individual closure and constitutive models and correlations are considered adequate if:

- The model pedigree is known, documented and acceptable,
- the model is generally acceptable for simulation of the physical processes of the application,
- the model predicts specific appropriate data with acceptable fidelity or accuracy, and
- the model is acceptable for the scale of the specific target application.

The performance of the integrated code is considered adequate if:

- The field equations represent the key processes and phenomena,
- the numeric solution approximates the equation set (field and closure) with acceptable accuracy,
- the code is generally acceptable for simulating the system components of the application,
- the model predicts the behavior of the important phenomena as observed in specific, appropriate integral effects tests with acceptable fidelity, and
- the model acceptably represents the interactions between the system components.

These performance measurement standards repeatedly invoke the term "acceptable" as the primary measure that the standard is satisfied. The most concrete measures of code performance relate to the fidelity with which experimental data are simulated, and judgments regarding fidelity are made throughout this report and its supporting documentation. In these judgments, "acceptability" is based on the application of a standardized and consistent set of criteria that has been previously applied in the assessment of USNRC-sponsored codes.[2-3, 2-7 and 2-8] The standardized acceptance criteria are applied to fidelity assessment, whether the data are from fundamental tests, separate effects tests, component tests, or integral effects tests, and are defined as follows:

<u>"Excellent"</u> agreement applies when the code exhibits no deficiencies in modeling a given behavior. Major and minor phenomena and trends are correctly predicted. The calculated results are judged to agree closely with the data. The calculation will, with few exceptions, lie within the specified or inferred uncertainty bands of the data. The code may be used with confidence in similar applications. (The term "major phenomena" refers to the phenomena that influence key parameters such as fuel rod cladding temperature, pressure, differential pressure, mass flow rate, and mass distribution. Predicting major trends means that the prediction shows the significant features of the data. Significant features include the magnitude of a given parameter through the transient, slopes, and inflection points that mark significant changes in the parameter.)

<u>"Reasonable"</u> agreement applies when the code exhibits minor deficiencies. Overall, the code provides an acceptable prediction. All major trends and phenomena are correctly predicted. Differences between calculation and data are greater than deemed necessary for excellent agreement. The calculation will frequently lie outside but near the specified or inferred uncertainty bands of the data. However, the correct conclusions about trends and phenomena would be reached if the code were used in similar applications. The code models and/or facility model noding should be reviewed to see if improvements can be made.

"Minimal" agreement applies when the code exhibits significant deficiencies. Overall, the code provides a prediction that is only conditionally acceptable. Some major trends or phenomena are not predicted correctly, and some calculated values lie considerably outside the specified or inferred uncertainty bands of the data. Incorrect conclusions about trends and phenomena may be reached if the code were used in similar applications, and an appropriate warning needs to be issued to users. Selected code models and/or facility model noding need to be reviewed, modified and assessed before the code can be used with confidence in similar applications.

"Insufficient" agreement applies when the code exhibits major deficiencies. The code provides an unacceptable prediction of the test. Major trends are not predicted correctly. Most calculated values lie outside the specified or inferred uncertainty bands of the data. Incorrect conclusions about trends and phenomena are probable if the code is used in similar applications, and an appropriate warning needs to be issued to users. Selected code models and/or facility model noding need to be reviewed, modified and assessed before the code can be used with confidence in similar applications.

For PIRT high-rank phenomena, the minimum standard for acceptability with respect to fidelity is generally "reasonable" agreement. Although "excellent" agreement is desirable, historically it has rarely been achieved with integral thermal-hydraulic system analysis codes. If "minimal" or "insufficient" agreement is indicated for a PIRT high-rank phenomenon, a code could still be considered adequate despite this deficiency if: (1) the phenomenon can subsequently be demonstrated to not have the dominant influence on the course of an accident indicated by its PIRT rank or (2) an appropriate method can be demonstrated for quantifying the calculational uncertainty resulting from the deficiency and this uncertainty is acceptable. The minimum acceptability standards for PIRT medium and low-rank phenomena are lower than those applied for the PIRT high-rank phenomena.

2.2.3 Code Assessments

The code assessments are divided into two parts as shown in Figure 2-1. One part pertains to the "bottom-up" evaluation of the code closure relations and the other part pertains to the "top-down" evaluations of the code governing equations, numerics and integrated performance.

In the first part of the code assessments, important closure models and correlations are examined by considering their pedigree, applicability, fidelity to appropriate fundamental or separate effects test data, and scalability. This part of the assessment is termed the "bottom-up" review because it focuses on the fundamental building blocks of the code, for example, the closure relationship for interphase drag in rod bundle regions. The pedigree evaluation is related to the physical basis of a closure model, assumptions and limitations attributed to the model, and details of the adequacy characterization at the time the model was developed. The applicability evaluation is related to whether the model, as implemented in the code, is consistent with its pedigree or whether use over a broader range of conditions has been justified. The fidelity evaluation is related to the existence and completeness of validation efforts (through comparison to data) or benchmarking efforts (through comparison to other standards, for example, a closed-form solution or results obtained with another code), or some combination of these two. The scalability evaluation here is limited to whether the specific model or correlation is appropriate for applying to the configuration and conditions of the AP600 SBLOCA application.

In the second part of the code assessments, the integrated code is evaluated by examining the field equations, numerics, applicability, fidelity to component or integral effect data and scalability. This part of the assessment effort is called the "top-down" review because it focuses on capabilities and performance of the integrated code. The field equation evaluation considers the acceptability of the equations to the scientific community. The numeric solution evaluation considers convergence, stability, and property conservation. The applicability evaluation considers whether the integrated code is capable of modeling the key AP600 plant systems and components. The fidelity evaluation considers the comparison of code-calculated and measured test data from both component and integral effects experiments. The scalability evaluation here is limited to whether the assessment calculations and experiments exhibit differences among the facilities, or between the calculated and measured test data for the same facility, that indicate experimental or code scaling distortions.

2.2.4 Scaling Analysis of the Collective Experimental Data Base

Scaling analyses are employed to demonstrate the relevancy and sufficiency of the collective experimental data base for representing the behavior expected of AP600 during SBLOCAs and to investigate the scalability of RELAP5/MOD3 for representing the important phenomena. The scope of these analyses is much broader than for the scalability evaluations described in the previous section relating to individual models and correlations or scaling-related findings from the code assessments. Here, the need is to demonstrate that the experimental data base is sufficiently diverse, so that the expected AP600 SBLOCA response is included and that the code calculations are comparable to the corresponding tests in non-dimensional space. This demonstration allows extending the conclusions relating to code capabilities, drawn from assessments comparing calculated and measured test data, to the prediction of AP600 plant behavior.

The scaling analyses employ both "top-down" and "bottom-up" approaches. The "top-down" scaling approach evaluates the global system behavior of the data from the AP600-related integral test facilities. A "top-down" scaling methodology is developed and applied in which: (1) the non-dimensional groups governing similitude between facilities are derived, (2) it is verified that these groups scale the results among the experimental facilities, and (3) it is determined whether the ranges of the group values provided by the experiment set encompass the corresponding AP600 group values. The "bottom-up" scaling analyses address selected issues raised in the AP600 SBLOCA PIRT[2-6] relating to localized behavior. These analyses are used to explain differences observed among tests in different experimental facilities and to use these explanations to infer the expected AP600 behavior and determine whether the experiments provide adequate representations of AP600.

2.3 The Adequacy Decision

The code adequacy decision is the culmination of the adequacy demonstration process described in the previous section and diagramed in Figure 2-1. The knowledge of physical processes and the PIRT indicate the relative importance of phenomena in simulating AP600 SBLOCAs. The measurement standards establish the minimum levels of performance that are considered acceptable. Assessments focussing on the important phenomena are then performed to evaluate the acceptability of the code performance. Scaling analyses are performed to demonstrate that the collective experimental data base is relevant and sufficient for representing expected AP600 SBLOCA response; this allows extension of the conclusions regarding code capabilities drawn from experimental assessments to the prediction of AP600 behavior. If the assessments indicate unacceptable code performance relating to the prediction of an important phenomenon, then the code deficiency is corrected and assessments are repeated to evaluate the deficiency correction. The process continues until the assessments indicate that all important phenomena are acceptably predicted.

2.4 References

2-1. C. L. Nalezny, *Summary of Nuclear Regulatory Commission's LOFT Program Experiments*, Idaho National Engineering Laboratory, NUREG/CR-3214, EGG-2248, July 1983.

2-2. J. R. Gloudemans, *Multiloop Integral System Test (MIST): Final Report*, Babcock and Wilcox Company, NUREG/CR-5395, EPRI/NP-6480, BAW-2023, Volume 1, April 1991.

2-3. *2D/3D Program Work Summary Report*, prepared jointly by Japan Atomic Energy Research Institute, Gesellschaft fuer Anglagen-und Reaktorsicherheit, Siemens AG, UB KWU, U. S. Nuclear Regulatory Commission, Los Alamos National Laboratory and MPR Associates, Inc., International Agreement Report NUREG/IA-0126, also GRS-100 and MPR-1345, June 1993.

2-4. L. E. Hochreiter, L. E. Conway, S. V. Fanto and L. K. Lau, *Integral Testing of the AP600 Passive Emergency Core Cooling Systems*, Proceedings ANS 1994 International Topical Meeting on Advanced Reactor Safety, Volume 2, p. 991-1004, 1994.

2-5. B. Boyack, R. Duffey, P. Griffith, G. Lellouche, S. Levy, U. Rohatgi, G. Wilson, W. Wulff, N. Zuber, K. Katsma, D. Hall, R. Shaw, C. Fletcher and K. Boodry, *Quantifying Reactor Safety Margins: Application of Code Scaling, Applicability, and Uncertainty Evaluation Methodology to a Large-Break Loss-of-Coolant Accident*, U. S. Nuclear Regulatory Commission, NUREG/CR-5249, December 1989.

2-6. J. D. Burtt, C. D. Fletcher, G. E. Wilson, C. B. Davis and T. J. Boucher, *Phenomena Identification and Ranking Tables for Westinghouse AP600 Small Break Loss-of-Coolant Accident, Main Steam Line Break, and Steam Generator Tube Rupture Scenarios*, Idaho National Engineering Laboratory, INEL-94/0061, Revision 2, March 1997.

2-7. *Compendium of ECCS Research for Realistic LOCA Analysis*, U. S. Nuclear Regulatory Commission, NUREG-1230, p. 4-126, December 1988.

2-8. R. R. Schultz, *International Code Assessment and Applications Program: Summary of Code Assessment Studies Concerning RELAP5/MOD2, RELAP5/MOD3, and TRAC-B*, Idaho National Engineering Laboratory, NUREG/IA-0128, EGG-EAST-8719, December 1993.

3 REVIEWS OF CODE GOVERNING EQUATIONS AND NUMERICS

Reviews have been performed regarding inherent RELAP5/MOD3 code capabilities for predicting the behavior expected during AP600 SBLOCAs. These reviews of the code governing equations and numerics, which are provided as a part of the integrated or "top-down" code evaluation process shown in Figure 2-1, are documented in Appendix A and are summarized here.

A review of the code governing equations considered their pedigree and the key concepts and processes culminating in the governing equation set solved by RELAP5/MOD3. The objective of this review was to characterize the applicability of the governing equations for AP600 accident analysis. This was accomplished by considering the inherent characteristics of the fundamental governing equations. As mathematical operations are performed on the fundamental governing equations, they are transformed in a manner that either restricts their range of applicability or requires that additional information, e.g., constitutive relationships, be provided. These mathematical operations were reviewed. The implications of the restrictions and limitations for the AP600 SBLOCA application were then evaluated. The description of the governing equations solved in RELAP5/MOD3, which was based on information found in References 3-1 and 3-2, is documented in Section A.1 of Appendix A.

The key focus of the code numerics review was the accuracy, stability and convergence of code calculations to a solution of the original equations when applied to the target application. The objective of this review was to summarize information regarding the domain of applicability of the numerical techniques and user procedures that impact the accuracy, stability and convergence features of RELAP5/MOD3. The code numerics review, which was based on information found in References 3-1, 3-2, and 3-3, is documented in Section A.2 of Appendix A.

These reviews showed the code governing equations and numerics to be generally applicable for simulating SBLOCAs in AP600. These reviews indicated three specific limitations of the code for this application: the assumption of homogeneity within each phase, a defect in the momentum flux formulation, and a tendency to overpredict condensation. These limitations and their implications for AP600 SBLOCA analysis are discussed below.

3.1 Assumption of Homogeneity Within Phases

The inherent assumption of one-dimensional codes that the liquid and vapor phases each are homogeneous has implications for this application which the RELAP5/MOD3 user should consider and account for. These implications regard simulation of behavior in the AP600 cold legs and CMTs during situations when these components are liquid-filled but thermally stratified. These AP600 components are modeled using one-dimensional nodalization schemes, as described in Section 6.3. Simple examples illustrating two such situations are described here. The intent of these examples is to convey to the user the mechanisms by which this code assumption may affect the outcome of a simulation. With this understanding, the user may discern the effects of this assumption for a particular accident scenario and, if appropriate, perform bounding analyses to quantify the impact for a specific accident simulation.

Example 1 - Figure 3-1 represents one of the cold legs on the AP600 CMT coolant loop during the high-pressure portion of a cold leg break accident scenario. The cold leg is liquid filled during the period when the steam generator tubes are draining and the CMTs are recirculating. Assume, for purposes of illustration, that the break is on the bottom of the cold leg pipe at Location A, that the steam generator drain flow rate is one-third of the CMT recirculation rate and that the break flow rate is equal to the steam generator drain rate. In the physical situation (shown in the upper sketch of Figure 3-1), hot water draining from the steam generator tubes can thermally stratify and overlay cold

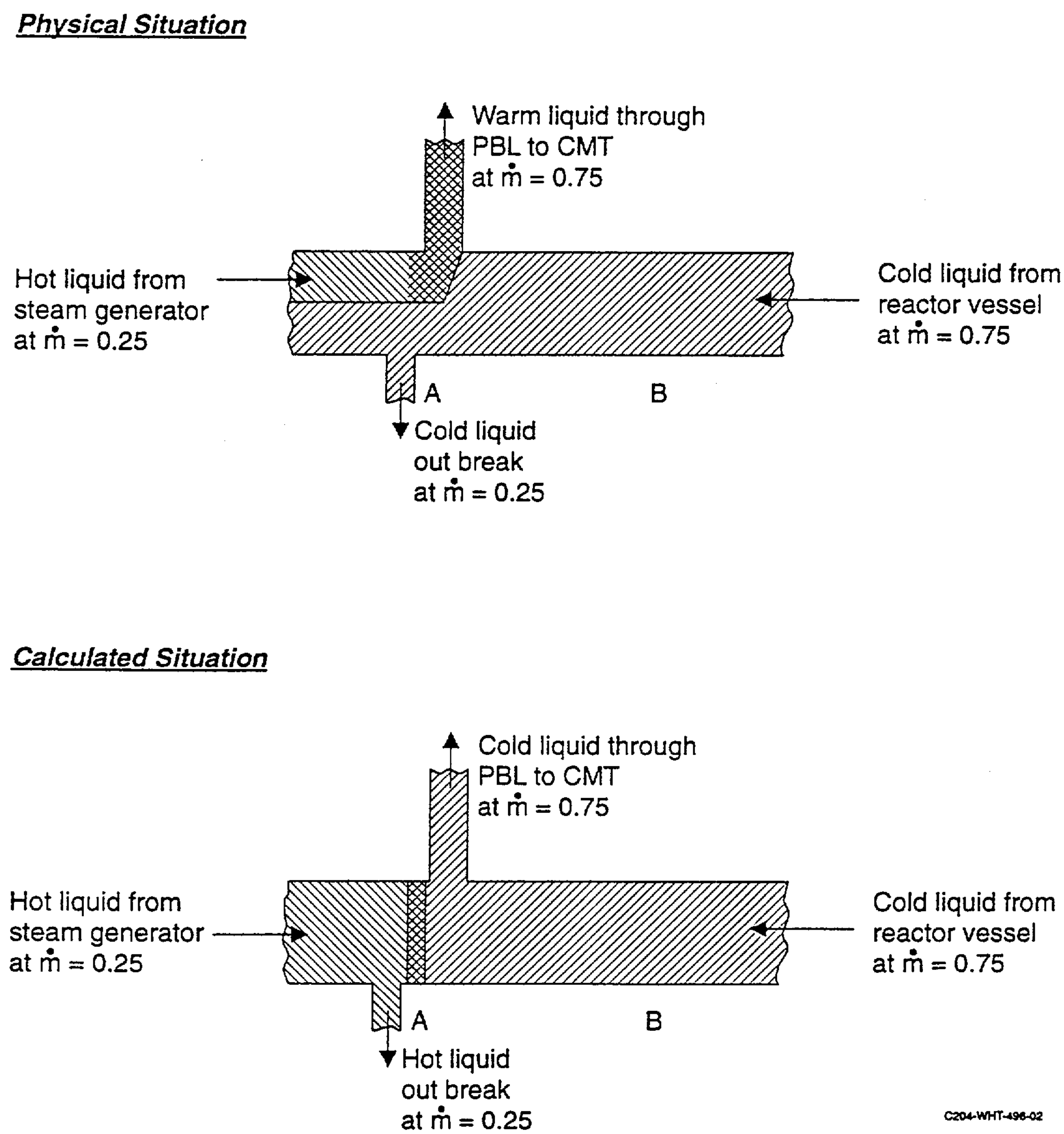

Figure 3-1. Example of cold-leg thermal stratification modeling distortion.

water within the horizontal cold leg. The water flowing through the break would be cold while the water flowing through the pressure balance line into the CMT would be warm (i.e., a mixture of the cold and hot liquids). The simulation, however, cannot represent thermal stratification in a horizontal component. Therefore, for the calculation of this example situation (shown in the lower sketch of Figure 3-1), hot liquid would flow out the break and cold liquid would flow into the pressure balance line. As a result of the homogeneous assumption, the simulation would, therefore, overstate the energy of the fluid exiting the break and understate the energy of the fluid entering the pressure balance line and CMT. For this case, the user might bound the effects of the uncertainty introduced into the simulation through this code limitation by relocating the break from Location A to Location B, repeating a portion of the simulation, and observing the differences between the two simulations.

Example 2 - Figure 3-2 represents one of the CMTs during the high-pressure portion of an SBLOCA. The CMT is initially filled with cold water. When recirculation begins, hot water enters the tank at the top and cold water exits the tank at the bottom. Unlike the cold leg in Example 1, the CMT is a vertical component and the code has some capabilities for representing thermal stratification effects within it (i.e., for resolving step type gradients using a subgrid resolution model). However, the code solution will provide a distorted CMT vertical thermal profile in situations where the temperature of water entering the tank declines. Warm water, entering the top of the tank after hot water has entered, may remain above the hot water in the simulation and this is non-physical behavior. The physical behavior is shown in the upper sketch and the calculated behavior is shown in the lower sketch of Figure 3-2. If this situation is encountered, the user might bound the effects of the uncertainty introduced into the calculation through this modeling distortion by altering the simulated thermal distribution (manually, at a calculation restart point) to remove the cumulative effects of the distortion and comparing the results of this sensitivity calculation with the base case calculation. Alternatively, the user might renodalize the CMT just before the time that it starts draining such that liquid above the thermal front is contained within a single control volume. This sensitivity calculation would show the effects of perfectly mixing all the water above the thermal front and thereby indicate the maximum delay expected in the onset of CMT draining that could be caused by thermal stratification effects.

Modeling distortions such as those portrayed in these two examples were observed in the code assessments against experimental data for the SBLOCA short-term phase summarized in Section 5.1. More detailed information on this subject appears in Appendix C of this report and Reference 3-4 (Volume 2, Appendix D). The assessment results indicate: (1) the cold leg thermal stratification distortion can have a minor effect on break flow and sequence event timing before ADS activation and (2) no significant effects of the CMT thermal stratification distortion were observed. In none of the assessments were the effects of these modeling distortions seen to be sufficiently large to render the code inadequate for generally representing the experimental data. However, as indicated above, code users need to be aware that judgments regarding the significance of effects such as these are, necessarily, accident-scenario specific.

The assumption of homogeneity within phases also plays a role in overpredicting interphase condensation as described in Section 3.3.

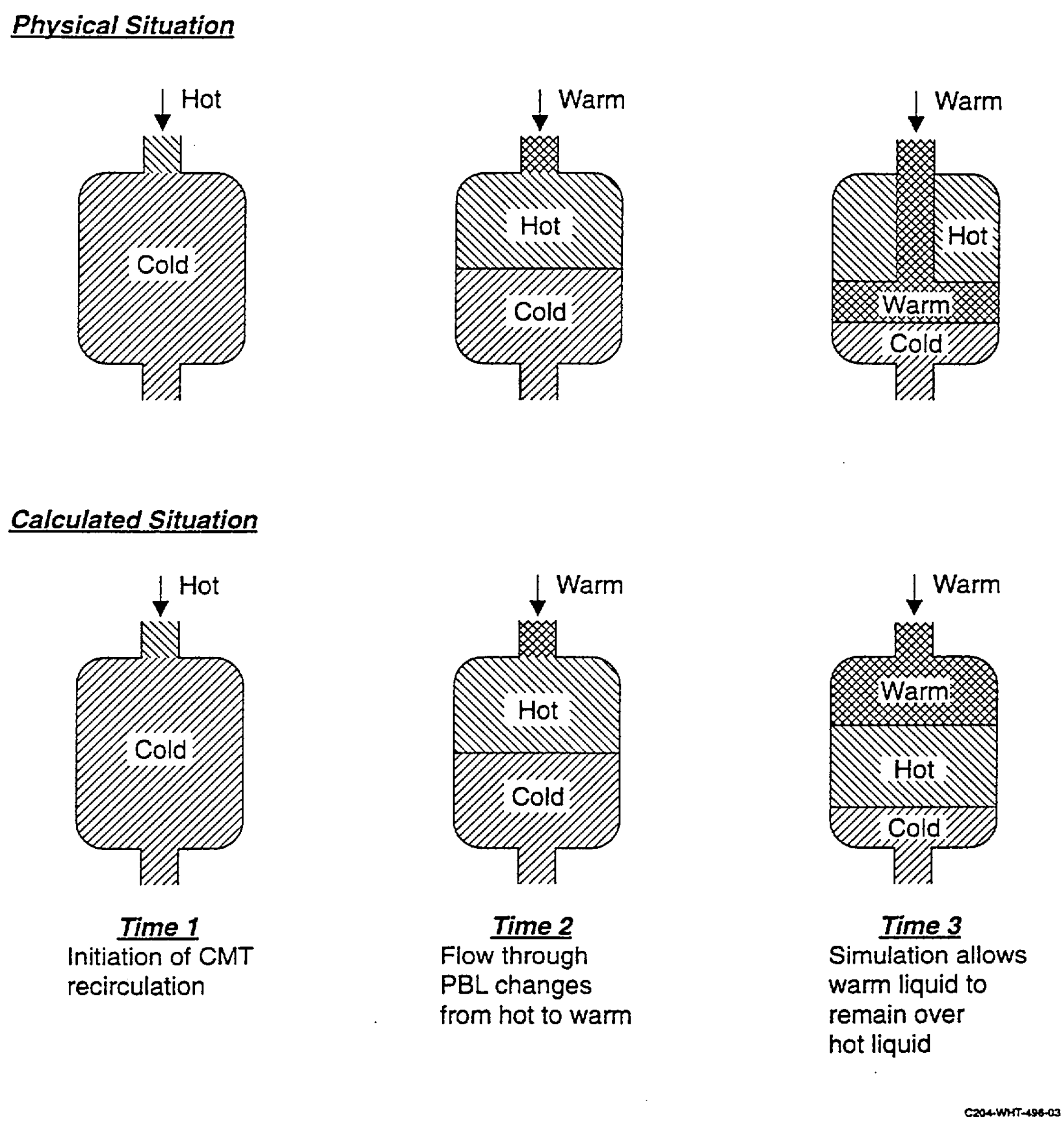

Figure 3-2. Example of CMT thermal stratification modeling distortion.

3.2 Momentum Flux Effects

An anomalous effect of the RELAP5 momentum flux formulation has been identified. This anomaly can result in non-physical circulations within otherwise-quiescent fluid regions that are modeled using quasi-multidimensional nodalization schemes. Prior to the AP600 RELAP5 application, some indications of this anomaly were reported; however, the source of the anomaly had not previously been identified and these prior indications were not widespread for two reasons. First, quasi-multidimensional nodalizations had not previously been extensively used. Second, system flow rates in most previous applications generally were high, for example due to the actions of pumps or coolant-loop natural circulation flows. The AP600 SBLOCA analysis application: (1) was originally approached using quasi-multidimensional noding schemes in many regions and (2) features many low-flow situations (where the anomalous acceleration due to the momentum flux defect can dominate a calculated solution). This section describes and illustrates this anomalous effect and describes a work-around that is demonstrated (through the assessments in Section 5) to be satisfactory for the AP600 SBLOCA analysis.

With RELAP5/MOD3, Version 3.2.1.2, it is possible for fluid to be artificially accelerated because of a defect in the momentum flux formulation. Figure 3-3 provides an illustrative example of a situation where acceleration due to this defect is likely to be experienced. The figure shows a nodalization for a portion of a reactor vessel downcomer. The downcomer nodalization features two annular azimuthal sections, shown as the left and right sides in the figure. These two vertical sections are interconnected over the downcomer height via cross-flow junctions (Junctions 101 through 113) and connected to plena (where boundary conditions are specified) at their tops and bottoms. Initially, liquid occupies the lower portion of the downcomer (shown as the dark region), steam occupies the upper portion and there are no flows through any of the junctions. When this model is run with momentum flux active at all junctions (this is the normal option), an internal circulation starts up and reaches a steady state. Liquid flows downward in the left section into the bottom plenum, then upward through the right section and across Junction 105, back into the left section. Steam flows upward in the left section into the top plenum, then downward through the right section and across Junction 105, back into the left section. These circulations are non-physical. When the run is restarted (from the circulating condition) with momentum flux disabled at all junctions, the recirculating flows decay away.

The currently recommended AP600 modeling approach (described in Section 6.3) limits the effects of the momentum flux anomaly in two ways. First, the recommended approach uses one-dimensional modeling schemes as much as is practicable. Preliminary quasi-multidimensional modeling schemes for the AP600 reactor vessel lower plenum, core, upper plenum and IRWST pool regions have given way in the recommended modeling approach to one-dimensional schemes in these regions. Second, in regions where quasi-multidimensional modeling is essential, the currently recommended modeling approach is to disable momentum flux in the normal and cross-flow junctions in which recirculation patterns can easily develop. In the AP600 SBLOCA application, only the reactor vessel downcomer region of the detailed model was judged necessary to model using quasi-multidimensional nodalization. The recommended detailed modeling approach disables momentum flux at all internal downcomer junctions and at the junctions connecting the downcomer to the reactor vessel lower plenum and upper head regions. This approach is justified because: (1) fluid velocities in the downcomer region generally are small, with the momentum equation dominated by the hydrostatic and frictional terms and not by the physical momentum flux effects and (2) changes in momentum flux within the downcomer are small because flow-area changes in this region are slight. The code assessments in Section 5 demonstrate that this approach to downcomer modeling represents a satisfactory work-around to momentum flux difficulties for the AP600 SBLOCA analysis application.

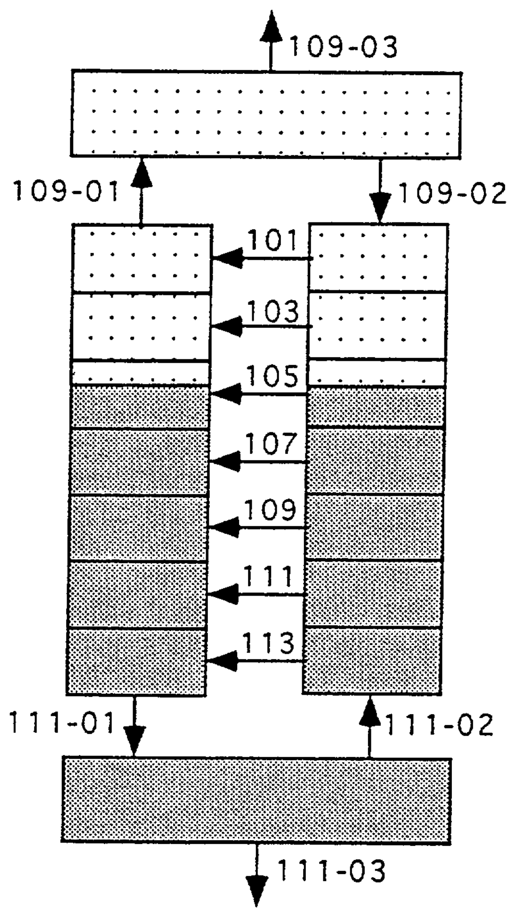

Figure 3-3. Example of quasi-multidimensional nodalization and effect of defect in the momentum flux formulation.

Work is under way toward correcting the momentum flux anomaly. This correction will appear in a code version subsequent to 3.2.1.2 that is the subject of this report. The use of the work-around described above will be discontinued following implementation and satisfactory demonstration of a correction.

3.3 Overprediction of Interphase Condensation

Two factors lead to a tendency, in certain situations, for the RELAP5/MOD3 code to overpredict interphase condensation: (1) the assumption of homogeneity within each phase and (2) the abruptness of changes in flow regime.

First, because of the assumption of homogeneity within each phase (as discussed in Section 3.1), all of the liquid within a control volume is calculated to be at a single temperature. As a result, it is not possible with RELAP5/MOD3 to represent a situation where condensation of steam on a free liquid surface locally warms the liquid at the surface, thus limiting further condensation. If sufficient steam is available, then condensation is calculated to continue until all subcooling has been removed from the liquid present in the control volume containing the steam/liquid interface.

Second, transitions in the flow regime cause corresponding transitions in the calculated interphase heat-transfer. For example, in a vertically-oriented volume, if conditions are quiescent a vertically-stratified flow regime is selected, while if conditions are dynamic a bubbly flow regime is selected. The steam/liquid interface area associated with the former is much less than that associated with the latter. Changing flow conditions can therefore lead to rapid changes in interface heat transfer area and interphase condensation rate.

For two reasons, interphase condensation in the CMT component was not observed to be overpredicted in the assessments described in Sections 5.1 and 5.2. First, the CMTs were modeled with the thermal stratification option activated. CMT response during SBLOCAs begins with a recirculation period, with warm water entering the top of the tank. When a steam/liquid interface is eventually formed within the tank, the potential for condensation is reduced because the local water temperatures near the interface are near saturation. Second, the flow conditions within the tank were not sufficiently dynamic to effect flow regime transitions that would alter the calculated interface heat transfer area.

Interphase condensation was observed to be overpredicted in the reactor vessel upper plenum region in several assessments for the OSU/APEX facility. During the short-term phase of the test for the 1-in. cold leg break scenario, an overprediction of condensation after IRWST injection began led to the calculation of a more rapid refill of the reactor vessel than was measured (see Section 5.1.2 and Appendix C). In this case, existing code capabilities were judged to be acceptable because the calculation of the minimum reactor vessel inventory condition (occurring just after onset of IRWST injection) was not affected. During the long-term phases of the tests for all three scenarios, overpredicted condensation caused by cyclic transitions between the vertically-stratified and bubbly flow regimes in the presence of cold water was seen to be one of the drivers for non-physical oscillations within the reactor vessel (see Section 5.2.2). It was concluded for these cases that, although improvement in the results could be obtained if the oscillations were reduced, existing code capabilities were acceptable because the calculated minimum vessel inventory during the long-term phase (occurring during sump injection) was not affected.

3.4 References

3-1. V. H. Ransom, *Course A - Numerical Modeling of Two-Phase Flows for Presentation at Ecole d'Ete d'Analyse Numerique*, EG&G Idaho, Inc., EGG-EAST-8546, May 1989.

3-2. A. S. Shieh, V. H. Ransom and R. Krishnamurthy, *RELAP5/MOD3 Code Manual, Volume 6, Validation of Numerical Techniques in RELAP5/MOD3*, Idaho National Engineering Laboratory, NUREG/CR-5535, EGG-2596, October 1994.

3-3. A. S. Shieh, R. Krishnamurthy and V. H. Ransom, "Stability, Accuracy and Convergence of the Numerical Methods in RELAP5/MOD3," *Nuclear Science and Engineering*, Vol. 116, p. 227-244, 1994.

3-4. *Adequacy Evaluation of RELAP5/MOD3 for Simulating AP600 Small Break Loss-of-Coolant Accidents*, Idaho National Engineering Laboratory, INEL-96/0380, (Proprietary), October 1996.

4 CODE MODEL AND CORRELATION REVIEWS

The RELAP5/MOD3 code has benefitted from extensive prior assessment, performed over a period of many years, related to predicting the accident behavior of existing reactors. Many of these prior assessments remain applicable for AP600 SBLOCA calculations. Recent examples of these assessments are found in the International Code Assessment Program,[4-1] the Code Applications and Maintenance Program,[4-2] and the RELAP5/MOD3 user guideline document.[4-3] This section summarizes additional studies conducted to determine the applicability of specific RELAP5/MOD3 models and correlations judged to be important for AP600 SBLOCA simulations. For the remaining models and correlations, the previous assessment base, strengthened by the assessments of integrated code performance against AP600-related experiments in Section 5, is considered adequate. These additional studies include reviews of recent developmental assessments[4-4] performed for RELAP5/MOD3, Version 3.2.1.2.

For the code model and correlation reviews, the capabilities of selected code models and correlations for predicting important behavior were individually studied. Importance is defined as influence upon the AP600 SBLOCA PIRT[4-5] high-ranked phenomena (these are listed in Table 2-1). This "bottom-up" review approach is in contrast with the "top-down" approach (which focuses on integrated code behavior) taken in the other code assessments of the code adequacy demonstration process shown in Figure 2-1.

Code model and correlation applicability was determined through evaluations of: (1) model pedigree, (2) the parameter ranges for which the model was originally developed, over which it is applied in RELAP5/MOD3, over which it has been assessed and those required for the AP600 SBLOCA application, (3) the fidelity with which the code model or correlation can replicate appropriate experimental data, and (4) the scalability of the model to AP600 plant geometry and SBLOCA conditions. The step-wise process diagramed in Figure 4-1 was used for this review as follows:

- AP600 SBLOCA PIRT high-ranked phenomena were listed and those that could best be evaluated using separate effects assessments were selected from the list. Phenomena more appropriately addressed through integral effects assessments were not considered in this review; these phenomena are covered through the assessments reported in Section 5.

- The RELAP5/MOD3 models and correlations that dominate code capabilities for predicting each of the selected PIRT high-ranked phenomena were determined. Seven such dominant models and correlations were identified. The models and correlations selected for review are listed in Table 4-1 along with the corresponding PIRT high-ranked phenomena that they influence.

- Key independent parameters or variables were determined for each of the dominant models and correlations.

- The parameter ranges of interest for the dominant models and correlations were determined. Sources of information for this step include the AP600 operating ranges and the experimental data from integral effects tests performed to represent AP600 SBLOCA behavior.

- Pertinent code developmental assessments that have not been addressed in previous RELAP5/MOD3 models and correlations documentation[4-6] were collected and evaluated.

The dominant models and correlations were then investigated individually as follows:

- Documentation and pedigree were reviewed.

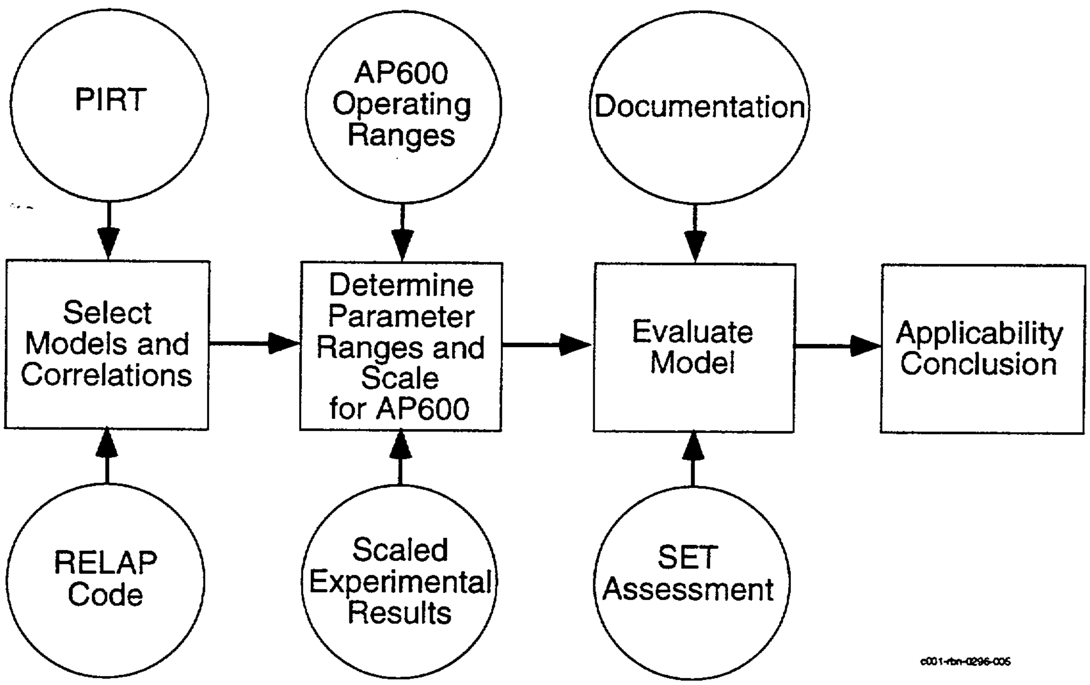

Figure 4-1. Models and correlations evaluation process.

Table 4-1. RELAP5/MOD3, Version 3.2.1.2 models and correlations selected for review and correspondence with PIRT high-ranked phenomena.

RELAP5 Model or Correlation	SBLOCA PIRT Short-term Phase High-ranked Phenomena Dominated by this Model	SBLOCA PIRT Long-term Phase High-ranked Phenomena Dominated by this Model
Accumulator Component	Accumulator Flow	
Critical Flow	ADS Energy Release, ADS Mass Flow, Break Mass Flow	ADS Energy Release, ADS Mass Flow
Decay Heat	Fuel Rod Core Power/Decay Heat	Fuel Rod Core Power/Decay Heat
Flow Resistance	Accumulator Flow, CMT Flow Resistance, IRWST Flow Resistance	IRWST Flow Resistance
Horizontal Stratification and Entrainment	ADS Energy Release, ADS Mass Flow, Break Mass Flow, Cold Leg-to-PBL Tee Phase Separation, Hot Leg Tee Phase Separation	ADS Energy Release, ADS Mass Flow
Interphase Drag in Bundles	Core Two-Phase Mixture Level	Core Two-Phase Mixture Level
Interphase Mass and Energy Transfer (Vapor Generation)	Core Flashing	

- The ranges of the model or correlation as originally developed, as applied in RELAP5, as assessed, and as required for the AP600 SBLOCA application were compared.

- Comparisons between the code model or correlation and appropriate experimental data were evaluated. Judgments regarding code model and correlation fidelity were made from these comparisons, using the same standardized and consistent set of criteria (see Section 2.2.2) that was used in the integral code assessments. Where appropriate and where sufficient information was available, the differences between experimental measurements and code calculations were quantified.

Conclusions

From these evaluations, overall judgments were made regarding the applicability of the dominant models and correlations for simulating AP600 SBLOCAs. All seven dominant models and correlations were judged to be applicable. Table 4-2 summarizes for each of these models and correlations the key parameters, special requirements or considerations for this application, and comments regarding applicability. Note that the example figures accompanying this table represent only a small part of the developmental assessment performed.[4-4] Although all the models were judged to be applicable, uncertainty in the models will cause uncertainty in the calculated results for AP600. The uncertainties associated with the critical flow, two-phase flow resistance, horizontal stratification and entrainment, and bundle interphase drag models are considered particularly noteworthy. The uncertainty in the critical flow model arises primarily because critical flow is sensitive to the geometry near the choking plane, particularly for low-quality flow. For optimal performance of the model, sufficient data to characterize the critical flow for a given geometry are required. Similarly, the two-phase pressure drops associated with valves and orifices depend on the geometry and the flow conditions. The scatter in the data used to develop the horizontal stratification and entrainment model and the possible influence of the absolute pipe size also leads to uncertainty in the calculated results for AP600. The evaluation showed that the interphase drag model overpredicted void fractions in the core by 5 to 9% at low pressures. The effects of uncertainty in these models on the AP600 response can be accounted for with sensitivity calculations, performed in the context of enhancing understanding of the underlying phenomenology. The code model and correlation reviews summarized here are fully documented in Reference 4-7.

Table 4-2. Summary of dominant RELAP5/MOD3, Version 3.2.1.2 model and correlation review results: all were judged to be applicable.

Dominant RELAP5 Model or Correlation	Key Parameters (and Special Considerations)	Comments
Accumulator Component	Flow, pressure, temperature (spherical tank, line orifice)	Model is based on conservation equations and poses no scaling issues. Correlations are applied to represent heat transfer from the walls and the liquid to the gas. The ranges of the application are within valid ranges of the correlations. As described in Reference 4-9, excellent pressure response agreement was obtained with data from LOFT Test L3-1.[4-10] Although the flow measurement remained within the dead bands of the instrument during this test, the agreement between calculated and measured flows can be inferred from Figure 4-2, which shows calculated and measured pressure versus gas volume. The excellent agreement between calculated and measured volume versus pressure and pressure versus time implies that the liquid volume versus time, and hence the accumulator flow, is also in excellent agreement.
Critical Flow	Pressure, temperature, quality (valves and break)	The Henry-Fauske model[4-11] has been implemented in RELAP5/MOD3, Version 3.2.1.2. The ranges of the AP600 application are within valid ranges of the correlation. Developmental assessments performed using experimental data from 16 sources indicate successful implementation and comparison to experimental data. An example comparison of calculated and measured critical flow data for a Marviken test[4-12] is presented in Figure 4-3. The RELAP5-calculated results with the Henry-Fauske model are in reasonable agreement with the test data. An applications assessment of the critical flow model, specific to the ADS Stage 1, 2 and 3 valves, appears in Section 5.4. For optimal performance of the model, the assessments indicated that sufficient data are required to characterize the two empirical constants, the discharge coefficient and the thermal nonequilibrium parameter, used in the model. In the absence of such data, default constants are generally utilized. The absence of characterization data leads to an increased level of uncertainty, but the additional uncertainty can be accounted for with sensitivity calculations.
Decay Heat	Time after scram	Established model[4-13] that is generally accepted by the scientific community. The ranges of the application are within the valid ranges of the model. An example comparison, showing excellent agreement of calculated results obtained with RELAP5 and the ORIGEN2[4-14] isotope buildup and depletion code, is presented in Figure 4-4. The difference in the integrated power at 10,000 s is less than 1%. The calculated results differ more after 10,000 s because the correction factor G(t) (applied to the fission product decay to account for neutron absorption effects in fission products) used in RELAP5 changes from a best-estimate equation to a conservative upper-bound tabulated value prescribed by the 1979 ANS standard. ORIGEN2 performs a best-estimate calculation throughout the transient.

Table 4-2. (continued).

Dominant RELAP5 Model or Correlation	Key Parameters (and Special Considerations)	Comments
Flow Resistance	Flow rate, pressure, void fraction (orifices, valves)	Form loss and wall friction models contribute to the calculation of flow resistance. For AP600 calculations, the dominant pressure drops are mainly due to form losses associated with orifices, valves, and tees. Form losses are modeled using a classical approach. Assessments have been performed using single-phase and two-phase pressure drop experiments. An example comparison,[4-15] showing reasonable agreement between the effective two-phase form loss multipliers derived from calculations and measurements from EPRI flow blockage tests, is presented in Figure 4-5. Because two-phase pressure drops depend on the geometry and flow conditions, uncertainty in two-phase resistance has the potential to affect AP600 SBLOCA calculations. Sensitivity calculations can be performed to bound the uncertainty associated with the flow resistance models in AP600 applications.
Horizontal Stratification and Entrainment	Flow rates, pressure, liquid level, densities (tees)	The horizontal stratification and entrainment model has a theoretical basis for determining the onset of liquid entrainment and vapor pullthrough but utilizes empirical constants to fit data. The model also uses empirical correlations for the fluid quality in the side pipe for different orientations of the side pipe (up, down, and side). The most significant application of the model for AP600 calculations is for an upwards orientation of the side pipe, corresponding to the hot leg-to-ADS-4 piping and cold leg-to-CMT PBL connections. The model was developed from experimental data that spanned the required range of thermodynamic conditions relative to AP600 SBLOCA applications. However, the geometry of the experiments did not span the geometry of the AP600. For example, the hot leg diameter in the AP600 is 0.787 m while the diameter of the main pipe in the largest facility was 0.284 m. Furthermore, the ratio of the side pipe diameter to the main pipe diameter ranged from 0.03 to 0.15 in the tests compared to 0.34 for the ADS-4 to hot leg connection in the AP600. The separate effects experiments described in Azzopardi and Hervieu[4-16] were reviewed to determine the data that would best represent the AP600 hot leg-ADS 4 tee configuration; the data by Azzopardi and Smith[4-17] were selected. A comparison, showing excellent agreement between a RELAP5 calculation and this data, is presented in Figure 4-6. The case shown is for a vertical upward-oriented side pipe, a main pipe diameter of 0.038 m and a side-to-main pipe diameter ratio of 0.67. The figure shows the fraction of liquid flowing through the main pipe taken off through the side pipe versus the fraction of gas taken off through the side pipe. Because the side pipe is oriented upwards, essentially no liquid is taken off through the side pipe until most of the gas is taken off. The figure also shows data from Mudde[4-18], in which the main pipe had a diameter of 0.23 m. A comparison of the data from Azzopardi and Smith and Mudde does not show a pipe-diameter effect for upward-oriented off-takes. However, the results on the effect of pipe diameter are not considered conclusive because the diameter ratio and flow conditions also varied between tests. The assessment calculations using data from Azzopardi and Smith and the comparisons with the data from Mudde have mitigated scale and geometry concerns relative to the horizontal entrainment model. However, the uncertainty in the model leads to uncertainty in AP600 applications, which can be bounded with sensitivity calculations.

Table 4-2. (continued).

Dominant RELAP5 Model or Correlation	Key Parameters (and Special Considerations)	Comments
Interphase Drag in Bundles	Flow rates, void fraction, pressure (bundles)	The RELAP5 rod-bundle interphase drag model is based on the empirical EPRI correlation[4-19] that is supported by extensive separate effects experiments covering a broad range of geometries and conditions. The ranges of the AP600 application are within the ranges of the correlation. An example comparison, showing excellent agreement between RELAP5-predicted and measured results for high-pressure FRIGG experiments,[4-20] is shown in Figure 4-7. The diagonal line represents a perfect match between the calculation and the test while the off-diagonal lines represent a 15% deviation. At low pressures, the code generally overpredicted void fraction and underpredicted bundle inventory. An example of this bias at low pressure is shown in Figure 4-8 for THETIS[4-21] boiloff tests. On average, the predicted void fraction was 9% greater than the measured value for the THETIS tests. A similar result was obtained for the low-pressure PERICLES tests[4-22] (see Figure 4-9), where, on average, the calculated void fraction was 5% greater than the measured value.
Interphase Mass and Energy Transfer (Flashing)	Flow rate, pressure, void fraction, phasic temperatures (bundle geometries)	The RELAP5 vapor generation model uses the maximum of the Plesset-Zwick[4-23] and Lee-Ryley[4-24] correlations to obtain interphase heat transfer coefficients for superheated liquid in bubbly flow. Measurements allowing direct comparisons of calculated and measured interphase mass and energy transfer are not available. The experiments used in assessing code capabilities for predicting interphase drag allow indirect assessments of interphase mass and energy transfer. An example, showing reasonable agreement between predicted and measured void fractions in GE level swell tests,[4-25] is provided in Figure 4-10. In these blowdown tests, the void fraction was determined by flashing, which generated steam, and by interphase drag, which affected the distribution of steam. Flashing is also an inherent phenomenon in system depressurizations such as occur during AP600 SBLOCAs, especially during the ADS blowdown period. Therefore, the integral systems experiment assessments in Sections 5.1 and 5.2 test this model. Early assessments of these experiments[4-26] identified oscillatory core behavior at low pressures, to which transitions in flashing models between the bubbly and slug flow regimes contributed. Changes in these flashing model transitions have been implemented in code version 3.2.1.2, which is the subject of this report.

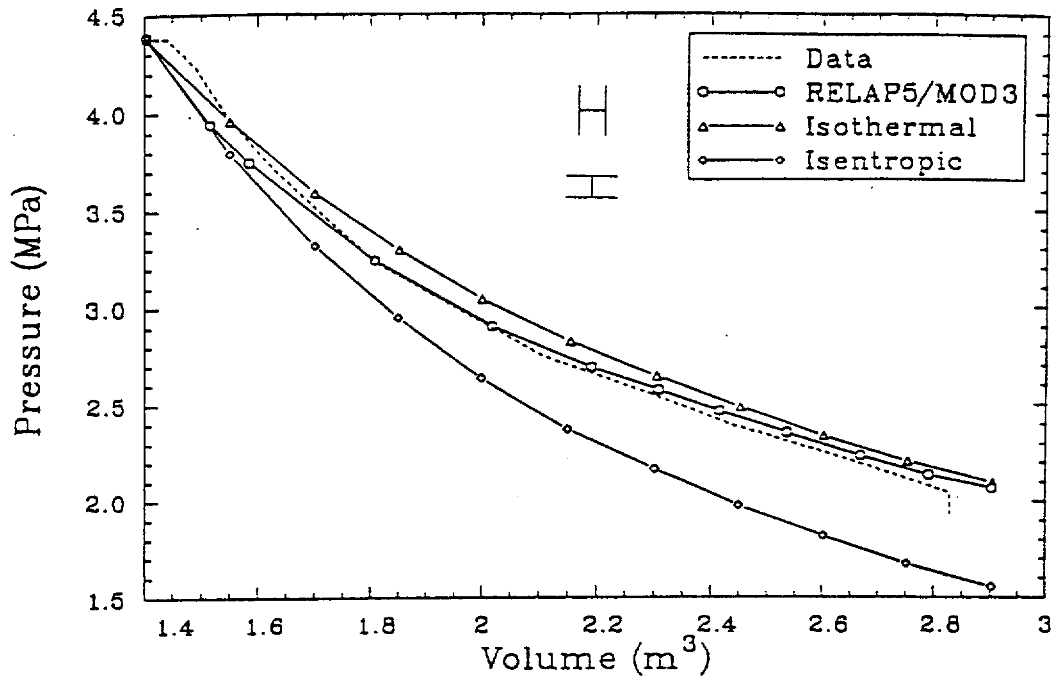

Figure 4–2. Accumulator gas pressure versus volume for LOFT Test L3–1.

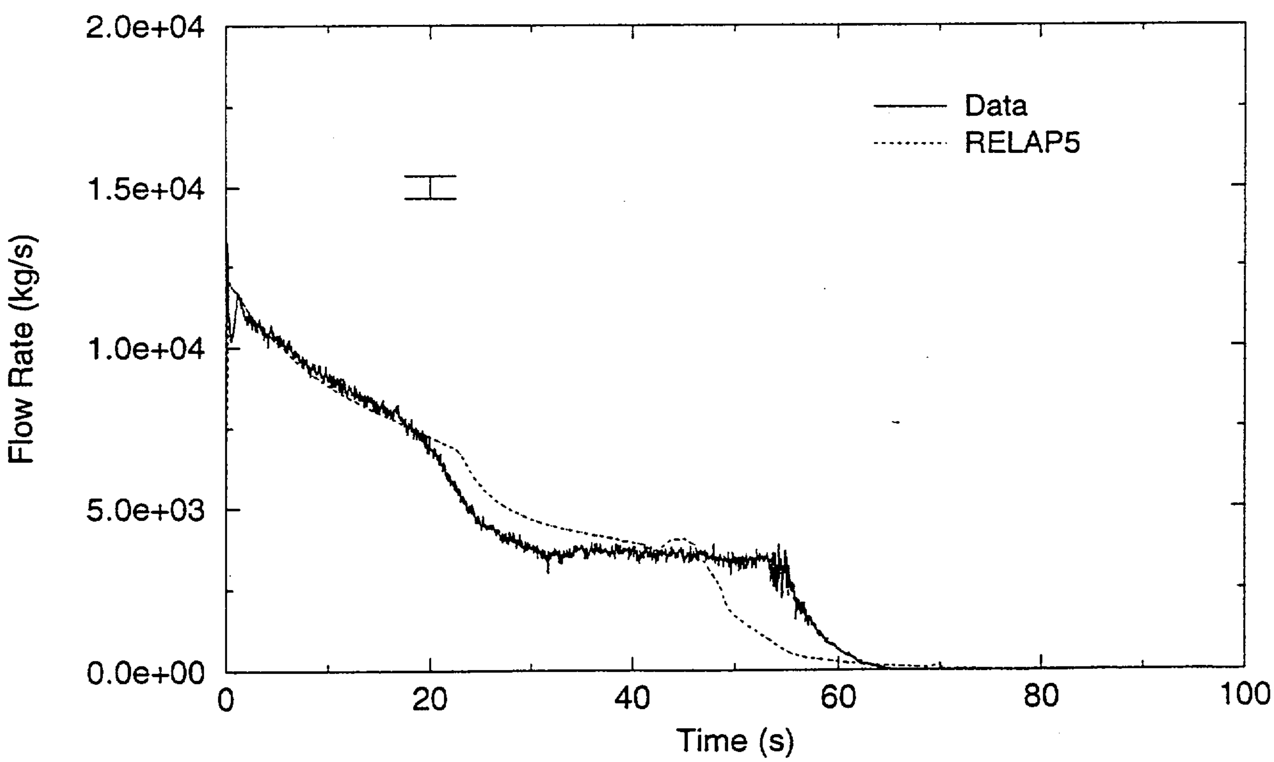

Figure 4–3. Discharge flow rates for Marviken Test 24.

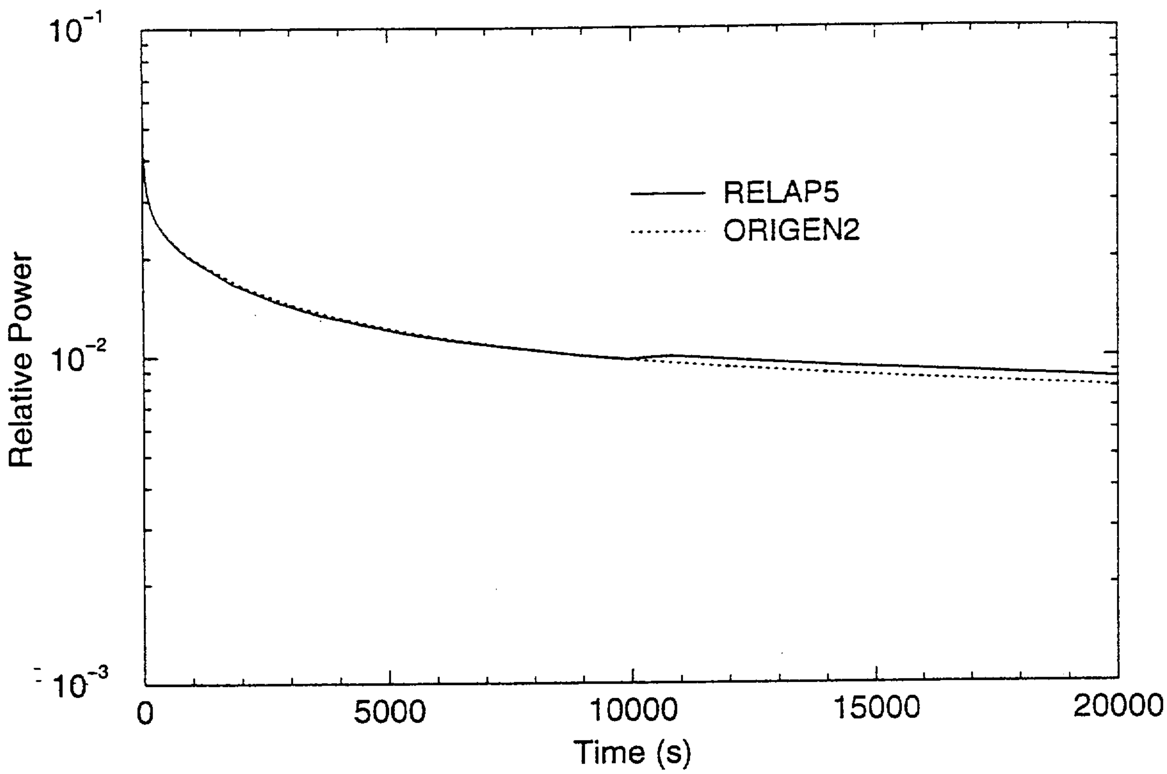

Figure 4–4. A comparison of decay heat from RELAP5 and ORIGEN2.

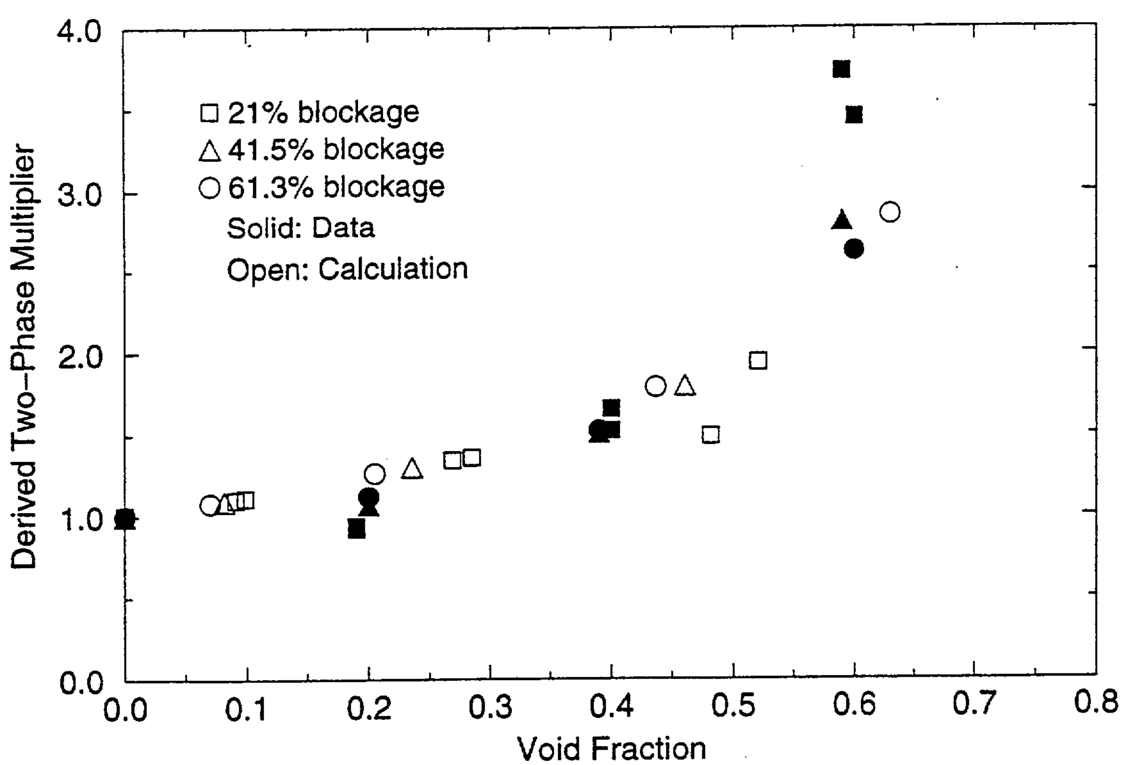

Figure 4–5. Two–phase pressure drop multipliers at the blockage in the EPRI tests.

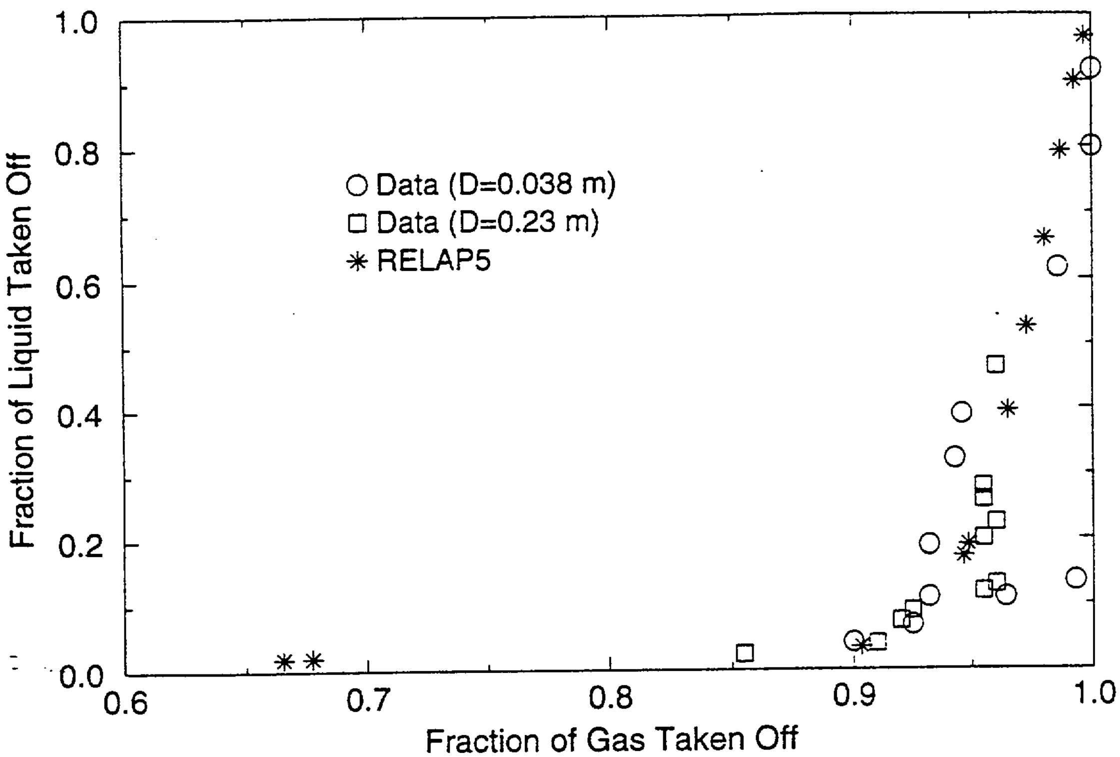

Figure 4–6. Phase separation in a horizontal pipe with an upwards side pipe.

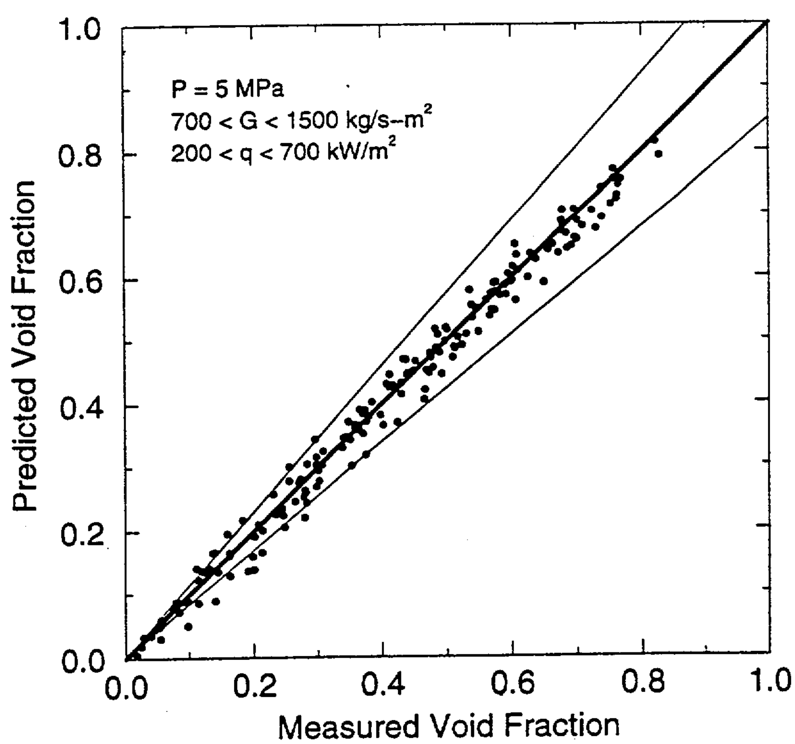

Figure 4–7. Calculated and measured void fractions from the FRIGG tests.

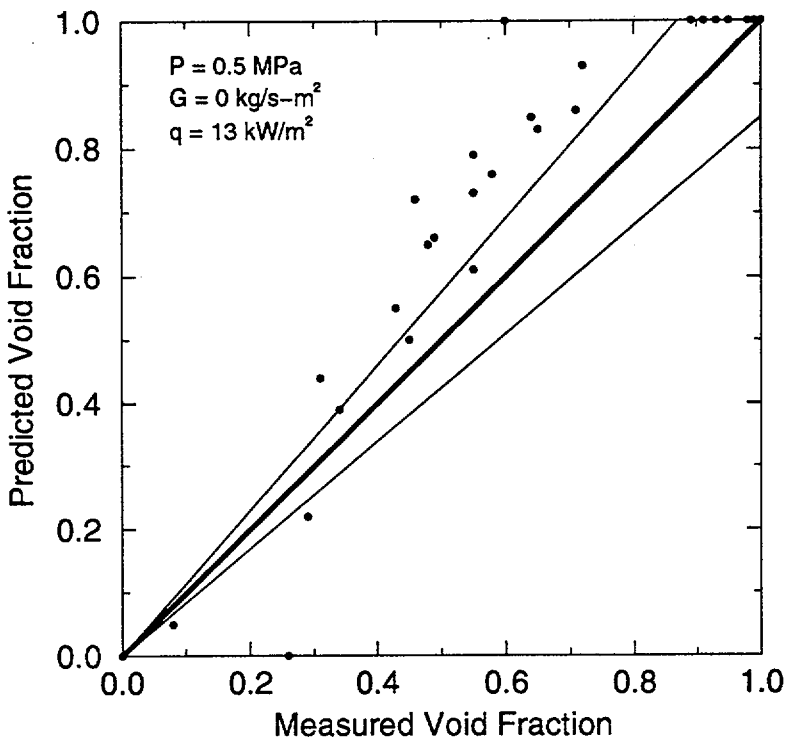

Figure 4–8. Void fractions from the THETIS tests.

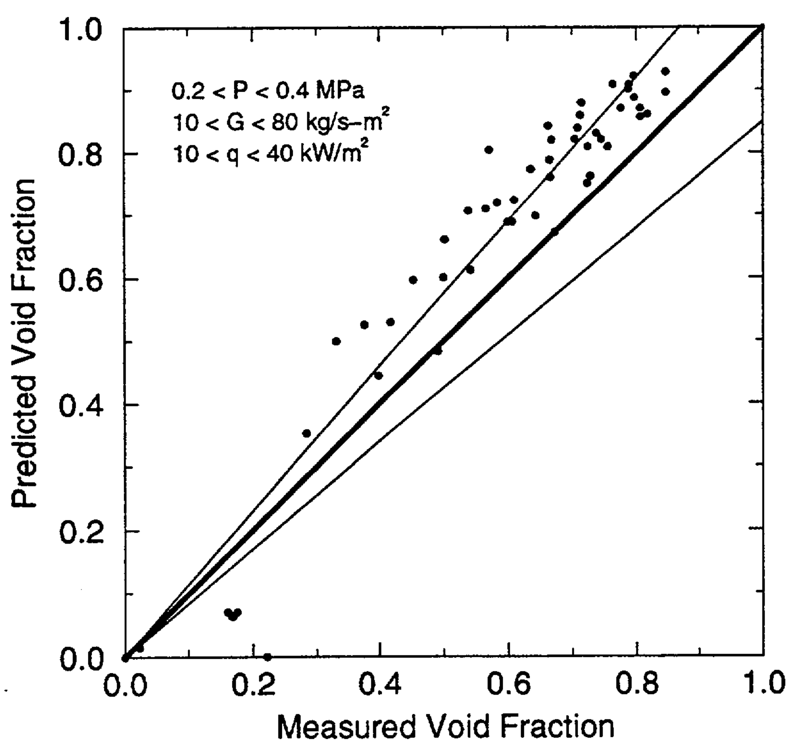

Figure 4–9. Void fractions from the PERICLES tests.

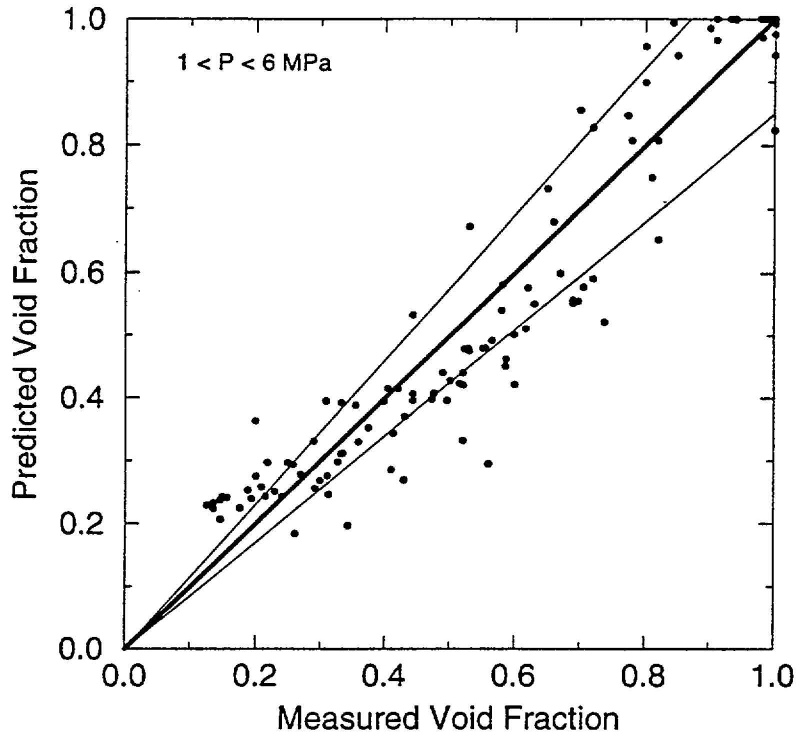

Figure 4–10. Void fractions from the GE level swell tests.

A part of the validation of the approach taken here for evaluating code model and correlation scalability and applicability is a comparison against a procedure independently developed by Dr. Ishii[4-8] for establishing the capability of a system code for scaling-up to the plant configuration and conditions of an advanced light water reactor (ALWR). The portion of Dr. Ishii's procedure relating to evaluation of code models and correlations is shown in Table 4-3. The approach taken here is very similar to that taken by Dr. Ishii.

Table 4-3. Steps relating to code models and correlations from Dr. Ishii's procedure for establishing code scale-up capability.

- Focus only on key phenomena in ALWR transients
- Identify the differences with present light-water reactor transients
- Identify related key models and correlations
- Evaluate ranges of key parameters in the plant and the experiments
  - Flow parameters (for example, velocities and void fractions)
  - Properties
  - System external scales (for example, diameters and lengths)
  - Internal scales (for example, bubble and droplet sizes and film thickness)
  - Flow regimes
- Evaluate data base for each key model and correlation
  - Basic scientific data base of original models
  - Integral test data
  - Separate effects test data
- Identify the ranges of extrapolation in the ALWR application
- Evaluate the impact of extrapolation (in particular, of the internal scale effects and flow regimes) in terms of parameter ranges and non-dimensional scaling parameters in models

---

4.1 References

4-1. R. R. Schultz, *International Code Assessment and Applications Program: Summary of Code Assessment Studies Concerning RELAP5/MOD2, RELAP5/MOD3, and TRAC-B*, Idaho National Engineering Laboratory, NUREG/IA-0128, EGG-EAST-8719, December 1993.

4-2. S. M. Sloan, R. R. Schultz and G. E. Wilson, *RELAP5/MOD3 Code Manual, Volume 7, Summaries and Reviews of Independent Code Assessment Reports*, Idaho National Engineering Laboratory, NUREG/CR-5535, INEL-95/0174, June 1994.

4-3. C. D. Fletcher and R. R. Schultz, *RELAP5/MOD3 Code Manual, Volume 5, User Guidelines*, Idaho National Engineering Laboratory, NUREG/CR-5535, INEL-95/0174, August 1995.

4-4. *RELAP5/MOD3 Code Manual, Volume 3, Developmental Assessment Problems*, Idaho National Engineering Laboratory, NUREG/CR-5535, INEL-95/0174, to be published May 1997.

4-5. J. D. Burtt, C. D. Fletcher, G. E. Wilson, C. B. Davis and T. J. Boucher, *Phenomena Identification and Ranking Tables for Westinghouse AP600 Small Break Loss-of-Coolant Accident, Main Steam Line Break, and Steam Generator Tube Rupture Scenarios*, Idaho National Engineering Laboratory, INEL-94/0061, Revision 2, March 1997.

4-6. *RELAP5/MOD3 Code Manual, Volume 4, Models and Correlations*, Idaho National Engineering Laboratory, NUREG/CR-5535, INEL-95/0174, August 1995.

4-7. C. E. Slater and C. B. Davis, *Applicability of Selected RELAP5/MOD3 Models and Correlations to AP600 Small Break Loss-of-Coolant Accidents*, Idaho National Engineering Laboratory, INEL-96/0440, (Proprietary), February 1997.

4-8. M. Ishii, Purdue University, "Procedure to Establish Code Scale-Up Capability to Plant," letter to F. Eltawila, USNRC, January 25, 1996.

4-9. K. E. Carlson et al., *RELAP/MOD3 Code Manual, Volume 3, Developmental Assessment Problems*, Idaho National Engineering Laboratory, NUREG/CR-5535, Draft, June 1990.

4-10. P. D. Bayless et al., *Experiment Data Report for LOFT Nuclear Small Break Experiment L3-1*, Idaho National Engineering Laboratory, NUREG/CR-1145, EGG-2007, January 1980.

4-11. R. E. Henry and H. K. Fauske, "The Two-Phase Critical Flow of One-Component Mixtures in Nozzles, Orifices, and Short Tubes," *Journal of Heat Transfer*, May 1971.

4-12. L. Ericson et al., *The Marviken Full-Scale Critical Flow Tests Interim Report: Results from Test 24*, A. B. Atomenergi Sweden, Report MXC-224, May 1979.

4-13. ANSI/ANS-5.1-1979, "American National Standard for Decay Heat Power in Light Water Reactors", American National Standards Institute/American Nuclear Society.

4-14. A. G. Croff, *ORIGEN2 - Revised and Updated Version of the Oak Ridge Isotope Generation and Depletion Code*, Oak Ridge National Laboratory, ORNL-5621, July 1980.

4-15. G. W. Johnsen, *RELAP5/MOD3.2.1.2 Developmental Assessment, Two-Phase Pressure Drop EPRI Flow Blockage Experiments*, Idaho National Engineering Laboratory, to be published.

4-16. B. J. Azzopardi and E. Hervieu, *Phase Separation at T Junctions*, Department of Chemical Engineering, University of Nottingham, U. K., 1991.

4-17. B. J. Azzopardi and P. A. Smith, "Two-Phase Flow Split at Tee Junctions: Effect of Side Arm Orientation and Downstream Geometry," *International Journal of Multiphase Flow*, Vol. 18, No. 6, p. 861, 1992.

4-18. R. F. Mudde, J. S. Groen and H. E. A. VanDen Akker, "Two-Phase Flow Redistribution Phenomena in a Large T-Junction," *International Journal of Multiphase Flow*, Vol. 19, No. 4, p. 563, 1993.

4-19. B. Chexal and G. Lellouche, *A Full-Range Drift-Flux Correlation for Vertical Flows (Revision 1)*, Electric Power Research Institute, NP-3989-SR, September 1986, as modified by: B. Chexal et al., *The Chexal-Lellouche Void Fraction Correlation for Generalized Applications*, NSAC-139, April 1991.

4-20. O. Nylund et al., *Hydrodynamic and Heat Transfer Measurements on a Full Scale Simulated 36-Rod Marviken Fuel Element with Uniform Heat Flux Distribution*, ASEA and AB Atomenergi, FRIGG-2, 1968.

4-21. K. Pearson, *Full Length Cluster Level Swell Data at Pressures of 2-40 Bar*, AEEW-R2193, November 1987.

4-22. R. Deruaz et al., *Study of Two-Dimensional Effects in the Core of a Light Water Reactor During the Reflooding Phase of a LOCA*, Commission of the European Communities, Contract No. SR002F, Final Report, 1984.

4-23. M. S. Plesset and S. A. Zwick, "The Growth of Vapor Bubbles in Superheated Liquids," *Journal of Applied Physics*, Vol. 25, No. 4, 1954, pp. 493-500.

4-24. K. Lee and D. J. Ryley, "The Evaporation of Water Droplets in Superheated Steam," *Journal of Heat Transfer*, American Society of Mechanical Engineers, November 1968, pp. 445-451.

4-25. J. A. Findlay and O. L. Sazzi, *BWR Refill-Reflood Program--Model Qualification Task Plan*, EPRI NP-1527, NUREG/CR-1899, GEAP-24898, October 1981.

4-26. *Adequacy Evaluation of RELAP5/MOD3 for Simulating AP600 Small Break Loss-of-Coolant Accidents*, Idaho National Engineering Laboratory, INEL-96/0380, (Proprietary), October 1996.

5 INTEGRATED CODE ASSESSMENTS

This section describes assessments of RELAP5/MOD3, Version 3.2.1.2, integrated code capabilities for predicting AP600 SBLOCA behavior. This activity represents a "top-down" code evaluation that complements the "bottom-up" evaluation of individual code models and correlations presented in Section 4. The assessments in this section use experimental data from both integral systems tests and component separate effects tests.

Evaluations of RELAP5/MOD3 capabilities for simulating AP600 SBLOCA transients were made using data from three integral test facilities, each of a different scale:

Facility	Location	Scale
ROSA/AP600[5-1]	Tokai, Japan	1:30.5 Volume, Decay Power & Flow Full Height Full Pressure
SPES-2[5-2]	Piacenza, Italy	1:395 Volume, Power & Flow Full Height Full Pressure
OSU APEX[5-3]	Corvallis, Oregon U.S.A.	1:192 Volume 1:96 Power & Flow 1:4 Height & Length 1:2 Velocity & Time Reduced Pressure

Reference 5-4 (Volume 2, Appendix A) provides concise descriptions of these experimental facilities and the extent and nature of their representations of AP600.

From the numerous experiments performed in the three integral test facilities, three postulated AP600 SBLOCA scenarios were selected for the code assessment effort. The initiating events for these accident scenarios were:

- 1-in. diameter cold leg break,
- Double-ended DVI line break (an 8-in. line, but smaller effective breaks on each side, see Section 5.1.1.2), and
- 2-in. diameter PBL break.

This set of SBLOCA accident scenarios was chosen because: (1) it results in a variety of challenges for the AP600 passive safety systems, (2) it represents a broad range of break sizes and locations, and (3) comparable tests simulating these scenarios were conducted in all three experimental facilities. A more limited set of data is available for assessing the behavior of the code after steady IRWST injection has been established, since only the OSU facility was designed for simulating the plant response during the long-term phase of the transient.

Assessment analyses were performed to evaluate the capabilities of the integrated code for predicting the behavior observed in the tests representing these accident scenarios. The first step in each analysis was to evaluate the experimental data to gain an understanding of the test behavior and any differences among the test responses that were attributable to differences in the dimensions or configurations of the facilities. The next step was to model each experimental facility and AP600 with RELAP5 using the consistent approach that is described in Appendix B. Performing calculations using the same code version and employing consistent approaches for nodalization and user option selection among the various facilities provides the necessary common basis from which to judge the performance of the code. This common basis is also needed in order to formulate a recommended AP600 modeling scheme based on the collective experiences drawn from the assessments.

RELAP5/MOD3 simulations of the tests and the comparable accidents in AP600 were then performed and analyzed. The results of the RELAP5 experiment simulations were compared with the corresponding test data (in the context of the uncertainty in the data) and these comparisons were used as indications of code performance. RELAP5 capabilities for simulating the behavior of important (as defined by the AP600 SBLOCA PIRT, see Section 2.2.1) processes and phenomena in the experiments were assessed using the acceptance criteria described in Section 2.2.2. The Integral Test Facility experimental uncertainties are documented in Appendix D. In these assessments, the responsible INEEL analyst made a preliminary judgment of the code capability for predicting each important PIRT phenomenon. Then, a meeting of the group of INEEL analysts performing the assessments for all facilities and accident scenarios was held to review the preliminary judgments and approve them. Subsequently, all judgments were reviewed by the USNRC Thermal-Hydraulic Consultants Committee. Scaling analyses were then performed, using the data from all tests and calculations, to demonstrate the relevancy and sufficiency of the experimental data set for representing the AP600 plant and the scalability of RELAP5 for representing the important phenomena. This demonstration allows the findings regarding RELAP5/MOD3 capabilities for predicting the behavior in the experiments to be extended to the prediction of the same behavior in AP600.

The assessments presented in Section 5.1 cover the SBLOCA PIRT short-term phase, the period from the accident initiating event through establishment of stable IRWST injection. The assessments of code capabilities for predicting experiment behavior over the SBLOCA long-term phase, the subsequent period of IRWST and sump injections, are described in Section 5.2. The integral facility scaling analysis, which supports the code assessments presented in this section, is summarized in Section 5.3. The scaling analyses include the results from preliminary assessment calculations of an inadvertent ADS opening transient, as well as from the three SBLOCAs described above. This transient was not included in the final assessment calculations because a comparable experiment was not performed in the SPES facility and because the preliminary assessment findings indicated that this transient posed no unique challenges to the code; the phenomena and assessment results were adequately covered by the other three SBLOCA scenarios. In addition to the assessments performed using data from integral system experiments, assessments were also performed using data from separate effects experiments pertinent to certain AP600-specific components. These component separate effects assessments are described in Section 5.4.

5.1 SBLOCA Short-Term Phase

This section summarizes assessments of RELAP5/MOD3, Version 3.2.1.2, capabilities for predicting the important AP600 PIRT SBLOCA short-term phase phenomena for three unique accident scenarios initiated by: a 1-in. diameter cold leg break, a double-ended rupture of a DVI line, and a 2-in. diameter pressure balance line break. Figure 5-1 shows the break locations, along with the location of the ADS Stage 4 (ADS-4) valve related to an additional assumed single failure as discussed below. Appendix C documents the assessments summarized in this section.

PROPRIETARY

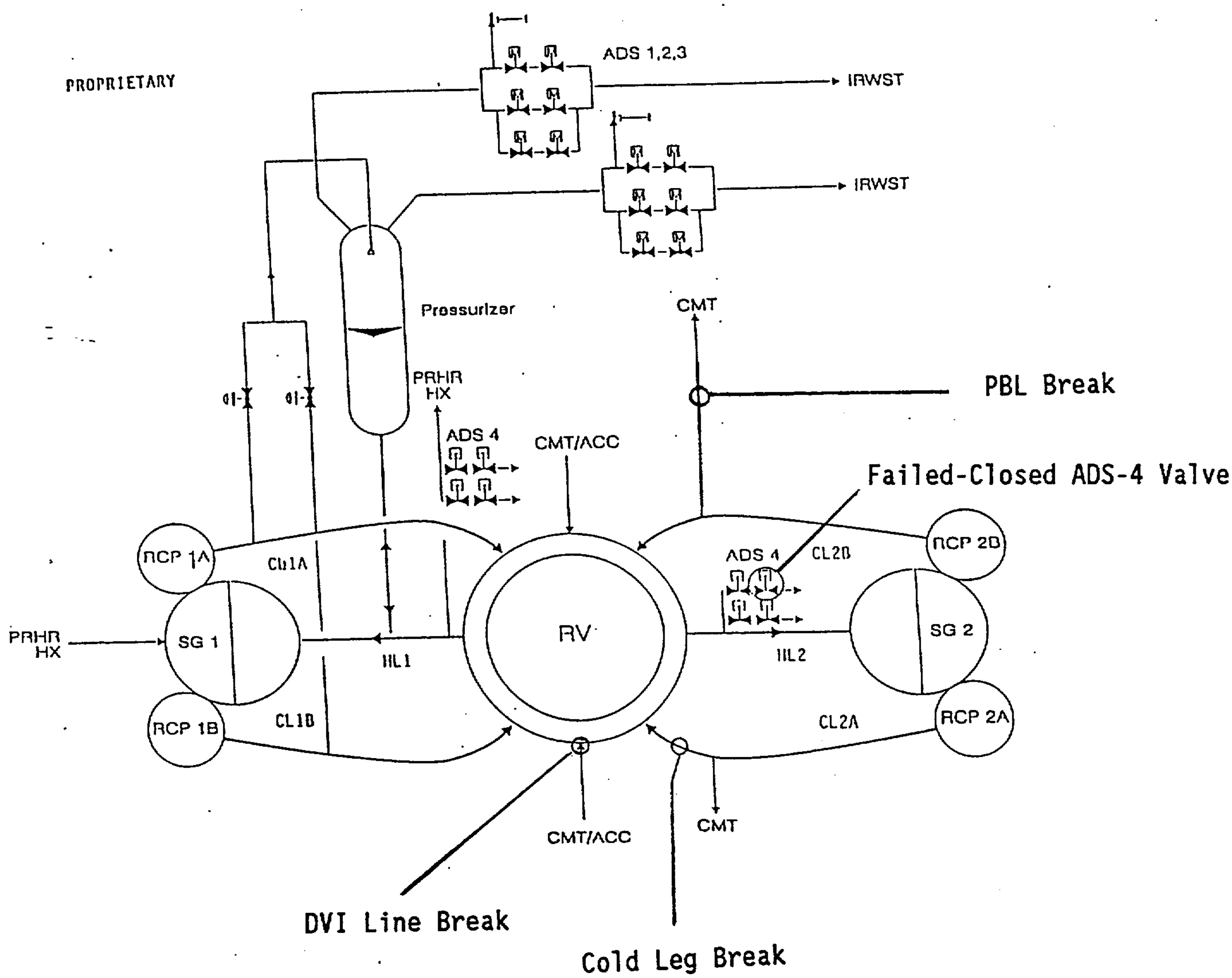

Figure 5-1. Locations of SBLOCA pipe ruptures and location of assumed ADS-4 valve additional single failure.

5.1.1 Accident Scenario and Experiment Descriptions

The overall AP600 SBLOCA short-term phase system response is summarized as follows. The break opening causes the RCS pressure and inventory to decline, generating a reactor trip and an S signal. The S signal activates the CMT and PRHR systems. The RCS pressure continues falling rapidly until flashing in the hotter RCS regions occurs, slowing the depressurization. The combination of RCS depressurization and inventory loss leads to an interruption of CMT recirculation and onset of CMT draining. The ADS is activated when the CMTs drain to a low setpoint level. First, ADS Stages 1, 2 and 3 (ADS-123) blow down the RCS from the top of the pressurizer through spargers into the IRWST pool; the RCS depressurization rate increases significantly during the ADS blowdown. The rapid depressurization increases the accumulator injection flow, such that the RCS and reactor vessel coolant inventories may temporarily increase shortly after the ADS blowdown begins. As the blowdown continues and the accumulators empty, the RCS inventory depletion accelerates. When CMT level has declined to a second low setpoint level, ADS-4 opens additional flow paths from the RCS hot legs directly into the containment loop compartments. The RCS blowdown continues and eventually the differential pressure between the RCS and containment is reduced below the head created by water standing in the IRWST. At that time, injection of IRWST water into the RCS begins. A period of oscillatory injection flow may result as the RCS inventory distribution adjusts itself to the new conditions created by the onset of IRWST injection. Eventually, the injection flow stabilizes, marking the end of the SBLOCA short-term phase. The minimums in the RCS and reactor vessel inventories occur either before, or shortly after, the time when the IRWST injection flow begins.

The following sections identify the experiments and describe the assumptions and unique aspects of system responses particular to the three accident scenarios used in the code assessments for the SBLOCA short-term phase.

5.1.1.1 1-in. Diameter Cold Leg Break. This postulated accident scenario is initiated by a 1-in. diameter, circular break on the bottom of a cold leg in the AP600 coolant loop that is connected to the CMTs. The break is assumed to be located between the reactor vessel and the PBL connection (see Figure 5-1). The scenario also assumes that one of the four ADS-4 valves fails to open. This assumption leaves 75% of the total ADS-4 flow area available for discharge from the RCS into the containment, thereby limiting RCS depressurization and increasing the time required to reach the onset of IRWST injection. The failed-closed ADS-4 valve is assumed to be one of the two parallel valves located in the discharge line connected to the hot leg on the same coolant loop that contains the break (see Figure 5-1).

The break for this scenario is much smaller than for the other two scenarios. This small break size results in a relatively slowly-developing event sequence. RCS depressurization is relatively slow and the period of CMT recirculation is relatively long. Once the ADS is activated, RCS pressure declines rapidly; the small break in the cold leg provides only limited RCS depressurization capability in addition to that provided by the ADS.

The data used in the code assessment were produced when the above accident scenario was simulated in each of the three experimental facilities. The test data came from ROSA/AP600 Test AP-CL-03,[5-5] SPES-2 Test S00401,[5-6] and OSU Test NRC22.[5-7] The assessment analysis was limited to the period from break opening until the establishment of steady IRWST injection. This period corresponds roughly to the first 8,000 s following break opening in AP600, ROSA and SPES, and to the first 4,000 s in OSU. Only the OSU test investigated behavior after this period. (An analysis of the longer-term behavior in this OSU test is presented in Section 5.2.)

5.1.1.2 Double-Ended DVI Line Break. This postulated accident scenario is initiated by a double-ended offset shear of one of the DVI lines (see Figure 5-1). In AP600, the DVI line nominal pipe size is eight-inch; however, the effective break diameters on both sides of the double-ended pipe rupture are smaller than the full pipe inner diameter. On the vessel side, an effective break diameter of four inches is created by the presence of the DVI line flow restrictor. On the line side, the effective break diameter is less than the full pipe diameter because of the presence of flow orifices in the IRWST, CMT, and accumulator discharge lines. The scenario also assumes another failure. In the ROSA and OSU experiments, the failure (to open) of one of the four ADS-4 valves was modeled. The failed-closed ADS-4 valve is assumed to be one of the two parallel valves located in the discharge line connected to the hot leg on the same coolant loop that contains the CMTs, as shown in Figure 5-1. In the SPES experiment, the failure (to open) of one of the two ADS-1 valves and one of the two ADS-3 valves was modeled. Because of this difference in the assumed additional failure, the SPES test is not an exact counterpart of the ROSA and OSU tests; however, this does not affect the usefulness of the SPES test for the purposes of code assessment.

The break size for this scenario is much larger than for the other two scenarios; the break is large enough to provide a significant RCS depressurization capability in addition to the ADS. The break location causes the early draining of the affected CMT through the ruptured DVI line into the containment. Therefore, relative to the other two scenarios, this event sequence develops quickly. For this scenario, the minimum reactor vessel inventory is attained well before the onset of IRWST injection. Inventory recovery is caused by unaffected accumulator injection and unaffected CMT draining. The broken DVI line assumed for this scenario roughly halves the full ECCS (accumulator, CMT, and IRWST) injection capabilities.

The data used in the code assessment were produced when the above accident scenario was simulated in the three integral experiment facilities. The test data came from ROSA/AP600 Test AP-DV-01,[5-8] SPES-2 Test S00706,[5-9] and OSU Test NRC20.[5-10] The assessment analysis was limited to the period from break opening until the establishment of steady IRWST injection. This period corresponds roughly to the first 2,000 s following break opening in AP600, ROSA, and SPES and to the first 1,000 s in OSU. Only the OSU test investigated behavior after this period. (An analysis of the longer-term behavior during this OSU test is presented in Section 5.2.)

5.1.1.3 2-in. Diameter Pressure Balance Line Break. This postulated accident scenario is initiated by a 2-in. diameter circular break in one of the PBLs (see Figure 5-1). The scenario assumes that one of the four ADS-4 valves fails to open (leaving 75% of the total ADS-4 flow area available for discharge from the RCS into the containment). The failed-closed ADS-4 valve was one of the two valves located in the ADS-4 discharge line connected to the hot leg in the CMT loop (i.e., the AP600 coolant loop that is not connected to the pressurizer; see Figure 5-1).

The break for this scenario is much larger than for the 1-in. diameter cold leg break scenario, resulting in a faster-developing accident sequence. However, the break size is still small in relation to the ADS openings and thus, once ADS opens, the break still provides only a limited additional RCS depressurization capability. The break location for this scenario results in asymmetric draining responses between the two CMTs. The level in the affected CMT (i.e., the one connected to the pressure balance line containing the break) declines slower due to break effects.

The data used in the code assessment were produced when the above accident scenario was simulated in each of the three experimental facilities. The test data came from ROSA/AP600 Test AP-PB-01,[5-11] SPES-2 Test S01007,[5-12] and OSU Test SB9.[5-13] The assessment analysis was limited to the period from break opening until establishment of steady IRWST injection. This period corresponds roughly to the first 4,000 s following break opening in AP600, ROSA, and SPES, and to the first 2,000 s in OSU. Only the

OSU test investigated behavior after this period. (An analysis of the longer-term behavior in this OSU test is presented in Section 5.2.)

5.1.2 Assessment Results for the SBLOCA Short-Term Phase

The AP600 SBLOCA PIRT figure of merit is "minimum reactor vessel inventory." As indicated in the scenario descriptions, the minimum inventory is attained during the short-term phase. This minimum occurs shortly after the break opens for the DVI line break scenario and shortly after the onset of IRWST injection for the other two scenarios. Table 5-1 compares the measured and calculated values for the reactor vessel minimum inventory (normalized to the initial inventory) for the three accident scenarios and three experimental facilities. For reference, the corresponding values for the calculated AP600 accident scenarios are also shown (analyses of the AP600 calculations appear in Appendix C). Note that the tabulated values for the SPES experiments are generally lower than for the other facilities because for SPES the decay heat and ADS-4 flow areas are overscaled while the PRHR system is underscaled (see Section 5.3.5). The table shows good agreement between the calculated and measured values; RELAP5 generally produced slight underpredictions of the minimum reactor vessel inventory, with the calculated value ranging from 5% (of the initial value) above to 13% below the measured value (an underprediction is conservative). Causes for this underprediction are discussed later, in Section 5.2.2. The scaling analysis in Section 5.3 compares and addresses the differences among the tests, calculations of the tests and calculations of the corresponding AP600 plant accident scenarios.

Table 5-1. Comparison of measured and RELAP5-calculated minimum normalized reactor vessel inventory during SBLOCA short-term phase.

Scenario, Facility/Test	Minimum Measured Reactor Vessel Inventory (Normalized to Initial Inventory)	Minimum Calculated Reactor Vessel Inventory (Normalized to Initial Inventory)
1-in. Cold Leg Break		
ROSA/AP-CL-03	0.70	0.60
SPES/S00401	0.49	0.45
OSU/NRC22	0.62	0.54
AP600	--	0.40
Double-Ended DVI Line Break		
ROSA/AP-DV-01	0.55	0.51
SPES/S00706	0.20	0.25
OSU/NRC20	0.46	0.44
AP600	--	0.44
2-in. Pressure Balance Line Break		
ROSA/AP-PB-01	0.77	0.64
SPES/S01007	0.62	0.53
OSU/SB9	0.70	0.68
AP600	--	0.56

Comparisons of the calculated and measured SBLOCA short-term phase overall system responses are shown in Figures 5-2 through 5-19 for the three experiments in each of the three experimental facilities. These overall responses are characterized by the RCS pressure, RCS mass inventory and reactor vessel inventory behavior. The behavior shown in these figures corresponds with the scenario descriptions provided in Section 5.1.1. The accident sequence of events is seen to be the same in both the calculation and the test for each experiment. The figures also show favorable comparisons between the calculated and measured system behavior for each experiment, providing general indications that the code is capable of simulating the SBLOCA behavior of a system of AP600 components (reactor vessel, steam generators, coolant loops, CMTs, PRHR system, ADS, accumulators, and IRWST).

While the code generally did a good job of calculating the overall system responses, there were specific experiments where some notable differences existed that are apparent in Figures 5-2 through 5-19. These are summarized in the following paragraphs; more detailed analysis is provided in Appendix C.

RELAP5 did not represent RCS coolant loop natural circulation flow well for the OSU 1-in. cold leg break test, leading to a much earlier CMT draining and ADS actuation in the calculation than in the experiment. There are no measurements of the loop flow rate in the experiment, but an estimate of the flow rate based on core power and loop temperatures indicates that the RELAP5 calculation overpredicted the natural circulation flow rate. The higher flow rate reduced the core vapor generation rate, which caused the RCS pressure to be lower than that measured (Figure 5-6). The reduced vapor generation also allowed natural circulation flow through the coolant loops to continue in the calculation, whereas in the experiment vapor collected in the steam generator U-tubes, stopping the loop natural circulation flow. In the calculation, the lower RCS pressure allowed liquid in the CMTs to flash, initiating an early CMT draining. It is suspected that the flow rate problem lies in the modeling of the pump flow resistance; insufficient facility data are available to allow an accurate characterization of this resistance with the pumps tripped. A sensitivity calculation performed with increased pump resistance was found to reduce the timing difference in the onset of CMT draining between the test and the calculation, and to change the mechanism for initiating CMT draining from flashing to vapor convection through the PBLs.

The calculated RCS mass inventory also recovered much faster in the calculation than in the test for the OSU 1-in. cold leg break (CLB) (Figure 5-7). This was primarily the result of cold water entering the upper plenum, which then condensed steam in the calculation. This condensation reduced the RCS pressure, allowing the initial flow from the IRWST to be higher than was measured. Cold water did not enter the upper plenum in the experiment at this time; its appearance in the calculation was caused by unphysical oscillatory flows in the reactor vessel. Because this occurred after IRWST injection had begun, however, these flows did not affect the calculated minimum vessel inventory or overall transient behavior; they merely accelerated the refill of the reactor vessel. Further discussion of the link between oscillations and condensation is provided in Section 5.2.

The faster mass inventory recovery was also seen in the OSU 2-in. PBL break calculation (Figure 5-19). Again, the initial IRWST flow was much higher than observed in the experiment, but in this calculation no significant condensation occurred in the upper plenum. Some condensation did occur in CMT-2 and its associated PBL, resulting in a partial refill of that CMT. The calculated RCS pressure was slightly lower than measured, which allowed a higher flow from the IRWST because of the reduced back pressure. As for the OSU 1-in. CLB calculation, the more rapid injection in this calculation did not affect the timing or magnitude of the minimum vessel inventory, it only accelerated the vessel refill.

The information deleted from this figure is considered proprietary by Westinghouse Electric Company

Figure 5–2. Measured and calculated short–term phase RCS pressure responses for the ROSA 1–inch diameter cold leg SBLOCA scenario.

The information deleted from this figure is considered proprietary by Westinghouse Electric Company

Figure 5–3. Measured and calculated short–term phase RCS and reactor vessel mass inventory responses for the ROSA 1–inch cold leg SBLOCA scenario.

The information deleted from this figure is considered proprietary by Westinghouse Electric Company

Figure 5–4. Measured and calculated short–term phase RCS pressure responses for the SPES 1–in. diameter cold leg SBLOCA scenario.

The information deleted from this figure is considered proprietary by Westinghouse Electric Company

Figure 5–5. Measured and calculated short–term phase RCS and reactor vessel mass inventory responses for the SPES 1–in. diameter cold leg SBLOCA scenario.

The information deleted from this
figure is considered proprietary by
Westinghouse Electric Company

Time (s)

Figure 5–6. Measured and calculated short–term phase RCS pressure responses for the OSU 1–in. diameter cold leg SBLOCA scenario.

The information deleted from this
figure is considered proprietary by
Westinghouse Electric Company

Figure 5–7. Measured and calculated short–term phase RCS and reactor vessel mass inventory responses for the OSU 1–in. diameter cold leg SBLOCA scenario.

The information deleted from this
figure is considered proprietary by
Westinghouse Electric Company

Figure 5–8. Measured and calculated short–term phase RCS pressure responses for the ROSA DVI line SBLOCA scenario.

The information deleted from this
figure is considered proprietary by
Westinghouse Electric Company

Figure 5–9. Measured and calculated short–term phase RCS and reactor vessel mass inventory responses for the ROSA DVI line SBLOCA scenario.

The information deleted from this figure is considered proprietary by Westinghouse Electric Company

Figure 5–10. Measured and calculated short–term phase RCS pressure responses for the SPES DVI line SBLOCA scenario.

The information deleted from this figure is considered proprietary by Westinghouse Electric Company

Figure 5–11. Measured and calculated short–term phase RCS and reactor vessel mass inventory responses for the SPES DVI line SBLOCA scenario.

The information deleted from this figure is considered proprietary by Westinghouse Electric Company

Figure 5–12. Measured and calculated short–term phase RCS pressure responses for the OSU DVI line SBLOCA scenario.

The information deleted from this figure is considered proprietary by Westinghouse Electric Company

Figure 5–13. Measured and calculated short–term phase RCS and reactor vessel mass inventory responses for the OSU DVI line SBLOCA scenario.

The information deleted from this figure is considered proprietary by Westinghouse Electric Company

Figure 5–14. Measured and calculated short–term phase RCS pressure responses for the ROSA 2–inch diameter PBL SBLOCA scenario.

The information deleted from this figure is considered proprietary by Westinghouse Electric Company

Figure 5–15. Measured and calculated short–term phase RCS and reactor vessel mass inventory responses for the ROSA 2–inch PBL SBLOCA scenario.

The information deleted from this figure is considered proprietary by Westinghouse Electric Company

Figure 5–16. Measured and calculated short–term phase RCS pressure responses for the SPES 2–in. diameter PBL SBLOCA scenario.

The information deleted from this figure is considered proprietary by Westinghouse Electric Company

Figure 5–17. Measured and calculated short–term phase RCS and reactor vessel mass inventory responses for the SPES 2–in. diameter PBL SBLOCA scenario.

The information deleted from this figure is considered proprietary by Westinghouse Electric Company

Figure 5–18. Measured and calculated short–term phase RCS pressure responses for the OSU 2–in. diameter PBL SBLOCA scenario.

The information deleted from this figure is considered proprietary by Westinghouse Electric Company

Figure 5–19. Measured and calculated short–term phase RCS and reactor vessel mass inventory responses for the OSU 2–in. diameter PBL SBLOCA scenario.

The RCS pressure in SPES was somewhat overpredicted in both the 1-in. CLB and 2-in. PBL break tests (Figures 5-4 and 5-16, respectively). This is believed to be the result of underpredicting the heat loss from the system (the ambient heat loss is not well characterized for this facility) and underpredicting the heat transfer in the PRHR heat exchanger. With a higher RCS pressure, vapor accumulated more slowly in the calculation than in the experiment. In both of these tests, CMT draining was initiated by vapor convection from the cold legs through the PBLs. Because there was less vapor present in the calculation, CMT draining occurred later than in the experiment. In the 2-in. PBL break test, this led to a correspondingly later ADS actuation in the calculation. In the 1-in. CLB test, a slightly faster calculated CMT draining resulted in ADS actuation at nearly the same time in the calculation and experiment. Despite the higher calculated pressure, the system mass inventory was well predicted. The pressure overprediction was not present in the DVI line break test, probably because of the relatively large break size, which drives the system depressurization without allowing much influence from heat losses through the piping or heat transfer in the PRHR system.

Assessment results covering the SBLOCA PIRT[5-14] short-term phase high-ranked phenomena are summarized in Table 5-2. This table shows "composite" judgments regarding code capabilities for predicting these phenomena. The term "composite" refers to a combined judgment for each accident scenario based upon the results of the individual assessments using data from the three experimental facilities. The judgments for each of the individual assessments were made using the acceptance criteria described in Section 2.2.2 and are provided in Appendix C, Table C.5-1. The composite judgments were made by taking into account uncertainties related to the quality of the test data and knowledge of the test facility configurations and operations. Table 5-2, therefore, provides a concise view of code capabilities for predicting the important AP600 behavior in the different SBLOCA scenarios. An overall judgment was also made for each high-ranked phenomenon based on a combination of the composite judgments for the individual accident scenarios; these overall judgments are presented and discussed later, in Section 6.2.

Table 5-2. Composite assessment results for AP600 PIRT SBLOCA short-term phase high-ranked phenomena.

High-Rank Phenomenon	Code Capability for 1-in. CLB	Code Capability for DVILB	Code Capability for 2-in. PBLB	See Note
Accumulator flow	Reasonable	Reasonable	Reasonable	1
ADS energy release	Reasonable	Reasonable	Reasonable	
ADS mass flow	Reasonable	Reasonable	Reasonable	2
Break mass flow	Reasonable	Reasonable	Reasonable	3
Cold leg-to-PBL tee phase separation	Reasonable	Reasonable	Reasonable	4
Core flashing	Reasonable	Reasonable	Reasonable	5
Core subcooling margin	Reasonable	Reasonable	Reasonable	6
Core two-phase mixture level	Reasonable	Reasonable	Reasonable	7
CMT flow resistance	Reasonable	Reasonable	Reasonable	
CMT level	Reasonable	Reasonable	Reasonable	8
Fuel rod core power/decay heat	None Made	None Made	None Made	9
Hot leg phase separation in tees	Reasonable	Reasonable	Minimal	10
IRWST flow resistance	Reasonable	Reasonable	Reasonable	11
Pressurizer level	Reasonable	Minimal	Reasonable	12

Note 1 - The code capability judgments for the OSU DVILB and pressure balance line break (PBLB) tests were excellent. The code capability judgments for the other seven cases were reasonable.

Note 2 - The code capabilities for this phenomenon were all judged to be reasonable, except for the SPES 1-in. CLB test for which the judgment was excellent, for the ROSA 2-in. PBLB test for which the judgment was minimal, and for the OSU direct vessel injection line break (DVILB) test for which no judgment was made.

Note 3 - The code capabilities for this phenomena were all judged reasonable, except for the SPES 1-in. CLB test and all three ROSA tests for which they were judged excellent.

Note 4 - No experimental instrumentation is available to directly measure this phenomenon. This phenomenon was indirectly assessed through comparison of measured and calculated behavior related to the onset of CMT draining. Also see "cold leg thermal stratification" in Table 5-3.

Note 5 - No experimental instrumentation is available to directly measure this parameter. However, reasonable agreement between measured and calculated RCS depressurization behavior is observed in all nine assessment cases. For examples, see Figures 5-2, 5-4 and 5-6. This agreement implies a reasonable prediction of overall RCS (not just core region) flashing. In Appendix C, code capability judgments were made only for the three ROSA test assessments, which were the most typical of the AP600 depressurization response (prototypical initial pressure and no core power augmentation to compensate for heat losses) and best instrumented (core thermocouples and hot leg densitometers) for indirect evaluation of core flashing.

Note 6 - The code capability judgment for the OSU 1-in. CLB test was minimal. The code capability judgments for the other eight assessment cases were reasonable.

Note 7 - The experimental facilities do not contain instrumentation to measure core two-phase mixture level. Code capabilities were judged instead upon comparisons between measured and calculated core collapsed levels.

Note 8 - Code capabilities for this phenomenon were judged to be reasonable for six of the nine cases. The capability was judged to be excellent for the OSU DVILB test. The capabilities were judged to be minimal for the SPES DVILB and OSU 2-in. PBLB tests.

Note 9 - Because core power was a boundary condition in all of the tests and calculations, no judgments of code capabilities were made for this phenomenon. These assessments do not provide data useful for evaluating code capabilities for predicting fuel rod core power/decay heat in AP600 (see Section 4 for a discussion of RELAP5 decay heat model applicability).

Note 10 - Experimental facility instrumentation to measure this phenomenon are generally limited. The ROSA facility contains instrumentation to measure hot leg and ADS-4 inlet fluid densities and the judgments for the ROSA test assessments were based on comparisons for these parameters. For ROSA, the judgments were reasonable for the 1-in. CLB and DVILB tests and minimal for the 2-in. PBLB test. These fluid densities were not measured in the SPES and OSU facilities and for the assessments of tests in these facilities the judgments were simply made to be consistent with those for ADS energy release and ADS mass flow (reasonable for all three tests in both facilities). The minimal composite judgment shown for the 2-in. PBLB scenario reflects the results from the ROSA assessment because that facility was the best instrumented to evaluate this phenomenon.

Note 11 - These judgments were based upon comparisons of the measured and calculated RCS pressures, IRWST pool levels and IRWST injection mass flow rates.

Note 12 - The code capability judgments for this phenomenon varied widely among the assessments cases. For the 1-in. CLB tests, the individual judgments were reasonable for ROSA, excellent for SPES and minimal for OSU. For the DVILB tests, the individual judgments were reasonable for ROSA and minimal for SPES and OSU. For the 2-in. PBLB tests, the individual judgments were reasonable for ROSA and SPES and minimal for OSU.

Table 5-2 shows that code capabilities were evaluated for 13 of the 14 PIRT short-term phase high-ranked phenomena. No code capability judgment could be made for the "fuel rod core power/decay heat" PIRT phenomenon. Core power was a boundary condition in all experiments and calculations of the experiments. Therefore, no information could be drawn from these assessments regarding code capability for predicting fuel rod core power/decay heat in AP600 (see Section 4 for a discussion of RELAP5 decay heat model applicability).

The composite code capabilities for the following 11 PIRT high-ranked phenomena were judged to be acceptable (reasonable) for all three accident scenarios: "accumulator flow," "ADS energy release," "ADS mass flow," "break mass flow," "cold leg-to-PBL tee phase separation," "core flashing," "core subcooling margin," "core two-phase mixture level," "CMT flow resistance," "CMT level," and "IRWST flow resistance."

Facility instrumentation was generally found to be limited for evaluating the "hot leg phase separation in tees" PIRT phenomenon (see Note 10 in Table 5-2). The code capability judgments made for this phenomenon in the SPES and OSU test assessments were indirect, based on the separate judgments made for the ADS energy release and mass flow phenomena. The ROSA instrumentation included measurements of hot leg and ADS-4 inlet fluid densities and the judgments for the ROSA tests were made based on comparisons of these parameters. The minimal composite judgment for the 2-in. PBLB scenario reflects difficulties in the code predictions of these parameters for this ROSA test. A minimal judgment was also made for the "ADS mass flow" phenomenon for the same ROSA test. The code capabilities for predicting both of these PIRT phenomena in the ROSA tests of the other two accident scenarios were judged reasonable. The fluid conditions at the hot leg to ADS-4 tee in the PBLB scenario are intermediate between those seen in the DVILB and CLB scenarios. In the former, the hot leg void fraction is higher, while in the latter the void fraction is lower, than in the PBLB scenario. It is the intermediate hot leg void fraction of the ROSA PBLB scenario test for which the calculated and measured results differed. A part of the difficulty is related to a distortion in the geometry of the hot leg to ADS-4 connection points in the ROSA facility. On one hot leg, the ADS-4 nozzle is situated on the top of the pipe while on the other hot leg the connection is rotated 45° from the vertical. The RELAP5/MOD3 code has the capability to represent off-take locations on the top, bottom, and side of pipes, but not at other intermediate orientations. This code limitation is not seen as significant for the AP600 application, where both ADS-4 connections are situated on the tops of the hot legs. However, this ROSA facility distortion does not explain all of the differences observed between the calculation and test data for this parameter in the PBLB scenario test. Therefore, the assessments have shown that RELAP5 modeling of the processes at the hot leg tee includes some uncertainties which, in turn, affect the prediction of ADS-4 mass flow. As will be shown in Section 6.2, a reasonable overall code capability judgment was made for this PIRT phenomenon.

For the "pressurizer level" PIRT phenomenon, the agreement between calculated and measured data varied widely among the accident scenarios and tests (see Note 12 in Table 5-2). The agreement was judged reasonable for all three ROSA tests. In the SPES DVI break calculation, the initial draining of the pressurizer was calculated well, but there was less water reintroduced into the pressurizer following ADS actuation and the subsequent draining behavior was somewhat different than in the experiment. For all three OSU experiments, the trends and maximum levels were calculated well, but the calculated draining of the pressurizer after the level was re-established following ADS actuation was too fast. For the OSU 1-in. CLB and 2-in. PBLB accident scenario tests, the calculated initial pressurizer draining was slower than measured. Plotted comparisons between the measured and calculated pressurizer behavior are found in Appendix C. The composite code capabilities for predicting pressurizer level were judged to be reasonable for the 1-in. CLB and 2-in. PBLB accident scenarios and minimal for the DVILB accident scenario. As will be shown in Section 6.2, a reasonable overall code capability judgment was made for this PIRT phenomenon.

All three composite code capabilities for predicting the "CMT level" phenomenon were judged to be acceptable (reasonable). However, for two of the nine assessment cases the results were found to be unacceptable (minimal): the SPES DVILB scenario and the OSU PBLB scenario. In both of these cases, the initial CMT draining behavior was well calculated. In the SPES case calculation, the intact CMT drained too slowly. In the OSU case calculation, CMT-1 drained too slowly and did not completely drain, and a refill of CMT-2 was predicted, but at an earlier time than observed in the test. Neither of these cases was judged to indicate a general code deficiency that would result in an unacceptable composite code capability judgment for this parameter (see Appendix C, Section C.5).

Although composite code capabilities for predicting "ADS mass flow" and "break mass flow" were judged reasonable, experience gained through these assessments indicated that the modeling of these flows is uncertain. As discussed above, one component of ADS-4 flow uncertainty is related to phase separation at the hot leg to ADS-4 tee. Another component of this uncertainty is related to ADS geometry and flow behavior. The AP600 ADS piping design has not been finalized, and the valve flow areas and resistances are currently specified using ranges. Code users should consider quantifying the effects of these uncertainties through bounding sensitivity studies for specific code applications. The effects of the calculational uncertainties in the ADS and break flows can be evaluated by observing results obtained when the ADS and break flow areas are varied over suitable ranges to account for these uncertainties.

The number of SBLOCA PIRT short-term phase high-ranked phenomena is small; to portray a more extensive view of code capabilities, evaluations were also made regarding composite code capabilities for predicting the 34 medium-ranked PIRT phenomena. The results of these evaluations are shown in Table 5-3. The individual assessment results covering the medium-ranked phenomena on a facility-by-facility basis are provided in Appendix C, Table C-5.2.

Table 5-3. Composite assessment results for AP600 PIRT SBLOCA short-term phase medium-ranked phenomena.

Medium-Rank Phenomenon	Code Capability for 1-in. CLB	Code Capability for DVILB	Code Capability for 2-in. PBLB	See Note
Accumulator noncondensible effects	None Made	None Made	None Made	
ADS choking in complex geometries	Reasonable	Reasonable	Reasonable	
ADS flow resistance	Reasonable	Reasonable	Reasonable	
ADS noncondensible effects	None Made	None Made	None Made	
Break energy release	Reasonable	Reasonable	Reasonable	
Break flow resistance	Reasonable	Reasonable	Reasonable	
Cold leg condensation	None Made	None Made	None Made	
Cold leg thermal stratification	Insufficient	Insufficient	Insufficient	1
Core boiling	Reasonable	Reasonable	Reasonable	
Core mass flow, including bypass	Reasonable	None Made	Reasonable	
Core stored energy release	Reasonable	None Made	Reasonable	
CMT-to-loop differential density	Reasonable	Reasonable	Reasonable	
CMT-to-IRWST differential head	Reasonable	Reasonable	Reasonable	2
CMT condensation	Reasonable	Reasonable	Reasonable	2
CMT flashing	Reasonable	Reasonable	Reasonable	
CMT thermal stratification and mixing	Reasonable	Reasonable	Reasonable	
Downcomer/lower plenum condensation	None Made	None Made	None Made	

Table 5-3. (continued).

Medium-Rank Phenomenon	Code Capability for 1-in. CLB	Code Capability for DVILB	Code Capability for 2-in. PBLB	See Note
Downcomer/lower plenum level	Reasonable	Reasonable	Reasonable	
Fuel rod CHF/dryout	None Made	None Made	None Made	
Fuel rod stored energy release	None Made	None Made	None Made	
Hot leg flashing	None Made	None Made	None Made	
IRWST pool flow	Insufficient	Insufficient	Insufficient	3
IRWST pool thermal stratification	Insufficient	Insufficient	Insufficient	3
IRWST sparger pipe level	None Made	None Made	None Made	
Pressurizer entrainment/de-entrainment	Reasonable	Reasonable	Reasonable	
Pressurizer flashing	Reasonable	Reasonable	Reasonable	
Pressurizer level swell	Reasonable	Reasonable	Reasonable	
PRHR heat transfer to IRWST	Reasonable	Reasonable	Reasonable	
Steam generator primary-to-secondary heat transfer	Reasonable	Reasonable	Reasonable	
Sump level	Reasonable	Excellent	Reasonable	4
Upper head/upper plenum entrainment/de-entrainment	None Made	None Made	None Made	
Upper head/upper plenum voiding	Reasonable	Reasonable	Reasonable	
Containment (interior) liquid distribution	None Made	None Made	None Made	
Containment (interior) pressure	None Made	None Made	None Made	

Note 1 - Code capabilities for predicting cold leg thermal stratification were judged insufficient (according to the criteria in Section 2.2.2) because no code model exists to represent this phenomenon. No cold leg thermal stratification was observed in the SPES tests. The ROSA 1-in. CLB assessment indicated that the absence of a model for this phenomenon had no effect on the prediction of PRHR-loop cold leg behavior and some effect on the prediction of CMT-loop cold leg behavior. The OSU 1-in. CLB assessment identified the lack of a thermal stratification model as affecting the CMT-loop cold leg behavior. For the 1-in. CLB accident scenario, the CMT loop cold legs contain the break (on the bottom of a pipe) in addition to the PBL connections (on the tops of the pipes). The inability to model cold leg thermal stratification therefore affected the temperatures of liquid presented at the break and PBLs. The assessments showed these effects to be small (relating to the break flow rate and timing of onset of CMT draining) and short-lived (occurring only over the period following S Signal and before ADS activation).

Note 2 - In the PIRT, the significance of the "CMT condensation" and "CMT-to-IRWST differential head" phenomena is related to the existence and cause of CMT refill behavior during the IRWST injection period. In the 1-in. CLB experiments, CMT refills were not observed in the ROSA test and calculation or in the SPES test and calculation (or in the AP600 calculation). However, condensation-induced CMT refills were observed in both the OSU test and calculation. CMT refills were not observed in any of the OSU tests or calculations for the other two accident scenarios. On this basis, reasonable composite code capability judgments have been assigned for these phenomena.

Note 3 - All facility input models used a "single-stack" nodalization approach to IRWST modeling. The insufficient code capability judgment indicates that this modeling approach cannot represent the pool flow and thermal stratification behavior within the IRWST. The assessments indicate that this IRWST modeling approach did not adversely affect the prediction of the IRWST-related functions and parameters (heat sink for the PRHR system, heat and mass sinks for the ADS-123 system, injection static head, and injection liquid temperature) over the duration of the SBLOCA short-term phase.

Note 4 - Only the OSU APEX facility contained a representation of the sump.

Because of limitations in the facilities and instrumentation, the composite judgments for the medium-ranked phenomena generally were based on fewer individual assessment cases than were the judgments for high-ranked phenomena. For 11 of the 34 medium-ranked phenomena, these limitations were sufficiently large so as not to allow code capability judgments to be made. For 20 of the remaining 23 medium-ranked phenomena, the evaluations resulted in acceptable (excellent or reasonable) composite judgments. Overall code capability judgments (combining the composite judgments from the three accident scenario assessments) for the medium-ranked PIRT phenomena are provided in Appendix C.

The three medium-ranked phenomena that were judged to be unacceptably predicted by the code were: "cold leg thermal stratification," "IRWST pool flow," and "IRWST thermal stratification."

RELAP5/MOD3 is a one-dimensional code which does not allow fluid within a liquid region to stratify vertically in a horizontal component such as the cold leg. Because the code does not contain models allowing for mechanistic simulation of this behavior, the composite code capabilities for representing cold leg thermal stratification were (according to the acceptance criteria in Section 2.2.2) judged to be insufficient. However, the significance of the differences between the calculated and measured behavior was observed to be small, affecting only event sequence timing in some of the assessment cases (see Note 1 in Table 5-3). Cold leg thermal stratification behavior was not observed in the SPES tests. In certain of the ROSA and OSU tests, cold leg thermal stratification behavior was observed and the lack of a RELAP5 modeling capability was seen to affect the timing of the onset of CMT draining. These timing differences were not seen to propagate into still-larger timing differences for subsequent sequence events nor were they seen to significantly affect the system behavior following ADS activation. The effects of this code limitation and suggestions for code users to account for them are further discussed in Section 3.1.

The code cannot currently mechanistically represent IRWST pool flow and thermal stratification behavior and the code capabilities for predicting these phenomena also were judged to be insufficient. The current IRWST modeling approach uses a single, vertical stack of hydrodynamic cells to represent the pool region. With this approach, thermal layers are predicted, but the temperature distribution is not realistic because hot water (produced from PRHR heat transfer and ADS sparger discharge) cannot rise and be replaced with cooler water from other tank regions. A parallel-stack modeling approach is needed to represent this behavior. Parallel-stack IRWST approaches have been attempted, but (for reasons related to the momentum-flux effects described in Section 3.2) the flow behavior produced was not physical. However, despite these judgments relating to behavior within the IRWST, all externally-related IRWST functions during the SBLOCA PIRT short-term phase (that extends up through establishment of steady IRWST injection) were seen in the assessments to be adequately represented in the simulations performed using the current modeling approach. These functions are: the heat sink for the PRHR system, the heat and mass sinks for the ADS-123, the injection static head and the injection liquid temperature. IRWST thermal stratification effects are further discussed in the long-term phase assessment analysis in Section 5.2.

5.1.3 Summary

Code capabilities for predicting the PIRT SBLOCA short-term phase high-ranked phenomena were judged through assessment against test data for three accident scenarios in three experimental facilities. All judgments made of overall code capabilities for predicting the high-ranked phenomena indicated acceptable code capabilities. This analysis shows that the code can acceptably represent the behavior of phenomena important for AP600 behavior, as observed in experimental facilities, during the SBLOCA short-term phase. Scaling analyses, discussing the suitability of the experimental data used in these assessments for representing AP600 behavior and supporting the code capability judgments made here, are presented in Section 5.3. The implications of the assessments presented here on the question of code adequacy for predicting AP600 SBLOCA behavior are addressed in Section 6.2.

5.2 SBLOCA Long-Term Phase

The previous section summarized assessments of code capabilities relative to the SBLOCA short-term phase, which extends from the time of break opening until steady IRWST injection has been achieved, a period of about 1-to-2 hours. These short-term phase assessments used data from ROSA, SPES and OSU experiments. The OSU experiments were continued until about 7 hours, simulating the entire IRWST injection period and into the sump injection period. Due to the OSU facility scaling, a 7-hour test period is equivalent to 14 hours in AP600.

The SBLOCA short-term phase assessments used detailed RELAP5 input models, each containing between 400 and 700 control volumes. Because the SBLOCA long-term phase involves less-dynamic behavior than the short-term phase, it was found that analysis of the long-term phase could be accomplished using simplified models without significant compromises in results. Simplified RELAP5 models of the AP600 and OSU facilities were developed so that the long-term phase could be analyzed more economically. These models, which are referred to as Long-Term Cooling Models (LTCMs), each contain about 100 control volumes and were developed by condensing the detailed models. LTCMs were not developed for ROSA and SPES because these facilities were not used to simulate SBLOCA long-term phase behavior. The OSU and AP600 LTCMs, which are described in Appendix B, were used to calculate the entire durations of SBLOCA transients. Because of their coarse nodalizations, the performance of the LTCMs over the SBLOCA short-term phase was generally not as good as that of the detailed models. However, benchmarks of the LTCMs against the detailed models and/or experimental data showed that the LTCMs provide reasonable entry conditions for the long-term phase analyses; these benchmark comparisons are described in Reference 5-15.

Using the LTCMs, RELAP5/MOD3, Version 3.2.1.2, calculations were performed to simulate the full durations of three OSU experiments along with the corresponding accident scenarios in AP600. This section summarizes assessments of code capabilities for predicting the important AP600 PIRT[5-14] SBLOCA long-term phase phenomena in these experiments. Detailed documentation of these assessments appears in Reference 5-15. The corresponding AP600 accident scenario calculations, which also are documented in Reference 5-15, are used in the scaling analyses described in Section 5.3.

5.2.1 Accident Scenario and Experiment Descriptions

The SBLOCA scenarios investigated and the OSU experiments used for the long-term phase assessments are the same as described in Section 5.1.1 for the assessments of the short-term phase. These scenarios were initiated by a 1-in. diameter cold leg break, a double-ended DVI line break and a 2-in. diameter PBL break (Figure 5-1 shows the break locations). The OSU facility tests representing these three accident scenarios are: NRC22,[5-7] NRC20,[5-10] and SB9,[5-13] respectively.

Several unique aspects of the short-term phase system responses for these three scenarios are described in Section 5.1.1. However, for the long-term phase the system responses for the three scenarios were found to be similar. This similarity results because during the long-term phase the RCS response is controlled by the resistance and area of flow paths from the RCS to the containment, and these are dominated by the ADS; the effects of differences among the scenario definitions (for example, break sizes and locations) are secondary.

The general system behavior during the long-term phase is described as follows. Two sub-phases are identified: IRWST injection and sump injection. The minimum reactor vessel inventory occurs during the short-term phase, before or just after the onset of IRWST injection. During the long-term phase, IRWST injection partially refills the RCS, but as the IRWST drains its injection flow slows, causing the RCS inventory to decline again. (A slower injection flow rate leads to less subcooling and more steam within the RCS). The sump level increases during the IRWST injection sub-phase due to flows from the break and ADS-4. Eventually, the liquid level in the sump reaches the elevation of the curb, allowing liquid to spill over the curb into AP600 containment dead-end rooms (from which liquid cannot be retrieved). These rooms are termed "normally non-flooded rooms" in AP600 design documents and are represented with the secondary sump tank in the OSU facility. Sump injection begins when the head associated with the IRWST pool level falls to that associated with the sump level at the curb elevation. The IRWST level continues falling and the sump recirculation valves (that allow direct equalization of the IRWST and sump pool levels) are opened. Afterwards, the overall system parameters (the injection flows and the RCS, reactor vessel, IRWST and sump inventories) stabilize to a final, quasi-steady condition. This final condition was found to be virtually the same for all three investigated scenarios. At the final condition, the levels in the IRWST and sump reside near the elevation of the curb. The reactor vessel inventory at the final condition is less than that experienced during most of the IRWST injection sub-phase, but greater than the minimum inventory attained near the beginning of IRWST injection. The core remains covered at all times.

5.2.2 Assessment Results for the SBLOCA Long-Term Phase

The AP600 SBLOCA PIRT figure of merit is the minimum reactor vessel inventory; the absolute minimum is reached during the short-term phase, either before or shortly after the onset of IRWST injection. During the long-term phase, a second minimum is experienced (at a higher inventory than the first) during sump injection. Table 5-4 compares the measured and calculated values for the reactor vessel minimum inventory during sump injection (normalized to the initial inventory) for the three OSU experiments. The table shows that the calculated results are in reasonable agreement with the measured values. However, RELAP5 consistently underpredicted the normalized minimum reactor vessel inventory by an average of 10%.

Table 5-4. Comparison of measured and RELAP5-calculated minimum normalized reactor vessel inventory during sump injection.

Scenario, Facility/Test	Minimum Measured Reactor Vessel Inventory (Normalized to Initial Inventory)	Minimum Calculated Reactor Vessel Inventory (Normalized to Initial Inventory)
1-in. Cold Leg Break OSU/NRC22	0.69	0.62
Double-Ended DVI Line Break OSU/NRC20	0.74	0.60
2-in. Pressure Balance Line Break OSU/SB9	0.74	0.65

The underprediction in minimum reactor vessel inventory during sump injection was related to an underprediction in the minimum core levels. The core level underprediction was primarily caused by a bias in the EPRI drift flux correlation. The average underprediction in minimum core liquid level during sump injection was 15% of the core height. Using measured boundary conditions representative of sump injection, the EPRI drift flux correlation was found to underpredict the measured core level by 10%. This finding is consistent with the finding related to rod-bundle interphase drag in the model and correlation reviews summarized in Table 4-2. Although this calculational accuracy is considered to be acceptable for systems calculations, it is important for the user to recognize that the EPRI drift flux correlation biases the calculation of core liquid levels and reactor vessel inventories at the low RCS pressures associated with this application. This bias is also present during the SBLOCA short-term phase, as evidenced by the underpredictions of the minimum reactor vessel inventories shown in Table 5-1.

Comparisons of the calculated and measured SBLOCA long-term phase overall system responses are shown for the three OSU experiments in Figures 5-20 through 5-28. These overall responses are characterized by the RCS pressure, RCS mass inventory and reactor vessel inventory behavior. The scaling analysis in Section 5.3 compares and addresses the differences among the tests, calculations of the tests and calculations of the AP600 plant accident scenarios. The figures show favorable overall comparisons between the calculated and measured system behavior for each experiment, providing general indications that the code is capable of simulating the behavior of a system of AP600 components (reactor vessel, steam generators, coolant loops, CMTs, PRHR system, ADS, and IRWST).

While the code did a good job in predicting the overall system response, there were specific instances where notable differences existed that are apparent in Figures 5-20 through 5-28. These are summarized in the following paragraphs; more detailed analysis is provided in Reference 5-15.

The RCS pressure was near atmospheric pressure during the long-term phase in both the tests and the calculations. On average, the calculated pressures were in at least reasonable agreement with the measured values. The code also represented the different trends occurring among the tests during IRWST injection as evidenced by a comparison of Figures 5-20, 5-23, and 5-26. However, the calculations exhibited significantly larger oscillations than were measured, particularly during the IRWST injection period. These oscillations were numerically induced and generally corresponded to periods of subcooled boiling in the core. The code's subcooled boiling model causes and/or aggravates the oscillations during the IRWST injection sub-phase.

The responses of the calculated and measured RCS and reactor vessel mass inventories were generally consistent with the scenario description provided in Section 5.2.1. The calculated trends were similar to those observed in the tests. However, the RCS and reactor vessel refilled more in the early portion of the IRWST injection sub-phase in the CLB and PBLB calculations than in the corresponding tests. Similar results were obtained with the detailed RELAP5 input model as described in Section 5.1.2. As will be discussed below, there were also larger and more rapid swings in vessel inventory during the IRWST injection period in the calculations than in the tests. However, because the second vessel inventory minimum occurs during sump injection, the sump injection sub-phase is the most important portion of the long-term phase. As shown in Figures 5-22, 5-25 and 5-28 and Table 5-4, the minimum calculated vessel inventory during the long-term phase was in reasonable agreement with the measured value for each test.

The code predicted unphysically-large oscillations during the long-term phase. Some of the oscillations caused relatively large swings in vessel inventory, in particular during the IRWST injection sub-phase. These swings, which for example are evidenced from 4,000 to 12,000 s in Figure 5-22, were found to be caused by condensation events associated with transitions between the vertically stratified and bubbly flow regimes in the reactor vessel upper plenum and head regions. These vessel inventory swings

The information deleted from this figure is considered proprietary by Westinghouse Electric Company

Figure 5–20. Measured and calculated long–term phase RCS pressure responses for the OSU 1–in. diameter cold leg SBLOCA scenario.

The information deleted from this figure is considered proprietary by Westinghouse Electric Company

Figure 5–21. Measured and calculated long–term phase RCS mass inventory responses for the OSU 1–in. diameter cold leg SBLOCA scenario.

The information deleted from this figure is considered proprietary by Westinghouse Electric Company

Figure 5–22. Measured and calculated long–term phase reactor vessel mass inventory responses for the OSU 1–in. diameter cold leg SBLOCA scenario.

The information deleted from this figure is considered proprietary by Westinghouse Electric Company

Figure 5–23. Measured and calculated long–term phase RCS pressure responses for the OSU DVI line SBLOCA scenario.

The information deleted from this figure is considered proprietary by Westinghouse Electric Company

Figure 5–24. Measured and calculated long–term phase RCS mass inventory responses for the OSU DVI line SBLOCA scenario.

The information deleted from this figure is considered proprietary by Westinghouse Electric Company

Figure 5–25. Measured and calculated long–term phase reactor vessel mass inventory responses for the OSU DVI line SBLOCA scenario.

The information deleted from this figure is considered proprietary by Westinghouse Electric Company

Figure 5–26. Measured and calculated long–term phase RCS pressure responses for the OSU 2–in. diameter PBL SBLOCA scenario.

The information deleted from this figure is considered proprietary by Westinghouse Electric Company

Figure 5–27. Measured and calculated long–term phase RCS mass inventory responses for the OSU 2–in. diameter PBL SBLOCA scenario.

The information deleted from this figure is considered proprietary by Westinghouse Electric Company

Figure 5–28. Measured and calculated long–term phase reactor vessel mass inventory responses for the OSU 2–in. diameter PBL SBLOCA scenario.

also are non-physical, however they were not seen to affect the minimum vessel inventory calculated during the long-term phase. The condensation occurred relatively early in the long-term phase while the minimum vessel inventory was achieved at the steady end-point condition during sump injection. These vessel inventory swings were not observed in the calculations of the AP600 accident scenarios corresponding to the OSU experiments. Because of scaling compromises in the OSU facility core, subcooled boiling is more important in the OSU facility than in the AP600. Consequently, the oscillations caused by the subcooled boiling model are more important in the OSU calculations than in the AP600 calculations. See Reference 5-15 for further discussion regarding these oscillations. In the OSU calculations, the oscillations caused by the subcooled boiling model resulted in the condensation events that caused the relatively large swings in vessel inventory. Thus, the combination of the subcooled boiling model and flow regime transitions caused the large swings in vessel inventory. While code capabilities are considered acceptable at this time, improvement in the results can be expected if the oscillations can be reduced.

Indications of specific code capabilities are provided by the results of detailed code assessments covering the AP600 PIRT SBLOCA long-term phase high-ranked phenomena for the three OSU experiments. These results are summarized in Table 5-5. The table lists the 11 PIRT high-rank phenomena and the judgments regarding code capabilities for predicting them in each of the three accident scenarios. These judgments were made using the acceptance criteria described in Section 2.2.2. An overall judgment was also made for each high-ranked phenomenon based on a combination of the judgments shown for the individual accident scenarios; these overall judgments are presented and discussed later, in Section 6.2. Detailed documentation of this assessment analysis is presented in Reference 5-15.

Table 5-5. Assessment results for AP600 PIRT SBLOCA long-term phase high-ranked phenomena.

High-Rank Phenomenon	Code Capability Judgment for OSU 1-in CLB Test (NRC22)	Code Capability Judgment for OSU DVILB Test (NRC20)	Code Capability Judgment for OSU 2-in PBLB Test (SB9)	See Note
ADS energy release	Excellent	Reasonable	Excellent	
ADS mass flow	Excellent	Reasonable	Excellent	
Core two-phase mixture level	Reasonable	Reasonable	Reasonable	1
Downcomer level	Reasonable	Reasonable	Reasonable	
Fuel rod core power/decay heat	None Made	None Made	None Made	2
IRWST flow resistance	Reasonable	Reasonable	Reasonable	3
IRWST pool level	Excellent	Excellent	Excellent	
IRWST pool thermal stratification	Insufficient	Insufficient	Insufficient	4
Sump fluid temperature	Reasonable	Reasonable	Reasonable	
Sump level	Reasonable	Excellent	Excellent	
Upper plenum two-phase mixture level	Reasonable	Reasonable	Reasonable	1

Note 1 - The experimental facilities do not contain instrumentation to measure core or upper plenum two-phase mixture level. Code capabilities were judged instead upon comparisons between measured and calculated collapsed levels.

Note 2 - Because core power was a boundary condition in all of the tests and calculations, no judgments of code capabilities were made for this phenomenon. These assessments do not provide data useful for evaluating code capabilities for predicting fuel rod core power/decay heat in AP600 (see Section 4 for a discussion of RELAP5 decay heat model applicability).

Note 3 - This judgment was based upon comparisons of measured and calculated reactor vessel pressures, IRWST pool levels and IRWST injection mass flow rates.

Note 4 - Based strictly on the results of comparisons of calculated and measured temperatures in the IRWST, the code capability for calculating IRWST thermal stratification would appear to be reasonable. However, this capability was instead judged to be insufficient because the code does not have a mechanistic model for this phenomenon. Rather than develop a code model for IRWST thermal stratification, it is recommended that the effects of stratification be bounded using sensitivity calculations. Two sensitivity studies were performed to bound the effects of uncertainty in modeling the IRWST thermal distribution. The first sensitivity study, for an OSU experiment of an inadvertent ADS actuation accident scenario, is reported in Volume 6 of Reference 5-4. The results indicate that thermal stratification effects can be large at the beginning of the IRWST injection period, but diminish with time, and are negligible during the sump injection period (when the minimum vessel inventory during the long-term phase is experienced). The second study, which is reported in Reference 5-15, yielded a similar finding for a 1-in. CLB accident in AP600. These results may be scenario specific; code users can perform similar studies to evaluate the effects of this uncertainty for other accident scenarios.

No judgment could be made for the "fuel rod core power/decay heat" phenomenon. Core power was a boundary condition in all experiments and calculations of the experiments. Therefore, no information can be drawn from these assessments regarding code capability for predicting fuel rod core power/decay heat in AP600 (see Section 4 for a discussion of RELAP5 decay heat model applicability).

Code capabilities for all three accident scenarios were judged to be acceptable (excellent or reasonable) for nine of the remaining ten high-rank phenomena: "ADS energy release," "ADS mass flow," "core two-phase mixture level," "downcomer level," "IRWST flow resistance," "IRWST pool level," "sump fluid temperature," "sump level" and "upper plenum two-phase mixture level."

The code does not currently have the models necessary to mechanistically represent the "IRWST thermal stratification" phenomenon (see discussion in the last paragraph of Section 5.1.2). In accordance with the evaluation criteria in Section 2.2.2, the code capability for predicting this phenomenon was judged to be insufficient. Despite this judgment, the IRWST functions during this phase, injection static head and injection fluid temperature, were seen to be adequately represented with the existing code and facility input model. Examples of sensitivity studies evaluating the effects of the uncertainty resulting from this modeling limitation are referenced in Table 5-5, Note 4. Similar sensitivity studies are recommended to code users for evaluating these effects in other accident scenarios. With the provision that the effects of this uncertainty be considered, the existing code and modeling approach are considered acceptable for representing the IRWST behavior during the SBLOCA long-term phase.

Although the code capabilities for predicting "ADS mass flow" were judged excellent or reasonable, experience gained through the assessments indicated that the modeling of ADS flow is inherently uncertain. This is particularly true for AP600, where the design of the ADS geometry has not been finalized and the flow behavior has not been fully characterized. Therefore, code users should consider quantifying the effects of this uncertainty through bounding sensitivity studies for specific code applications. For example, the effects of the uncertainty in ADS flow can be evaluated by observing results obtained when the ADS flow area is varied over its design range.

The number of SBLOCA PIRT long-term phase high-ranked phenomena is small; to portray a more extensive view of code capabilities, judgments were also made regarding prediction of selected additional PIRT phenomena. The additional phenomena are primarily medium ranked in the current PIRT. Assessment results for these selected additional phenomena are summarized in Table 5-6. Code capabilities were judged for ten long-term phase non-high-rank phenomena. Overall capabilities (combining the capabilities from the three individual assessments) were judged to be acceptable (excellent or reasonable) for eight of these phenomena: "ADS flow resistance," "break mass flow," "containment liquid distribution," "CMT-to-IRWST differential head," "CMT condensation," "CMT noncondensible effects," "hot leg fluid stratification and phase separation," and "sump flow resistance." The "containment liquid distribution phenomena" was evaluated based on comparisons of calculated and measured inventories in the OSU primary and secondary sump tanks.

The overall code capabilities for predicting "core boiling" and "core subcooling margin" were judged to be minimal. The minimal judgment for "core subcooling margin" was given because the code-calculated lower plenum (core inlet) fluid subcooling was consistently underpredicted during the long-term phase. This underprediction was found to result from excessive numerical flow oscillations that mixed the core and downcomer fluids, dissipating the core inlet fluid subcooling in the process. Figures 5-20 through 5-28 show that oscillations are observed in both the test data and calculations but that the magnitude of the oscillations is overpredicted in the calculations. The code capability for predicting "core boiling" was judged minimal because the subcooled boiling model was found to contribute to these oscillations.

Table 5-6. Assessment results for selected AP600 PIRT SBLOCA long-term phase non-high-ranked phenomena.

Non-High-Rank Phenomenon	Code Capability Judgment for OSU 1-in CLB Test (NRC22)	Code Capability Judgment for OSU DVILB Test (NRC20)	Code Capability Judgment for OSU 2-in PBLB Test (SB9)	See Note
ADS flow resistance	Reasonable	Reasonable	Reasonable	
Break mass flow	Excellent	Reasonable	Excellent	
Containment liquid distribution	Reasonable	Reasonable	Reasonable	
Core boiling	Minimal	Minimal	Minimal	
Core subcooling margin	Minimal	Minimal	Minimal	
CMT-to-IRWST differential head	Reasonable	Reasonable	Minimal	1
CMT condensation	None Made	None Made	Reasonable	1
CMT noncondensible effects	None Made	None Made	Reasonable	1
Hot leg fluid stratification and phase separation	Reasonable	Reasonable	Reasonable	
Sump flow resistance	Reasonable	Reasonable	Reasonable	

Note 1 - The significance of the "CMT condensation" and "CMT noncondensible effects" phenomena in the SBLOCA PIRT relates to CMT refills during the long-term phase. No refills occurred in the experiments and calculations for Tests NRC20 and NRC22. For Test SB9, refills of one CMT were observed in both the test and calculation. For those reasons, code capabilities for predicting these two phenomena were judged to be reasonable. However, in Test SB9 the calculated CMT level during refill was lower than that observed in the test and the calculated draining behavior in the other CMT was different in the test and calculation. For those reasons, the code capability for predicting "CMT-to-IRWST differential head" was judged to be minimal for that test.

5.2.3 Summary

RELAP5/MOD3 has been shown to be capable of simulating the overall behavior of a system of AP600 components during the SBLOCA long-term phase, as observed in tests representing three different accident scenarios in the OSU scaled experimental facility. With one exception, all code capability judgments regarding prediction of the high-ranked PIRT phenomena were acceptable. The exception was "IRWST thermal stratification" for which the capability was judged insufficient because the code currently does not have the models necessary to mechanistically represent this behavior. Despite this judgment, the IRWST functions during this phase (injection static head and injection fluid temperature) were seen in the assessments to be adequately represented. Therefore, as long as the uncertainty introduced by this code limitation is accounted for, the acceptability of the code for this application is not impacted. This assessment has shown that the code can acceptably represent the behavior of phenomena important for AP600 behavior during the SBLOCA long-term phase, as observed in tests in the OSU scaled experimental facility. Scaling analyses, discussing the suitability of the experimental data used in these assessments for representing AP600 SBLOCA behavior and supporting the code capability judgments made here, are presented in Section 5.3. The implications of the experimental assessments presented here on the question of code adequacy for predicting AP600 SBLOCA behavior are addressed in Section 6.2.

5.3 Scaling Analyses

A systematic "top-down" scaling analysis procedure was developed[5-16] and applied[5-17] to evaluate the global system behavior of the data from the AP600-related integral test facilities. The objectives of this analysis relating to code adequacy demonstration are:

- To determine the sufficiency of the integral test data base for code assessment. The criterion for sufficiency is that the data bound (as defined in Section 5.3.1) the expected AP600 behavior. As with the other reviews and assessments described in this report, the AP600 SBLOCA PIRT[5-14] is used to focus the scaling analysis. Conversely, information generated through scaling analysis of the physical data base is valuable for confirming the PIRT.

- To determine the relevance of the data. The criterion for relevancy is typicality; if behavior is typical of AP600, then it is relevant. It is possible that behavior observed in the experiments is peculiar to the experiments (due to distortions) and is not expected in the plant. The effects of known and potential sources of distortions are investigated.

- To uncover, through comparisons between test data and corresponding calculations, any biases that the code may produce with respect to the evaluated phenomena and to examine the impact of any biases on the AP600 prediction. The scaling similarity between a code prediction and its counterpart experiment is determined, indicating that the code prediction represents the processes and interactions involved in the experiment.

Additionally, "bottom-up" scaling analyses were performed to address selected issues raised by the AP600 SBLOCA PIRT[5-14] that are related to localized behavior. The objectives of the bottom-up scaling analysis relating to code adequacy demonstration are:

- To explain behavior differences observed among tests in the different experimental facilities by linking facility behavior to scaling distortions.

- To use these explanations to infer the expected AP600 behavior and determine whether the experimental data provide sufficient representation of AP600.

This section summarizes the results of both the top-down and bottom-up scaling analyses. The top-down scaling analyses investigate the same three AP600 SBLOCA scenarios used in the code assessments described in Sections 5.1 and 5.2. These three SBLOCA scenarios are initiated by: a 1-in. diameter break in a cold leg, a double-ended rupture of a DVI line, and a 2-in. diameter break in a PBL. The general top-down scaling methodology and application procedure are described in Section 5.3.1. Top-down scaling analysis results for the AP600 PIRT SBLOCA short-term phase (the period from the time the break opens until stable IRWST injection is established) are summarized in Section 5.3.2. Results for the AP600 PIRT SBLOCA long-term phase (the period encompassing the remainder of IRWST injection and sump injection) are summarized in Section 5.3.3. Bottom-up scaling analysis results are summarized in Section 5.3.4. A summary of results from all scaling analyses is provided in Section 5.3.5.

5.3.1 General Top-Down Scaling Methodology and Application Procedure

The top-down scaling methodology provides a procedure through which: (1) the main nondimensional groups (Πs) that govern similitude between facilities (with regard to the key system response, reactor vessel mass inventory) are derived, (2) it is verified that these nondimensional groups scale the results among the various experimental facilities of different sizes, (3) it is determined whether the ranges of the nondimensional group values provided by the set of experiments encompass the corresponding AP600 values (thereby indicating the assessments using the experimental data are applicable to AP600), and (4) the scalability of RELAP5 is verified by qualitative and quantitative comparisons of data and the corresponding calculations in non-dimensional space.

The top-down scaling methodology considers the interconnections among system components, leading to nondimensional groups involving parameters from more than one component. The methodology evaluates the relative importance of the nondimensional groups and the processes they represent with regard to their influence upon the key system response. These evaluations show that the vast majority of nondimensional groups are of secondary importance; the system response is generally governed by a limited number of processes. The theory is then validated through comparison with the experimental data, verifying that the important nondimensional groups selected adequately scale results from among the various facilities.

The top-down scaling methodology consists of the following eight steps, which are described in detail in Reference 5-16:

1. Define the phenomenologically distinct periods of the transient, clearly identifying the initiating and ending events for these periods. These periods are the "sub-phases" of the accident when different system components come into play. Here, the term "sub-phase" is used to indicate a portion of SBLOCA PIRT short-term and long-term phases (see Section 2.2.1). The remaining steps are performed separately for each sub-phase.

2. Identify and define the participating subsystems and components and the interactions of importance (the topology of the system).

3. Develop governing equations for the topology defined in Step 2 along with the closure equations necessary to create a complete and closed equation set.

4. Nondimensionalize the equation set from Step 3.

5. Define and select reference parameters to be used in the order-of-magnitude analyses.

6. Perform order-of-magnitude analyses to identify dominant nondimensional groups and equations. The magnitude of each nondimensional group is evaluated, allowing a simplification of the analysis through discarding of relatively minor terms.

7. Validate, to the extent possible, each equation against test data.

8. Compare the magnitudes of the non-dimensional groups among the experimental facilities and AP600 to elucidate the applicability of the test data to AP600.

The application of this top-down scaling methodology is described as follows:

Selection of key variables to be compared

a. Based on the PIRT and the reduced set of governing equations describing the system topology, select the phenomena and variables for scaling analysis (e.g., the vessel liquid level, the CMT draining behavior and the lower plenum temperature behavior).

b. Manipulate the equations for these phenomena and variables into workable forms, through integration, differentiation and combination with other equations. A workable form is one in which the phenomenon or variable is expressed as a function of measured quantities, providing a relationship that can be compared with test data.

Verification of modeling assumptions

c. Verify the theoretical relationships through comparison with experimental data. The scaling model assumes that the dominant terms in the right hand side of the equation, overshadow the low order terms. For example, consider Equation 1 in which the Πs represent nondimensional coefficients and the χs are the normalized variables (always of Order 1):

$$L.H.S.=\Pi_i\chi_i^* + \Pi_j\chi_j^* + \Pi_k\chi_k^* \qquad \textbf{(1)}$$

Since the normalized variables are of order one, the importance of each term is given by the relative values of the nondimensional coefficients (Πs). Suppose that Π_i is orders of magnitude larger than Π_j and Π_k. This means that the equation can be approximated (if the theory[a] is correct) to:

$$L.H.S.\approx\Pi_i\chi_i^* \qquad \textbf{(2)}$$

We then plot the left hand side (L.H.S.) vs. the right hand side (R.H.S.) using the data (or calculation) values of the relevant normalized (starred) variables, and verify that indeed

a References to "the theory" throughout the scaling analyses refer to the model from which the equations and Πs are derived and have no relation to RELAP5 models or calculations. In the plots. there are no "traces" that result from the theory, only the 45° slope.

their relationship is a straight line with a 45° slope. Figure 5-29 illustrates such a plot, along with the significance of having +65% and -45% departures from the 45° line.

By comparing the slopes of the data with the theory, we are verifying that the processes represented in the equations are the dominant ones. Note that the equations are time derivatives and, therefore, indicate trends and the mechanisms that govern those trends; the nondimensional coefficients are measures of slopes, as opposed to magnitudes. Throughout this report, scaling comparisons are almost always comparisons between slopes and not between magnitudes. The system is a time varying system, whose physical configuration varies, sometimes abruptly, from one phase to the next. A measure of departures from the theory in terms of magnitude would assume that the equations are solved to yield the magnitudes, and any *errors* evaluated this way can accumulate from phase to phase, therefore biasing the evaluation of the latter phases.

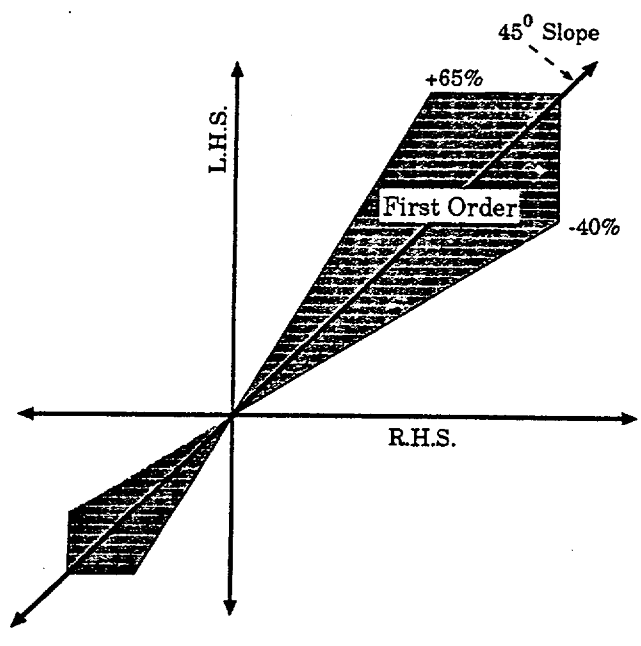

Figure 5-29. Illustration of the regions of First Order agreement between data and theory in graphical terms.

Comparing slopes, instead of magnitudes, can still provide a quantitative measure of comparison. Since equations are manipulated to provide a linear relationship between the left and right hand sides, a linear regression of the results is both a measure of slope and a measure of linearity. The dominant mechanisms (and nondimensional coefficients) were determined based on the Order of Magnitude analysis, therefore a departure of the resulting traces of about ±10% from the theory is generally expected. We also know that the variables themselves carry some uncertainty due to imperfect instrumentation. Based on uncertainty evaluations made to all relevant instruments and measurement techniques,[b] we assigned a maximum uncertainty of ±20% to all starred values.[c] If these uncertainties were only in the right hand side of the equation, the result of these measurement uncertainties would be a bias. But since both sides of the equations are a function of some starred quantity, uncertainties on both sides will result in a change of slope. Equations 3, 4 and 5 illustrate this concept. The factors in parentheses account for the ±20% uncertainty (on both sides of the relationship) and the ±10% from the Order of Magnitude analysis.

$$L.H.S.(1.2)\ or\ (0.8) = R.H.S.(1.1)\ or\ (0.9)\ \text{"and"}\ (1.2)\ or\ (0.8) \tag{3}$$

In the worst cases, this could be:

$$L.H.S. = R.H.S.\frac{(1.1)(1.2)}{0.8} = R.H.S.(1.65) \tag{4}$$

or

$$L.H.S. = R.H.S.\frac{(0.8)(0.9)}{1.2} = R.H.S.(0.6) \tag{5}$$

or a range of -40% to +65% departure between L.H.S. and R.H.S. due to lower order terms and measurement uncertainty. Therefore, the theory can be correct and accurate to a **First Order** approximation, even when departures of -40% or +65% are evaluated from the plots. This is, of course, the extreme. We find that in many cases the departure from the theory (45° slope) is within this band, and the RELAP5 calculations (which have no contribution from measurement uncertainty) also depart from the theory more than ±10%, indicating that the departure is more due to uncertainties in the evaluations of the Πs than on the data itself. Π values are evaluated using nominal values of the facility's geometry, operating parameters, and other characteristics. Such parameters may vary somewhat from scenario to scenario, and our knowledge of the facility may not be perfect. For example, some Π values are quite sensitive to line resistances, and these seem to vary significantly

b Reference 5-4, Volume 5, Appendix D.

c This seems like a high estimate of uncertainty since for most instruments the uncertainty is 10% or less. However, in these comparisons, we use many derived quantities (e.g., flow values derived from tank level data), which carry a larger uncertainty value than direct measurements.

between tests. The lines of most concern to us are expected to always be full of liquid (i.e., DVI lines, CMT injection lines); however, if gas enters these lines (i.e., nitrogen from the accumulators or steam from the downcomer at the DVI injection nozzle when the downcomer level drops below the DVI elevation), the effective line resistance increases, thus causing the departure seen in the plots between data (or calculation) and the nominal 45° slope. A departure from the theoretical 45° slope due to factors of this kind does not negate the validity of the model, it only points to deficiencies in our sources of information.

For simplicity, **First Order** agreement is defined as a case in which the difference in slopes between the lines representing the theory and measurements is no more than ±50% (this is a rough approximation of the +65% and -40%). Note that even if the departure from the 45° slope is more than ±50%, but the traces are straight lines, it means that the numerical value of the dominant Π is probably incorrect, but the starred key variables chosen still represent the dominant phenomena.

If departure from the theory is caused by phenomena or mechanisms unaccounted for in the theory, such departure is expected to be large in both slope and linearity. Unaccounted phenomena may not conform to our definition of phase and its assumptions, and make the trace non-linear (having abrupt changes of slope or loops). This is expected to occur in the beginnings and ends of phases, or when component interactions are significant enough to affect the overall behavior.

Verification of data sufficiency

d. It is very unlikely that one can produce a facility in which all dimensions are ideally scaled for a time-varying configuration, such as AP600. In all the test facilities examined, there were compromises that needed to be made in order to build them. There is no perfect match of Πs and responses. The approach is then to determine, by examining the relative values of the dominant non-dimensional coefficients, whether the AP600 *solution*[d] can be expected to exist between the responses exhibited by facilities whose dominant Πs envelop those of AP600.

If the theoretical relationships are verified, then we can use the nondimensional coefficients (Πs) to "collapse" the data. This collapsing process applies the facility scaling factors, attempting to make the data from all facilities appear as parallel straight lines on nondimensional plots. At this point, compare, via the nondimensional coefficients and relationships, the behavior of the facilities with the AP600 expected performance and determine whether the test data envelops AP600 behavior (i.e., the Π_{AP600} is included within the range of Π covered by the experimental facilities). Note that in this context, experiment facility "distortions" actually help widen the spectrum of solutions, rather than disqualify them. A single facility can (and does) exhibit different Π values for different tests, when a physical parameter of the facility is systematically changed (e.g., a valve size, a heat input, or an initial level). In this fashion a single facility can provide sufficient data to encompass AP600 expectations if the range of the varying Πs contains the AP600 values of those Πs.

d Having demonstrated that the scaling model is correct, the data from the facilities are solutions to the model equations. The inherent assumption in this approach is that in the space of solutions there are no discontinuities between different values of the Πs and that solutions for Πs contained in the range of the tests will also be similar.

Effect of distortions

e. If the behavior of the test data does not support the theory (as represented by the equation), then review the theory assumptions and the test data to determine the source of the discrepancy and its impact upon the relationship between the test facility and plant behavior (i.e., is the discrepancy due to an unsuspected or overlooked phenomenon that may be present in AP600 also, or is it due to a distortion?). In this manner, unsuspected sources of distortion are uncovered and evaluated.

In these analyses, most known sources of distortions are already accounted for in the equations and system parameters. The nondimensional coefficients (Πs) are made up of parameters that in some cases do not conform to an "ideal" dimensional value; oversized valves, atypical elevations and shapes, and non-prototypical operating conditions are examples of the types of *distortions* that are accounted for in the numerical value of a Π. Quite often, these non-prototypical coefficients are the ones neglected in the analysis because their order of magnitude is lower than that of the dominant Π. The fact is that the dominant Πs are seldom identical for all facilities; which points to the distortions in a less traditional but more meaningful fashion.

Verification of Integrated Code Behavior

f. Along with the test data from the experimental facilities, corresponding RELAP5/MOD3 simulations of the tests and the corresponding accident in AP600 are included in the comparison. Comparisons are made directly between the facility test data and the calculations simulating the tests. A direct comparison is also made between the RELAP5/MOD3 AP600 calculations and the scaling-analysis model expectations. Measured and calculated phenomena and variables are compared in a nondimensional domain, establishing whether the AP600 simulation is "similar" to the test data and in what range. Note that the so-called AP600 theoretical expectations result from scaling analysis and not from the simulations of AP600 response. In this fashion, data and calculations are compared quantitatively. The slopes of the traces are used to determine a quantitative measurement of the difference between RELAP5 calculations and the data. The code results do not carry with them the measurement uncertainties indicated for the data. When the code follows the data, it indicates that measurement uncertainties are not a main cause of deviation, but rather that "unimportant" mechanisms are having more of an impact in the response than anticipated by the theory. Significant deviations warrant a closer look, which in most cases indicate that differences in the system conditions, rather than code limitations, are responsible for the discrepancy. **This is not intended as a substitute for the code assessments presented in Sections 5.1, 5.2, and 5.4 of this report.** It is, however, new quantitative comparison information supporting the evaluation of code adequacy.

Scaling analysis observations and conclusions are summarized in the context of the objectives stated above.

5.3.2 Top-Down Scaling Analysis Results for the SBLOCA Short-Term Phase

The sub-phases for the scaling analysis of the SBLOCA short-term phase were defined as follows:

- **Subcooled blowdown:** Starts at time zero (break opening) and ends with the "S" signal that activates the CMT and PRHR systems.

- **Intermediate:** Starts with the "S" signal and ends with the opening of ADS-4 valves. This is a complex, scenario-dependent phase that is subdivided, for analysis purposes, into the following:
  - Initial period: Starts with the activation of the CMT and PRHR systems and ends when the system reaches the saturation pressure of the secondary system.
  - Middle (Recirculation) period: Starts when the system reaches the secondary saturation pressure and ends with the onset of accumulator injection or the opening of ADS-1 valves.
  - ADS-123 blowdown period: Starts with the onset of accumulator injection or the opening of ADS-1 valves, and ends with the opening of ADS-4 valves.
- **ADS-4 blowdown:** Starts with the opening of ADS-4 valves and ends with the onset of IRWST injection.
- **IRWST injection:** Starts with the onset of IRWST injection and ends when the collapsed vessel level reaches the hot leg centerline.

Of these sub-phases, ADS-4 blowdown was deemed the most important because it is during this period when the reactor vessel inventory, which is the SBLOCA PIRT primary figure of merit, typically reaches its minimum.

The phenomena and variables selected for scaling analysis are listed in Table 5-7. The measured and calculated experimental data used for this analysis are summarized in Section 5.1 and are presented in more detail, along with the calculated data for AP600, in Appendix C.

Table 5-7. Variables selected for the scaling analysis of the SBLOCA short-term phase.

Sub-phase of the SBLOCA Short-Term Phase	Analysis Variables Selected
Subcooled blowdown	Pressurizer pressure Pressurizer level
Intermediate	System pressure System liquid fraction
ADS-4 blowdown	CMT level Vessel inventory
IRWST injection	Vessel inventory

The scaling methodology report[5-16] demonstrated the eight-step procedure for the subcooled blowdown, the "Intermediate Phase" (which encompasses what we call the initial, middle (recirculation), and ADS-123 blowdown periods), the ADS-4 blowdown, the IRWST injection, and the long-term cooling

(LTC) sub-phases for a 1-in. diameter CLB accident scenario. In Reference 5-17, this demonstration was revisited and expanded to include the analyses of the double-ended DVILB and 2-in. diameter PBLB accident scenarios.[e]

The remainder of this section discusses results of the scaling analysis covering the four sub-phases of the SBLOCA PIRT short-term phase for the three accident scenarios. Although, according to the PIRT, these three scenarios are controlled by the same important mechanisms and processes, for some cases the scaling analysis found that the system configurations and timings of events are sufficiently different to warrant considering the DVILB scenario separately from the other two. For these cases, reasons for the separate treatment of the DVILB scenario are provided.

5.3.2.1 ***Subcooled Blowdown Sub-Phase.*** This sub-phase is common to all three accident scenarios and to all facilities except OSU, in which experiments are initiated within the intermediate sub-phase. The system configuration pertinent for the subcooled blowdown sub-phase is shown in Figure 5-30. With the exception of the pressurizer, the RCS fluid is subcooled during this sub-phase. The energy flows into and out of the RCS are roughly in balance. When the break opens, the pressurizer supplies the remainder of the RCS with liquid to make up for the fluid volume lost through the break. This sub-phase ends when the system configuration changes because the "S" signal activates the PRHR and CMT systems.

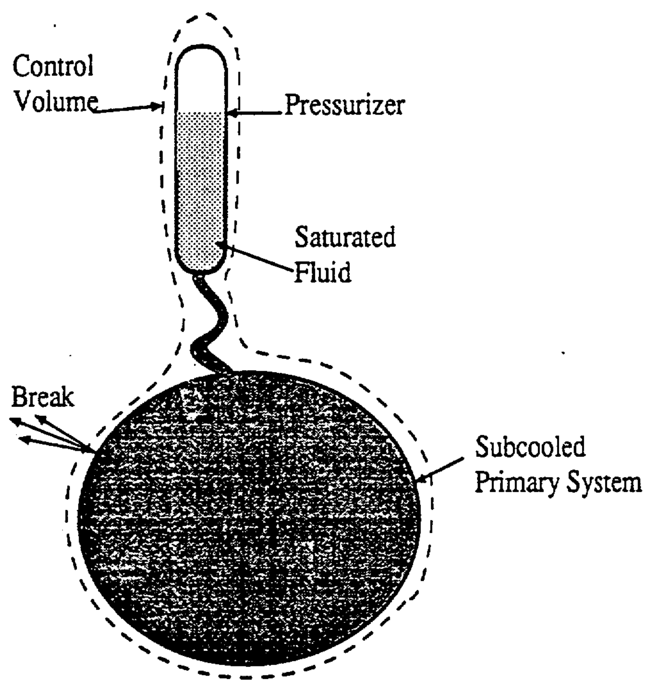

Figure 5-30. Subcooled blowdown sub-phase: system configuration.

The scaling analysis variables selected for this sub-phase are pressurizer pressure and pressurizer liquid level (or liquid mass). The governing equations for these variables are presented in Reference 5-17 and details regarding their development are provided in Reference 5-16. These equations describe the time rates of change of the variables in terms of nondimensional groups and reference parameters. With this theory, a net RCS heat balance (with core power balanced by steam generator heat removal) is assumed.

---

e This reference also includes the inadvertent opening of ADS-1 (IADS) scenario which was part of the early horizontal integration efforts.[5-4]

The nondimensional groups derived from the equations, their values for each facility and their physical interpretations are listed in Table 5-8. The table shows that $\Pi_{7\text{-}pzr}$ is orders of magnitude larger than any other nondimensional coefficient and, therefore, it is the dominant one.[f] Note also that the values of the other Πs listed, although small, place the AP600 Π value as contained in the range covered by the experimental facilities. Thus, the pressurizer behavior, according to the scaling model (the theory) can be described by an equation (relating normalized pressurizer pressure and mass) of the form:

$$L.H.S.(P*) \approx R.H.S.(\Pi_{7\text{-}pzr}, M*) \qquad \textbf{(6)}$$

Table 5-8. Nondimensional coefficients in scaling equations for the subcooled blowdown sub-phase.

Coefficient	AP600	ROSA	SPES	OSU	Physical Interpretation
$\Pi_{0\text{-}pzr}$	0.0021	0.0023	0.0014	NA	Ratio of manometric pressure to thermodynamic pressure
$\Pi_{7\text{-}pzr}$	1.0	1.0	1.0	NA	Pressurizer emptying time ratio
$\Pi_{8\text{-}pzr}$	0.0130	0.0129	0.0130	NA	Ratio of energy input to energy storage
$\Pi_{11\text{-}pzr}$	0.016	0.016	0.016	NA	Ratio of potential energy to enthalpy

Figure 5-31 shows both sides of Equation 6 plotted against each other, for all applicable scenarios. From a sequence timing perspective, the transients begin at the upper right hand corner of the figure and proceed downward and to the left. The normalizations are made with respect to the "nominal" initial values of pressurizer pressure and mass. The deviations in the starting points for the curves are a result of deviations of the initial conditions in the tests and calculations from their nominal values. Measured data are shown for tests representing all three accident scenarios in the ROSA and SPES experimental facilities. Calculated data also are shown for all of these tests as well as the corresponding calculations for AP600. The theory (Equation 6) is represented by two straight lines with 45° slopes. The measured and calculated traces are not all perfectly-straight lines. Terms neglected in the equations as a result of the order of magnitude analysis have some influence. For clarification, the same data have been broken up and presented by scenario in Figures 5-32, 5-33, and 5-34.

f The Πs listed in Table 5-8 are all of the coefficients of the governing equation defined for this sub-phase. An order of magnitude analysis leads to the conclusion that there is only one dominant Π amongst these and it is $\Pi_{7\text{-}pzr}$, and this is clearly shown in Table 5-8. All Πs are all listed here to illustrate the process. In the summaries of the subsequent sub-phase scaling analyses, only the dominent Πs will be tabulated.

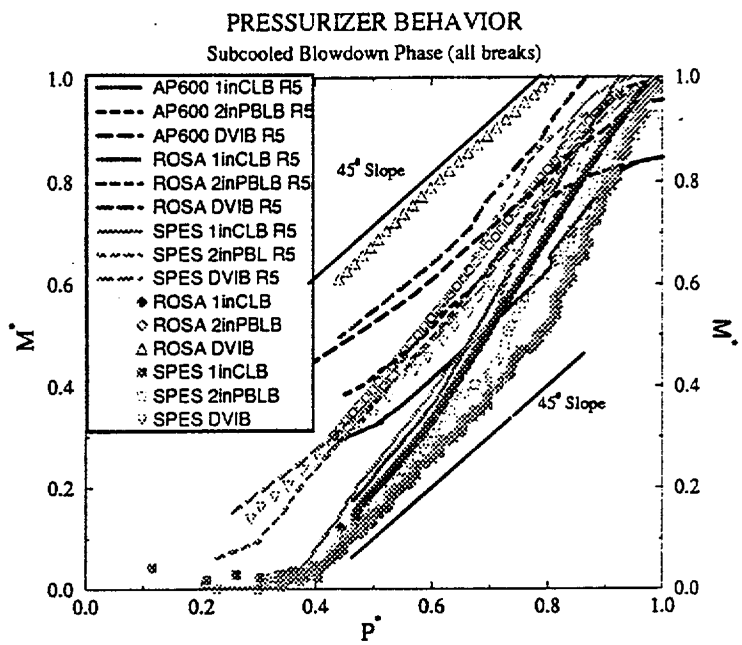

Figure 5-31. Subcooled blowdown sub-phase: normalized pressurizer mass vs. normalized pressure for all three test scenarios and RELAP5 calculations.

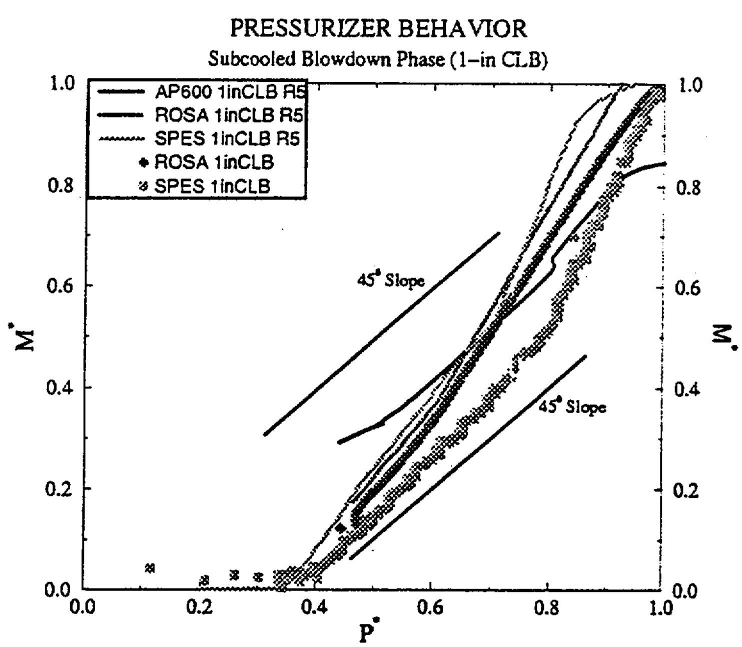

Figure 5-32. Subcooled blowdown sub-phase: normalized pressurizer mass vs. normalized pressure for the 1-in. CLB scenario.

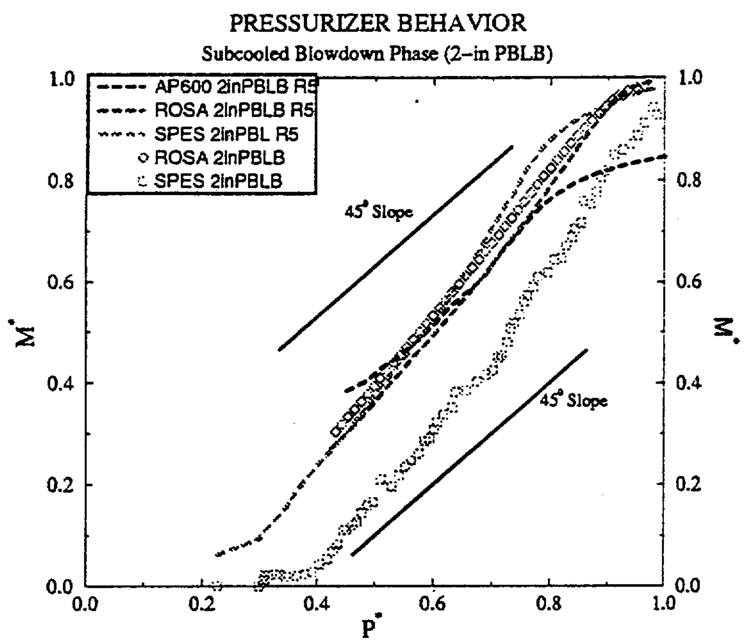

Figure 5-33. Subcooled blowdown sub-phase: normalized pressurizer mass vs. normalized pressure for the 2-in. PBL break scenario.

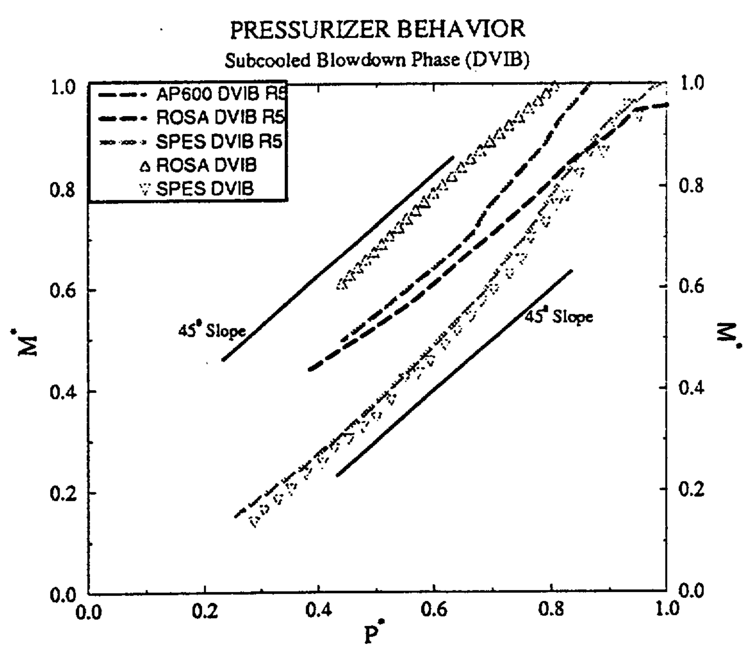

Figure 5-34. Subcooled blowdown sub-phase: normalized pressurizer mass vs. normalized pressure for the DEGB of the DVI line scenario.

The data from Figure 5-31 are quantified in Table 5-9 that shows the slopes of the measured and calculated curves obtained from a linear regression analysis. Here, the scaling theory is represented by a slope of 1.0. The "correlation coefficient" is a measure of the "goodness" of the linear fit, with 1.0 as the ideal. The table also includes the percent deviation between the *theory* and the *data*, and the percent deviation between the *data* and the corresponding RELAP5 *calculations*.

Table 5-9. Quantitative comparison of the M^* vs. P^* slopes for the subcooled blowdown sub-phase.

System and Scenario	Slope	Data Deviation from the Theory [%]	Correlation Coefficient	RELAP5 Deviation from the Data [%]
AP600 1-in. CLB	1.04	4	0.999	
AP600 2-in. PBLB	1.17	17	0.997	
AP600 DVIB	0.99	-1	0.999	
ROSA 1-in. CLB	1.77	77	0.999	
ROSA 1-in. CLB R5	2.00	100	0.999	13
ROSA 2-in. PBLB	1.41	41	0.999	
ROSA 2-in. PBLB R5	1.42	42	0.999	1
ROSA DVIB	1.04	4	0.999	
ROSA DVIB R5	1.37	37	0.998	32
SPES 1-in. CLB	1.20	20	0.998	
SPES 1-in. CLB R5	1.73	73	0.992	44
SPES 2-in. PBLB	1.58	58	0.996	
SPES 2-in. PBLB R5	1.60	60	0.997	1
SPES DVIB	1.09	9	0.998	
SPES DVIB R5	1.42	42	0.997	30

- **Verification of Modeling Assumptions**

Figure 5-31 shows that every test and calculation trace follow essentially the same trend, and specifically the trend expected by the theory. A closer look as offered by the numbers in Table 5-9 shows that a few of the results deviate from the theory beyond the 50% established limit for First Order agreement. A review of our assumptions indicated that, although the dominant $\Pi_{7\text{-}pzr}$ (Table 5-8) was the one associated with break flow, as soon as scram occurs, the net heat balance brings another Π ($\Pi_{8\text{-}pzr}$) into the picture. This lack of balance increases the slope of the traces and its contribution is greater for smaller breaks. The data points out this effect, as the deviation from the theory becomes smaller for larger breaks. Bounding calculations of this effect indicate that the theory (with the inclusion of $\Pi_{8\text{-}pzr}$) is correct. The third column of Table 5-9 is calculated as follows:

$$Deviation_{Data} = (Slope_{Data} - 1) \times 100$$

- **Verification of Data Sufficiency**

  It was noted earlier that the value of the dominant $\Pi_{7\text{-}pzr}$ for AP600 is the same as for the test facilities. Furthermore, the other Πs (such as $\Pi_{8\text{-}pzr}$) for the facilities encompass the corresponding values for the AP600 Πs. Therefore, the data contains, within its range, the expected behavior of AP600.

- **Evaluation of Distortions**

  The examination of the Πs indicates no identifiable distortion large enough to affect the overall ("top-down view") system behavior (same trends are exhibited by all traces in Figure 5-31). Numerical differences between the AP600 slopes and those of the tests are attributable to atypicalities in the steam generators of both facilities and the initial core heat input. Yet, as Figure 5-31 shows, they do not make the behavior of the test results dissimilar.

- **Verification of Integrated Code Behavior**

  The last column in Table 5-9 records the deviation of the slope in the calculation with respect to the slope in the respective test.

$$Deviation_{R5} = \frac{(Slope_{R5} - Slope_{Data})}{Slope_{Data}} \times 100$$

  The results are within our assumed data uncertainty range, ±20% (that translates onto a slope departure range of ±50%), indicating that RELAP5 is representing the phenomena that the facilities are experiencing during this early phase. Furthermore, since the facilities encompass the range expected of AP600, RELAP5 is, therefore, also representing that range of phenomena.

5.3.2.2 ***Intermediate Sub-Phase.*** This is a complex, scenario-dependent, sub-phase that occurs in the three scenarios in slightly different ways. It encompasses the plant behavior after the "S" signal and the energy transfer processes (steam generators, PRHR, and CMT recirculation and draining), as well as the mass transfer processes (break, CMT and accumulator injection, ADS-1 through ADS-3 blowdown), appear, disappear, interact, and compete to dominate the system response. To systematize its analysis, this sub-phase was divided into three periods, based on system configuration and flow paths. Not all of these periods occur in all scenarios, but the overall process of bringing the system down from the end of the subcooled blowdown to ADS-4 actuation still presents strong similarities, from a *top-down* point of view. Figure 5-35 is a schematic representation of the system and its components during this sub-phase. At the onset of the sub-phase, the pressurizer is empty; the steam generators and the PRHR are actively removing heat, and the CMTs have begun to recirculate. During this initial period, the system depressurizes due to the energy transfer to the steam generators and the PRHR, and through the break. This (*Initial blowdown period*) ends when the system reaches saturation, at about the pressure of the secondary, losing the steam generators as a heat sink. The second period begins at this time and the depressurization slows. This slow depressurization (*Middle or recirculation period*) period ends when the net inflow of coolant to the primary is significantly increased by the injection of the accumulators or by the CMTs beginning to drain. The third and last subdivision of this sub-phase (*ADS-123 blowdown period*) begins at this time. The depressurization is accelerated by the incoming cold water and by the opening of first three stages of ADS valves. The period, and the subphase, end when the ADS-4 valves open. Because of the complexity of the intermediate sub-phase, the application of the scaling analysis methodology requires: (1) detailed information regarding the distributions of saturated and subcooled fluids within the reactor coolant system,

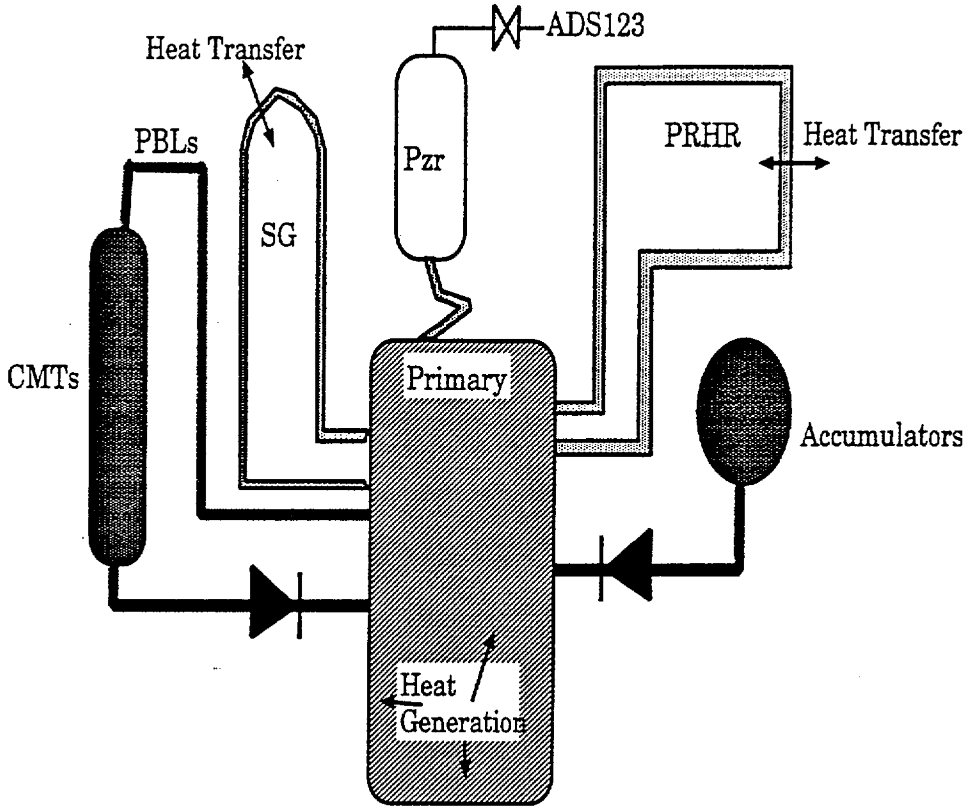

Figure 5-35. System components during the "Intermediate" sub-phase.

(2) numerous assumptions regarding thermodynamic variables, and (3) that integrals of certain thermodynamic functions be evaluated in order to determine the reference parameters and perform the order of magnitude analysis. The scaling methodology report[5-16] analyzed this phase in detail for the 1-in. CLB scenario. With this approach, the intermediate subphase is evaluated through investigations of the total reactor coolant system inventory (1-α) as a function of normalized system pressure. Figure 5-36 shows the results of this investigation for the calculations and measurements from the three experimental facilities and the calculation for AP600 for the 1-in. CLB accident scenario. The pressure is normalized as follows:

$$P^{*} = \frac{P_{max} - P}{P_{max} - P_{0\text{-}ADS4}} \tag{7}$$

$P_{0\text{-}ADS4}$ is the reference value (theory) of system pressure for the ADS-4 blowdown sub-phase. This is an *externally* calculated value, based on our modeling of the system for the purposes of scaling analysis. P_{max} is the system's pressure at the beginning of this phase.

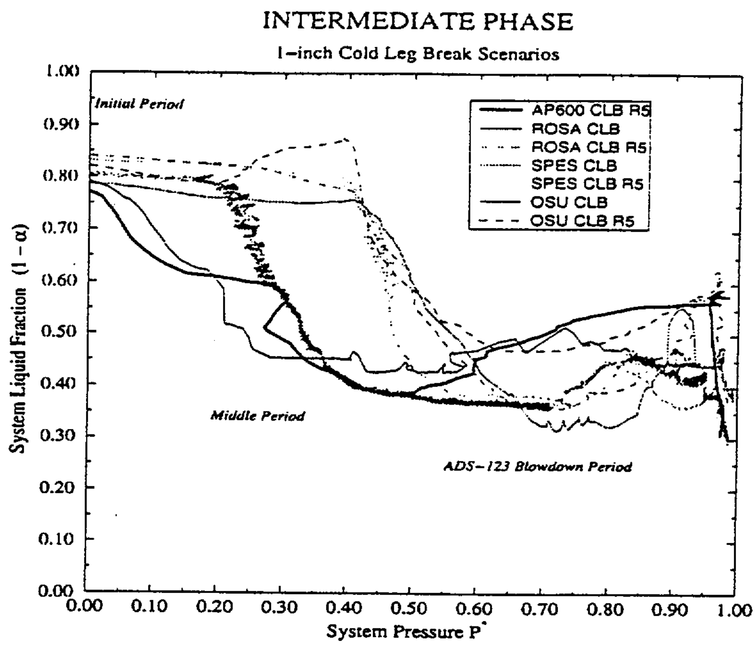

Figure 5-36. Key system performance parameters ((1-α) vs. P^*) during the entire Intermediate sub-phase.

However, the scaling methodology report analysis for the 1-in. CLB accident scenario also indicated that the developments and complex interactions during the intermediate sub-phase have little effect on the system conditions present at the beginning of the next sub-phase (ADS-4 blowdown) or on the SBLOCA PIRT figure of merit (minimum reactor vessel inventory). As a result, a simplified scaling applications approach was justified and used to evaluate the intermediate sub-phase for the remaining accident scenarios. The simplified approach represents the reactor coolant system as a large control volume with a break into containment and investigates the "reserve mass", M_r, the reactor coolant system inventory residing above the elevation of the break. A normalized reserve mass, M_r^*, is defined as the reserve mass as a fraction of its initial value at the beginning of the intermediate sub-phase.

Figure 5-37 shows the results using the simplified scaling approach corresponding to the detailed approach results in Figure 5-36. The initial, middle and ADS-123 blowdown periods are more evident in the plotted results using the simplified approach. There is an initial period of pressure loss without much mass loss; ADS-1 opens and the mass loss matches the pressure loss; ADS-3 opens and the mass drops "faster". The figure shows how the effect of accumulator injection is not perceived in the higher regions of the system. The key variables shown in Figure 5-36 are consistent with the variables used in the methodology development report.[5-16] The application, however, of the two-field model developed for this was found not to be practical. Therefore, the application scaling report[5-17] uses the variables in Figure 5-37 with the simplified model to analyze this sub-phase. Figure 5-37 indicates similarity between the responses of the different facilities for the 1-in. CLB, and this is true of the other scenarios as well. Note that because of the way in which the pressure has been normalized, the event sequence proceeds left to right in this figure, with $P^* = 1.0$ corresponding to the point where ADS-4 is actuated.

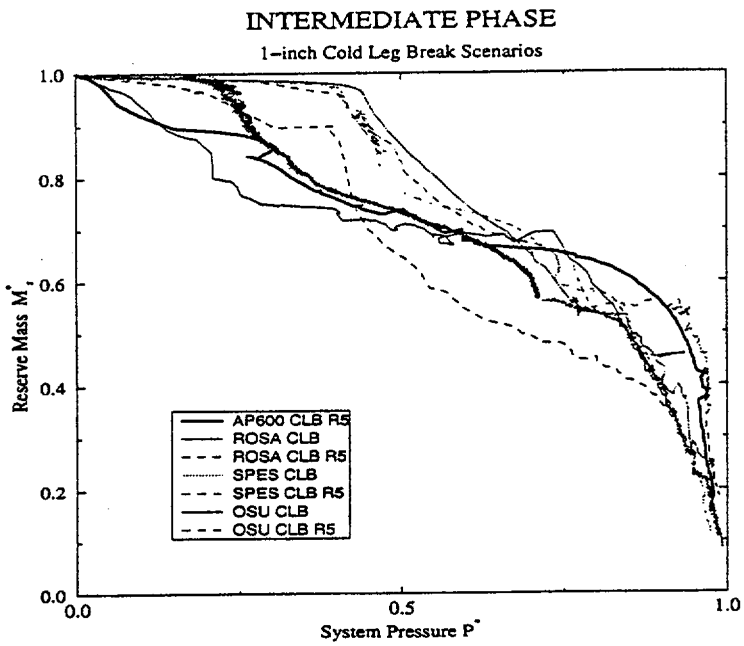

Figure 5-37. Normalized liquid mass above the loops vs. normalized pressure during intermediate sub-phase, for the 1-in. CLB scenario.

Unlike other sub-phases, the intermediate sub-phase does not lend itself to easy verification of the theory. The numerical estimates of Π_2 in Table 5-10 do suggest that AP600 (represented in the plot by a RELAP5 calculation) and ROSA will have a larger initial slope (as they do), while SPES will remain flatter. Table 5-10 shows that this situation does not change significantly during the *middle* or recirculation period. OSU comes into the picture at the beginning of the second period.[g] In the last period, the slope of mass loss with respect to system pressure is expected to be flatter yet. What the traces show is an initial loss of pressure at constant mass, due to energy transfer (SGs, PRHRs, CMTs); followed, in the middle period, by a loss of pressure and mass. (This is actually a relatively long period of time after the SGs are isolated.) In the last period, there is a loss of pressure and some mass through the ADS Stages 1 and 2; the mass lost, however, is replenished by the accumulators, which actually increases the liquid fraction in the system, until ADS-3 actuation and accumulator emptying bring the system down to the conditions at ADS-4 opening. The analysis of the ADS-4 phase assumes that these conditions are quite the same for all scenarios, regardless of their prior history. The traces in Figure 5-36 support that assumption.

g The early portions of OSU data and calculation are included in the plot for convenience of the construction of the plot. OSU was not designed to represent the early depressurization of AP600, and its transients begin at about the time that saturation is reached in the primary.

Table 5-10. Values of the relevant Πs throughout the intermediate sub-phase for the 1-in. CLB scenario.

Initial Period					
Π	**AP600**	**ROSA**	**SPES**	**OSU**	**Physical Interpretation**
Π_2	0.04	0.02	0.14	N/A	Ratio of pressure change due to change in specific energy of subcooled field from heat transfer to the reference pressure
Middle (CMT/PRHR Recirculation) Period					
Π	**AP600**	**ROSA**	**SPES**	**OSU**	**Physical Interpretation**
Π_2	0.11	0.12	0.53	0.06	Ratio of pressure change due to change in specific energy of subcooled field from heat transfer to the reference pressure
ADS-123 Blowdown Period					
Π	**AP600**	**ROSA**	**SPES**	**OSU**	**Physical Interpretation**
Π_3	14.8	15.6	17.8	40.5	Ratio of pressure change due to change in specific energy of saturated field from mass inflows to the reference pressure

- **Verification of Modeling Assumptions**

The system pressure is dominated by the energy and mass transfer. These two processes compete and at times alternate control of the depressurization. Both transfer processes are quite difficult to measure in the experiments and particularly in this sub-phase. Analysis of the tests indicates that the theory can offer an explanation for the observed behavior. Yet, assumptions made about mass and energy distribution in the system cannot be accurately confirmed. One can also readily observe in Figures 5-36 and 5-37 that the assumption that the liquid fraction is a function only of pressure is not always true (there are multivalued loops in all of the traces), but on the average (from beginning to end of the sub-phase), all traces do follow a "similar" path, and they all end at about the same liquid fraction in the non-dimensional space.

- **Verification of Data Sufficiency**

Table 5-10 shows that the magnitude of the evaluated Πs for the test facilities contain the values evaluated for the plant; except in the case of Π_3 in which AP600 is slightly outside of the estimated range. The tests results cover a wide variety of slopes, and despite their differences, the final *state* of the system is similar for all of them. One can say that the data is, therefore, sufficient, with the same reservations made for the assumptions (it shows depressurizations from the operating pressure of the system to the theoretical value at ADS-4 actuation, while all systems lose and gain the same proportion of liquid coolant). Figures 5-36 and 5-37 show the close agreement amongst the traces at near the ADS-4 actuation point and that the AP600 calculation generally is contained within the envelope of the test data. Table 5-11 lists the quantitative results depicted in Figure 5-36 (and in analogous figures for the other scenarios[5-17]) and evaluates the deviation from the theory, represented by the ADS-4 initial pressure, and the deviation between tests and calculations.

Table 5-11. Numerical values of ADS-4 conditions in nondimensional space coming out of the intermediate sub-phase, corresponding deviations with respect to theoretical assumptions, and the deviation of the RELAP5 calculations.

1-inch CLB Scenario							
	AP600 (R5)	**ROSA**	**ROSA (R5)**	**SPES**	**SPES (R5)**	**OSU**	**OSU (R5)**
P*	0.974	0.993	0.989	0.987	0.975	0.937	0.939
(1-α)	0.308	0.375	0.366	0.287	0.307	0.446	0.576
P Deviation from the theory (%)	2.6	0.7	1.1	1.31	2.5	6.3	6.1
RELAP5 Deviation in P* from the data (%)			-0.403		-1.21		0.213
RELAP5 Deviation in α from the data (%)			-2.45		6.97		29.15
2-inch PBL Break Scenario							
	AP600 (R5)	**ROSA**	**ROSA (R5)**	**SPES**	**SPES (R5)**	**OSU**	**OSU (R5)**
P*	0.990	0.959	0.987	0.992	0.973	0.995	1
(1-α)	0.361	0.413	0.371	0.330	0.425	0.413	0.5
P Deviation from the theory (%)	1.0	4.1	1.3	0.8	2.7	0.5	0
RELAP5 Deviation in P* from the data (%)			2.92		-1.92		0.50
RELAP5 Deviation in α from the data (%)			-10.1		29.1		21.2
DEGB of the DVI Scenario							
	AP600 (R5)	**ROSA**	**ROSA (R5)**	**SPES**	**SPES (R5)**	**OSU**	**OSU (R5)**
P*	0.944	0.921	0.950	0.930	0.915	0.943	0.905
(1-α)	0.277	0.274	0.302	0.177	0.151	0.34	0.320
P Deviation from the theory (%)	5.6	7.93	5	7	8.48	5.7	9.5
RELAP5 Deviation in P* from the data (%)			3.18		-1.59		-4.03
RELAP5 Deviation in α from the data (%)			10.2		-14.9		-5.76

- **Evaluation of Distortions**

From a "top-view" approach, this is as difficult and involved as the verification of the modeling assumptions. Local values of heat transfer are not "typical" of AP600; however, these atypicalities were compensated for and in the overall picture did not prevent the facility from producing the expected result (the proper intermediate sub-phase end point conditions, at ADS-4 actuation).

- **Verification of Integrated Code Behavior**

  RELAP5 represented the ranges of phenomena seen in Figures 5-36 and 5-37 in each facility. There are local differences, but the "shapes" of the traces indicate that RELAP5 covered the range well. A quantitative comparison of P^* and α for tests and the corresponding calculations (Table 5-11) yielded errors between -2.5% and 29%. Note that even the 29% is within our ±50% criterion for First Order agreement.

5.3.2.3 ADS-4 Blowdown Sub-Phase. The ADS-4 blowdown sub-phase begins when the ADS Stage 4 valves open and continues until the RCS pressure declines sufficiently to allow the onset of IRWST injection flow. During ADS-4 blowdown, the only source of coolant to the RCS for replenishing the vessel inventory is the liquid remaining in the CMTs. Based on the dominant system equations, the scaling analysis variables selected for this phase are:

- The CMT level, and

- The reactor vessel inventory.

The governing equations describing the behavior of these variables are presented in Reference 5-17 and are derived in Reference 5-16. These equations represent the time rates of change of these variables. In the scaling theory, the ADS Stage 4 mass flow is evaluated using the Homogeneous Equilibrium Model (assuming constant upstream pressure and flow quality).

For several reasons, scaling of this sub-phase for the DVILB scenario was significantly different from the CLB and PBLB scenarios. In the DVILB scenario, the break flow area is large and is comparable to the ADS flow area; this is not the case for the other scenarios. For the DVILB scenario, the affected CMT drains quickly and activates ADS-4 early as compared with the other scenarios. As a result, in the DVILB scenario, one of the CMTs remains full of water, even up to the beginning of this sub-phase, while in the other scenarios, both CMT levels are low. During this sub-phase, the vessel inventory is rising (due to CMT injection) in the DVILB scenario, but is falling in the other scenarios. In addition, the ECCS injection capability (accumulators and CMTs) is degraded for the DVILB scenario but not for the others. Finally, scaling of this sub-phase for the PBLB scenario differed moderately from the CLB scenario because the location of the break in the PBLB scenario slows the draining process in the affected CMT. As a consequence of this, the two types of scenarios have different numerical values for the dominant Πs and are treated differently.

Figures 5-38, 5-39, and 5-40, respectively, show schematics of the system configurations during the ADS-4 blowdown sub-phase for the CLB, PBLB and DVILB scenarios. The nondimensional groups used in the governing equations, their values for each facility and their physical interpretations are listed in Table 5-12 for the CLB and PBLB scenarios. For the DVILB scenario, the values for some of the nondimensional groups are different, as shown in Table 5-13. The scaling analysis for this sub-phase verified that the data were collapsed. Examples illustrating this verification are provided here; full documentation is provided in Reference 5-17.

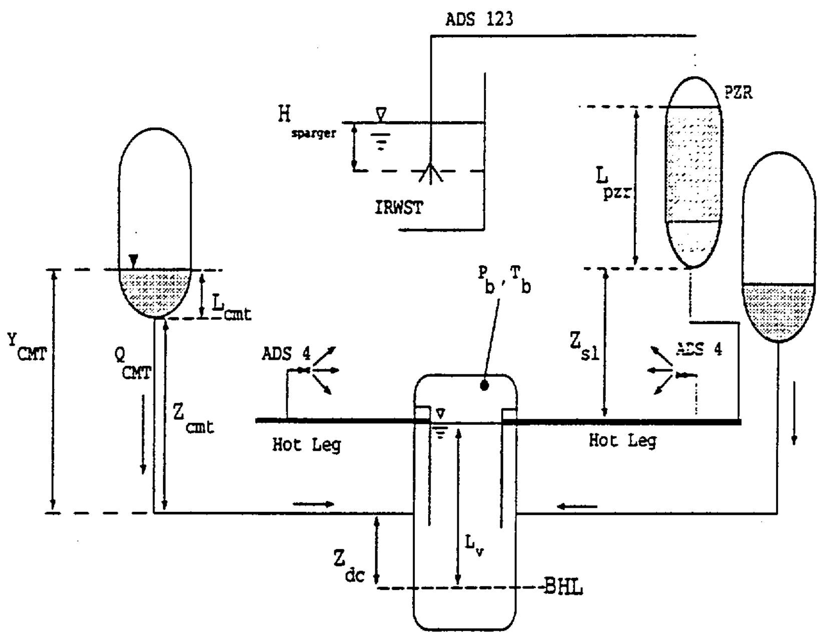

Figure 5-38. ADS-4 blowdown sub-phase: schematics and important components for a CLB scenario.

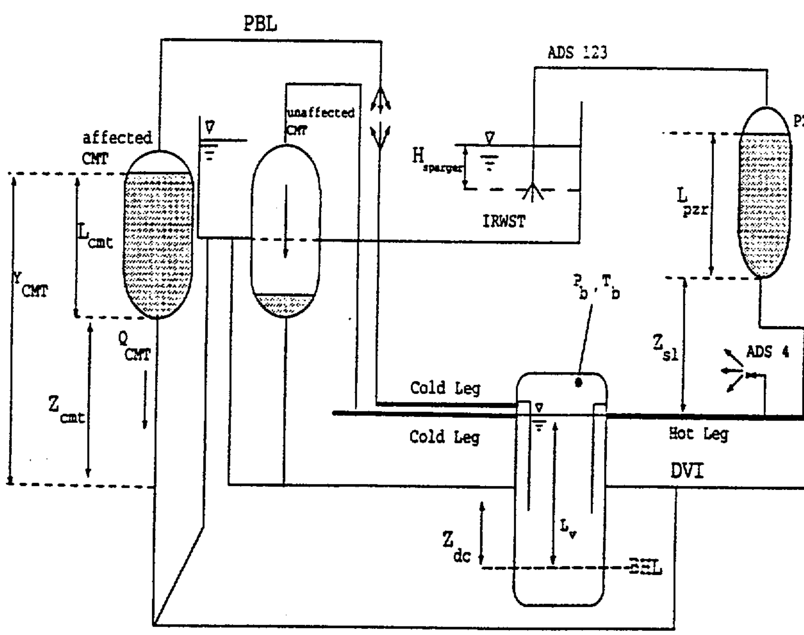

Figure 5-39. Schematic description of the system configuration at the beginning of ADS-4 blowdown for the pressure balance line break scenario.

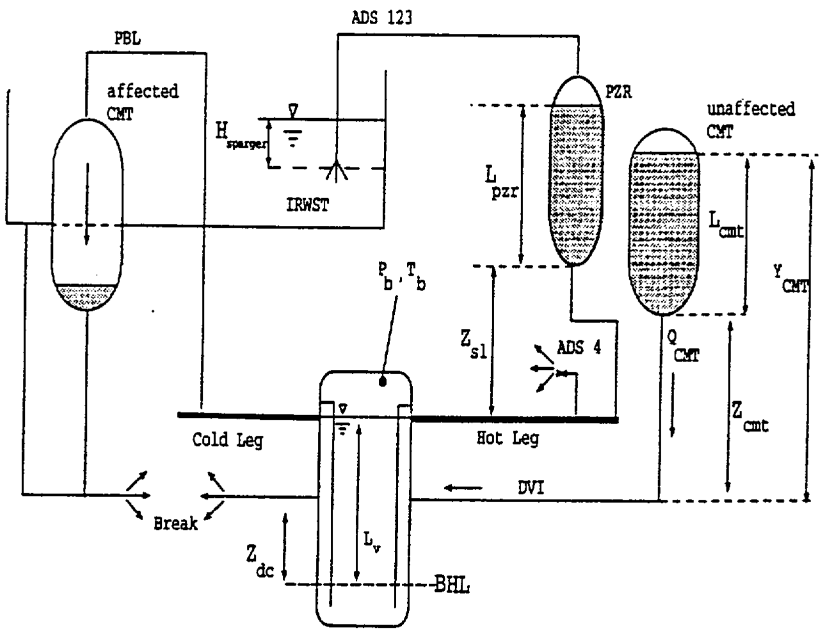

Figure 5-40. Schematic description of the system configuration at the beginning of ADS-4 blowdown for the DVILB scenario.

Table 5-12. Numerical values of the nondimensional coefficients in the ADS-4 blowdown sub-phase dominant equations for the 1-in. CLB and 2-in. PBLB scenarios.

Coefficient	AP600	ROSA	SPES	OSU	Physical Interpretation
$\Pi_{7-vessel}$	1.0	1.0	1.0	1.0	Nondimensional rate of vessel draining
$\Pi_{15-cmt}\Pi_{17-cmt}$	1.63	1.94	0.69	0.75	Nondimensional CMT draining rate
Π_{16-cmt}	1.16	2.00	0.56	0.90	Fraction of CMT flow over the system out-flow

Table 5-13. Numerical values of the nondimensional coefficients in the ADS-4 blowdown sub-phase dominant equations for the DEGB of the DVI scenario.

Coefficient	AP600	ROSA	SPES	OSU	Physical Interpretation
$\Pi_{7-vessel}$	1.0	1.0	1.0	1.0	Nondimensional rate of vessel draining
$\Pi_{15-cmt}\Pi_{17-cmt}$	0.45	0.53	0.21	0.40	Nondimensional CMT draining rate
Π_{16-cmt}	0.75	1.19	0.40	0.48	Fraction of CMT flow over the system out-flow

- **Verification of Modeling Assumptions**

  - CMT level Figure 5-41 shows the CMT draining responses for the 1-in. diameter CLB tests and calculations. This figure presents the integral of the CMT level rate equation; the normalized CMT level is shown as a function of the integral of the square root of the CMT head. The figure also shows the expected slope of the traces based on the scaling theory. The data are shown to behave quite well. The traces for the measured and calculated data are nearly-straight lines and the lines for the theory and measured test data are nearly parallel. This indicates that the theory is correct because it captures the dominant features of the processes observed in the test. The lines for the calculations of the tests also are nearly parallel with the theory, indicating the code well represents the phenomena captured by the test.

  - Vessel Inventory Figure 5-42 shows the vessel inventory responses for all of the 1-in. diameter CLB tests and calculations. For ideal agreement, the traces should lie on a 45° line. The lines bounded by arrows in the figure indicate the portions of the test data over which comparison with the theory held valid. Table 5-14 quantifies the vessel level responses from the scaling analyses for the results shown in Figure 5-42. This table shows the slopes of the measured and calculated data as obtained from a regression analysis. The scaling theory is represented by a slope of 1.0; the deviation in the slope of the data from the theory is shown in Column 4 of Table 5-14, and Column 5 shows the deviation of the calculation from the tests. The "correlation coefficient" is a measure of the linearity, with a coefficient of 1.0 the ideal. The figure displays First Order agreement between the theory, test data, and calculations. The irregularities in the tests caused by oscillatory pressurizer and other interactions are the causes of the numerical deviations shown in the table. The figure shows that the theory is supported by the test data when the latter are smoothed.

- **Verification of Data Sufficiency**

  Tables 5-12 and 5-13 show that the dominant nondimensional coefficients of AP600 are contained within the range of numerical values exhibited by the test facilities.

- **Evaluation of Distortions**

  None of the known sources of facility distortions were observed to result in atypical behavior. The oversized ADS-4 valves in SPES were handled within the scaling tools.

- **Verification of Integrated Code Behavior**

  Figures 5-41 and 5-42 display First Order agreement between the calculations and test data when compared in the scaling context for the ADS-4 blowdown sub-phase. In addition, divergences between the scaling theory and test data are well simulated with RELAP5.

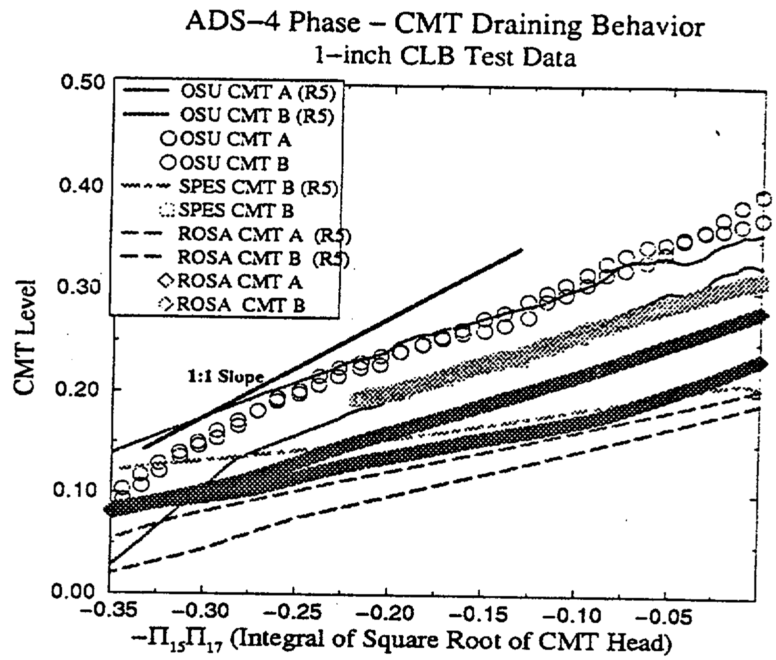

Figure 5-41. ADS-4 blowdown sub-phase CMT level equation results for 1-in. CLB.

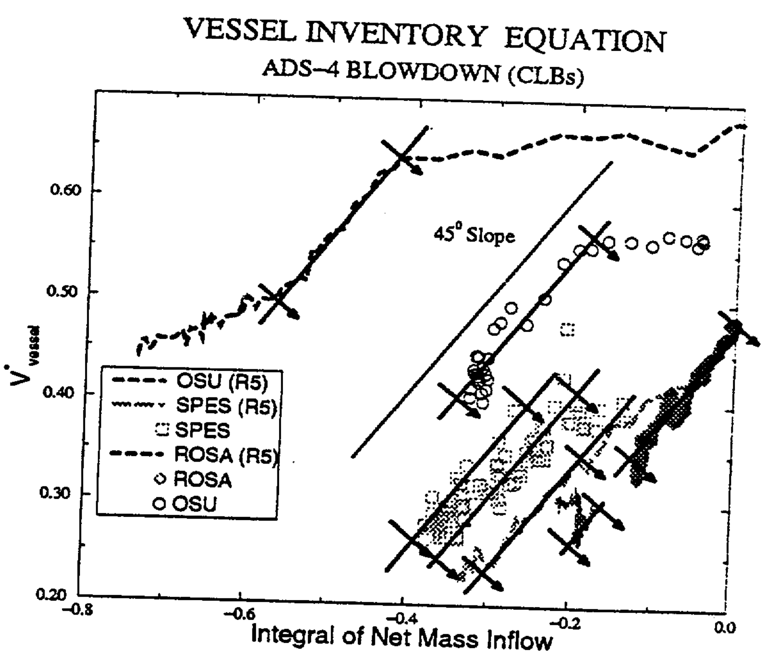

Figure 5-42. Plot of the relationship between vessel liquid inventory and the net inflow during the ADS-4 blowdown sub-phase of the 1-in. CLB scenario.

Table 5-14. Quantitative evaluation of agreement between vessel inventory traces and the expected theoretical behavior, via linear regression, for the ADS-4 blowdown sub-phase.

Scenario	Slope	Correlation Coefficient	Deviation from Theory	RELAP Deviation from Data
		1-inch. CLB		
AP600 R5	0.660	0.990	-34	
ROSA R5	1.152	0.980	15	10
ROSA	1.051	0.934	5	
SPES R5	0.630	0.891	-37	-59
SPES	1.540	0.820	54	
OSU R5	0.470	0.950	-53	-40
OSU	0.780	0.991	-22	
		2-inch PBL break		
AP600 R5	0.630	0.975	-37	
ROSA R5	-0.220	-0.516	-122	214
ROSA	-0.070	-0.079	-107	
SPES R5	0.620	0.960	-38	82
SPES	0.340	0.863	-66	
OSU 5R	0.040	0.113	-96	33
OSU	0.030	0.392	-97	
		DEGB of the DVI		
AP600 R5	-0.070	-0.268	-107	
ROSA R5	0.458	0.841	-54	35
ROSA	0.340	0.557	-66	
SPES R5	0.100	0.756	-90	-66
SPES	0.290	0.187	-71	
OSU 5R	0.003	0.037	-99	-100
OSU	-2.020	-0.759	-302	

5.3.2.4 IRWST Injection Sub-Phase. The IRWST injection sub-phase begins with the onset of flow from the IRWST into the RCS. This occurs when the RCS pressure becomes lower than the IRWST head. For the purposes of the scaling analysis, the period investigated was assumed to end with the refilling of the vessel up to the level of the hot legs. During this sub-phase, cold water from the IRWST floods the downcomer and core, reducing core boiling and altering the condition of fluid leaving the RCS through the ADS-4 valves. Both vessel and pressurizer levels may oscillate during the beginning of this sub-phase. At the initiation of this sub-phase, the pressurizer level is of about the same elevation as the IRWST water level; the contents of the pressurizer slowly drain into the hot leg.

The scaling analysis variable selected for the IRWST injection sub-phase is reactor vessel inventory. The governing equation describing the behavior of this variable is presented in Reference 5-17 and is derived in Reference 5-16. This equation represents the time rate of change of the variable. In the theory, the ADS Stage 4 mass flow is evaluated using either the Homogeneous Equilibrium Model (assuming constant upstream pressure and flow quality) or a friction-dominated model. The pressurizer vapor-space pressure is assumed to be a constant boundary condition. Because of timing considerations, the theory also assumes that the IRWST appears to the RCS as an imposed pressure boundary condition. The DVI line component is represented as an algebraic relationship between head difference across it and the flow rate through it.

As in the prior sub-phase, scaling of the IRWST injection sub-phase for the DVILB scenario was different than for the other two scenarios. The DVI break flow area is large and is comparable to the ADS flow area; this is not the case for the other scenarios. In addition, the IRWST injection capability is degraded in the DVILB scenario but not in the others.

Figure 5-43 shows a schematic of the system configuration during the IRWST injection sub-phase for the CLB and PBLB scenarios. Figure 5-44 shows the system configuration for the DVILB scenario. The nondimensional groups used in the governing equations, their values for each facility and their physical interpretations are listed in Table 5-15 for the CLB and PBLB scenarios and in Table 5-16 for the DVILB scenario. The scaling analysis for this sub-phase verified that the data were collapsed. Examples illustrating this verification are provided here; full documentation is provided in Reference 5-17.

Table 5-15. Numerical values of the relevant Πs of the IRWST injection sub-phase dominant equations for the CLB and PBLB scenarios.

Πs	AP600	ROSA	SPES	OSU	Physical Interpretation
$\Pi_{7\text{-vessel}}$	1.0	1.0	1.0	1.0	Nondimensional rate of vessel filling
$\Pi_{1\text{-dvi}}/\Pi_{3\text{-dvi}}$	2.00	1.49	1.96	4.79	Ratio of pressure forces over friction forces in the line
$\Pi_{16\text{-dvi}} = \rho_l Q_{dvi}/\dot{m}_0$	1.57	1.52	1.53	1.01	Ratio of DVI flow over total net inflow
$\Pi_{16\text{-sl}} = \rho_l Q_{sl}/\dot{m}_0$	0.24	0.16	0.53	0.22	Ratio of surge line flow over total net inflow

Table 5-16. Numerical values of the relevant Πs for the IRWST injection sub-phase dominant equations for the DEGB of the DVILB scenario.

Πs	AP600	ROSA	SPES	OSU	Physical Interpretation
$\Pi_{7\text{-vessel}}$	1.0	1.0	1.0	1.0	Nondimensional rate of vessel filling
$\Pi_{1\text{-dvi}}/\Pi_{3\text{-dvi}}$	1.97	1.49	1.97	4.79	Ratio of pressure forces over friction forces in the line
$\Pi_{16\text{-dvi}} = \rho_l Q_{dvi}/\dot{m}_0$	2.20	2.10	2.60	1.80	Ratio of incoming flow over total net inflow
$\Pi_{16\text{-sl}} = \rho_l Q_{sl}/\dot{m}_0$	1.40	1.10	3.80	0.60	Ratio of surge line flow over total net inflow

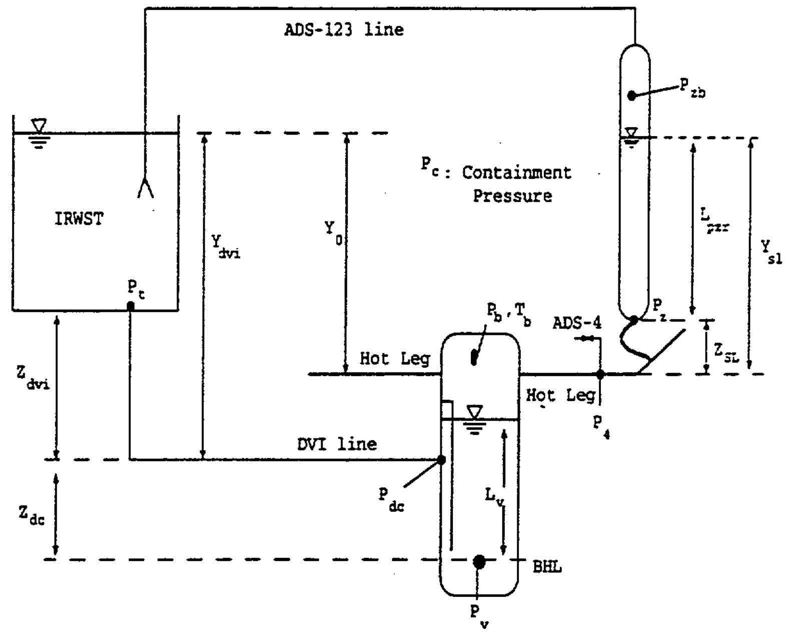

Figure 5-43. Schematic description of the system configuration during the IRWST injection sub-phase for the CLB and PBLB scenarios.

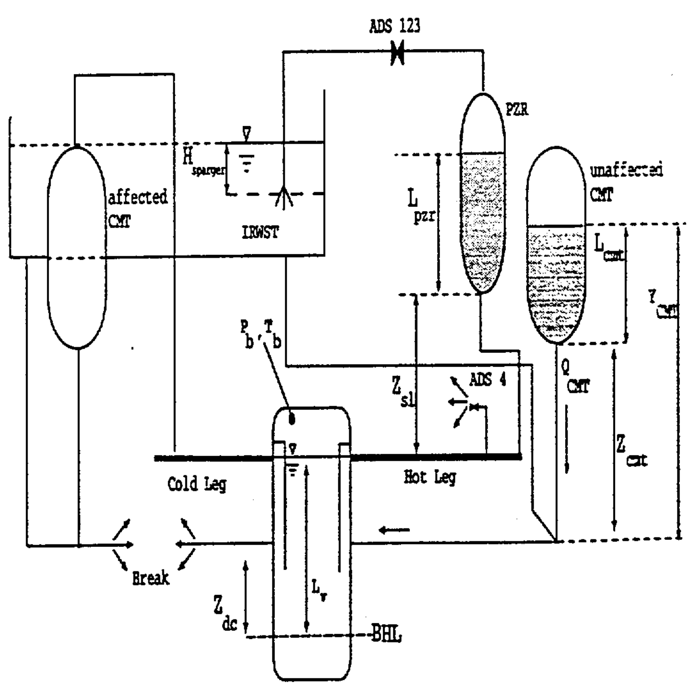

Figure 5-44. Schematic description of the system configuration at the beginning of the IRWST injection sub-phase for the DVILB scenario.

- **Verification of Modeling Assumptions**

The vessel inventory responses during the IRWST injection sub-phase of all 1-in. diameter CLB tests are shown in Figure 5-45. This figure compares the normalized vessel inventory against the net vessel mass inflow. The slopes of the test data and the RELAP5 calculations are compared against the theory. Table 5-17 shows for all three accident scenarios the numerical values of these slopes along with deviations in percent for the theory and the RELAP5 calculations. As shown in the Figure 5-45, overall the test data are quite noisy. The noise is caused because the net reactor vessel inflow is a small-valued parameter that is calculated as the difference between two large-valued parameters. The noise is more apparent in Figures 5-46 and 5-47 that show detailed views of the same data for the ROSA and SPES tests, respectively. The usefulness of the data needed for the scaling comparison thus is limited because of instrument uncertainty and measurement noise in all of the test facilities. An additional factor is that the measured data channels needed to make the comparisons often are discontinuous, as evidenced by a more detailed view of the ROSA comparison. The ADS-4 mass flow measurement is based upon catch-tank readings and the catch-tank is periodically drained and refilled, leading to the repetitive looping appearance of the ROSA test data trace. These factors complicate both the quantitative and qualitative comparisons between the data and theory. The scaling analysis concluded that the general qualitative trends of the test data support the scaling theory for the IRWST injection sub-phase. However, the data appear to indicate that the scaling theory assumption that the ADS-4 upstream conditions (and therefore ADS-4 mass flows) are constants is a weak one, and this weakness leads to the divergences noted between the scaling theory and the measured and calculated data.

In summary, the scaling analysis for the IRWST injection sub-phase showed that the assumptions made to model the behavior of the important components were valid and that the results can be used to analyze and compare the trends among the various facilities.

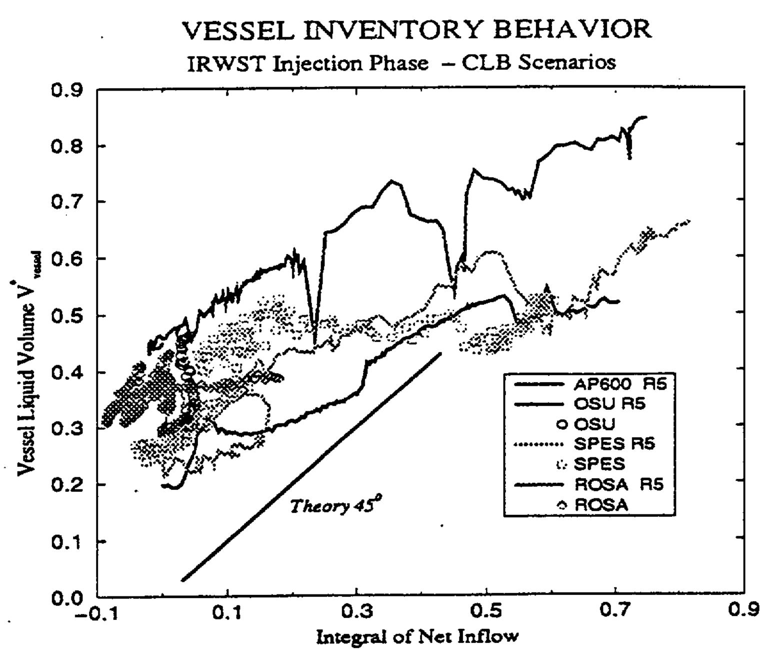

Figure 5-45. Plot of the relationship between vessel volume and net inflows during the IRWST sub-phase of the 1-in. CLB scenario.

Table 5-17. Quantitative evaluation of agreement between vessel inventory traces and the expected theoretical behavior, via linear regression, for the IRWST injection sub-phase.

Trace	Slope	Regression Coefficient	Deviation from Theory [%]	RELAP5 Deviation from Data [%]
1-inch CLB				
AP600	0.54	0.946	-46	
ROSA (R5)	0.83	0.552	-17	196
ROSA	0.28	0.498	-72	
SPES (R5)	0.45	0.933	-55	50
SPES	0.30	0.749	-70	
OSU (R5)	0.47	0.958	-53	151
OSU	-0.91	0.163	-191	
2-inch PBL break				
AP600	0.36	0.921	-64	
ROSA (R5)	0.05	0.641	-95	0
ROSA	0.05	0.365	-95	
SPES (R5)	0.31	0.939	-69	7
SPES	0.29	0.715	-71	16
OSU (R5)	0.26	0.623	-74	
OSU	0.31	0.727	-69	
DEGB of the DVI				
AP600	0.03	0.162	-97	
ROSA (R5)	0.61	0.745	-39	916
ROSA	0.06	0.328	-94	
SPES (R5)	0.39	0.980	-61	179
SPES	0.14	0.963	-86	
OSU (R5)	0.39	0.891	-61	50
OSU	0.26	0.993	-74	

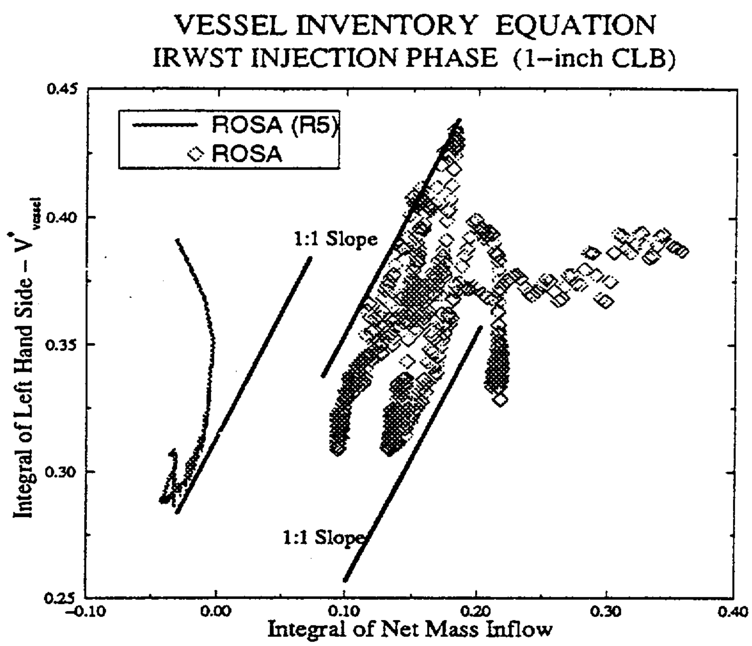

Figure 5-46. Detail of the relationship between vessel volume and net inflows during the IRWST sub-phase of the ROSA 1-in. CLB scenario.

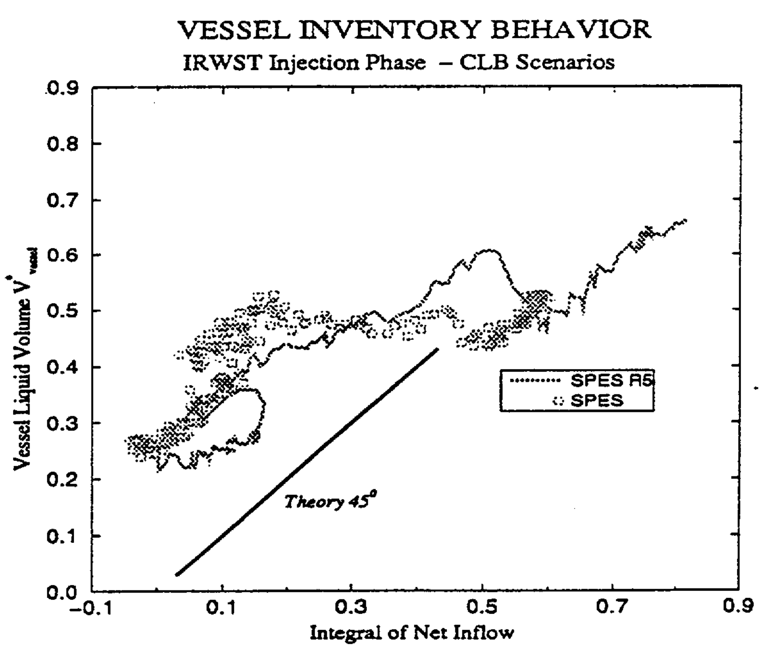

Figure 5-47. Detail of the relationship between vessel volume and net inflow during the IRWST injection sub-phase of the SPES 1-in. CLB scenario.

- **Verification of Data Sufficiency**

  As shown in Tables 5-15 and 5-16, with only one exception, the nondimensional group values (Πs) for AP600 are bounded by those of the other facilities. The exception is for the ratio of DVI line flow to total net inflow, $\Pi_{16\text{-}dvi}$ for the CLB and PBLB accident scenarios. This exception is not considered significant because: (1) the AP600 value lies only slightly outside the range of the experiments, (2) the AP600 value is conservative with respect to the range of the experiments (because the vessel refills slightly faster in the plant than in the experiments), and (3) the Π values shown are for a nominal case with failure of 25% of the ADS-4 capacity and the composite experimental data base includes certain ROSA experiments (where the ADS-4 capacity has been reduced to 50%) with a much higher Π value.

- **Evaluation of Distortions**

  None of the known sources of facility distortions were observed to result in atypical behavior. The oversized ADS-4 valves in SPES were accounted for within the scaling tools.

- **Verification of Integrated Code Behavior**

  Table 5-17 quantifies the "error" in the RELAP5 calculation with respect to its experimental counterpart. However, because of noise and instrumentation uncertainties, these comparisons are not reliable and therefore Figures 5-46 and 5-47 more clearly show that the RELAP5 calculations follow closely the behavior (in terms of slopes) of the tests. RELAP5 is seen to represent the different phenomena that dominate this sub-phase, including those that the scaling analysis theory neglected in the beginning and end of the sub-phase.[h]

A variable-by-variable comparison of data, theory, and calculations was performed and the results show that the scaling approach captures the most dominant processes in its nondimensional equations and coefficients defined for the different sub-phases. Using these coefficients, we are also able to conclude that the data base is sufficiently large to contain the expected AP600 range of dominant phenomena. The direct comparison of data with their corresponding RELAP5 calculations in nondimensional space indicates that the code represents the phenomena of relevance to predict AP600 behavior.

5.3.3 Top-Down Scaling Analysis Results for the SBLOCA Long-Term Phase

For the scaling analysis of the SBLOCA long-term phase, the sub-phases were defined as follows:

- IRWST draining: starts with IRWST injection and ends when the IRWST level has declined sufficiently to open the sump recirculation valves.

- Long-term cooling: starts when the sump recirculation valves open (allowing equalization of the IRWST and sump levels) and continues thereafter.

h In the beginning of this sub-phase, the inflow into the vessel may still oscillate between the IRWST, the CMTs, and the accumulators; the scaling theory assumes that only the IRWST is injecting liquid into the system. At the end of the phase, the level in the vessel reaches the hot leg and increases no further, therefore flattening the trace and departing from the 45° slope. RELAP5 is seen to represent this behavior.

The reactor vessel inventory, which is the SBLOCA PIRT primary figure of merit, reaches a second minimum during the long-term cooling sub-phase. However, the minimum achieved in the long-term phase is above that achieved before or shortly after the onset of IRWST injection during the short-term phase.

The phenomena and variables selected for scaling analysis of the long-term phase are listed in Table 5-18. The measured and calculated experimental data used for this analysis are summarized in Section 5.2 and are presented in more detail, along with the calculated data for AP600, in Reference 5-15.

Table 5-18. Variables selected for the scaling analysis of the SBLOCA long-term phase.

Sub-phase of the SBLOCA Long-Term Phase	Analysis Variables Selected
IRWST draining	DVI line mass flow IRWST level
Long-term cooling	Vessel inventory

The scaling methodology report[5-16] documents the eight-step procedure developed for the IRWST draining and long-term cooling sub-phases. Reference 5-17 documents the application of this methodology for these two sub-phases in 1-in. diameter CLB, double-ended DVILB and 2-in. diameter PBLB accident scenarios. This reference also documents application of the methodology for a fourth scenario, inadvertent opening of ADS Stage 1.

As was discussed for the short-term phase, the scaling analysis found that the system configurations and timings of events for the long-term phase are sufficiently different to warrant considering the DVILB scenario separately from the other two scenarios. Unlike the short-term phase, however, experimental data covering the long-term phase is available only from only one facility, APEX at OSU. Therefore, for the long-term phase, the sufficiency and relevancy of the data is judged based on evaluation of the deviation of results between AP600 and OSU, rather than on the inclusion of the AP600 results within the envelope of results for the ROSA, SPES and OSU facilities, as was done for the short-term phase.

The remainder of this section summarizes the results (from Reference 5-17) of the scaling analysis covering the two sub-phases of the SBLOCA PIRT long-term phase for the three accident scenarios.

5.3.3.1 IRWST Draining Sub-phase. This sub-phase starts with the beginning of IRWST injection.[i] Injection into the RCS lowers the level in the IRWST, reducing its driving head and thereby reducing the injection rate. Flow exits the RCS primarily through the ADS-4 valves. Eventually, the IRWST level reaches the setpoint where the sump recirculation valves are opened, allowing the sump and IRWST levels to equalize. This event marks the end of this sub-phase. The system configuration pertinent for the IRWST draining sub-phase of the 1-in. CLB and 2-in. PBLB accident scenarios is shown in Figure 5-48. The system configuration pertinent for the DVILB scenario is similar, with the exceptions that: (1) because one of the DVI lines is ruptured, the IRWST is free to drain directly into the sump through the broken DVI line and (2) the break is relatively large and located below the cold leg elevation.

i It is important to note that the way this sub-phase is defined, it overlaps the IRWST Injection sub-phase described in Section 5.3.2.4. In this case, however, we are examining a much longer time scale than before.

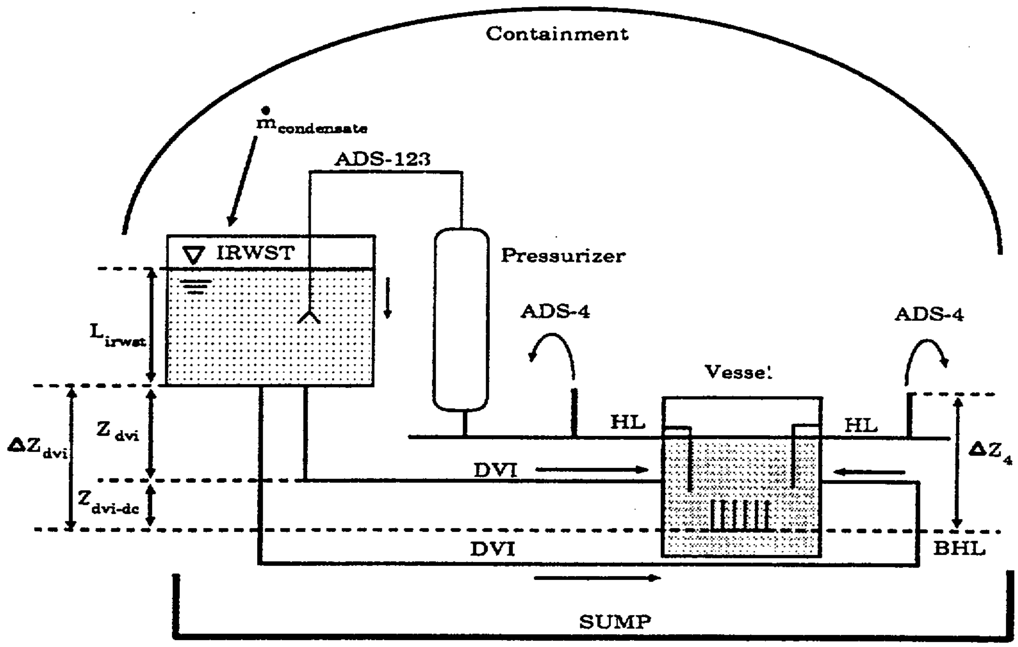

Figure 5-48. System configuration during IRWST draining (prior to sump injection).

The scaling analysis variables selected for this sub-phase are DVI line mass flow rate and IRWST level. The governing equations for these variables are presented in Reference 5-17 and details regarding their development are provided in Reference 5-16. The equations describe these variables in terms of nondimensional groups and reference parameters. The scaling theory assumes that, at the beginning of this sub-phase, the pressurizer has emptied and the vessel level is at the elevation of the hot legs. In this summary, we will focus on the DVI line mass flow response.

The theory also assumes a quasi-steady condition: (1) the ADS-4 steam flow is fully condensed on the containment shell and returned to the IRWST, (2) this steaming and condensation rate is small in relation to the DVI line flow rate, (3) wall heat transfer changes relatively slowly and therefore may be considered as a constant boundary condition, (4) the ADS-4 fluid quality is the same as that at the core exit, and (5) the RCS inflow rate at the DVI line equals the outflow rate through the ADS-4 (plus the break for the case of the DVILB accident scenario). The nondimensional groups used in the equations, their values for AP600 and the OSU facility, and their physical interpretations are listed in Table 5-19. The values of all Πs for AP600 are near the corresponding values for OSU experiments. The last column in the table compares the plant and facility Πs as a ratio.

Table 5-19. Relevant Π ratios in the IRWST draining sub-phase.

CLB and PBLB Scenarios				
Nondimensional Coefficients	**AP600**	**OSU**	**Physical Interpretation**	Π_{OSU} / Π_{AP600}
$\Pi_{2-ads4} / \Pi_{2-dvi}$	0.63	0.58	Ratio of ADS-4 to DVI line manometric heads	0.92
$\frac{\Pi_{3-dvi} + \Pi_{3-ads4}}{\Pi_{2-dvi}}$	0.37	0.42	Ratio of friction forces to available head	1.14
Z^{*}_{dvi}	0.43	0.40	Nondimensional DVI line head	0.93
DVILB Scenario				
$\frac{\Pi_{3-dvi} + \Pi_{3-ads4}}{\Pi_{2-dvi}}$	1.0	1.0	Ratio of friction forces to available head	1.0
Z^{*}_{dvi}	0.114	0.104	Nondimensional DVI line head	0.91

- **Verification of Modeling Assumptions**

The test data and RELAP5 calculations for the tests and AP600 accidents of the CLB and PBLB scenarios are compared against the DVI mass flow scaling equation in Figure 5-49. The calculated data are seen to be much more oscillatory than the measured data; the causes for these oscillations are discussed in Section 5.2.2. The data from this figure, along with those for the DVILB scenario, are quantified in Table 5-20. The table shows the slopes of the measured and calculated curves obtained from regression analysis. The correlation coefficient is a measure of the linearity of the curves, with 1.0 the ideal. The figure and table both show first order agreement between the measured data and the scaling theory, thus verifying the theory. The figure and table also show first order agreement between the smoothed calculated data and the measured data in the context of the nondimensional scaling comparison.

Table 5-20. Quantitative comparison of the slopes shown by the head-flow traces in experiments and calculations during the IRWST draining sub-phase.

System and Scenario	Slope	Data Deviation from the Theory (%)	Correlation Coefficient	RELAP5 Deviation from the Data (%)
		SBLOCA Scenarios		
OSU CLB	0.69	-31	0.7035	
OSU PBL	0.56	-44	0.5297	
OSU IADS	0.70	-30	0.7092	
OSU CLB (R5)	0.82	-18	0.5346	17
OSU PBLB (R5)	1.36	36	0.8667	142
AP600 CLB (R5)	1.03	3	0.6491	
AP600 PBLB (R5)	1.54	54	0.8800	
		DVIB Scenario		
OSU DVIB	1.18	18	0.9638	
OSU DVIB (R5)	1.77	77	0.9322	50
AP600 DVIB (R5)	0.82	18	0.9417	

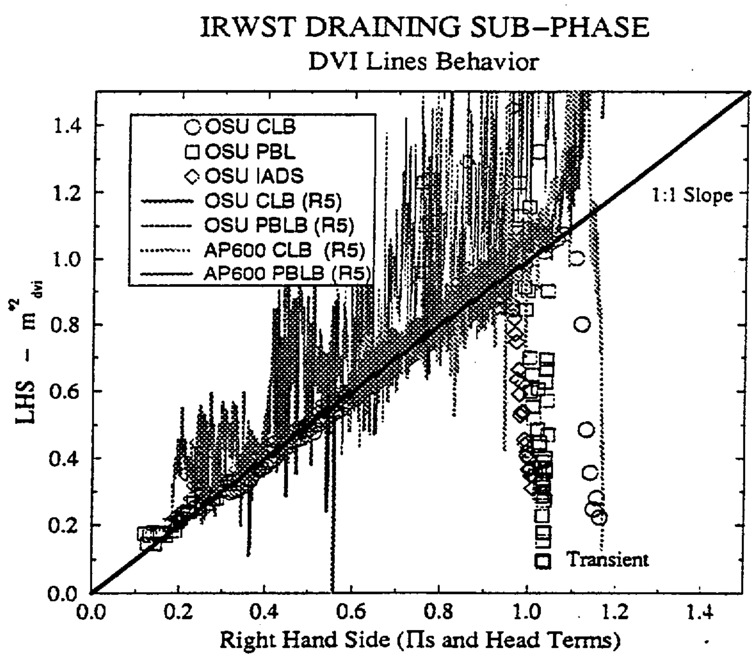

Figure 5-49. Plot of the relationship between mass flow through the DVI lines and the available head, in nondimensional space for the CLB and PBLB scenarios.

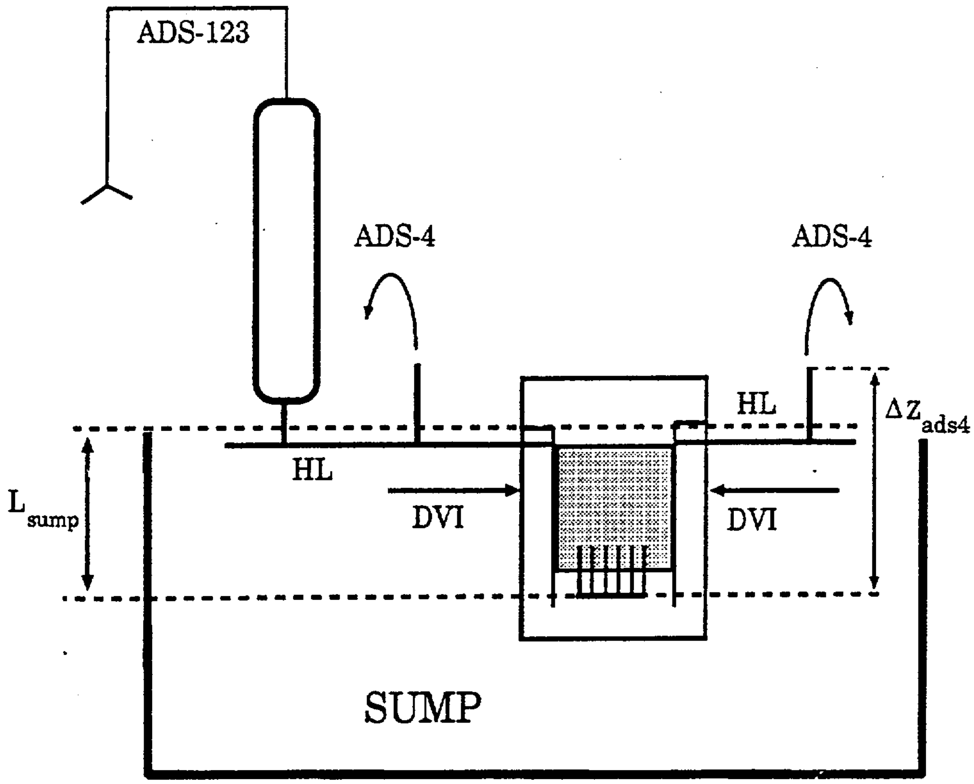

Figure 5-50. System configuration during long-term cooling sump injection.

- **Verification of Data Sufficiency**

  The experimental data are sufficient because all relevant Π ratios for the OSU experiments are within about 14% of those for AP600, as shown in Table 5-19. Furthermore, existing variations in the test configurations, such as failure of a smaller or larger percentage of ADS-4, vary these coefficients in ways that include the nominal AP600 situation. Thus, even though we only have one facility to represent this phase of the transient, variations in the configurations among the OSU tests make up for the absence of ROSA and SPES tests.

- **Evaluation of Distortions**

  No behavior is observed in the experimental responses for this sub-phase that is significantly atypical of AP600. This was expected because this is a very simple sub-phase and the experiment (OSU) was specifically designed to represent it. The OSU facility includes representations of the AP600 containment sump and containment normally non-flooded (dead-end) rooms. The OSU primary and secondary sump tanks, respectively, represent these regions. The facility does not represent the condensation processes on the inside of the AP600 containment shell nor the return of condensate to the IRWST. However, this distortion is not significant because the ADS-4 flow quality is low.[5-15] As a result, the steam flow rate to the containment and, therefore, the condensate return rate to the IRWST is only a small fraction of the total DVI line flow rate.

- **Verification of Integrated Code Behavior**

  Table 5-20 lists the deviation of RELAP5 calculations from the respective tests in nondimensional space. The results show First Order agreement between calculation and data. Note that wherever the data deviated from the theory, so did the calculation. The effect of lower order phenomena, neglected by the theory, are captured by the RELAP5 calculations.

In summary, the scaling assumptions were verified and we used them to collapse the data. The data includes the expected *top-down* behavior of AP600. There was no evidence of distortions affecting the behavior of the facility. Quantitative comparisons between code and test data show that the code represents the dominant phenomena well.

5.3.3.2 Long-Term Cooling Sub-Phase. This phase begins when the sump starts to participate in the process; the system configuration is shown in Figure 5-50. There is a brief initial transition period in which the IRWST and sump equalize levels and become a single pool. This sump is not *draining* its contents into the primary system, as was the case for the IRWST, but the fluid is rather recirculating between the primary system and the sump. The quasi-steady state that results can be seen as an extrapolation of the equations in the previous sub-phase, in which certain parameters and relations have changed. However, this sub-phase is actually a little more complex because it includes the containment dynamic contributions to the process (for example, the heat capacitance of the concrete and metal structures, the storage of water as a film throughout the containment surfaces, and the heat transfer to the walls in the tank, etc.). None of the test facilities represent the AP600 containment and, therefore, there is no data to analyze which would include the containment. The scaling applications analysis evaluates equations for the system quasi-steady state at the long-term cooling end condition. These equations are for the system (DVI line and ADS-4) mass flow rate, the system outlet quality, the hot-side (core, hot leg and ADS-4) density and reactor vessel inventory. The analysis leads to evaluation of nondimensional reactor vessel mass at the end condition as the primary indication of the system steady state. Table 5-21 shows the results of the analysis; the nondimensional vessel mass for the OSU facility is within 2% of that for AP600, thereby indicating verification of the data sufficiency. No experimental distortions, other than the aforementioned containment-related ones, are seen to be significant. The code capabilities for simulating the end condition are discussed in Section 5.2.

Table 5-21. Relevant nondimensional parameters for the long-term cooling sub-phase.

Nondimensional Parameter	AP600	OSU	Physical Interpretation	Π_{OSU} / Π_{AP600}
M^*_{ss}	0.358	0.352	Nondimensional vessel inventory	0.98

5.3.4 Bottom-up Scaling Analysis

This section summarizes the bottom-up scaling analyses performed to complement the top-down scaling analysis approach. Section 5.3.4.1 discusses the methodology, Section 5.4.3.2 discusses CMT draining behavior, and Section 5.4.3.3 discusses oscillatory IRWST injection behavior. These analyses are fully documented in Reference 5-18.

5.3.4.1 ***Bottom-up Scaling Analysis Methodology and Data Evaluation***. The data base from the three AP600 integral test facilities is extensive. On average, more than a dozen transient tests are available from each facility. The typical transient test in the ROSA/AP600[5-1] and SPES-2[5-2] facilities may last two to three hours; in the OSU/APEX[5-3] facility, the typical test may last seven or more hours. The instrumentation is sampled frequently (at 0.2 to 2 Hz) and the number of data channels ranges from several hundreds to thousands. This means that the overall data base extends to several gigabytes of information. Thus, the general supply of information is almost overwhelming. Paradoxically, when a particular process is identified and investigated, there can be a dearth of information available to identify the mechanisms of that process.

An efficient methodology must be laid out which is comprehensive, as well as capable of providing detailed information on the specific phenomena occurring. It is easy to get lost in a sea of phenomena, not all of which are of equal importance for the system as a whole. Therefore, triage is in order. "Comprehensive" means that all the data base should be scanned for similar phenomenological behavior. The large amount of information requires the identification of a relatively simple figure of merit, which can be extracted from the data base with a reasonable effort for all transients. However, the selection of a figure of merit must clearly convey the occurrence of the various phenomena under investigation.

The process of identifying the figure of merit and its use in the determination of similar phenomenological occurrences is called pattern recognition. This pattern recognition process goes on to outline the consistencies and differences among the various transients. If the selection of the figure of merit is effective and if the transients are sufficiently diverse, then it follows that the various phenomena will be observed in some transients and will be absent in others. Further, one can also consider the intensity and duration of each event (as deduced by the values and variations of the figure of merit) to refine the classification of specific phenomenologies among the various transients. With this set of observations summarized in tabular form, the pattern recognition process is completed.

The next step in the data evaluation methodology is the mechanistic explanation. The pattern recognition process identifies the relevant players in the phenomena of concern. A component (or a set of components) is usually identified as the core of the action associated with a specific phenomenon. Note that, most of the time in integral facilities, there are complex system interactions. However, usually it is reasonably easy to focus the attention on the major players while setting temporarily aside those components that (while nonetheless contributing to the phenomena) are not absolutely necessary to the occurrence of the observed phenomenon or to the understanding of the detailed mechanism.

This "sorting out" process is fundamental in the quest for the mechanistic explanation. In fact, the guiding principle should be the search for the simplest explanation of the process. Once the core of the process has been identified, it is easy to fit all the other subordinate pieces to it in a complementary manner. It is not very efficient to try to solve the puzzle with all the pieces at once, since the effort is too cumbersome and most of the time inconclusive. It is far better to proceed with small system subsets in an iterative mode, which allows for periodically revisiting the overall picture in order to verify how all the various interactions fit together.

Assuming that a simple subset of the overall system has been identified as the core of the phenomenological action, there are a variety of tools that investigators may use to prove or disprove their theories. The objective is to construct causal relationships between the various signals associated with the thermal-hydraulic behavior of a component or of a set of components.

The analysis of precursors is one of the most effective tools used to establish causal relationships between events. It is based on the comparison of the trace variations. In particular, it points out the temporal shifts between related traces (e.g., an inflow and an outflow, or a level and a pressure).

As an example, consider the changes in the discharge flow at an orifice and the associated change in the upstream pressure. The analysis of the precursors could be used to establish if the upstream pressure changes as a result of an increase in the liquid fraction at the discharge orifice or if the flow increases in response to an increase in upstream pressure. This information can be validated with voidage and level measurements in the proximity of the discharge orifice, and the final determination can then be made as to the causal relationship between flow and pressure.

The magnitude of the various signals is not paramount in this type of analysis provided that the signal variation is large compared to the signal noise or interferences. Care should be exercised in the study of the spatial relationships between instruments and in the assessment of the effect of capacitances and resistances on the original signal (e.g., the presence of a catch tank or the position of a flow meter in a line may introduce time delays in the detected flow response). There might be other considerations based on experience and phenomenological insight that are equally valuable in the pursuit of the mechanistic explanation of the phenomena.

When a mechanistic explanation is obtained that can explain all the transients observed, the last step of the methodology can be performed. The objectives of the last step are: (1) to determine the applicability of the phenomena observed in the facility(ies) to the AP600 prototype and (2) to determine the importance of the phenomena vis-à-vis safety.

The first objective is usually met by considering the mechanistic explanation especially when there is evidence that the phenomena are linked to components which are nonexistent at the prototypical scale (e.g., collection systems, separators and valves). If the observed phenomena cannot be conclusively related to facility atypicalities and a clear case cannot be made that they will not be present in the prototype, then the phenomena observed in the integral facility(ies) are considered to be plausible for the prototype. In these situations, a scaling analysis becomes necessary.

The second objective of this last step is also addressed by scaling considerations. In some cases, these considerations are limited to simple, inventory-bounding estimates which can be used to satisfy the reactor vessel inventory requirement. Simple inventory considerations or scaling analyses based on energy considerations or nondimensionalization of the complete set of conservation statements may be necessary to properly rank the phenomena of concern within the AP600 PIRT framework.

The data evaluation process is integrated with the PIRT. Therefore, the phenomena identification coincides with the first objective of this step, while the second objective complements the expert judgment on which the PIRT is originally based. For AP600 SBLOCA, the overall criterion guiding the ranking process is the reactor vessel inventory.

In general the scaling effort is also characterized within the hierarchical two tier scaling methodology framework.[5-19] This framework identifies a top-down and a bottom-up approach to scaling. This is not inconsistent with the previous description of the last step of the methodology. The mechanistic explanation identifies a core component or set of components where the key events controlling a specific phenomenon take place. This information is needed for the bottom-up scaling formulation.

The top-down or system-level scaling is pursued independently from the experimental evidence and is based on the dimensional analysis of the system governing equations. By "dimensional analysis" we mean the nondimensionalization of the conservation statements followed by order-of-magnitude considerations to rank the various terms in order of importance. Each term of the equations relates to specific phenomena. Therefore, by ranking the terms, one also generates information which must be integrated into the AP600 PIRT.[5-14]

It is necessary to identify a hierarchical level which bounds the top-down scaling effort. The complexity of system interactions must be incorporated in the top-down scaling. Therefore, it was decided to extend this scaling effort down to the component level and to match it with bottom-up scaling considerations which are limited to the specific component (or a set of components) as previously described.

The third step of the methodology is linked to the identification of the facility distortions and to the evaluation of their effect on the overall system behavior. It is most efficient to proceed from the PIRT phenomena and rankings to the facility distortions rather than in reverse. One approaches the data initially with certain suspicions based on preconceived views relating to facility distortions and their possible effects and proceeds accordingly. In identifying seemingly-obvious distortions in a facility and studying their effect on the system behavior one may find that: (1) the specific distortion may be irrelevant to the system behavior in portions of the transient and (2) there are other, less obvious, distortions that may play a far more significant role in a given portion of a transient.

For completeness, it is always possible to summarize the overall effect of a specific "obvious" facility distortion once all other effects are quantified within the methodology described here. To use an analogy, provided many keys and many doors, it is far more practical to ask which key will open the door of primary interest, rather than trying to define which door each key might open.

Figure 5-51 depicts the methodology flow diagram within the overall code validation process. Figure 5-52 describes the iterative paths to the PIRT, and to the experimental program and the code analyses associated with the local (bottom-up) and system (top-down) level scaling. In Figure 5-53, the linkages between the various items in Figure 5-52 and the overall advanced light-water reactor (ALWR) thermal-hydraulic research plan are identified to relate the methodology to the overall research effort. Two examples illustrating this process follow: CMT draining and oscillatory IRWST injection.

5.3.4.2 CMT Draining. In this section, the phenomena of the events leading to the CMT draining are described.

Discussion

As will be seen, the onset of draining is controlled by a number of equally important parameters. A strong distinction can be made between the processes leading to initiation of CMT draining based on break size. For small breaks (circular breaks with diameters on the order of 1 in. or less), the initiation of draining is difficult to predict. There is a long period of recirculation and heating of the CMTs. For larger breaks (2 in. or more), the process is more straightforward. The recirculation period is short and draining begins when the primary system mass is lost to the point at which the cold leg begins to uncover and steam enters the pressure balance line (PBL).

To further complicate the issue for small breaks, the potential for CMT draining is present for a long period of time. Minor offsets of the delicate balance between flashing, subcooling, and heat losses cause a liquid level to form in the CMT. Conclusions will be drawn as to the scalability and predictability of the CMT behavior in the integral facilities and in the prototype for relatively large and small breaks.

The phenomena associated with the onset of draining in the CMTs are complex and are caused by combinations of equally-important events. According to the data evaluation methodology, the first step is to consider the patterns associated with all transient types in the three experimental facilities. At first, the picture that emerges is not consistent because: (1) the timing of onset of draining varies and (2) the conditions present in the CMT at the onset of draining can differ even for similar transients.

The CMT recirculation process takes place in all three facilities when the CMT outlet valve is open. This is a single-phase natural circulation process, which has the interesting feature of thermal stratification within the CMT; warm water slowly flows into the CMT on top of the cold water that is already there. The temperature gradient between these two water masses is very sharp at first and then it gradually broadens. The wall heat transfer and local mixing effects are the most interesting aspect of this process.

Wall heat transfer and local mixing are important for determining the vertical temperature gradient. At the onset of CMT draining the water low in the CMT is still at its initial cold temperature. Therefore, the heated zone resulting from recirculation is still completely contained within the CMT. The recirculation gradually lowers the position of the thermal center, which may affect the natural circulation flow rate.

Earlier RELAP5 code versions overestimated this mixing because of unphysical numerical diffusion. The calculated temperature of the fluid leaving the bottom of the CMT was too high and this affected the overall system behavior. From the beginning of the ALWR research program, this issue was anticipated. Steps were taken to incorporate into RELAP5/MOD3 a thermal stratification model to alleviate this problem and Version 3.2.1.2 contains this model.

We now consider the conditions leading to the onset of CMT draining. We will compare the behavior of ROSA/AP600 and SPES-2 and then show how OSU/APEX comprises both of these behaviors. Figures 5-54 and 5-55, respectively, show the CMT temperature profiles for experiments in ROSA/AP600 and SPES-2. The saturation temperature is shown at the top of each plot. Temperature indications from vertical rakes containing thermocouples located in the center of the CMTs also are shown. Note the advancement of the thermal front downward, as the warm water progressively reaches lower locations in the CMT. The onset of draining is identified by the arrow in both plots.

The different temperature trace patterns in the two plots are due to different processes associated with the draining. The onset of CMT draining and level formation in ROSA/AP600 is due to flashing of the water inside the CMT while the PBL is filled with liquid. In SPES-2, the level formation is due to inflow of vapor from the PBL, which is voided. These two draining mechanisms bound the possible range of behavior and will be referred to as "draining by flashing" and "draining by inflow," respectively.

As mentioned earlier, OSU/APEX encompasses both behaviors within the same test. Figure 5-56 shows the temperature traces for CMT2 which exhibit a periodic flashing/condensation pattern. This pattern is similar to the ROSA/AP600 behavior where the level formation is due to internal flashing. The difference here is that cold water from the PBL is able to recondense the vapor periodically, thus refilling the CMT. The PBL is filled with liquid in this case. Figure 5-57 illustrates the behavior in CMT1 for the same OSU/APEX test. Here, a pattern of draining by inflow is observed. Note that the same temperature jump observed in the SPES-2 traces is present here. This indicates that vapor is flowing into the CMT through the PBL.

Figure 5-58 illustrates the different behavior observed in the two CMTs for this OSU/APEX experiment. It is possible for both mechanisms to coexist in the same facility at the same time, as can be seen from the two CMT level traces. This asymmetrical CMT behavior is related to break location. The results shown in these figures relate an OSU/APEX test representing a break located on the top of the cold leg that connects to the PBL for CMT1. Examination of other OSU/APEX transients where the break is on the bottom of the cold leg connecting to the PBL of CMT1 reveals somewhat similar behavior.

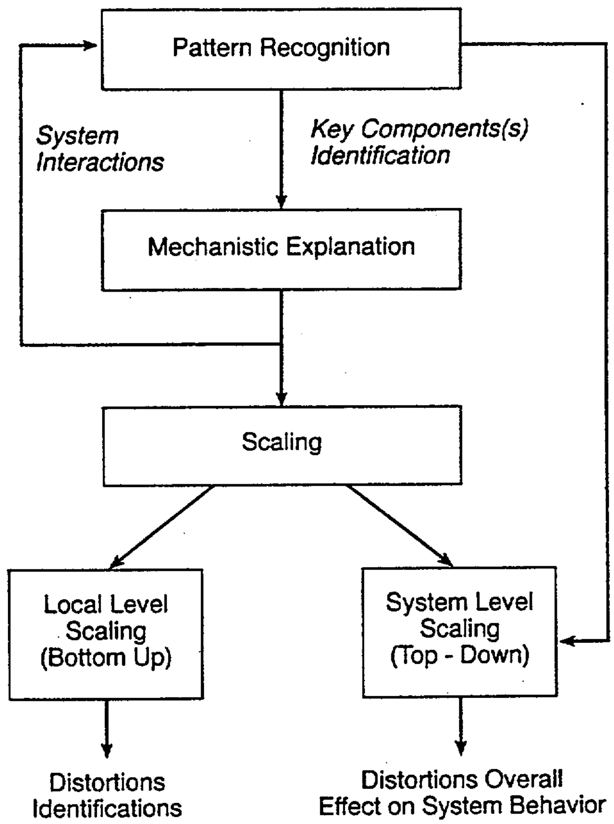

Figure 5-51. Scaling methodology flow diagram.

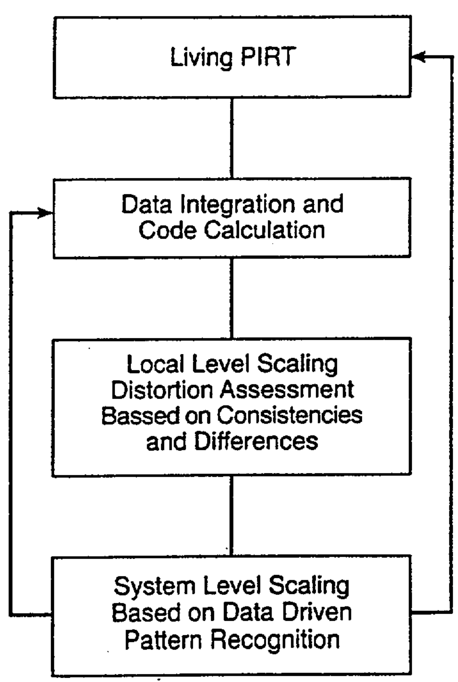

Figure 5-52. Interactions between PIRT, bottom up scaling and top-down scaling.

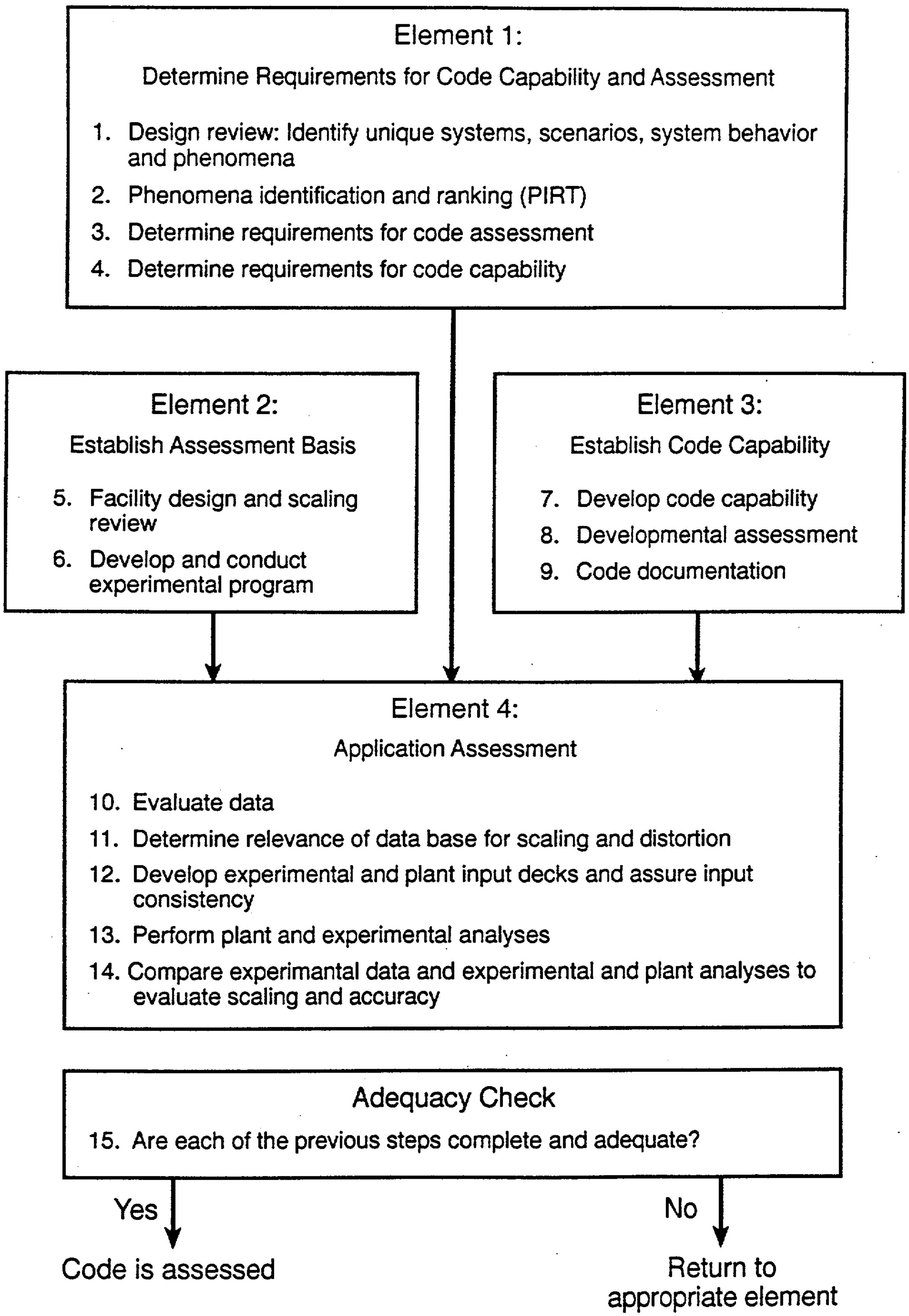

Figure 5-53. PIRT and scaling methods in the context of the ALWR research plan.

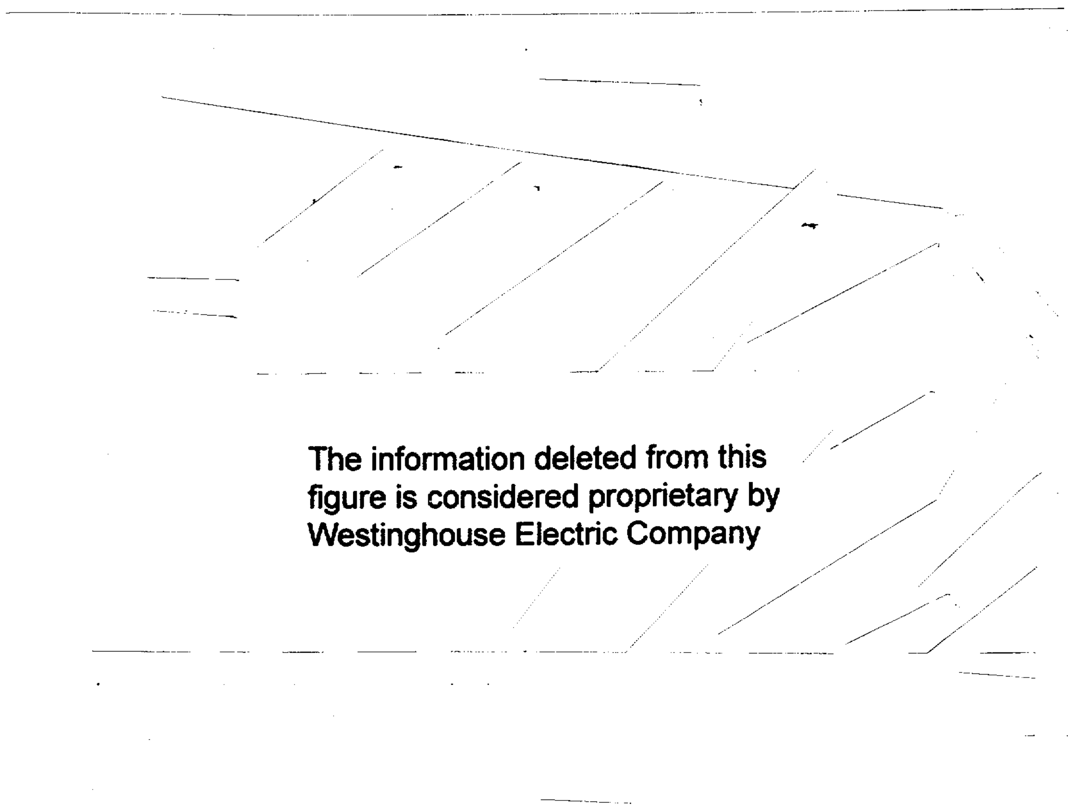

Figure 5-54. CMT thermal profile response during a ROSA/AP600 experiment.

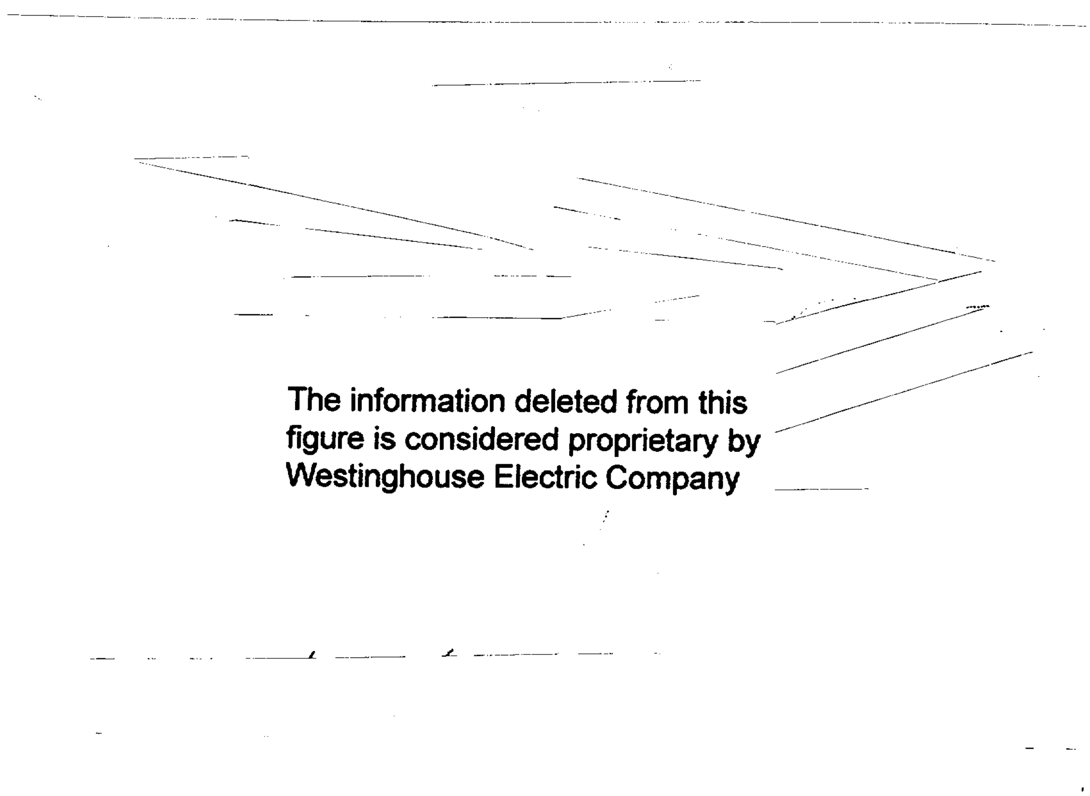

Figure 5-55. CMT thermal profile response during a SPES-2 experiment.

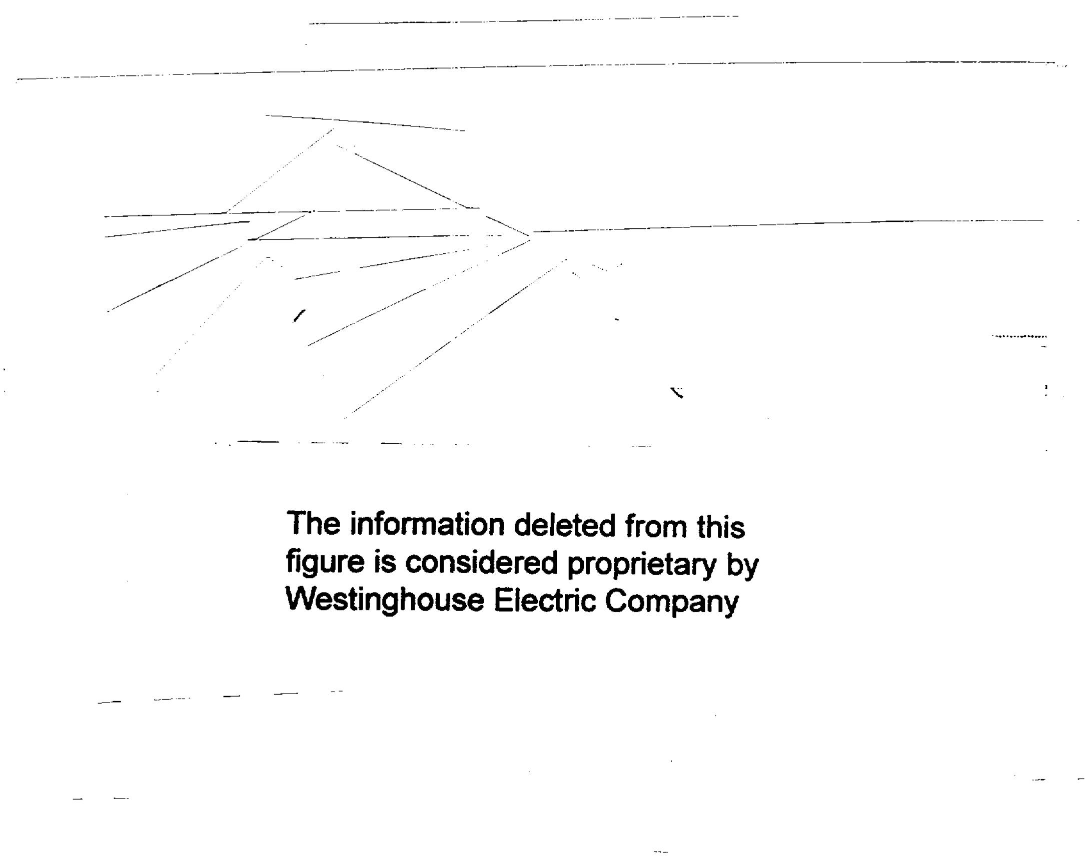

Figure 5-56. CMT2 thermal profile response during an OSU/APEX experiment.

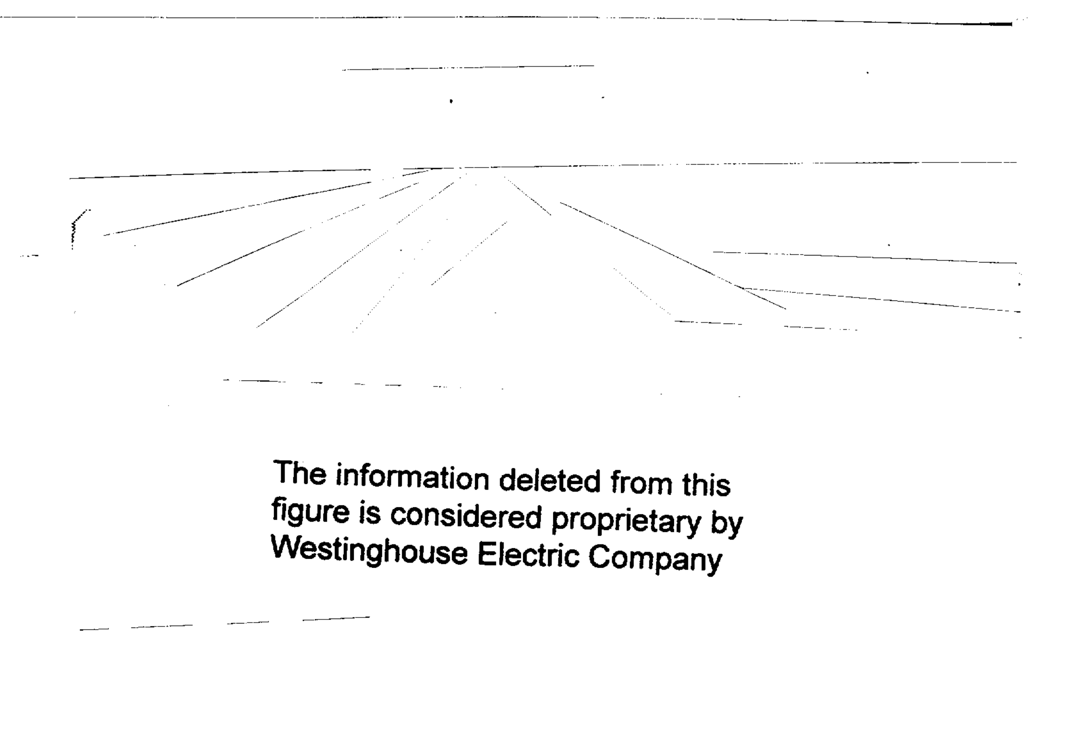

Figure 5-57. CMT1 thermal profile response during an OSU/APEX experiment.

The information deleted from this figure is considered proprietary by Westinghouse Electric Company

Figure 5-58. Comparison of the two CMT responses for an OSU/APEX experiment.

These observations suggest the intuitive conclusion that the break tends to favor vapor inflow at the PBL on the broken cold leg by reducing the inventory with respect to the intact cold leg. Regardless of this difference, the imbalance between the two CMTs is shown to be minimal. Figure 5-58 provides evidence of this fact, since the CMT draining rate changes at about 500 s, when the ADS is activated. This is due to a slight variation in the direct vessel injection (DVI) line piping arrangement which allows accumulator injection to preferentially reduce the draining of CMT1 and thus causes CMT2 to lead in the draining process thereafter.

In view of the effect of minute differences on the CMT draining process, a number of scaling approaches have been attempted. Two system-level scaling efforts were inconclusive since the detailed distribution of inventory and energy turn out to be important for this process. Therefore, the attempt to lump these quantities at a system level is not a viable alternative. A local scaling effort has shed some light on the causes of the different behaviors observed in the three facilities. Next we will review these three scaling efforts.

The first scaling approach is based on global inventory considerations. This idea relates to the fact that as the cold-leg level drops, it uncovers the inlet to the PBL, thus causing vapor inflow and draining of the CMT. This approach provides a bounding value of the global inventory where CMT draining will occur.

Table 5-22 lists inventories for the ROSA/AP600 and SPES-2 facilities. All values are normalized with respect to the initial system inventory. The SPES-2 ranges are broad due to the uncertainties associated with some of the data. The ROSA/AP600 data show that for all transients the bounding value is lower by far than any of the actual values. In summary, the table shows that the bounding value of the global inventory does not provide a good representation of the phenomena; inventory distribution plays a far more important role than is assumed by the global approach.

Table 5-22. System level inventory scaling.

Transient	Normalized Inventory ROSA/AP600	Normalized Inventory SPES-2
200% PBL break	0.69	
1-in. diameter cold leg bottom break with failure of ADS-123	0.69	0.76
1/2-in. cold leg bottom break	0.74	
200% DVI line break	0.75	0.92-0.97
2-in. PBL break	0.80	0.64-0.83
2-in. cold leg bottom break	0.81	0.81
Bounding value	0.38	

The second scaling approach involves global energy and inventory considerations. Consider normalizing the internal energy of the overall system with respect to the internal energy at the initial steady state and with reference to the internal energy of liquid water at ambient temperature. Similarly, one can define a normalized internal energy for the CMT. Both internal energies should be specific to the mass in the volume of concern in order to be comparable. Figure 5-59 illustrates the behavior of these two normalized specific internal energies as plotted against the system inventory, which is normalized with respect to its initial value.

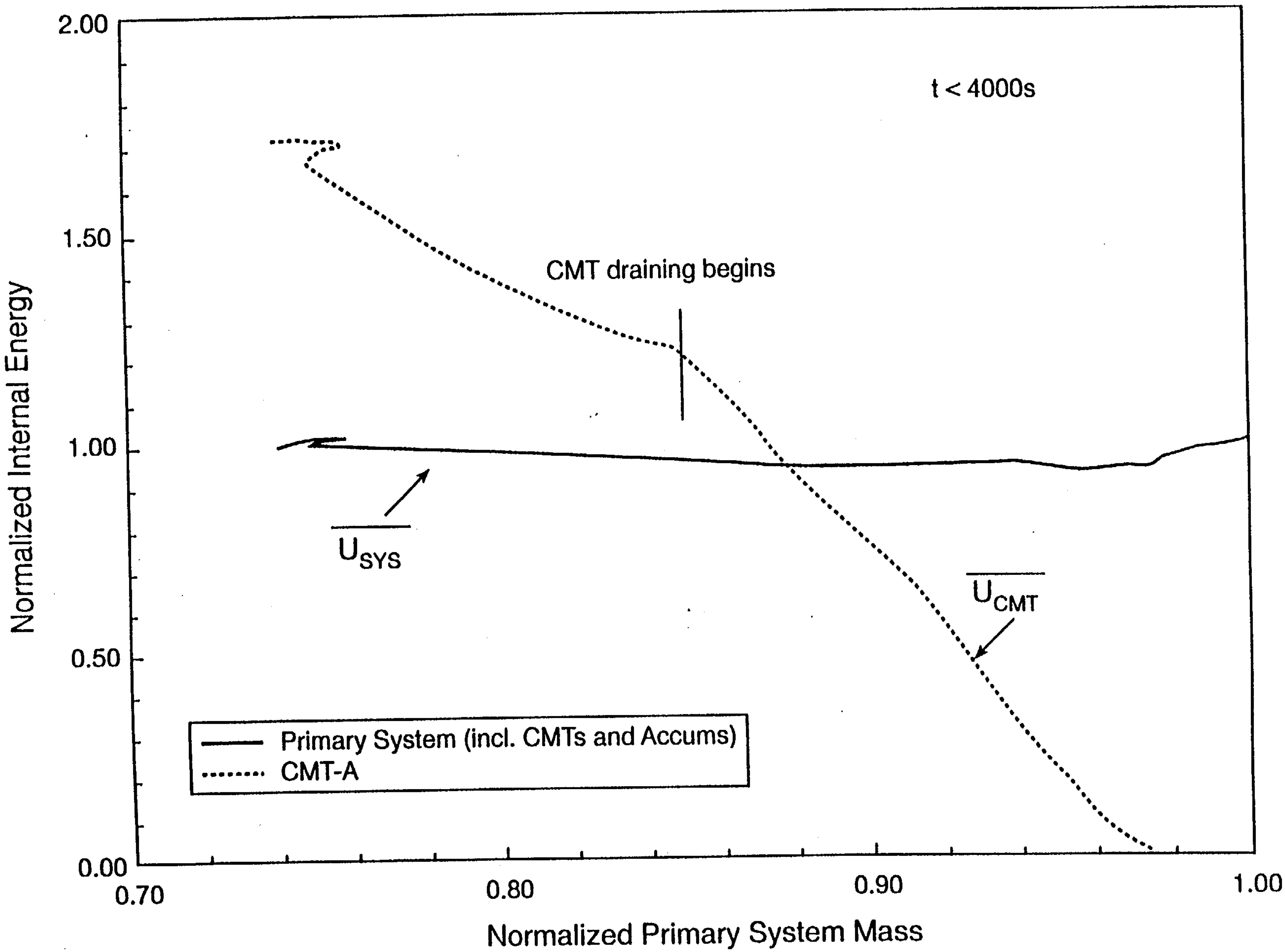

Figure 5-59. CMT and system energies as function of system inventory.

The relative internal energy of the CMT with respect to the system internal energy can be obtained by determining the ratio between the CMT and system values. If one plots this ratio against the system inventory which is rescaled (with respect to a maximum and minimum value of the inventory bounding the CMT draining range), a draining criterion should emerge. Figure 5-60 qualitatively depicts this criterion. CMT draining can occur at low CMT energies when the system inventory is low, but it requires a higher CMT energy if the system inventory is high.

This global approach is based on lumped CMT and system energies. Unfortunately, the energy distribution, as well as the inventory distribution, play a determinant role in the CMT behavior. Therefore, this approach is inconclusive. Further, the process of data reduction required to obtain the normalized specific energies is cumbersome, and the uncertainties associated with the data are large. In conclusion, this global scaling approach was not found to be viable.

Recalling that the partition between system level scaling and local level scaling is drawn at the component level, a local level scaling is pursued. Figure 5-61 depicts the control volume that is considered for the proposed bottom-up scaling analysis. The control volume is the portion of the CMT that is occupied by warm water, and it is assumed that the interface between the warm and cold water regions within the CMT is sharply defined. The local energy balance is written as:

$$S\,h\,(T_s - T_w) + G\,A\,c_f\,(T_s - T_{CL}) = M_f\,c_f\,\frac{dT_s}{dt}$$

where S is the CMT surface area exposed to hot water,
h is the convection heat transfer coefficient,
T_s is the fluid saturation temperature,
T_w is the CMT wall temperature,
G is the PBL mass flux,
A is the PBL cross sectional flow area,
c_f is the heat capacity of the fluid,
T_{CL} is the cold leg fluid temperature,
M_f is the mass of the hot fluid in the CMT and
t is time.

The three terms in this equation represent the heat losses through the CMT wall, the slightly-subcooled PBL water inflow, and the energy associated with the system depressurization. The gradual system depressurization caused by PRHR cooling and CMT recirculation results in flashing of the saturated water in the CMT. At the onset of flashing, this energy is used to raise the temperature of the incoming PBL flow. Note that this inflow becomes progressively colder (also because of PRHR cooling and CMT recirculation effects).

$$\overline{U_{SYS}} = \frac{U_{SYS} - U_{\infty}}{U_O - U_{\infty}}$$

$$\overline{U_{CMT}} = \frac{U_{CMT} - U_{\infty}}{U_O - U_{\infty}}$$

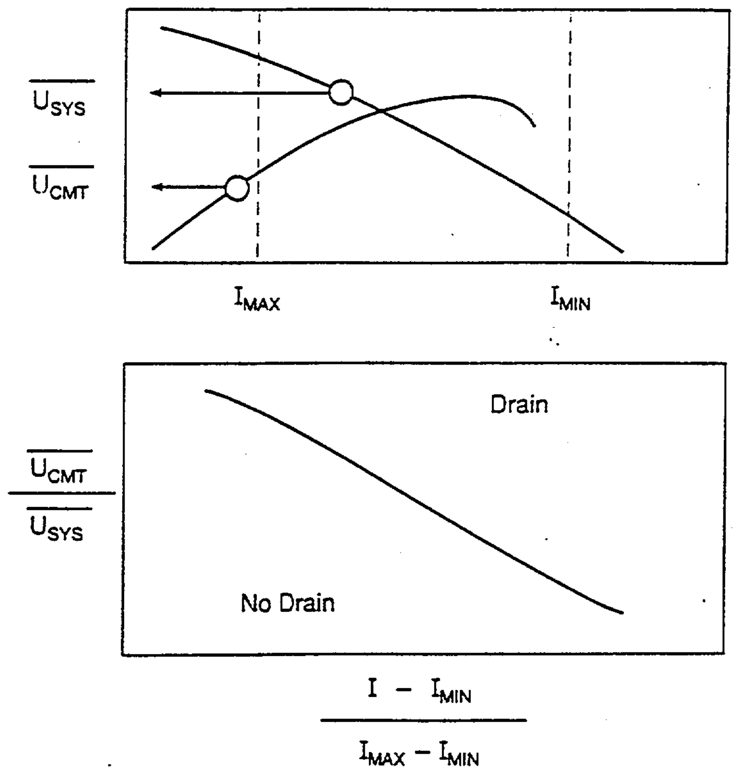

Figure 5-60. CMT and system energies as a function of rescaled system inventory.

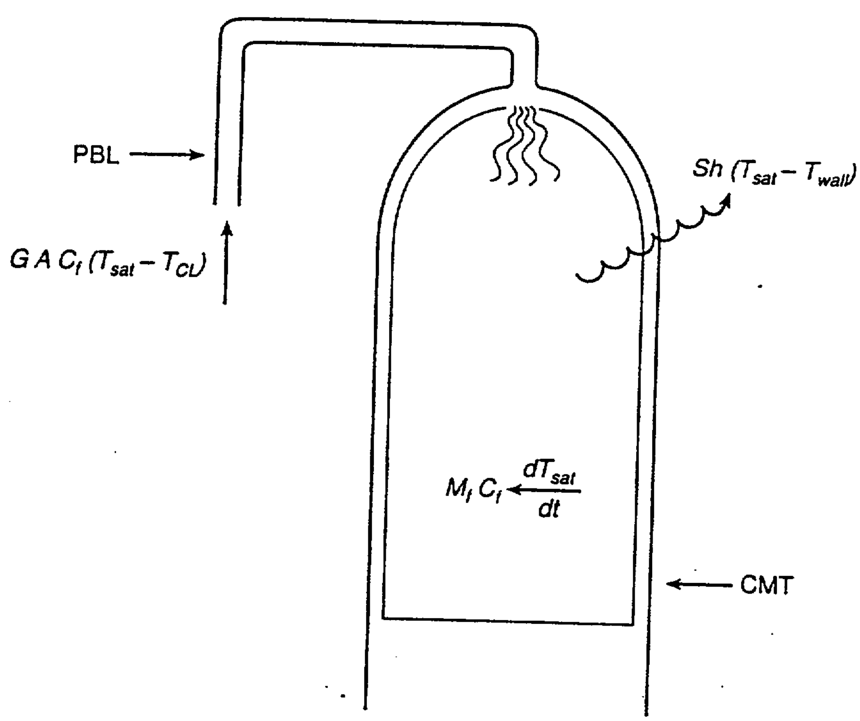

Figure 5-61. Control volume description for proposed bottom-up local CMT scaling.

In essence, there is a race between the CMT flashing capability (which increases as the volume of saturated water in the CMT increases) and the PBL flow subcooling which also increases (as more and more cold water flows into the cold legs). The energy equation is simplified by assuming that most of the heat losses are associated with the heat capacity of the CMT wall rather than with losses to the ambient environment. Further, it is also assumed that the temperature ramp in the metal wall matches the temperature ramp in the fluid. By considering the mass balance on the CMT, written with a constant inflow of water through the PBL, one can write the term

$$GA = \rho_f V_f / \tau$$

where ρ_f is the fluid density
V_f is the fluid volume
τ is a characteristic time.

Note that the warm front in the CMT progresses downward with a velocity in the range of 1.4 to 2.1 mm/s. The time τ is taken from the onset of CMT recirculation. With this notation, the energy balance is cast as

$$\left(\rho_f c_f - \frac{V_m}{V_f} \rho_m c_m\right) \frac{dT_f}{dt} = \frac{\rho_f}{\tau} c_f (T_s - T_{CL})$$

where V_m is the volume of the metal of the CMT,
c_m is the heat capacity of the metal and
T_f is the fluid temperature.

By introducing the Clausius-Clapeyron relationship, to relate the depressurization to the fluid temperature ramp, the final formulation is obtained as:

$$\frac{\dfrac{dP}{h_{fg}\,\rho_v}}{\dfrac{dt}{\tau}} = \frac{1 - \dfrac{T_{CL}}{T_s}}{1 - \dfrac{(\rho\, c\, V)_m}{(\rho\, c\, V)_f}}$$

where h_{fg} is the latent heat of vaporization.

In the right hand side of this equation, the denominator is well scaled for all three facilities, since the CMT wall thickness has been scaled appropriately so that the ratio of the CMT diameter and the CMT wall thickness is the same for all the facilities as for the AP600. The reason for casting the energy balance in this form is that the term $dP/h_{fg}\rho_v$ is consistent with the OSU/APEX pressure scale and it is fully preserved for the two full-pressure facilities (ROSA/AP600 and SPES-2). The time is scaled with the overall time, which makes all chronological scales consistent.

The numerator on the right hand side deals with subcooling of the inflow from the PBL. This term effectively couples the rest of the system with the CMT. It is in this term that all the subtle system interactions in the system are buried. In particular, one should recall PIRT discussion of cold-leg stratification, tee phase separation and downcomer flow distribution effects.

Figure 5-62 plots this term as a function of time. For OSU/APEX, the time has been doubled as required by the 1/4-height scale of that facility. The arrows in the figure identify the timing associated with the onset of CMT draining. It is reassuring that similar patterns are present in the three traces. Figure 5-63 compares the CMT level responses for these tests. Note that OSU/APEX initiates CMT draining at about the same time as the other two facilities. However, a cold slug of water enters the OSU/APEX PBL, vapor is condensed and the draining process is retarded. Draining resumes at about 4000 s.

The comparison of the behavior in the three facilities is drawn on the basis of the traces presented in Figure 5-62. A minimum condition for the PBL inflow subcooling scaling term is achieved within the first 1000 s or so. Figure 5-64 provides an enlargement of the same plot in that region. The minimum values of the scaling term are similar for OSU/APEX and ROSA/AP600, while SPES-2 exhibits a significantly higher minimum value.

This finding is consistent with the comparisons of the surface-to-volume ratios presented in Table 5-23. In this table, the ROSA/AP600 and OSU/APEX surface-to-volume ratios are 0.18 and 0.15, respectively. The highly-elongated SPES-2 facility, on the other hand, exhibits a value of 0.048, which is about 3 to 4 times lower than for the other two facilities. This means that the heat losses in the SPES-2 facility are higher. Therefore, in the energy balance, one can expect higher subcooling of the PBL inflow which is clearly reflected in the raised value of the minimum in Figure 5-64.

Table 5-23. Surface-to-volume ratios for the three facilities (inventory at onset of CMT draining).

Ratio	AP600/ROSA	AP600/OSU	AP600/SPES
Volume Ratio	30	192	395
Height Ratio (L)	1	4	1
Equivalent Diameter Ratio (D)	5.5	6.9	21
L/D Ratio	0.18	0.58	0.048
Surface-to-Volume Ratio	0.18	0.15	0.048

A far more important insight emerges from this analysis. One should ask why CMT draining begins later than, not at or near, the times when the minimums in Figure 5-64 are reached. To address this question, we need to compare similar transients with different break sizes. The OSU/APEX facility provides a set of four such transients. Figure 5-65 shows results for four tests with break diameters of 0.5, 1.0 and 2.0 in. These are nominal diameters, which correspond to actual AP600 scaled sizes of 0.8, 1.7 and 2.2 in., respectively. There are two 2.2-in. breaks, one on the bottom of the cold leg and one on the top. It is clear from this figure that, indeed, for all the larger breaks CMT draining begins at or near the minimum condition. It is only for the 0.8-in. break that CMT draining begins much later, at about 4000 s. This is the test plotted in Figures 5-62 and 5-64.

It is reasonable to conclude that the system has an early, first opportunity to drain if subcooling in the PBL flow is unable to overwhelm the flashing due to depressurization. If this opportunity is missed, then the system will drain when the fluid flashing rate is large enough to generate vapor while compensating for the heat losses and for the subcooled inflow. Transients with larger break sizes evolve rapidly and, therefore, PRHR cooling is less than for transients with smaller break sizes, for which the response is slower.

The information deleted from this figure is considered proprietary by Westinghouse Electric Company

Figure 5-62. Comparisons of the energy balance PBL subcooling term for ROSA/AP600, SPES-2, and OSU/APEX cold leg break tests.

The information deleted from this figure is considered proprietary by Westinghouse Electric Company

Figure 5-63. CMT level responses for ROSA/AP600, SPES-2, and OSU/APEX cold leg break tests.

The information deleted from this figure is considered proprietary by Westinghouse Electric Company

Figure 5-64. Expanded-scale comparisons of the energy balance PBL subcooling term for ROSA/AP600, SPES-2, and OSU/APEX cold leg break tests.

The information deleted from this figure is considered proprietary by Westinghouse Electric Company

Figure 5-65. Comparisons of the energy balance PBL subcooling term for OSU/APEX cold leg break tests with three different break sizes.

This analysis provides insights and explains the different CMT draining onset behavior observed in the three experimental facilities. However, the phenomena associated with CMT draining are even more complex. Consider the SBLOCA with failure of ADS-123 for which results are depicted in Figures 5-66 and 5-67. Here, draining occurs at point A. Since ADS-123 is not activated, CMT draining continues below the 67.5% level setpoint (where ADS would be activated). At a level of about 40%, the draining stops because the CMT internal flashing ceases due to the matching of the system pressure and the saturation temperature of the CMT water. The stepwise drain that occurs at about 9000 s is due to the intermittent uncovery of the PBL, which allows for intermittent flow of vapor into the top of the CMT.

Another aspect, and a rather surprising one, is that conditions for CMT draining are present for a long time (i.e., 1 hour or more). It is conceivable that a small perturbation in the temperature of the flow from the PBL or a sudden drop in pressure caused by a small localized condensation event in the primary system may trigger CMT draining. As the draining begins, inflow from the PBL stops and this results in the elimination of one of the heat sinks in the energy balance. This event reinforces the draining process due to internal flashing.

In spite of these complexities, there is no safety issue associated with CMT draining because it is impossible for the liquid level in the vessel to go lower than the top of the cold-leg elevation without uncovering the PBL inlet. If the PBL inlet uncovers, it is impossible for the CMT not to drain. As far as operator training and the predictability of the CMT draining event, there is little hope to effectively account for all of the complexities associated with this phenomenon. The use of a one-dimensional system code, such as RELAP5/MOD3, does not allow for the modeling of liquid-liquid stratification phenomena in pipes. Therefore, it is unrealistic to expect that RELAP5 computations will predict the details of the CMT draining process.

Relevance to the Prototype

The complex phenomenology associated with CMT draining, as described above, is expected for the prototype. The broad spectrum of phenomena observed in the experiments should reasonably map the prototypical behavior. It is not reasonable to expect that the RELAP5 code will precisely predict mechanisms and timings of CMT draining during SBLOCAs. As an example of the difficulty of the problem, consider the delicate balance of flashing, PBL flow, and subcooling. It is clear that, given the limitations of predicting liquid-liquid thermal stratified behavior in the cold leg, the modeling of the PBL intake region will not allow for accurately representing the conditions of the fluid entering the PBL.

The level of effort required to model all the phenomena contributing to CMT draining is far beyond the scope of system codes such as RELAP5/MOD3. As to the future capability of system codes to address such a complex situation, it may still remain a questionable endeavor. Therefore, the implications to the prototype should be cast in terms of system design for safety performance, rather than for system predictability and scaling. By that we mean that the present design might well satisfy the safety requirements in terms of bounding system behavior, while the specific system trajectory within those bounds may remain extremely difficult to predict.

The information deleted from this figure is considered proprietary by Westinghouse Electric Company

Figure 5-66. Energy balance PBL subcooling term for a failure of ADS-123 transient.

The information deleted from this figure is considered proprietary by Westinghouse Electric Company

Figure 5-67. CMT level response for a failure of ADS-123 transient.

Conclusions

The data show that the CMTs approach a possible draining condition early during SBLOCAs, when the subcooling introduced by the PBL flow competes with the flashing associated with the system depressurization. A minimum of the PBL inflow subcooling is observed when the effects of PRHR cold water return spread throughout the system. If this spreading effect is fast, then the CMT will not drain at the minimum subcooling condition and draining will instead occur later, due to PBL vapor inflow or to the progressively increased flashing associated with the larger CMT saturated liquid volume. If the PRHR cooling effect is slow relative to the length of the SBLOCA short-term phase, then CMT draining will occur at the minimum subcooling condition. This second possibility is observed for the larger breaks, where the depressurization is faster than the spreading of the cooling associated with PRHR return flow.

Reactor coolant system level, with respect to cold leg elevation, is definitive as far as CMT draining is concerned. If the level is above the cold leg, the CMT may not drain. Once level has declined to the cold leg elevation, the CMT will drain. The cold leg is about 2 m above the top of the core. Ergo, as long as water remains in the CMT, core uncovery is not a problem.

There is no safety issue associated with the timing of CMT draining because it is impossible for the vessel liquid level to drop lower than the cold leg elevation without uncovering the PBL inlet. It is also impossible to keep the CMT from draining as the PBL inlet uncovers. However, as far as predictability of the timing of CMT draining, the draining condition is caused by several competing mechanisms dominated by second-order effects. Prediction of these effects is a large challenge for system codes.

Assessments of RELAP5/MOD3 capabilities for predicting CMT behavior in the ROSA/AP600, SPES-2 and OSU/APEX facilities for three different SBLOCA scenarios (cold leg break, DVI line break, and PBL break) are summarized in Section 5.1 and documented in Appendix C. Results from these assessments pertinent to CMT draining are described as follows. In all but one of the nine assessment cases, the code was seen to predict the same initiator for CMT draining (i.e., either CMT flashing or PBL voiding) as observed in the experiment. (The exception was for the ROSA/AP600 test of the PBL break accident scenario, in which a PBL configuration unlike that of AP600 was used. When this test irregularity was accounted for with the model, the code predicted the same cause of CMT draining as observed for this test as well). Code predictions of the timing of onset of CMT draining were seen to vary from test to test. No overall predictive bias was observed (i.e., the code prediction was about as likely to be late as early); over the nine tests, the mean predictive timing error was only 11 s early. The root-mean-square timing error was seen to vary inversely with break size; 658 s for the 1-in. cold leg break, 250 s for the 2-in. PBL break and 6 s for the DVI line break. The overall root-mean-square timing error for the nine tests was 406 s. The code also had difficulty in predicting intermittent CMT refills following the onset of draining. This complex refill behavior was observed in some experiments and in some of the calculations, but timing predictions were erratic. Most importantly, the assessments showed that, despite the difficulties in predicting the timing of onset of CMT draining and the particulars of the draining process, predictions of the overall system behavior, the vessel inventory (the PIRT figure of merit) and subsequent events were seen to be acceptable. Therefore, code weaknesses related to prediction of CMT draining behavior were not seen to adversely affect the overall adequacy of the code for predicting AP600 SBLOCA behavior.

5.3.4.3 Oscillatory IRWST Injection.

Discussion

In this section, the oscillatory behavior associated with the beginning of IRWST injection will be studied. The phenomena are most evident in the ROSA/AP600 facility; therefore, we will use the data from this facility to generate the mechanistic explanation and the bottom-up scaling approach. The scaling approach extended to the OSU/APEX facility will justify that facility's behavior in light of its distortions and will provide foundation for the extrapolation to the prototypical scale. Because of its major distortion of the ADS-4 valve sizing, the SPES-2 facility does not provide data relevant for evaluating this behavior.

The long-term source of inventory for AP600 during SBLOCAs is first the IRWST and ultimately the sump. In order for the IRWST to inject, the primary system pressure must decrease below the IRWST static head, which corresponds to approximately 1 bar. The primary system depressurization is due to the ADS activation and, in its final stage, to the opening of ADS-4.

Following the opening of ADS-4 there is: (1) entrainment of water above the hot legs out ADS-4, (2) continued drainage of water from the CMTs, and (3) increased flashing and boiling in the core. This vapor generation results in the lowest core inventory observed throughout the transient. The vapor generation and overall system inventory depletion must be overturned by the initiation of IRWST flow, which reduces voidage in the core and replenishes system inventory.

Upon first examination, the IRWST injection phenomena observed in the three integral experimental facilities do not provide a cohesive, unified picture of the behavior. Figure 5-68 typifies the IRWST injection behavior seen in the three facilities. The absolute time shown in this figure should be ignored, the relative times are as occurred in the experiments. The ROSA/AP600 facility exhibits a recognizable, significant IRWST flow oscillation. The OSU/APEX facility shows what might be oscillations, but at a much higher frequency. Finally, the SPES-2 facility appears to inject in an almost continuous fashion, with only two cycles apparent. The corresponding pressurizer level responses, depicted in Figure 5-69, suggest that the oscillatory behavior is related to the outflow of water located above the elevation of the ADS-4 discharge.

The data evaluation methodology will be followed to address the issue of the IRWST injection and to clarify the different behavior observed in the three facilities. The pattern recognition does not yield significant information in this case; there is only an indication of some interactions between pressurizer inventory and IRWST inflow.

A qualitative examination of the SPES-2 data shows a sharp depressurization associated with ADS-4 actuation, which almost immediately lead to continuous IRWST injection. The SPES-2 ADS-4 valve flow areas are overscaled by 270%. The Westinghouse rationale for this significant distortion was grounded in the notion that the heat stored in the metal masses might reduce the depressurization rate and consequently delay IRWST injection. This rationale was not guided by a comprehensive scaling analysis. Consider, for instance, that ADS-4 oversizing results in a core inventory (preceding IRWST injection) which is consistently and significantly lower than the minimum inventory observed in both ROSA/AP600 and OSU/APEX. Due to these strong atypicalities in this portion of the transient, we do not consider the SPES-2 data to be useful for evaluating AP600 oscillatory IRWST injection behavior.

The high frequency of the oscillations in OSU/APEX, coupled with the low sampling rate of its data acquisition system, pose difficulties in the identification of the precursors which is the basis for developing a mechanistic explanation. There is an absence as well of information on flow densities. Therefore, ROSA/AP600 appears to be the facility best suited to gain insight into these phenomena, since instrumentation is relatively more extensive, the oscillation frequency is low and the data acquisition sampling rate is high.

The information deleted from this figure is considered proprietary by Westinghouse Electric Company

Figure 5-68. IRWST injection flow responses for the ROSA/AP600, SPES-2 and OSU/APEX SBLOCA tests.

The information deleted from this figure is considered proprietary by Westinghouse Electric Company

Figure 5-69. Pressurizer level responses for the ROSA/AP600, SPES-2 and OSU/APEX SBLOCA tests.

The main features apparent in the ROSA/AP600 data are: (1) system interactions and (2) small driving forces (i.e., gravity heads). These features may result in extremely complex causal relationships among the various components. For oscillating IRWST injection, a number of components play a role. However, the heart of the mechanism can be confined to a few key components with the others playing contributing roles. With this in mind, we will now provide a mechanistic explanation of the phenomena which strives to be inclusive of all effects while emphasizing the essential elements.

Figure 5-70 shows the overall trends relevant to the ROSA/AP600 IRWST injection phenomena. As the IRWST injection flow rate increases, the core level increases and the core voidage decreases. This conclusion is common to all observed transients and it frames the overall understanding of the behavior.

The study of precursors is used to determine the causal relationships between upper plenum pressure, ADS-4 flow, and pressurizer level. To sort out the experimental information, we need to identify the various instruments that generated the data. The upper plenum pressure is measured by a pressure transducer. The pressurizer level is measured by a differential pressure cell. Both these instruments have negligible time lags. The same is not true for the ADS-4 flow measurement. ADS-4 flow is measured from levels of catch tanks, which are located about 44 m from the hot leg ADS-4 offtake. This information clearly is subject to a time lag. To quantify the associated ADS-4 flow measurement time delay, we need to examine additional measurements which relate to the timing of the outflow.

To identify the locations of the various instruments, we examine the geometrical configuration of the facilities. Figure 5-71 provides a plan view of the ROSA/AP600 hot and cold legs. Figure 5-72 provides an isometric drawing of portions of the pressurizer surge and ADS-4 discharge lines. On the ADS-4 line, the short arrow indicates the location of the γ-densitometer labeled "DE431." Data from this instrument are plotted in Figure 5-73. The same figure also shows flow data, deduced from the catch tank level (IM-CT-A), and a differential pressure indication from the ADS-4 line. This figure is used to quantify the time lag between the peak of the flow rate at the gamma densitometer and at the catch tank.

Consider the peak in the γ-densitometer trace at 6661 s and the peak in the catch tank trace at 6673 s. The time delay is about 12 s. The length of the 4-in. diameter piping associated with the 12-s time delay is 38 m. The additional 4.1-m long pipe that separates the location of the γ-densitometer from the ADS-4 hot-leg connection is of variable diameter, from 2.5 to 3 in. This length of pipe introduces a time delay of about 1 s. Therefore, the total time delay between the ADS-4/hot leg connection and the catch tank is approximately 13 s.

Consider the relative timing of the ROSA/AP600 upper plenum pressure, pressurizer level and ADS-4 mass flow rate during one pressurizer drain event shown in Figure 5-74. At the initiation of draining, the pressurizer level trace leads both the pressure trace and the ADS-4 mass flow rate trace. The question is, does the ADS-4 mass flow rate lead or follow the pressure increase? At first, one might have concluded that pressure increased before ADS-4 flow increased. When the 13-s measurement delay is factored in, this is seen not to be the case. Therefore, the causal relationship is as follows: when the pressurizer drains, water floods the ADS-4 ports, causing the upper plenum pressure to rise. In other words, the upper plenum pressure depends on the flow conditions at the ADS-4 discharges.

Figure 5-75 provides a comparison between the differential pressure across the pressurizer surge line (i.e., upper plenum pressure minus pressurizer pressure) and the pressurizer and surge line static head. The traces are subjected to identical running averages and the pressure differential is shifted upward by 40 kPa. Note that the upper plenum and pressurizer pressures are measured using independent pressure transducers which operate up to the full system pressure. Therefore, the 40 kPa adjustment is well within the measurement error. This figure shows that the liquid level in the pressurizer clearly responds to the

The information deleted from this figure is considered proprietary by Westinghouse Electric Company

Figure 5-70. ROSA/AP600 core collapsed level and IRWST injection flow responses.

The information deleted from this figure is considered proprietary by Westinghouse Electric Company

Figure 5-71. Plan view of ROSA/AP600 hot and cold legs.

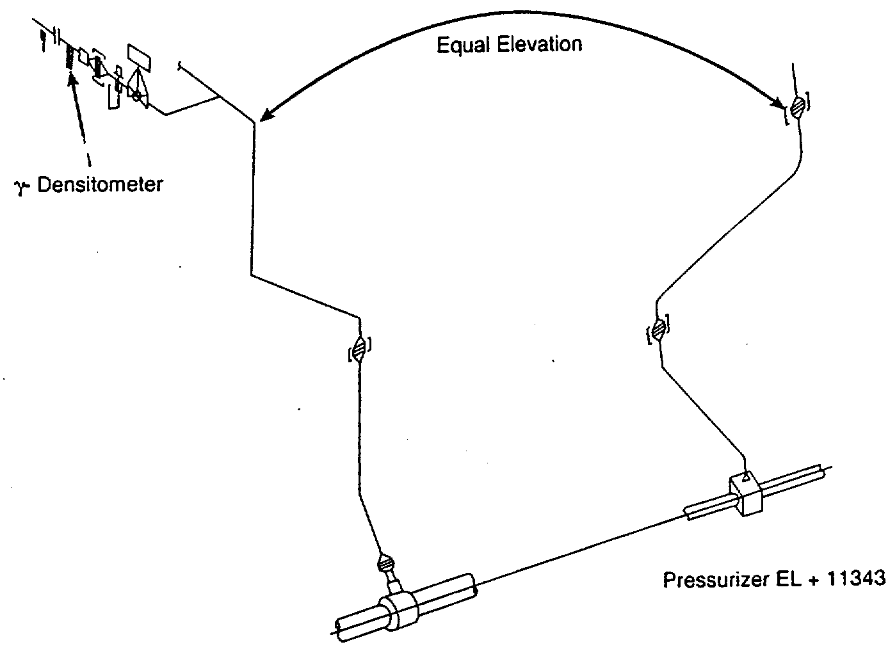

Figure 5-72. Isometric drawing of the ROSA/AP600 pressurizer surge and ADS-4 discharge lines.

The information deleted from this figure is considered proprietary by Westinghouse Electric Company

Figure 5-73. Responses of ROSA/AP600 ADS-4 density, ADS-4 differential density, and catch tank level.

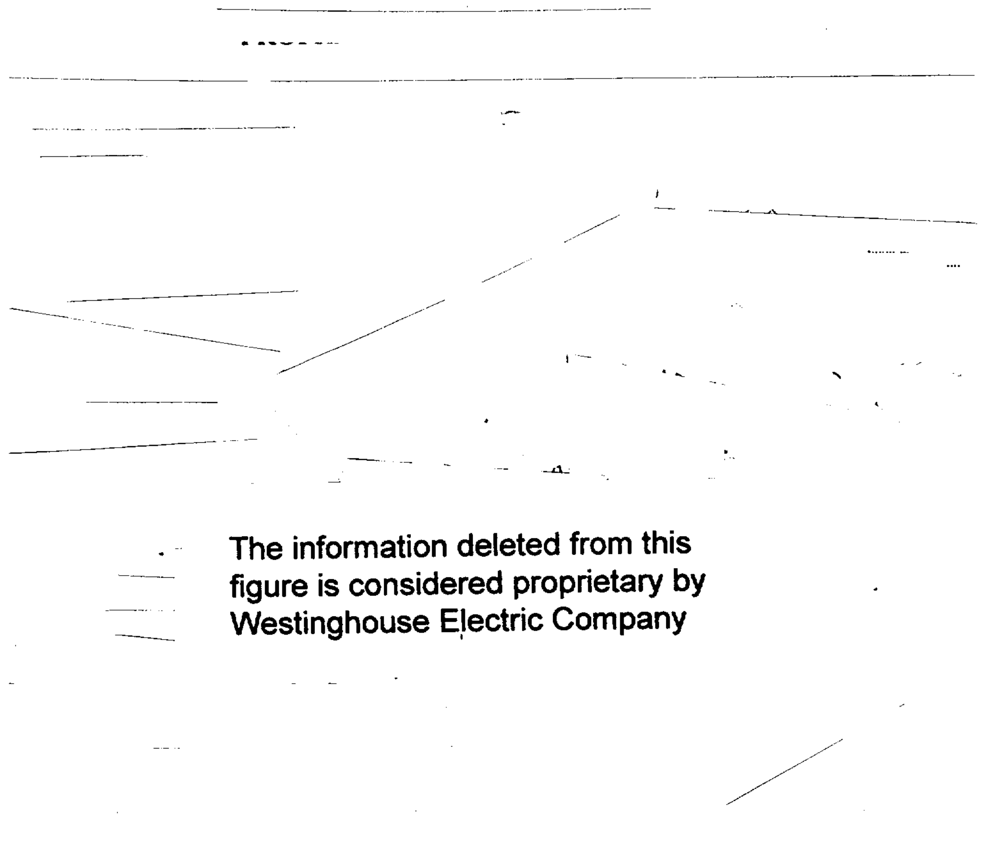

Figure 5-74. Responses of ROSA/AP600 pressurizer level, upper plenum pressure and ADS-4 flow.

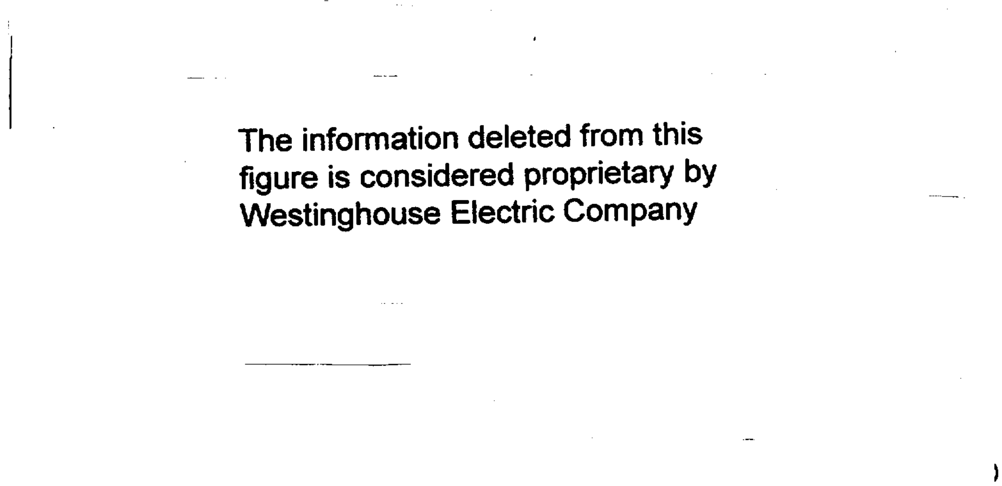

Figure 5-75. Comparison of ROSA/AP600 pressurizer surge line differential pressure and pressurizer and surge line static head.

differential pressure. Hence, a feedback is established between the liquid inventory in the pressurizer and the upper plenum pressure which can be stated as:

Level → Flow → Pressure → Level.

In the formulation of the surge line and pressurizer head trace, the surge line collapsed liquid level used is from the measurement of a differential pressure cell spanning the surge line. The frictional pressure drop through the surge line is significant during periods of pressurizer refill. In Figure 5-75, this is evident in the difference of about 1 m observed for the early refill events.

The dynamic effects associated with fluid acceleration are depicted in Figure 5-76. The draining portion of the transient occurs rapidly, while the refill portion occurs slowly. A detailed comparison of the traces in Figure 5-76 at the beginning of a pressurizer draining event reveal the imbalance between differential pressure and static head. There is a dynamic effect corresponding to a 2-to-3 m/s downward velocity of the liquid in the surge line. This value is consistent with the velocity deduced from the time response of pressurizer level.

Figure 5-76 shows the inventory distribution between the pressurizer and the surge line. It is apparent that substantial voids are present in the surge line before the pressurizer drains. This implies that vapor is flowing upwards in the surge line during the pressurizer refill portion of the transient. Deductive reasoning indicates that, even though vapor flow through the pressurizer tank inlet sparger has ceased, there must be continued condensation within the surge line piping leading to the sparger, since the evidence of continued upward surge line vapor during the pressurizer refill period is irrefutable.

At this point, we need to establish a consistent precursor for the pressurizer draining event. Consider the combined head of pressurizer and surge line expressed as:

$$\rho_L \, g \, H = \rho_L \, g \, H_{L,PZR} + \rho_L \, g \, H_{L,SL} \, (1 - \alpha)$$

where ρ is density,
g is acceleration due to gravity,
H is the height of the liquid column,
α is the void fraction and
the subscripts L, PZR and SL are liquid, pressurizer and surge line.

From this equation and from inspection of Figure 5-76, it is clear that the surge line-pressurizer gravity head distribution is unstable. Should liquid holdup increase in the surge line, the second term of the right hand side of this equation will increase. The left hand side of the equation is nearly constant, given the relative insensitivity of the differential pressure to an increase in liquid holdup and the balance between differential pressure and total head.

Therefore, the pressurizer must drain in order to reduce the first term on the right hand side of the equation and thus balance the total head. This exacerbates the increase in liquid holdup in the surge line and quickly leads to the rapid pressurizer drain observed in Figure 5-77. With this mechanism for the pressurizer drain, it is now necessary to find a plausible cause for the increase in surge line liquid holdup.

The information deleted from this figure is considered proprietary by Westinghouse Electric Company

Figure 5-76. ROSA/AP600 pressurizer and surge line inventory distributions.

The information deleted from this figure is considered proprietary by Westinghouse Electric Company

Figure 5-77. Comparison of ROSA/AP600 net reactor coolant system flow, reactor vessel level and pressurizer level.

As a pressurizer refill phase ends, the two-phase upward flow in the surge line stops. The overall reactor coolant system pressure is decreasing at this time, which indicates that the vapor generation rate is less than vapor outflow rate. Therefore, the vapor velocity in the surge line must be decreasing. This, in conjunction with the gradual filling of the primary system shown in Figure 5-77, is the cause for the surge line void fraction decrease. Note that liquid flooding also limits the vapor access to the surge line, as the net system inflow is shown to increase prior to the pressurizer draining events. As for the source of this water, in the early portion of the transient it is furnished by continued CMT draining. Later, IRWST injection flow becomes the main source.

Note that the IRWST injection water is cold, relative to the CMT water, and that IRWST injection reduces the vapor generation rate. This explains why the early pressurizer draining events are preceded by the pressurizer level holding nearly constant for a short period of time; there is sufficient vapor velocity to hold up the liquid in the surge line. In the later portion of the transient (when the vapor velocity is lower), as soon as the upward vapor flow ceases, there is an immediate flow reversal and pressurizer draining.

This mechanistic explanation relates the roles of IRWST flow, core vapor generation and pressurizer level in this process. Figure 5-78 clearly establishes that the IRWST flow and upper plenum pressure are in opposition of phase. Therefore, as the pressure increases, the IRWST flow decreases and vice-versa.

The sequence of events governing the oscillatory behavior can be summarized as follows:

1. The reactor vessel upper plenum pressure is balanced by a two-phase column of liquid and vapor in the pressurizer surge line and by liquid in the pressurizer.

2. As the hydrostatic equilibrium is reached, the upward liquid flow in the surge line stops.

3. Afterward, the surge line upward vapor flow decreases because vapor generation is insufficient to maintain it. In fact, as the vapor is vented out of the ADS-4 and surge line, the reactor coolant system pressure drops. The falling pressure favors the increased IRWST injection flow, which increases the core inlet subcooling and further decreases the vapor generation rate. The liquid inventory in the reactor coolant system increases, and this further limits the upward vapor flow into the surge line because the hot legs become flooded with water.

4. The liquid column in the pressurizer and in the surge line cannot be sustained and a draining event takes place (i.e., the surge line floods and the pressurizer drains).

5. The water draining from the pressurizer finds its way out of the system via the ADS-4 discharge line. The pressure drop across the ADS-4 discharge line increases, and this causes the upper plenum pressure to rise.

6. The upper plenum pressure increase causes a two-phase mixture to flow up the surge line to reach again the hydrostatic balance. Note that the frictional pressure drop associated with the upward two-phase flow in the surge line is significant.

7. Once the hydrostatic balance point is reached, the cycle described here is repeated.

The information deleted from this figure is considered proprietary by Westinghouse Electric Company

Figure 5-78. Comparison of ROSA/AP600 primary pressure and IRWST injection flow responses.

The last step of the data evaluation methodology consists of scaling considerations. For this particular phenomenon, both the top-down and bottom-up approaches will be pursued. The strength of the top-down scaling is in the clearly identifiable initial and boundary conditions. Its weakness is in the necessary global nature of the governing equations, which cannot provide a detailed representation of the local distributions of energy, inventory and momentum.

On the other hand, the bottom-up approach is complementary to the top-down approach since it lacks detailed description of the initial and boundary conditions. In fact, the components that are included in the bottom-up control volume are disconnected from the integral system and, therefore, the feedback with it is artificially modeled. However, detailed representation of the distributions is possible with this approach. The benefit of the bottom-up approach is in the identification of the effect of the local distortions on the various phenomena.

When these findings are integrated in the top-down approach, the overall integral effect of the local distortions is elucidated and their effect at prototypical scale can be inferred. The interface between the two scaling approaches is at the component level. We will now look at the bottom-up scaling to identify the relevant distortions of the various facilities and their effect on the local behavior.

With this background, the focus of the bottom-up scaling is placed on the surge line region. A momentum balance on the surge line can be written as:

$$P_{UP} = P_{PZR} + \rho g H_{L,PZR} + \rho g H_{SL}(1 - \alpha) + \frac{1}{2}\rho v_{L,SL}^2 \left(f\frac{L}{D} + K\right)\Phi_{LO}^2$$

where P is pressure, the subscript UP referring to upper plenum
v is velocity
f is the friction factor
L/D is the length-to-diameter ratio
K is the resistance coefficient
Φ is the Martinelli-Nelson friction multiplier.

Here the inertia forces are neglected because the transient is relatively slow. McCreery[5-20] has shown that this assumption is reasonable for the ROSA/AP600 configuration. The upward two-phase flow in the surge line is modeled with the Martinelli-Nelson flow multiplier, which is recommended for mass fluxes up to 1,300 kg/m^{2}s. In this case the mass flux is about half this value.

As the pressurizer level drops, the surge line density increases (i.e., the surge line floods). The water then makes its way into the ADS-4 discharge line and causes the pressure in the reactor vessel upper plenum to increase as it blocks the ADS-4 ports. The propagation of these events suggests that a link needs to be introduced between the pressurizer level and the upper plenum pressure. Consider the hydrostatic balance at the onset of draining:

$$P_{UP} \sim P_{PZR} + \rho g H_{L,PZR} + \rho g H_{SL}(1 - \alpha)$$

When draining begins, the change in surge line void fraction is linked to the pressurizer level as follows:

$$\Delta\alpha = \frac{\Delta H_{L,SL}}{H_{SL}} = \frac{A_{PZR}}{A_{SL}}\frac{\Delta H_{L,PZR}}{H_{SL}}$$

where A denotes area.

By noting that the variation in the upper plenum pressure is much larger than the variation in the pressurizer pressure during the initial draining period, and that the cross-sectional area of the pressurizer is far larger than the cross-sectional area of the surge line, one obtains:

$$P_{UP} \sim P_{UP^0} + \rho g \frac{A_{PZR}}{A_{SL}} \left(H^0_{L,PZR} - H_{L,PZR} \right)$$

where the superscript "0" indicates conditions at draining onset. This functional relationship can be written as:

$$P_{UP} = C \; (H^0_{PZR} - H_{L,PZR})$$

H^0 can be approximated as the pressurizer height, H_{PZR}, and a nondimensional pressurizer level can be introduced as:

$$Z = H_{L,PZR}/H_{PZR}$$

and a nondimensional liquid velocity given as

$$\dot{Z}_{PZR} = \frac{v_{L,SL}}{\sqrt{g H_{PZR}}} \left(\frac{A_{PZR}}{A_{SL}} \right)$$

The nondimensional form of the momentum equation for the surge line becomes

$$\dot{z}\,|\dot{z}| + \frac{\dfrac{C}{\rho g} + 1}{\dfrac{\Phi^2_{LO}}{2} \left(\dfrac{A_{PZR}}{A_{SL}} \right)^2 \left(f\dfrac{L}{D} + K \right)} Z = \frac{\dfrac{C}{\rho g} + \dfrac{P_{PZR}}{\rho g H_{PZR}} - (1-\alpha)\dfrac{H_{SL}}{H_{PZR}}}{\dfrac{\Phi^2_{LO}}{2} \left(\dfrac{A_{PZR}}{A_{SL}} \right)^2 \left(f\dfrac{L}{D} + K \right)}$$

which can be expressed in the simple form:

$$\dot{Z}|\dot{Z}| + A Z = B.$$

Table 5-24 summarizes the values of the parameters A and B for the facilities and for the AP600. Table 5-25 provides the ratios of parameters A and B for the facilities to the AP600. This simple model can capture the main features of the phenomena. The void fraction α in the upward two phase flow is estimated at 0.85 from the data. Figure 5-79 shows the effect of α on the duration of the draining event. This model has reduced the process to the refill/drain sequence, which is dominated by the frictional resistances in the surge line. Table 5-26 provides a summary of the results for $\alpha = 0.85$.

Table 5-24. Nondimensional parameters for AP600, ROSA/AP600, and OSU/APEX.

	AP600	ROSA	OSU surge line 1:4	OSU surge line 1:7
A ($\alpha = 0$)	1.7E-3	1.4E-3	42E-3	4.6E-3
A ($\alpha = 0.8$)	0.056E-3	0.046E-3	1.4E-3	0.15E-3
B ($\alpha = 0$)	0.25E-3	0.212E-3	8.0E-3	0.89E-3
B ($\alpha = 0.8$)	0.012E-3	0.012E-3	0.33E-3	0.037E-3

Note: The surge line aspect ratio in OSU/APEX is preserved due to flow pattern considerations. Therefore, the surge line cross-sectional area is 1/16 of the AP600 instead of 1/48.

Table 5-25. AP600 plant-to-facility ratios of nondimensional parameters.

Parameter	AP600/ROSA	AP600/OSU as built	AP600/OSU ideal
A	1.2	0.040-0.041	0.36-0.37
B	1.0-1.2	0.031-0.037	0.28-0.32

Table 5-26. AP600 plant-to-facility ratios for amplitude and period for a void fraction of 0.85.

Parameter	AP600/ROSA	AP600/APEX
Amplitude, given as the ratio B/A	0.83-1.0	0.78-0.88
Period	0.82	4.2

	AP600	ROSA	OSU
Calculated event duration (s)	102	165	12
Measured event duration (s)	N/A	49-535 100-300	8-40
Calculated pressurizer level span (m)	1.1	1.4	0.25
Measured pressurizer level span (m)	N/A	1-3	0.12-0.5
Surge line elevation span (m)	4.1	5.9	1.1
Surge line length (m)	28	12	7.6
Pressurizer area/surge line area	28	31	9.5

These results indicate that ROSA/AP600 scales the local phenomena reasonably well. The cause of discrepancies observed in the OSU/APEX data are clearly identified in the oversized pressurizer surge line, which is scaled linearly (i.e., an L/D about 1). Note that Ishii scaling would have required a diameter of the surge line 60% smaller than the one associated with the linear scale.

The event duration is obtained by integrating the momentum equation as

$$event\ duration = 2\sqrt{\frac{B}{A}}$$

$$\times \left(\frac{A_{PZR}}{A_{SL}}\right)\sqrt{\frac{\Phi_{LO}^{2}\left(f\frac{L}{D}+K\right)}{\frac{C}{\rho g}+1}}$$

where C is a constant of proportionality.

In OSU/APEX, the oversized surge line and a larger value of the constant C both contribute to a decrease in the event duration by a factor of about five. This value is consistent with the measured event durations. In fact, for OSU/APEX the event durations are from 16 to 80 s, while in ROSA/AP600 they are from 100 to 300 s. Therefore, the time duration ratio between ROSA/AP600 and OSU/APEX ranges from 3.8 to 6.3.

Conclusions

The mechanism governing the oscillatory IRWST injection is reasonably well understood. The effects of the ADS-4 size, of the IRWST injection flow and subcooling and of the vapor generation rate are clarified and integrated into the mechanism. The phenomena are modeled focussing on the pressurizer drain/refill behavior and the associated the surge line flow. The overall event duration is deduced from a surge line momentum balance. The integrated scaling results show that:

1. The SPES-2 facility is distorted in the overall system level timing because the ADS-4 ports are oversized. Therefore, in this facility the system behavior traverses this portion of the transient much more rapidly than in the prototype. As a result of this accelerated timing, oscillatory IRWST injection is almost completely absent in the SPES-2 test responses. There is little evidence to comment about the adequacy of the local surge line scaling for SPES-2 and, in any case, it is inconsequential.

2. The OSU/APEX facility represents the global system timing well. However, the surge line behavior is locally distorted because the surge line is overscaled. This results in an accelerated drain/refill cycle, which is atypical. Therefore, the oscillatory IRWST phenomena observed in OSU/APEX exhibits a far shorter cycle period than the one expects in AP600.

The information deleted from this figure is considered proprietary by Westinghouse Electric Company

Figure 5-79. Effect of void fraction on the duration of the pressurizer draining event.

3. The ROSA/AP600 facility provides a reasonable representation of AP600 oscillatory IRWST injection phenomena. This behavior does not impact the safety of the plant, since it is caused by excessive liquid inventory held above the ADS-4 ports by the ADS-4 vapor outflow. With 75% of ADS-4 activated, the vapor outflow rate exceeds the vapor generation rate; therefore, one can exclude liquid hold up in the ADS-4 discharge lines under those conditions. Consequently, the PIRT does not show high rankings associated with these phenomena.

The capabilities of the RELAP5/MOD3 code for predicting oscillatory IRWST injection behavior in a ROSA/AP600 1-in. cold leg break experiment were previously analyzed in detail.[5-21] This previous analysis was performed using code version 3.1.2.2, a predecessor of the code version examined in this report. The previous analysis showed that the code reasonably predicted all aspects of oscillatory IRWST injection behavior, including the magnitude, period and shape of its cyclic phenomena. A detailed assessment analysis of oscillatory injection behavior was not repeated for the purpose of updating it to reflect code version 3.2.1.2, which is the subject of this report. However, the code assessments reported here include evaluations of RELAP5/MOD3, Version 3.2.1.2 capabilities for predicting IRWST injection flow rate and pressurizer level responses, which are top-level indicators of this oscillatory behavior. These assessments, performed for the ROSA/AP600, SPES-2 and OSU/APEX facilities for three different SBLOCA scenarios (cold leg break, DVI line break, and PBL break), are summarized in Section 5.1 and documented in Appendix C. Results from these assessments pertinent to oscillatory IRWST injection behavior are described as follows.

For the experiments in the ROSA/AP600 and OSU facilities, oscillatory IRWST injection behavior was observed in both the tests and the RELAP5 calculations of the tests simulating all three accident scenarios. For the SPES-2 experiments, no oscillatory IRWST injection behavior was observed in the test and calculation of the test for the DVI line break scenario and only minor oscillatory behavior was observed in the tests and calculations for the other two scenarios. Figures comparing measured and calculated IRWST injection rate and pressurizer level responses for all of these tests appear in Appendix C.

These figures show that code predictions of oscillatory IRWST injection behavior in the tests to be acceptable, but not as favorable as in the previous analysis.[5-21] As an example, the calculated and measured pressurizer level responses for the ROSA/AP600 1-in. cold leg break test are provided in Figure C.2.2-13 and the calculated and measured IRWST injection responses for the same test are provided in Figure C2.2-28. While the calculated cyclic amplitude is similar to the measured one, the calculated period is longer and the shapes of the traces differ (with the test data showing a flat-top trace and the calculated data showing a saw-tooth trace). The reduced calculational fidelity with code version 3.2.1.2 was found to be caused by the implementation of a new code option related to interphase heat transfer in bubbly and slug flow regimes and a modification of the criteria for vertical stratification (Option 61, see Section 6.3.3). This option, which was implemented to help rectify excessive core flow oscillation behavior identified in previous analyses, was seen to have a moderately adverse effect on prediction of oscillatory IRWST injection behavior. Such trade-offs are necessary features of system code predictions. As described in Section 5.1, the assessment analysis judged that overall code capabilities for predicting both IRWST injection flow rate and pressurizer level were reasonable.

5.3.5 Summary of Scaling Analyses

The top-down scaling analysis tools were applied for AP600 integral tests in three experimental facilities for three SBLOCA scenarios. In this analysis: (1) the sufficiency of the experimental data used for the code assessments in Sections 5.1 and 5.2 was evaluated by investigating whether the experimental data contains the ranges of important phenomena expected of AP600, (2) the relevance of the data was evaluated by investigating the effects of experimental distortions on the observed behavior with respect to the behavior expected in AP600, and (3) similarity was evaluated by comparing the responses of RELAP5 calculations of the experiments with the test data.

The results of the top-down scaling analysis show that the data base provided by the three integral test facilities (ROSA, SPES and OSU) sufficiently represents the AP600 SBLOCA PIRT high-ranked phenomena and, therefore, the data base is adequate for assessing the RELAP5/MOD3 code. Tables 5-27 and 5-28 summarize the results regarding data sufficiency. These tables show the scaling analysis nondimensional groups pertinent to the SBLOCA PIRT high-ranked phenomena for which nondimensional coefficients were derived. Sufficiency is indicated if the Π value for AP600 is enveloped by those of the experiments.

Table 5-27. Summary of top-down scaling data sufficiency evaluations for AP600 SBLOCA short-term phase PIRT high-ranked phenomena.

SBLOCA SHORT-TERM PHASE						
		Π Values				
PIRT High-Ranked Phenomenon	**Pertinent Nondimensional Variables (Πs)**	**AP600**	**ROSA**	**SPES**	**OSU**	**Notes**
Accumulator flow	Π_3	14.8	15.6	17.8	40.5	1
ADS energy release	Π_3	14.8	15.6	17.8	40.5	1
ADS mass flow	Π_7	1.0	1.0	1.0	1.0	1
Break mass flow	$\Pi_{7\text{-pzr}}$	1.0	1.0	1.0	---	2
Cold leg-to-PBL tee phase separation						3
CMT flow resistance	$\Pi_{15\text{-cmt}}\Pi_{17\text{-cmt}}$	1.63 0.45	1.94 0.53	0.69 0.21	0.74 0.40	4
CMT level	$\Pi_{15\text{-cmt}}\Pi_{17\text{-cmt}}$	1.63 0.45	1.94 0.53	0.69 0.21	0.74 0.40	4
Core flashing						5
Core subcooling margin	$\Pi_{9\text{-dc+lp}}$	7.45 4.84 5.62 13.7	12.7 8.17 8.81 14.1	2.93 2.11 7.31 13.3	6.03 3.21 6.08 14.9	6 6 6 6
Core mixture level	$\Pi_{16\text{-dvi}}$	1.39 2.19	1.33 2.13	1.43 2.63	1.08 1.77	5 5
Core power / decay heat						7
Hot leg tee phase separation						8
IRWST flow resistance	$\Pi_{1\text{-dvi}} / \Pi_{3\text{-dvi}}$	2.01 1.97	1.49 1.49	1.97 1.97	4.99 4.79	9
Pressurizer level	$\Pi_{7\text{-pzr}}$	1.0	1.0	1.0	---	2

Note 1 Πs without a component index, such as Π_3 or Π_7 refer to the entire system. Several of the components tabulated in Tables 5-27 and 5-28 operate during the intermediate sub-phase and therefore do not have a component specific Π. In the case of Π_3, AP600 is not included in the facilities range but it is very close to it. Given the uniformity of the response of the facilities during this sub-phase, and the small relative impact of this sub-phase on the primary safety criterion, this small deviation is not considered to be a problem.

Note 2 OSU was not designed to represent the subcooled blowdown sub-phase in which the break flow and pressurizer level are important. The system can be represented in such a simple way that any differences can be included in the scaling, and different scenarios can be collapsed together in the same plot.

Note 3 This is a local phenomenon with no representation in the top-down approach at any time. It is deemed important during the intermediate sub-phase where only global Πs come into play.

Note 4 CMT levels and CMT flow resistance are important during the ADS-4 blowdown sub-phase. AP600 values are contained within the range of the facilities for all scenarios examined. (The two sets of values listed correspond to the different scenarios. The first line is for the CLB and PBLB scenarios and the second line is for the DVILB scenario.)

Note 5 Core flashing and core mixture level are local phenomena. Representation of these phenomena is outside the scope of the top-down scaling approach. $\Pi_{16\text{-dvi}}$ is the closest that the top-down approach gets to representing core level. The numerical values show that AP600 is close to the range exhibited by the facilities and, given the definition of $\Pi_{16\text{-dvi}}$, the facilities are more conservative than AP600. The two values shown for core mixture level correspond to the values for the CLB and PBLB combined and for the DVILB scenario.

Note 6 Core subcooling margin is represented in the scaling analysis through $\Pi_{9\text{-dc+lp}}$, which is a nondimensional number that describes the mixing in the lower reactor vessel region. The values of $\Pi_{9\text{-dc+lp}}$ show that AP600 is within the range of the experiments for all transients examined. (The four sets of values listed correspond to the ADS-4 blowdown and IRWST injection sub-phases for the CLB and PBLB scenarios combined and for the DVILB scenario.)

Note 7 This phenomenon is a boundary condition in all tests and calculations and cannot be addressed through top-down scaling.

Note 8 Phase separation in tees during the ADS-4 blowdown sub-phase and afterward is recognized by the top-down approach as an extremely important phenomenon. Yet, the scaling approach does not view the system with the fine definition required to develop a corresponding Π. Assumptions and simplifications were required to handle this local issue with global consequences. Overall, we do not think that this source of uncertainty is significant enough to change our conclusions regarding the safety criterion. But from our top-down results, we cannot state that the data base includes the AP600 phase separation mechanism.

Note 9 This phenomenon is important during the IRWST injection sub-phase in all scenarios. AP600 values are included in the data-base range. The two values shown correspond to the CLB and PBLB scenarios combined and to the DVILB scenario.

Table 5-28. Summary of top-down scaling data sufficiency evaluations for AP600 SBLOCA long-term phase PIRT high-ranked phenomena.

SBLOCA LONG-TERM PHASE				
		Π Values		
PIRT High-Ranked Phenomenon	**Pertinent Nondimensional Variables (Πs)**	**AP600**	**OSU**	**Notes**
ADS energy release				1
ADS mass flow	$\Pi_{3\text{-dvi}} / \Pi_{2\text{-dvi}}$	1.550	1.497	2
Core mixture level	$Z^*_{dvi} + Z^*_{dc\text{-}dvi} - L^*_v$	0.059	0.053	2
Core power / decay heat				1
Downcomer level	$Z^*_{dvi} + Z^*_{dc\text{-}dvi} - L^*_v$	0.059	0.053	2
IRWST flow resistance	$\Pi_{3\text{-dvi}} / \Pi_{2\text{-dvi}}$	1.55	1.50	2
IRWST pool level	$\Pi_{17\text{-dvi}}$	0.86	0.99	2
	$Z^*_{dvi} + Z^*_{dc\text{-}dvi} - L^*_v$	0.059	0.053	2

Table 5-28. (continued).

PIRT High-Ranked Phenomenon	Pertinent Nondimensional Variables (Πs)	Π Values AP600	OSU	Notes
IRWST pool thermal stratification				1
Sump fluid temperature				1
Sump level	$Z^*_{dvi} + Z^*_{dc\text{-}dvi} - L^*_v$	0.080	0.077	2
Upper plenum mixture level	$Z^*_{dvi} + Z^*_{dc\text{-}dvi} - L^*_v$	0.080	0.077	2

Note 1 This phenomenon does not have a corresponding Π in the top-down analysis.

Note 2 ROSA and SPES are not designed to perform in this period of the transients. Some ROSA experiments were prolonged to include parts of this behavior but their analyses have not been a part of this study.

A number of facility and component distortions, having to do with facility configuration, set points, and modes of operation, had been identified early in the scaling effort and were a concern in terms of the potentially-distorted behavior that they could produce. From the *top-down* viewpoint, these distortions did little to cause the observed behavior of the facilities to deviate from the expected behavior of AP600. In fact, as discussed previously, some of the distortions have had the unexpected effect of broadening the range of the nondimensional coefficients, therefore ensuring that AP600's behavior is included in the data base. Among these three facilities, there is no overall "best representor of AP600", and in fact we did not expect one. The differences among facilities have actually enhanced, rather than hindered, the usefulness of the data base. The scaling methodology allowed many of the distortions and accounted for in the way the data is analyzed and collapsed. Here, we discuss the facility distortions and their impact on facility behavior in the *top-down* context.

- **ROSA**

  Cold leg loop seals ROSA loop seals were expected to affect the way in which the CMTs begin to drain, and they did. This happens, however, during the intermediate sub-phase, in which the system behavior is viewed coarsely by the scaling analysis and the loop seals correspond to a finer description of the components. The loop seals did not prevent the CMTs from draining, and their presence caused only a minor effect on event timing.

  Single cold leg on each coolant loop and single PBL ROSA cannot represent asymmetries between the cold legs on the same loop as the break because it only has one cold leg per loop. Furthermore, the non-symmetric accident scenarios, such as the PBL break, cannot be exactly represented with the ROSA facility configuration. The asymmetric behavior, and the recirculation within the same loop that was expected to occur in AP600 because of the two-cold-legs-per-loop configuration were not found to be as relevant as initially anticipated. The AP600 design does not feature pumps which inject fluid into only one of the two cold legs on the same loop. Thus, sources for asymmetries among the cold legs are limited. Further, such asymmetries, in the data base during the subcooled blowdown and intermediate sub-phases of the short-term phase, were not found to be significant from the top-down scaling perspective.

  Cold leg lower elevation There was no effect observed due to this scaling distortion.

Small IRWST Due to AP600 design changes, the IRWST in ROSA is smaller than the corresponding AP600 scaled volume. The expected effect is a limited ability to remove the energy from the PRHR and hotter water at the time of IRWST Injection. Neither of these effects was significant enough to cause ROSA's behavior to deviate from the expected trends.

High elevation IRWST The IRWST in ROSA is somewhat higher than the prototypic elevation. As a result, ROSA would have a higher head available IRWST injection at the beginning of that sub-phase. This effect is accounted for in the relevant Πs of that phase and it actually helps broaden the range of Πs to include AP600's.

- **SPES**

Large primary and secondary system heat losses Being tall and thin, SPES has greater heat losses than the properly scaled values. Westinghouse attempted to make up for this by adding to the decay heat in the core. The result was a skewed distribution of energy during the early phases of the transients. The oversized ADS valve openings, however, act to homogenize this skewed distribution and the effects of the heat losses lose importance in the overall behavior of the facility. In the process, SPES provides a wider range of states that then ensure that the data base will include AP600 behavior.

One-dimensional tubular downcomer geometry It was originally thought that the tubular configuration of SPES's downcomer would preclude it from potentially important asymmetric behavior. While this is true, in the other facilities the loop asymmetries were only seen to be present during early portions of the transients and their effect was not significant enough to be detected later.

Oversized ADS-4 The sizes of breaks and valves affect the nondimensional numbers generated for each facility. If the behavior between facilities is similar, the nondimensional number is used for collapsing the data and ensuring that AP600 is contained in the range. Different nondimensional numbers of facilities with similar behavior is what allows us to have a range. Differences, such as with the size of ADS-4, while still important, are therefore absorbed into the analysis. The situation would be different if, because of the different size, the resulting behavior departed from similarity. This did not happen in the tests.

One pump per coolant loop The pumps were not powered during any of the pertinent test periods, and the fact that there was only one per loop in SPES did not have any visible consequences in the system behavior in the top-down scaling analysis. However, from a bottom-up perspective, this distortion results in a lower resistance to recirculating flows between the cold legs on the same coolant loop.

Pressurizer small aspect ratio The SPES pressurizer is short and fat with respect to an ideally scaled pressurizer. This makes the SPES pressurizer relatively slow to drain and the most significant effect is to delay IRWST injection. The pressurizer, however, does not act alone in the integral tests. Its behavior is included in the scaling analysis in combination with its surge line.

Lack of ADS-123 sparger This is perhaps the most significant atypicallity of SPES. Its ADS-123 discharges directly to the atmosphere, which then affects the conditions in the pressurizer itself and impacts the entire system. It affects, for instance, the magnitude of the system pressure at the opening of ADS-4 and the onset of IRWST injection. Both of these conditions were accounted for during the selection of reference parameters, and therefore were absorbed into the scaling analysis.

Underscaled PRHR system Most SPES tests were performed with a single PRHR heat exchanger tube, while volume scaling requires two tubes. This distortion lowered the RCS depressurization rate, reduced heating of the IRWST, and affected the involvement of steam generator heat transfer prior to activation of ADS. The reduced effectiveness of the PRHR system was also one contributor to generally lower minimum core and vessel inventories in the SPES tests than observed in the corresponding tests of the other facilities. Despite these effects, however, this distortion was not seen to significantly impact the global system behavior evaluated in the top-down scaling analysis.

Lower plenum The reactor vessel lower plenum is tall and contains fluid volume that is not directly involved with the flow path from the downcomer to the core inlet. Fluid mixing in this region affects the core inlet temperature and this is atypical of AP600. No significant effects of this distortion were observed in the top-down scaling analysis.

Upper plenum/upper head plate Small holes in the separating plate between the reactor vessel upper plenum and head created a high resistance to flow, resulting in slow draining of liquid from the upper head to the upper plenum. No significant effects of this distortion were observed in the top-down scaling analysis.

- **OSU**

Reduced primary and secondary pressures This is a design atypicality. It precludes OSU from representing the SBLOCA subcooled blowdown sub-phase.

Initial energy distribution This is also a design atypicality that results from the reduced pressure. It affects the behavior of the system at the beginning of each transient.

Reduced height Another design atypicality prevents choking of ADS-4 flow during the ADS-4 blowdown and into the IRWST injection sub-phases. This modifies slightly the timing of ADS-4 and IRWST injection, and makes the downstream piping and conditions important earlier than they should be.

Core Heat Flux OSU has fewer and larger than appropriately-scaled core heater rods. As a result, it has a 10 times higher-than-prototypic heat flux on the surface of rods. From the top-down viewpoint, the required scaled heat is being supplied, but from a local level this was found to place a portion of the core into the wrong heat transfer regime in some situations (for example, see Reference 5-15).

The known and suspected distortions in the three experimental facilities and the effects of these distortions observed in the analyses are presented above. Despite known sources of distortions in all of the facilities, none of them was seen to invalidate the data from any facility; therefore, the data base was judged to be relevant for AP600.

The scaling analysis comparisons between the RELAP5-calculated and measured test data show that the code well represents the responses of the scaling variables related to the AP600 SBLOCA PIRT high-ranked phenomena.

Bottom-up scaling analyses were performed to evaluate localized phenomena associated with CMT draining and oscillatory IRWST injection behavior. The results of these analyses are described as follows.

The bottom-up analysis of CMT draining behavior was performed using test data from the ROSA/AP600, SPES-2 and OSU/APEX experimental facilities. The analysis showed that the CMTs approach a possible draining condition early during SBLOCAs, when the subcooling introduced through the PBL competes with flashing behavior in the depressurizing reactor coolant system. For the larger break sizes, the CMTs are seen to drain at this point, but for smaller breaks the onset of draining is delayed. The reactor coolant system level relative to the cold leg elevation is definitive for CMT draining. If the level is above the elevation span of the cold leg, the CMTs may not drain, but once level has declined to the top elevation of the cold leg the CMTs will drain. Since the cold leg elevation is about 2 m above the top of the core, as long as water remains in the CMT, core uncovery is not a concern. There is no safety issue associated with the timing of CMT draining because it is impossible for the vessel level to drop lower than the cold leg without uncovering the PBL inlet. It is also impossible to prevent the CMT from draining once this inlet is uncovered. However, the timing of CMT draining was seen to be controlled by several competing mechanisms dominated by second-order effects; prediction of these effects is a large challenge for system codes. The integral code assessments described in Section 5.1 confirm the difficulty of predicting certain details and the timing of CMT draining with RELAP5/MOD3. However, the assessments showed that, despite the difficulties in predicting the timing of CMT draining and the details of the draining process, the predictions of overall system behavior, the vessel inventory and subsequent events were seen to be acceptable.

The bottom-up analysis of oscillatory IRWST injection behavior started with data from the ROSA/AP600, SPES-2 and OSU/APEX experimental facilities. A distortion in the SPES-2 facility (oversized ADS-4 flow areas) prevented this behavior from being observed in the tests from that facility. The OSU/APEX facility was seen to represent the global system timing well but, because the pressurizer surge line flow area was overscaled, the oscillation period was far shorter than that expected for AP600. The ROSA/AP600 test data were seen to provide reasonable representations of oscillatory IRWST injection behavior in AP600. A plausible mechanism governing this behavior was developed and verified through comparisons with the ROSA/AP600 data. The mechanism portrays a delicate balance among the reactor vessel upper plenum pressure, the pressurizer and surge line inventories and the IRWST injection flow rate. The code assessments in Section 5.1 present code/data comparisons for pressurizer level and IRWST injection flow rate responses; the overall code capabilities for predicting these phenomena were judged to be reasonable.

5.4 Component Separate Effects Analysis

This section summarizes the separate effects code assessments performed for two unique AP600 components: the CMTs and ADS-123. Additional assessments using separate effects experiments related to the PRHR system are not yet available because of delays in documentation of these experiments. All of these assessments use data obtained from Westinghouse AP600 separate effects test (SET) facilities. The assessments reported here were based on judgments of code capabilities made through comparisons of measured data and calculations performed using RELAP5/MOD3, Version 3.2.1.2. For consistency with other code assessment efforts documented in this report, the same set of acceptance criteria given in Section 2.2.2 was used to make these judgments.

5.4.1 CMT Test Code Assessment

The objective of this study was to assess RELAP5/MOD3 using AP600 CMT SETs performed by Westinghouse Electric Corporation.[5-22] The capabilities of RELAP5/MOD3 for predicting AP600 PIRT[5-14] SBLOCA phenomena related to operation of the CMT were evaluated through comparison of RELAP5/MOD3 calculation results against experimental data from the CMT tests. The analysis and assessment effort was directed toward the CMT recirculation and draining portions of the SBLOCA short-term phase. The CMT-related phenomena that were assessed in this study (and their corresponding PIRT rankings) are: level response (high), condensation (medium), thermal stratification and mixing (medium), and noncondensible effects (low). Other phenomena related to CMT performance which could not be assessed because of test facility configuration or instrumentation limitations were: flow resistance (high), CMT-to-loop differential density (medium), CMT-to-IRWST differential head (medium), and flashing (medium). Of particular note, CMT flow resistance could not be evaluated because the CMT test facility was not representative of the entire AP600 CMT system (i.e., the inlet line, the tank region full scaled volume and elevation, and the discharge line).

The Westinghouse CMT test facility[5-23] consisted of a scaled, instrumented test vessel (representing the upper half of an AP600 CMT). The test facility vessel inner diameter was 0.491 m (1.61 ft) as compared with an AP600 CMT inner diameter of 3.81 m (12.5 ft). A steam/water reservoir acted as both the test vessel fluid source and discharge flow sink. Piping connecting the test vessel and reservoir supplied steam and/or liquid to the top of the CMT and allowed discharge flow from the bottom of the CMT back to the steam/water reservoir. The test vessel inlet piping was attached to the top of the tank through a flow distribution nozzle.

Westinghouse conducted testing in the CMT facility to study four different operating conditions. The tests are grouped into four series investigating: (1) CMT wall condensation with and without the presence of noncondensible gas, (2) CMT draining from initially-cold conditions at constant pressure, (3) CMT draining from initially-cold conditions concurrent with depressurization, and (4) natural circulation of liquid into the CMT followed by draining of the heated liquid under depressurization conditions. Sixteen of these tests were selected to be used for code assessment.

The results of the assessment effort are summarized in Table 5-29. Representative CMT SET assessment results are illustrated in Figures 5-80 through 5-82. These results are for CMT tests where the tank is heated to various depths before draining begins, thus simulating likely CMT operating conditions during AP600 SBLOCA scenarios. Figure 5-80 compares the measured and RELAP5-calculated average discharge mass flow rates. The code is seen to provide very good agreement at low flow rates, but it somewhat underpredicts the draining rate at the higher flow rates. Figures 5-81 and 5-82, respectively, compare measured and RELAP5-calculated CMT level responses for low and high draining rate cases. These figures illustrate that the CMT level response is reasonably predicted for both cases. Other information obtained from the CMT separate effects assessments is summarized as follows.

Table 5-29. Summary of code assessment results from CMT separate effects experiments.

SBLOCA PIRT CMT-Related Phenomenon (and PIRT Ranking)	Code Capability Judgment
Level response (High)	Reasonable
Condensation (Medium)	Reasonable
Thermal stratification and mixing (Medium)	Reasonable
Noncondensible effects (Low)	Reasonable

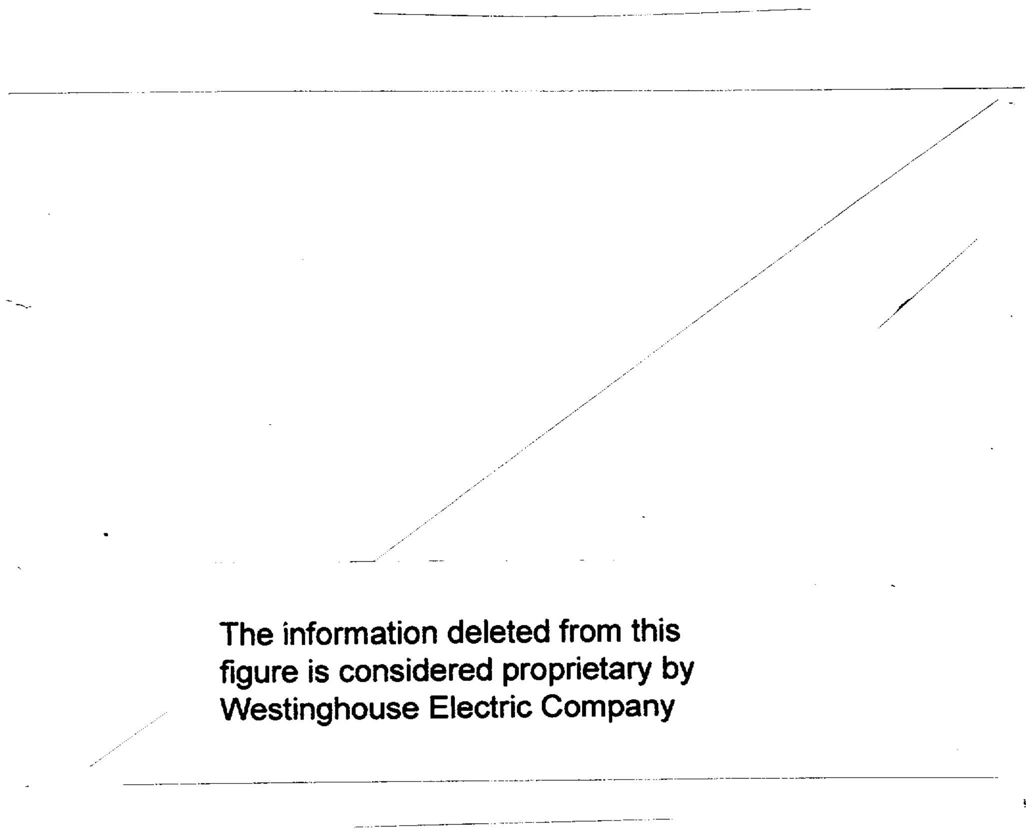

Figure 5-80. Discharge mass flow rate comparison for CMT heated draining tests.

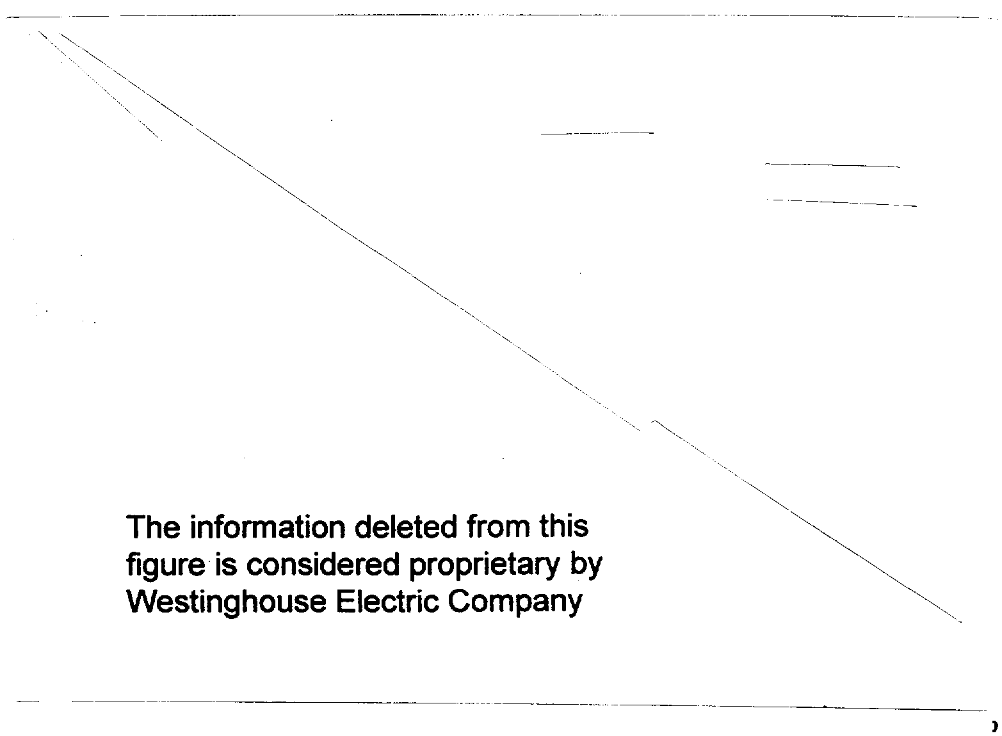

Figure 5-81. CMT level response comparison for Test C071505.

The information deleted from this figure is considered proprietary by Westinghouse Electric Company

Figure 5-82. CMT level response comparison for Test C075508.

Results for the wall condensation tests showed that RELAP5/MOD3 reasonably predicted condensation and noncondensible effects phenomena. The code calculation initially provided excellent agreement in predicting condensate mass, but later diverged from the test data due to a lower calculated CMT pressure. Also, air was expelled from the CMT at a faster rate in the calculations than observed in the tests, which exposed additional wall surface to steam and increased condensate mass in the code predictions.

The assessments for the cold draining tests showed that RELAP5/MOD3 reasonably predicted the CMT level response. In most tests, the code prediction lay outside the small uncertainty bands of the data but typically paralleled the test response. RELAP5/MOD3 did not capture the draining delay due to condensation in the CMT that occurred in the cold draining tests. However, because all AP600 transients that activate the CMTs involve some degree of CMT recirculation, which reduces the condensation potential of the liquid, prediction of this draining delay is not considered a significant issue.

The overall code capability for predicting thermal stratification and mixing in the CMT was judged to be reasonable. A discussion of the general limitations related to the modeling of CMT thermal stratification effects using a one-dimensional computer code is provided in Section 3.1. In these assessments, the best agreement of calculated thermal stratification behavior with the data was seen for the cold draining tests. Timing in the calculations slightly lagged that in the test, which shifted the temperatures outside the uncertainty bands of the thermocouple data, but the overall trends were well predicted. The calculated temperature profiles for the natural circulation and heated draining tests did not follow the trend of the tests as closely as for the cold draining tests; the calculated temperature response was erratic, not smooth as indicated by the test data. For this reason, the assessment for those tests resulted in a judgment of minimal. However, because the overall temperature profile trends were reasonably predicted even in those tests and because the cold draining tests showed good agreement, the composite judgment is reasonable.

Two nodalization sensitivity studies were performed to investigate areas in which the model nodalization used in these assessments was not entirely consistent with the CMT nodalization in the AP600 model described in Appendix B. The first study involved a change to the diffuser connection at the top node of the CMT tank to duplicate exactly the modeling options used in the AP600 model. The level response results were slightly improved, thus verifying that the noding of the diffuser connection in the AP600 CMT model is appropriate. The second study involved a reduction in the axial nodalization of the CMT test tank in order to be completely consistent with the modeling of the corresponding portion of the CMT in the AP600 model. One case was run (draining at constant pressure) and the results showed a better prediction of CMT level response, leading to excellent agreement with the test data. This study (along with basic model nodalization convergence confirmation that was performed) confirms that the axial nodalization used in the AP600 CMT model is appropriate. Another sensitivity study was performed regarding the number and spacing of CMT wall heat structure mesh points. This study indicated that the CMT heat structure modeling used in the AP600 model provides converged solutions of the wall heat transfer processes. All of these sensitivity studies support the manner in which the CMTs are represented in the AP600 model described in Appendix B.

This study showed that RELAP5/MOD3, Version 3.2.1.2, acceptably predicted the SBLOCA PIRT high-ranked phenomenon (CMT level) along with the lower-ranked phenomena of condensation, thermal stratification and mixing and noncondensible effects. The other CMT-related PIRT phenomena could not be evaluated in these assessments due to limitations of the experimental facility. These CMT test assessments are documented in detail in a separate report.[5-24]

5.4.2 ADS-123 Test Code Assessment

The capability of RELAP5/MOD3 to calculate phenomena associated with ADS-123 operation was assessed using data from the VAPORE experimental facility.[5-25] This facility is a full-scale representation of one train of the AP600 ADS-123 system including the inlet piping, the valve cluster (with separate flow paths for ADS-123), the discharge piping and the sparger. A pressurized tank supplies combinations of steam and water through the network. After exiting the valve cluster, fluid flows through discharge piping and a sparger into a quench tank, which is vented to atmosphere. The assessment model extended from upstream of the valve network through the location in the discharge piping where the flows exiting ADS-123 are recombined. The nodalization and user input option selections of the VAPORE assessment model are consistent with ADS-123 modeling in the AP600 and other experimental facility models described in Appendix B.

The assessment effort was directed toward ADS-123 phenomena that are identified in the AP600 PIRT[5-14] SBLOCA short-term phase. Only ADS mass flow (high rank in the PIRT) was directly assessed. Because the upstream fluid conditions were specified as boundary conditions in the assessment model, an assessment of ADS energy release (high rank) is inherent in the mass-flow assessment. Due to facility limitations, choking in complex geometries (medium rank) could not be assessed. Instrumentation was not sufficient to identify choking locations within the network, but assessment of the overall choking behavior is indirectly indicated through comparisons between the measured and calculated mass flow rates. Noncondensible effects (medium rank) could not be assessed because none of the tests evaluated working fluids other than mixtures of steam and water. Flow resistance (medium rank) could not be assessed because the calculations showed choked and not friction-dominated flow conditions. In the assessment model, the network flow resistances were set as a result of benchmark calculations using data from tests other than those used in the assessments. In this benchmarking process, we identified the importance of correctly characterizing the resistances of the ADS valves (particularly the isolation valves, which are likely to remain unchoked). Finally, because of instrumentation limitations and because the calculations showed choked flow conditions, condensation in ADS spargers (low rank) could not be assessed.

The assessments used data from 11 tests of the VAPORE Phase B1 test series. For this series, the two valves in each AP600 ADS stage (i.e., the actuation valve and the control valve) were represented in both the test facility and assessment model using combinations of a valve and an orifice. The tests evaluated various combinations of valve cluster inlet pressures (from 191 to 1965 psia, 1.32 to 13.55 MPa) and qualities (from 0.07 to 0.28). The tests also evaluated different combinations of ADS-123 activations.

The main assessment results for the VAPORE tests, comparisons between measured and calculated mass flow rates for the 11 tests, are shown in Figure 5-83. This figure includes the effects of two uncertainties related to the experiments. First, the horizontal error bars represent the uncertainty in the observed flow rate as a result of flow-measuring instrumentation error. Second, the vertical error bars represent the effects caused by a large uncertainty in the measured test inlet quality. These effects were accounted for by performing three separate calculations for each test: one using the nominal (i.e., reported) inlet quality, one using zero quality and one using twice the nominal quality. The span of the vertical error bar represents the range created by the latter two calculations. Based on the calculations using the nominal inlet qualities, the code on-average slightly underpredicted the measured flow rates. The average calculated flow rate was 95% of the measured flow rate, with two standard deviations of 18%.

Table 5-30 summarizes the code capability judgments made through these assessments. The assessments indicate that (assuming valve-related parameters are characterized and proper inlet conditions are provided) RELAP5/MOD3, Version 3.2.1.2, can reasonably predict the PIRT high-ranked phenomena (the mass flow and energy release) associated with the ADS-123 system. The VAPORE assessments are documented in detail in a separate report.[5-26]

Table 5-30. Summary of code assessment results from ADS-123 separate effects experiments.

AP600 SBLOCA PIRT ADS-123-Related Phenomenon (and PIRT Ranking)	Code Capability Judgment
Mass flow (High)	Reasonable
Energy release (High)	Reasonable

5.4.3 Combination and Summary of Separate Effects Code Assessments

The CMT and ADS-123 separate effects test assessments indicate that RELAP5/MOD3 is capable of acceptably representing the PIRT high-ranked phenomena that could be evaluated using these tests. The RELAP5 test facility input models used in these assessments are consistent with those used for AP600 and the integral test facilities. Separate-effects tests addressing PRHR system behavior were not completed in time so that assessments using them could be included in this report; these assessments will be reported later.

The information deleted from this figure is considered proprietary by Westinghouse Electric Company

Figure 5-83. Comparison of calculated and measured results for VAPORE ADS-123 experiments.

5.5 References

5-1. *Large Scale Test Facility System Description for the ROSA/AP600 and ROSA-V Configurations*, Japan Atomic Energy Research Institute, Memo 09-070, March 1976.

5-2. M. Rigamonti, *SPES-2 Facility Description*, Sezione Reattori Innovativi (SIET), 00183RI92, Revision 0 (Proprietary), April 1994.

5-3. Westinghouse Electric Corporation, *Westinghouse AP600 Long Term Cooling Test at Oregon State University, Facility Drawings, Piping and Instrumentation Diagrams*, LTCT-T3-300 (Proprietary), December 1, 1994.

5-4. *Adequacy Evaluation of RELAP5/MOD3 for Simulating AP600 Small Break Loss-of-Coolant Accidents*, Idaho National Engineering Laboratory, INEL-96/0380, (Proprietary), October 1996.

5-5. R. A. Shaw, T. Yonomoto and Y. Kukita, *Quick Look Report for ROSA/AP600 Experiment AP-CL-03*, Japan Atomic Energy Research Institute, Memo 06-249, October 1994.

5-6. Westinghouse Electric Corporation, *Quick Look Report for SPES-2 Matrix Test S00401*, PXS-T2R-020 (Proprietary), Preliminary, July 1994.

5-7. J. T. Groome, *CL#3, 1" Bottom of Pipe Break with Modified ADS 1, 2, and 3 Logic and ROSA ADS Setpoints, NRC-22*, Oregon State University, OSU-APEX-96007, Revision 0, June 19, 1996.

5-8. R. A. Shaw, T. Yonomoto and Y. Kukita, *Quick Look Report for ROSA/AP600 Experiment AP-DV-01*, Japan Atomic Energy Research Institute, Memo 07-189, September 1995.

5-9. L. Conway, R. Hundal, M. Loftus, V. Merrit and M. Ogrinsh, *AP600 Design Certification Program, SPES-2 Tests, Final Data Report*, Westinghouse Electric Corporation, WCAP-14309, Revision 1 (Proprietary), Volume II, p. 5.1-4, July 1995

5-10. J. T. Groome, *Double-Ended DVI Break with Modified ADS 1, 2, and 3 Logic, NRC-20*, Oregon State University, OSU-APEX-96005, Revision 0, May 1, 1996.

5-11. Y. Anoda, R. A. Shaw, T. Yonomoto and Y. Kukita, *Quick Look Report for ROSA/AP600 Experiment AP-PB-01*, Japan Atomic Energy Research Institute, Memo 06-310, January 1995.

5-12. Westinghouse Electric Corporation, *Quick Look Report for SPES-2 Matrix Test S01007*, PXS-T2R-025 (Proprietary), Preliminary, July 1994.

5-13. M. J. Loftus, *Quick Look Report for OSU Matrix Test SB9 (Blind Test)*, Westinghouse Electric Corporation, LTCT-T2R-029 (Proprietary), September 1994.

5-14. J. D. Burtt, C. D. Fletcher, G. E. Wilson, C. B. Davis and T. J. Boucher, *Phenomena Identification and Ranking Tables for Westinghouse AP600 Small Break Loss-of-Coolant Accident, Main Steam Line Break, and Steam Generator Tube Rupture Scenarios*, Idaho National Engineering Laboratory, INEL-94/0061, Revision 2, March 1997.

5-15. C. B. Davis, P. D. Bayless, J. E. Fisher, P. A. Roth and S. T. Polkinghorne, *Evaluation and Assessment of RELAP5/MOD3 Version 3.2.1.2 for Simulating the Long-Term Phase of Small Break Loss-of-Coolant Accidents in the AP600*, Idaho National Engineering Laboratory, INEL-96/0395, (Proprietary), October 1996.

5-16. S. Banerjee, M. G. Ortiz, T. K. Larson and J. M. Cozzuol, *Top-Down Scaling Analysis Methodology For AP600 Integral Tests*, Idaho National Engineering Laboratory, INEL-96/0040, (Proprietary), to be published April 1997.

5-17. M. G. Ortiz, C. E. Lenglade, S. M. Sloan and L. Teerlink, *Top-Down Scaling Analysis of AP600 Integral Test Data in Support of RELAP5 Adequacy Assessment*, Idaho National Engineering Laboratory, INEL-96/0117, (Proprietary), to be published April 1997.

5-18. D. Bessette, M. DiMarzo and P. Griffith, *Phenomenology Observed in the AP600 Integral Systems Test Programs Conducted in ROSA-AP600, APEX, and SPES-2 Facilities*, U.S. Nuclear Regulatory Commission, (Proprietary), draft, December 1996.

5-19. Technical Program Group, *An Integrated Structure and Scaling Methodology for Severe Accident Technical Issue Resolution*, Idaho National Engineering Laboratory, NUREG/CR-5809, EGG-2659, Draft Report for Comment, November 1991.

5-20. G. E. McCreery, *Adequacy Evaluation of RELAP5/MOD3 for Simulating AP600 Small Break Loss-of-Coolant Accidents, Volume 2, Appendix C, Attachment 1: Calculations of Pressurizer Liquid Level Oscillations for ROSA Test AP-CL-03 and for AP600 and OSU Geometries*, Idaho National Engineering Laboratory, INEL-96/0380, (Proprietary), October 1996.

5-21. J. M. Cozzuol, *Adequacy Evaluation of RELAP5/MOD3 for Simulating AP600 Small Break Loss-of-Coolant Accidents, Volume 2, Appendix D, ROSA/AP600 Test AP-CL-03 RELAP5 Calculation Assessment*, Idaho National Engineering Laboratory, INEL-96/0380, (Proprietary), October 1996.

5-22. *Core Makeup Tank Test Data Report*, Westinghouse Electric Corporation, WCAP-14217, (Proprietary), November 1994.

5-23. *Facility Description Report for AP600 Core Makeup (CMT) Test Program*, Westinghouse Electric Corporation, WCAP-14132, (Proprietary), July 1994.

5-24. L. A. Stickler and S. M. Sloan, *RELAP5/MOD3.2.1.2 Application Code Assessment Using the Westinghouse CMT Separate Effects Tests*, Idaho National Engineering Laboratory, September 1996, (Proprietary), transmitted by letter DGH-02-96, November 15, 1996.

5-25. V. V. Miselis, A. J. Brockie and J. S. Nitkiewicz, *Facility Description Report: AP600 Automatic Depressurization System Phase B1 Tests*, Revision 0, Westinghouse Electric Corporation, WCAP-14303, (Proprietary), March 1995.

5-26. L. S. Ghan, J. P. Adams and S. M. Sloan, *Assessment of RELAP5/MOD3 using Data from the Westinghouse VAPORE ADS-123 Test Facility*, Idaho National Engineering Laboratory, September 1996, (Proprietary), transmitted by letter DGH-02-96, November 15, 1996.

6 SUMMARY OF ADEQUACY FINDINGS

This section addresses the adequacy of the RELAP5/MOD3, Version 3.2.1.2, computer code for performing confirmatory analyses of AP600 design-basis SBLOCAs. The adequacy case is made by combining the results from the various reviews, evaluations and assessments summarized in this report. The organization and content of this section is diagramed in Figure 6-1. A summary of reviews of the RELAP5/MOD3 code governing equations and numerics (from Section 3 and Appendix A) and the applicability of selected code models and correlations (from Section 4) is presented in Section 6.1. The performance of the integrated code for predicting AP600-specific component separate effects (from Section 5.4) and scaled integral effects experiments representing AP600 (from Sections 5.1 and 5.2) is summarized in Section 6.2. Recommended AP600 modeling approaches and user guidance for performing confirmatory SBLOCA analyses are given in Section 6.3. The combination of the code evaluation results from the reviews and assessments into the case for code adequacy is given in Section 6.4.

6.1 Code Governing Equations, Numerics and Applicability of Models and Correlations

Reviews of the RELAP5/MOD3 code governing equations and numerics were conducted. The reviews concentrated upon the assumptions underlying the basis for the computer code and the significance of those assumptions for AP600 SBLOCA analysis. These reviews are summarized in Section 3 with details presented in Appendix A. The reviews uncovered three specific limitations of the code for this application: the assumption of homogeneity within the liquid and vapor phases, a defect in the momentum flux formulation, and a tendency to overpredict condensation. The first limitation results from the basic inability of a one-dimensional code to predict single-phase thermal stratification behavior within horizontal components. For the AP600 application, this limitation prevents simulation of warm water residing over cold water within the cold legs. As described in Section 5.1, cold leg thermal stratification modeling distortions caused by this limitation were observed to affect the temperatures of water presented to the break and PBL inlet for the ROSA and OSU 1-in. diameter cold leg break tests. However, the assessments for these tests showed that the effects of these distortions on the break flow, CMT draining and vessel inventory were not significant. The second limitation can result in artificial fluid accelerations in regions modeled using quasi-multidimensional noding. In the facility input models described in this report, the effects of this limitation have been minimized by: (1) restricting such noding only to regions where it is essential (this was judged to be only in regions of the detailed models representing annular reactor vessel downcomer geometry) and (2) disabling momentum flux in those regions. The assessments in Section 5.1 show that this approach to reactor vessel downcomer modeling represents a satisfactory work-around to momentum flux difficulties in RELAP5/MOD3, Version 3.2.1.2 (an effort is under way to remedy this situation in later code versions). The third limitation is caused by the assumption of homogeneity within the liquid phase and large interphase heat transfer area changes associated with transitions between flow regimes. The integral assessments showed that the overprediction of condensation did not impact the calculation of the minimum vessel inventory in either the short or the long term phases. In summary, the reviews have shown the code governing equations and numerics to be generally applicable for the AP600 SBLOCA application.

Other studies were conducted to determine the applicability of selected RELAP5/MOD3 models and correlations for AP600 SBLOCAs. These studies, reported in Section 4, were based on a "bottom-up" review. With this approach, the capabilities of seven code models and correlations important for predicting the AP600 SBLOCA PIRT high-ranked phenomena were evaluated. These seven important models were: the accumulator lumped-parameter component, critical flow, decay heat, form friction, horizontal stratification and entrainment, interphase drag in bundles, and interphase mass and energy transfer. For the other models and correlations, the extensive historical RELAP5 code assessment

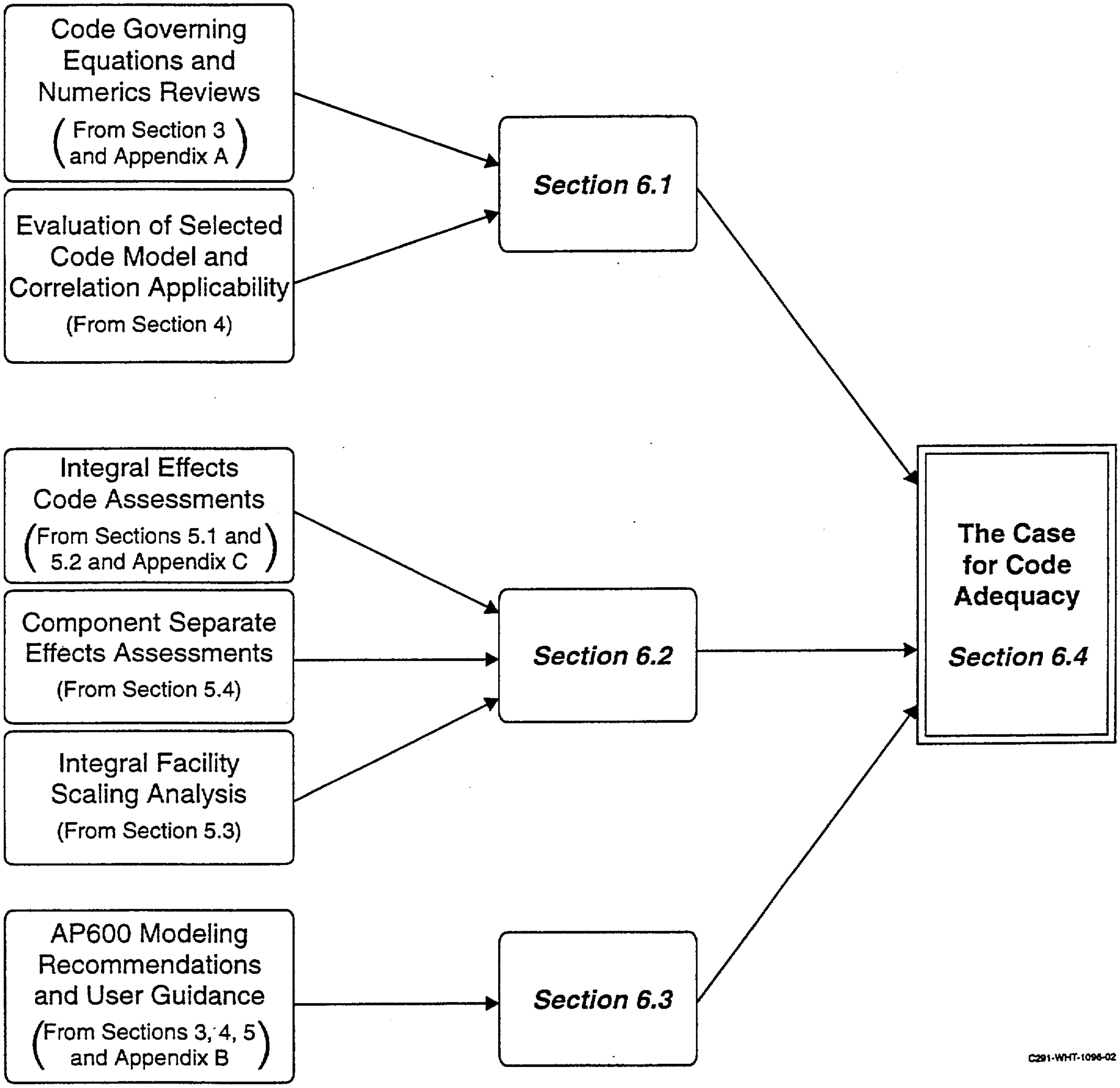

Figure 6-1. Development of the Adequacy Case.

base[6-1, 6-2, 6-3] is considered adequate. Applicability for the important code models and correlations was evaluated through reviews of: (1) model pedigree, (2) the parameter ranges for which models were originally developed, over which they are applied in RELAP5/MOD3, over which they have been assessed, and the ranges required for the AP600 SBLOCA application, (3) the fidelity with which the code model or correlation replicates appropriate experimental data, and (4) the scalability of models to AP600 plant geometry and dimensions. All seven dominant models and correlations were judged to be applicable for the AP600 SBLOCA application.

6.2 Integrated Code Performance

This section summarizes the results from the assessments of integrated code performance for predicting AP600 SBLOCA PIRT high-rank phenomena and the scaling analysis described in Section 5.

The code assessments for the PIRT SBLOCA short-term phase used data from the ROSA, SPES and OSU integral experimental facilities for tests simulating three different AP600 SBLOCA scenarios. The scenarios are initiated by a 1-in. diameter cold leg break, a double-ended DVI line break and a 2-in. diameter PBL break. These assessments are summarized in Section 5.1; a full accounting of the individual assessment judgments made for each test in each facility is found in Appendix C, Table C.5-1. Assessment results on a facility-by-facility basis are summarized in Table 6-1. This table indicates the composite judgments made of code capabilities for predicting the 14 AP600 SBLOCA PIRT short-term phase high-ranked phenomena, based on averages of the judgments from the three individual test assessments for each facility. The assessment results also are summarized in Table 6-2, which shows composite judgments representing averages of the judgments from the individual assessments using data from ROSA, SPES and OSU experiments for each accident scenario. In addition, Table 6-2 shows an overall judgment for each phenomenon that was made based on a combination of the composite judgments for the three accident scenarios.

Table 6-1. Assessment results by test facility for AP600 SBLOCA PIRT short-term phase high-ranked phenomena.

SBLOCA Short-Term Phase High-Rank Phenomenon	Composite Code Capability Judgment for the 3 ROSA Tests	Composite Code Capability Judgment for the 3 SPES Tests	Composite Code Capability Judgment for the 3 OSU Tests
Accumulator flow	Reasonable	Reasonable	Excellent
ADS energy release	Reasonable	Reasonable	Reasonable
ADS mass flow	Reasonable	Reasonable	Reasonable
Break mass flow	Excellent	Reasonable	Reasonable
Cold leg-to-PBL tee phase separation	Reasonable	Reasonable	Reasonable
Core flashing	Reasonable	None Made	None Made
Core subcooling margin	Reasonable	Reasonable	Reasonable
Core two-phase mixture level	Reasonable	Reasonable	Reasonable
CMT flow resistance	Reasonable	Reasonable	Reasonable
CMT level	Reasonable	Reasonable	Reasonable
Fuel rod core power/decay heat	None Made	None Made	None Made
Hot leg phase separation in tees	Reasonable	Reasonable	Reasonable
IRWST flow resistance	Reasonable	Reasonable	Reasonable
Pressurizer level	Reasonable	Reasonable	Minimal

Table 6-2. Assessment results by accident scenario for AP600 PIRT SBLOCA short-term phase high-ranked phenomena.

SBLOCA Short-Term Phase High-Rank Phenomenon	Composite Code Capability Judgment for the 1-in. CLB	Composite Code Capability Judgment for the DVILB	Composite Code Capability Judgment for the 2-in. PBLB	Overall Judgment
Accumulator flow	Reasonable	Reasonable	Reasonable	Reasonable
ADS energy release	Reasonable	Reasonable	Reasonable	Reasonable
ADS mass flow	Reasonable	Reasonable	Reasonable	Reasonable
Break mass flow	Reasonable	Reasonable	Reasonable	Reasonable
Cold leg-to-PBL tee phase separation	Reasonable	Reasonable	Reasonable	Reasonable
Core flashing	Reasonable	Reasonable	Reasonable	Reasonable
Core subcooling margin	Reasonable	Reasonable	Reasonable	Reasonable
Core two-phase mixture level	Reasonable	Reasonable	Reasonable	Reasonable
CMT flow resistance	Reasonable	Reasonable	Reasonable	Reasonable
CMT level	Reasonable	Reasonable	Reasonable	Reasonable
Fuel rod core power/decay heat	None Made	None Made	None Made	None Made
Hot leg phase separation in tees	Reasonable	Reasonable	Minimal	Reasonable
IRWST flow resistance	Reasonable	Reasonable	Reasonable	Reasonable
Pressurizer level	Reasonable	Minimal	Reasonable	Reasonable

Code capabilities were assessed for 13 of the 14 PIRT short-term phase high-ranked phenomena. The "fuel rod core power/decay heat" phenomenon could not be assessed because it represented boundary conditions in all tests and calculations. The models and correlations reviews described in Section 6.1 indicate that the RELAP5 decay heat model is applicable for AP600 SBLOCAs. Code users may, as needed, analyze the effects of uncertainty in this phenomenon through sensitivity studies investigating variations in the assumed initial core power and rate of decay heat.

For the remaining 13 PIRT short-term phase high-ranked phenomena, a total of 107 individual judgments were made of code capabilities for predicting the behavior observed in the experiments. Of these judgments, 97 indicated acceptable code performance (i.e., with either excellent or reasonable agreement between RELAP5-calculated and measured test data). The assessments found that the code had difficulty in predicting the pressurizer level for some of the tests, and for the DVI line break accident scenario and OSU facility in particular. The code had difficulty in predicting phase separation in the hot leg/ADS-4 tees that affected the ADS-4 flow for the ROSA test simulating the PBL break scenario. The code also had difficulty predicting the CMT level responses in one SPES test and one OSU test and the core subcooling response for another OSU test. However, for reasons presented in Appendix C, Section C.5, on a case-by-case basis, these difficulties were seen to be isolated cases and not indicative of general code deficiencies. Accordingly, the overall code capabilities for predicting these phenomena were judged to be reasonable.

The code assessments for the PIRT SBLOCA long-term phase used test data from OSU integral experiments for the same three accident scenarios described above. These assessments are summarized in Section 5.2. The assessment results relating to code capabilities for predicting the 11 AP600 PIRT SBLOCA long-term phase high-ranked phenomena in each of the accident scenarios are given in Table 6-3. An overall judgment was made for each phenomenon based on an average of the individual judgments made for the three accident scenario assessments. Again, no judgments could be made for the "fuel rod core power/decay heat" PIRT phenomenon because this represented boundary conditions in all tests and calculations. Code capabilities for predicting nine of the ten remaining long-term phase high-ranked phenomena were judged to be acceptable (indicating either excellent or reasonable agreement). Code capabilities for predicting "IRWST pool thermal stratification" were judged "insufficient" according to the standardized acceptance criteria because the code does not have a mechanistic model for representing this phenomenon. Despite the "insufficient" judgment, the assessments showed that the functions of the IRWST during the long-term phase (i.e., providing the injection static head and injection fluid temperature) can be adequately represented if sensitivity calculations are employed to evaluate the effects of uncertainties introduced by code limitations related to IRWST modeling. Therefore, these code limitations were not seen to impact the adequacy of the code for this application.

Table 6-3. Assessment results for AP600 PIRT SBLOCA long-term phase high-ranked phenomena.

SBLOCA Long-Term Phase High-Rank Phenomenon	Code Capability Judgment for the 1-in. CLB	Code Capability Judgment for the DVILB	Code Capability Judgment for the 2-in. PBLB	Overall Judgment
ADS energy release	Excellent	Reasonable	Excellent	Excellent
ADS mass flow	Excellent	Reasonable	Excellent	Excellent
Core two-phase mixture level	Reasonable	Reasonable	Reasonable	Reasonable
Downcomer level	Reasonable	Reasonable	Reasonable	Reasonable
Fuel rod core power/decay heat	None Made	None Made	None Made	None Made
IRWST flow resistance	Reasonable	Reasonable	Reasonable	Reasonable
IRWST pool level	Excellent	Excellent	Excellent	Excellent
IRWST pool thermal stratification	Insufficient	Insufficient	Insufficient	Insufficient
Sump fluid temperature	Reasonable	Reasonable	Reasonable	Reasonable
Sump level	Reasonable	Excellent	Excellent	Excellent
Upper plenum two-phase mixture level	Reasonable	Reasonable	Reasonable	Reasonable

The top-down scaling analyses demonstrate that the experimental data base provided by the integral test data encompasses the important phenomena and ranges expected of AP600 during the short-term phase of the SBLOCA scenarios investigated. For the SBLOCA long-term phase, the top-down scaling analyses evaluate the important phenomena ranges with respect to the experimental data base provided with the OSU facility. While each experimental facility has known sources of distortions, none of these was found to make the data from any of the facilities irrelevant for AP600. The top-down scaling analysis considered these known distortions and included their effects in the data-collapsing process. Bottom-up scaling analyses into CMT draining and oscillatory IRWST injection behavior showed that the experimental data base contains information sufficient for representing these behaviors in AP600. Because the experimental data base has been shown to be sufficient and relevant for AP600, the code assessment results obtained using this data are considered to be representative for code predictions of AP600 behavior.

Additional code assessments were performed using test data from separate effects experimental facilities representing the AP600 CMT and ADS-123 components. The results from these assessments pertaining to AP600 SBLOCA PIRT high-rank phenomena are given in Table 6-4. The table shows that code capabilities for predicting all of these phenomena were judged to be acceptable.

Table 6-4. Component separate effects assessment results for SBLOCA PIRT high-ranked phenomena.

High-Ranked Phenomenon	Code Capability Judgment
ADS-123 energy release	Reasonable
ADS-123 mass flow	Reasonable
CMT level	Reasonable

6.3 AP600 Modeling Recommendations and Guidance

This section describes the recommended RELAP5/MOD3 models and user guidance for performing AP600 SBLOCA analysis. These recommendations are based on the collective experience gained through the assessment analyses presented in this report.

The AP600 plant employs a combination of proven component designs and new, untested, advanced conceptual designs. For example, the AP600 pressurizer design is very similar to the pressurizers used in operating plants, whereas core makeup tanks have never before been used in commercial PWRs. Development of the recommended RELAP5 AP600 plant models paralleled the AP600 design approach. Proven component designs used in AP600 were modeled using proven nodalization practices employed in a generation of PWR models of currently-operating plants (see Reference 6-3). New component designs, specific or unique to AP600, were modeled using a four step approach: (i) the phenomena likely to occur in the component were identified and the code correlations were reviewed to determine their applicability, (ii) a proposed nodalization of the component was produced based on knowledge of the correlations and engineering judgment, (iii) the proposed component nodalization was tested by performing convergence studies and by comparing code assessment calculations to integral systems data, and (iv) the component nodalization was either verified as adequate and left unchanged or was determined as inadequate and revised accordingly. The separate effects assessments documented in Section 5.4 were a key part of identifying appropriate modeling approaches for the new component designs. The integral effects assessments documented in Sections 5.1 and 5.2 support the acceptability of the modeling approaches adopted for the new component designs.

The code assessments in this report, which form the basis for item (iii) above, were all related to SBLOCAs. Consequently, the recommendations and guidance provided here are specific to SBLOCAs. When available, modeling recommendations and guidance will be given in subsequent documents to address other AP600 transients.

6.3.1 The AP600 Models

Two recommended AP600 plant models have been developed: a detailed model for studying plant behavior during the SBLOCA short-term phase and a long-term-cooling model (LTCM) designed for studying the SBLOCA long-term phase. Both recommended models are summarized here and are documented fully in Appendix B.

The AP600 detailed model and the AP600 LTCM were developed for different purposes. The detailed model was designed to study the complex transient behavior during the SBLOCA short-term phase while the LTCM was designed to study the slowly-varying system transient behavior during the SBLOCA long-term phase. Because the missions of the two models are different, the levels of detail used in them also are quite different. The numbers of hydrodynamic cells and heat structures used for representing a component in the detailed model generally is much larger than those used for representing the corresponding component in the LTCM. The detailed model is used to study the portion of the

SBLOCA accident scenario when steep gradients and rapidly-varying behavior play an important role and require fine resolution of the behavior. The LTCM is designed to study the portion of the scenario when bulk flow phenomena dominate and the system is in a quasi-steady condition.

The SBLOCA short-term and long-term phases also differ in that the containment is effectively isolated from the RCS by choking planes (at the break and ADS) during most of the short-term phase whereas little or no choking is experienced during the long-term phase, allowing the containment to communicate with the RCS. In the AP600 detailed model, containment features are represented using constant-pressure boundary conditions. In the AP600 LTCM, a parametric approach to modeling containment response is taken. The containment continues to be represented with boundary conditions, but they are varied such that the containment behavior response is bounded. This parametric approach is currently recommended. Sensitivity studies[6-4] were used to evaluate the effects of large variations in the containment parameters on the RCS response; these studies showed that the RCS response was insensitive to those variations. Therefore, the simple parametric containment modeling approach is considered adequate for analysis of the SBLOCA long-term phase. Alternate approaches to containment modeling continue under development; these are discussed in Appendix B, Section B.4.8.

6.3.2 AP600 Model Nodalizations

Nodalization diagrams for the recommended AP600 detailed and long-term-cooling models are shown in Figures 6-2 and 6-3, respectively. The basis for the nodalizations is described in Appendix B.

6.3.3 New Modeling Recommendations

The recommended AP600 modeling practices described in Appendix B include two "new" practices that have evolved as a result of the code assessments presented in this report.

In preliminary assessment analyses,[6-5] two problems were seen to plague the calculations: (1) critical flow modeling difficulties and (2) non-physical recirculating flows in regions of the model containing quasi-multidimensional nodalization (parallel stacks of hydrodynamic cells interconnected with cross-flow junctions). As demonstrated through the assessments in Section 5, the first problem has been eliminated as a result of implementing the Henry-Fauske critical flow model in RELAP5/MOD3, Version 3.2.1.2. The Henry-Fauske model is activated by using Card 1 Option 53. The choking option should only be specified at junctions where choking is expected to occur, e.g., at the break, the ADS valves, and the CMT discharge line orifice during the DVI double-ended guillotine break. The second problem has been addressed by: (1) limiting quasi-multidimensional nodalization only to regions where deemed essential; for this application, this was the reactor vessel downcomer region and (2) by specifying "no momentum flux" for certain junctions associated with the reactor vessel downcomer in the detailed AP600 model. Momentum flux is disabled by setting "s" = 3 in the "efvcahs" junction control flags (see Appendix A of Reference 6-6). The current recommendation is to disable momentum flux at all internal downcomer junctions and the junctions connecting the downcomer with the lower plenum and upper head regions. Momentum flux remains enabled at the cold leg and DVI junctions with the downcomer.

In addition to code-user Option 53 that activates the Henry-Fauske critical flow model, five other options activated on Card 1 also are currently recommended for use:

15 Does not allow violation of the Courant limit.

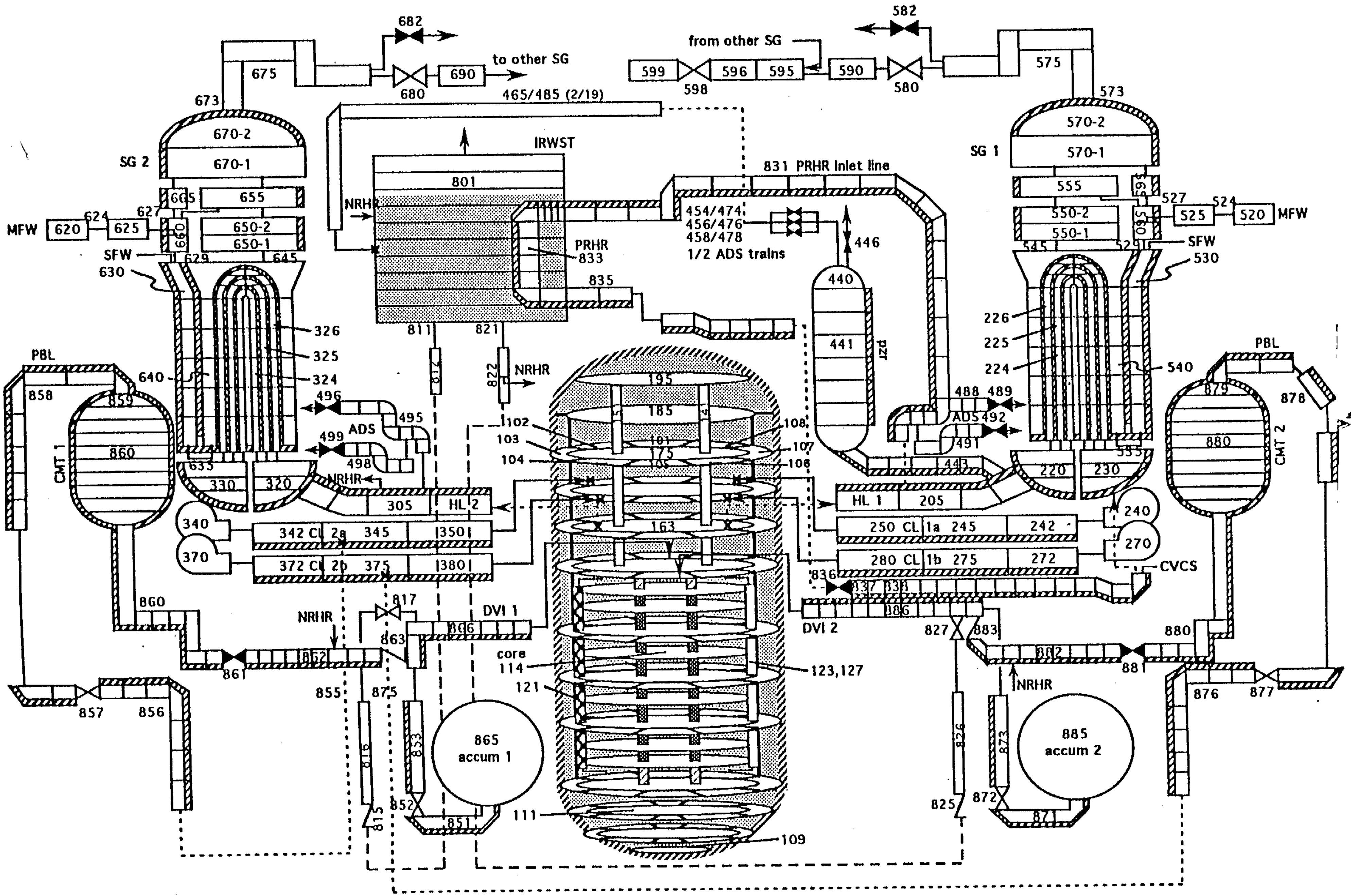

Note: All downcomer azimuthal junctions are crossflow.

Figure 6-2. AP600 plant detailed RELAP5 model nodalization.

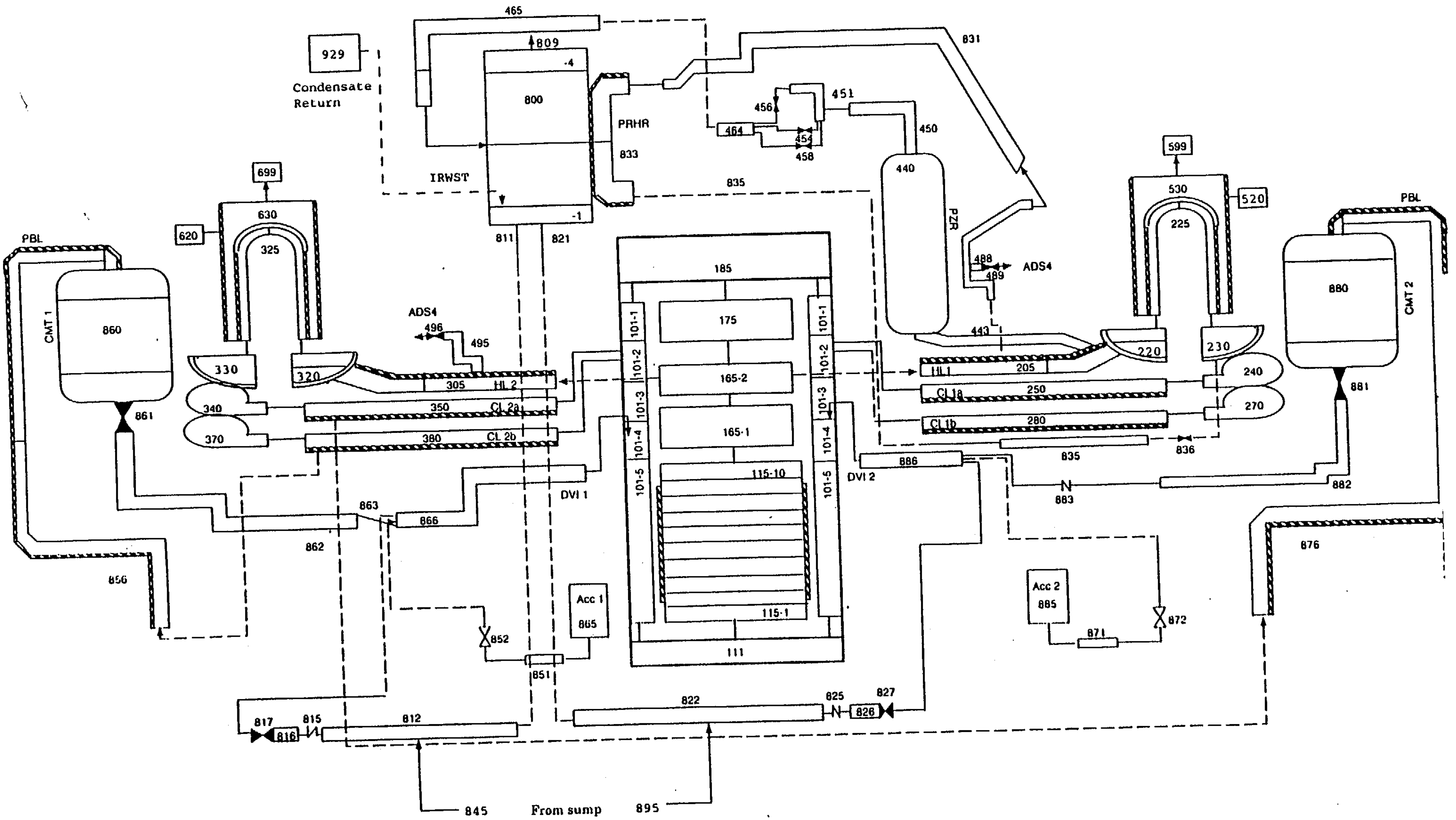

Figure 6-3. AP600 long-term cooling RELAP5 model nodalization.

55 Activates changes to interphase heat transfer coefficients (H_{if}) in the annular and annular-mist flow regimes, to subcooled boiling and to rod-bundle interphase drag.

57 Invokes the new annular wall-friction model.

58 Invokes changes to H_{if} modifying interpolation between subcooled and superheated liquids.

61 Invokes changes to H_{if} in bubbly and slug flow regimes and modifies the criteria for vertical stratification.

6.3.4 User Guidance

The following information is provided for analysts performing calculations with the AP600 RELAP5 models.

Both models were developed using the AP600 design information provided to the Idaho National Engineering Laboratory up to March 1, 1996. Design change information received after that date will be incorporated in future versions of the models.

Westinghouse Electric Corporation specified design ranges for the AP600 ADS valve flow areas and resistances. The nominal (middle-of-range) values were used in the recommended models. The assessments in Sections 5.1, 5.2, and 5.4 of this report show that the Henry-Fauske critical flow model possesses capabilities for acceptably predicting ADS flow rates when flow paths are properly characterized (i.e., the flow area, discharge coefficient and nonequilibrium parameter). The recommended AP600 models use the default values for the Henry-Fauske discharge coefficient (1.0) and thermal nonequilibrium parameter (0.14). The analyst should consider quantifying the effects of uncertainty in ADS characterization for specific applications by performing sensitivity studies in which the ADS parameters are appropriately varied. An example of such a sensitivity study, performed for an SBLOCA using the detailed AP600 facility model, is provided by Reference 6-7. The same situation exists for break flow; the recommended break modeling approach is to use the Henry-Fauske model with default input values and account for the uncertainty in break modeling by performing analyses covering a spectrum of break sizes.

In the AP600 models, the calculated core decay power is based on the American Nuclear Society 5.1 decay heat standard[6-8] with three fissile isotopes (U-235, U-239 and Pu-239), actinides, G-factor and end-of-equilibrium cycle burnup and fission product inventory. The models assume a nominal full reactor power of 1933 MW_t. A favorable benchmark comparison between RELAP5/MOD3 and ORIGEN2 decay heat responses is shown in Section 4. If desired, analysts can directly evaluate the effects of decay heat uncertainty for their specific application using sensitivity calculations in which the initial core power or decay heat multiplier are appropriately varied.

The assessments in Sections 5.1 and 5.2 of this report indicate that code solutions generated for SBLOCAs with the AP600 models will be oscillatory in the core region. These rapid oscillations are numerically induced (involving the subcooled boiling and other models) and have been seen to reduce fluid subcooling within the reactor vessel downcomer and core regions. The oscillations also have been seen to result in non-physical condensation in the reactor vessel upper head region of OSU experiment calculations (see Section 5.2.2). This condensation was not observed in the corresponding AP600 accident scenario calculations, but the user should be alert for this possibility.

The reviews and assessments in Sections 4, 5.1, and 5.2 indicate that interphase drag in the core fuel rod bundle region is overpredicted by the code under low pressure conditions, such as are experienced following ADS blowdown in AP600. This overprediction generally results in about a 10%

underprediction of the minimum core collapsed level. The minimum reactor vessel inventory also is generally underpredicted.

Both the detailed and long-term cooling recommended models contain features that "work around" the code difficulties related to the defect in the momentum flux formulation described in Section 3.2. Code development activities are continuing to address the momentum flux defect and eventual changes in the recommended modeling approach are anticipated. These work-arounds are summarized as follows:

- Both models currently employ one-dimensional modeling in the core and reactor vessel upper plenum regions; eventually, these regions may be modeled using a quasi-multidimensional nodalization scheme (cross-flow interconnected multiple parallel stacks of hydrodynamic cells).

- The detailed model currently employs a quasi-multidimensional representation of the reactor vessel downcomer region in which momentum flux has been disabled. This disabling eventually may not be required.

- Both models currently employ one-dimensional modeling of the IRWST pool; eventually the IRWST pool may be modeled using a quasi-multidimensional nodalization scheme.

The reviews and assessments in this report describe the capabilities and limitations of the code for predicting thermal stratification in various AP600 components. These reviews and assessments are summarized as follows:

- A one-dimensional code such as RELAP5 cannot represent warm water residing over cold water in horizontal components, such as the cold legs (see discussions in Sections 3.1 and 5.1).

- RELAP5 possesses a capability for representing warm water residing over cold water in the CMT component (as demonstrated by the assessments in Sections 5.1 and 5.4). However, users should be aware of, and account for, a code model limitation that can affect the calculated tank thermal profile in certain specific situations (as described in Section 3.1).

- Because of the work-around modeling approach for the IRWST component described above, the vertical thermal profile within the IRWST pool is not mechanistically represented with the code. However, this modeling approach was not seen in the assessments in Section 5.1 to adversely affect prediction of the IRWST functions during the SBLOCA short-term phase. This modeling approach was seen in the assessments in Section 5.2 to affect the response of the injection fluid temperature during the initial portion of the long-term phase. Sensitivity calculations (using bounding assumptions regarding the tank thermal profile) were performed to evaluate the effects upon the assessment calculations of the uncertainties resulting from the model limitation. The results of these sensitivity calculations are believed to be accident scenario specific; code users can perform similar studies to evaluate these effects for other scenarios.

6.4 Combination of Code Adequacy Evaluation Results

Table 6-5 summarizes the results from the various components of code adequacy evaluation described in this report. For each SBLOCA PIRT high-ranked phenomenon, the reviews and assessments that have been performed to investigate code adequacy are shown and the outcomes of the evaluations are indicated. The information shown in this table is described as follows:

Table 6-5. Summary of RELAP5 code adequacy evaluation results.

AP600 PIRT High-Ranked Phenomenon	RELAP5		Experimental Data	
	Closure Relation Applicability	Integrated Code Assessment	Sufficiency	Relevancy
SBLOCA SHORT-TERM PHASE				
Accumulator flow	✓	✓	✓	✓
ADS energy release	✓	✓	✓	✓
ADS mass flow	✓	✓	✓	✓
Break mass flow	✓	✓	✓	✓
Cold leg-to-PBL tee phase separation	✓	✓	✓	✓
Core flashing	✓	✓	✓	✓
Core subcooling margin	Not Applicable	✓	✓	✓
Core two-phase mixture level (see Note 1)	✓	✓	✓	✓
CMT flow resistance	✓	✓	✓	✓
CMT level	Not Applicable	✓	✓	✓
Fuel rod core power/decay heat	✓	Not Applicable	Not Applicable	Not Applicable
Hot leg phase separation in tees	✓	✓	✓	✓
IRWST flow resistance	✓	✓	✓	✓
Pressurizer level	Not Applicable	✓	✓	✓
SBLOCA LONG-TERM PHASE				
ADS energy release	✓	✓	✓	✓
ADS mass flow	✓	✓	✓	✓
Core two-phase mixture level (see Note 1)	✓	✓	✓	✓
Downcomer level (see Note 1)	Not Applicable	✓	✓	✓
Fuel rod core power/decay heat	✓	Not Applicable	Not Applicable	Not Applicable
IRWST flow resistance	✓	✓	✓	✓
IRWST pool level	Not Applicable	✓	✓	✓
IRWST pool thermal stratification (see Note 2)	Not Applicable	✓	✓	✓
Sump fluid temperature	Not Applicable	✓	✓	✓
Sump level	Not Applicable	✓	✓	✓
Upper plenum two-phase level (see Note 1)	Not Applicable	✓	✓	✓

Note 1 - Evidence from integral experiments is based on collapsed level, not two-phase mixture level indications.

Note 2 - Code capabilities for representing the IRWST functions (available static injection head and injection fluid temperature) were seen in the assessments to be acceptable, even though the code currently cannot mechanistically represent the thermal stratification behavior within the IRWST. The current recommendation is to use a one-dimensional approach for IRWST modeling and perform bounding sensitivity calculations to account for the uncertainties introduced in analyses by doing so.

A check mark in the "RELAP5 Closure Relation Applicability" column indicates that reviews of code models and correlations influencing the PIRT phenomenon were performed and that the results show applicability of those models and correlations for AP600 SBLOCA analysis. The correspondence between the models and correlations and the PIRT phenomena that they influence, and the review results, are discussed in Section 4.

A check mark in the "RELAP5 Integrated Code Assessment" column indicates that code capabilities for simulating the PIRT phenomenon were evaluated through comparisons between measured and code-calculated behavior and that the results show acceptable agreement. This table combines results from: (1) integral experiment assessments using tests performed in the ROSA, SPES and OSU facilities for the PIRT short-term phase, (2) integral experiment assessments using tests performed in the OSU facility for the PIRT long-term phase, and (3) separate effects experiment assessments using tests representing the AP600 CMT and ADS-123 components. These assessments are discussed in Sections 5.1, 5.2, and 5.4, respectively.

A check mark in the "Experimental Data Sufficiency" column indicates that scaling analyses evaluating pertinent ranges of conditions for the phenomenon have been performed and that the integral experiment data base used for the code assessments has been demonstrated to bound the expected AP600 behavior. A check mark in the "Experimental Data Relevancy" column indicates that the scaling analysis uncovered no integral experiment facility distortions that would significantly affect the simulations of the phenomenon. The scaling analysis is discussed in Section 5.3.

A "Not Applicable" entry indicates that it is not appropriate to evaluate the phenomenon identified with the table row using the evaluation method identified with the table column.

For each AP600 SBLOCA PIRT high-ranked phenomenon, favorable outcomes are indicated in Table 6-4 regarding: (1) applicability of code models and correlations and (2) code capabilities for predicting pertinent behavior as observed in experimental facilities scaled to AP600. The scaling analysis indicates that the experimental data base used in the integral assessments is both sufficient and relevant for representing the behavior expected of AP600. Therefore the code assessment results obtained are pertinent for AP600. This investigation demonstrates that the RELAP5/MOD3, Version 3.2.1.2, computer code, when used with the recommended AP600 modeling approach and guidance, is adequate for performing confirmatory AP600 SBLOCA analyses.

6.5 References

6-1. R. R. Schultz, *International Code Assessment and Applications Program: Summary of Code Assessment Studies Concerning RELAP5/MOD2, RELAP5/MOD3, and TRAC-B*, Idaho National Engineering Laboratory, NUREG/IA-0128, EGG-EAST-8719, December 1993.

6-2. S. M. Sloan, R. R. Schultz and G. E. Wilson, *RELAP5/MOD3 Code Manual, Volume 7, Summaries and Reviews of Independent Code Assessment Reports*, Idaho National Engineering Laboratory, NUREG/CR-5535, INEL-95/0174, June 1994.

6-3. C. D. Fletcher and R. R. Schultz, *RELAP5/MOD3 Code Manual, Volume 5, User Guidelines*, Idaho National Engineering Laboratory, NUREG/CR-5535, INEL-95/0174, August 1995.

6-4. C. B. Davis, P. D. Bayless, J. E. Fisher, P. A. Roth and S. T. Polkinghorne, *Evaluation and Assessment of RELAP5/MOD3 Version 3.2.1.2 for Simulating the Long-Term Phase of Small Break Loss-of-Coolant Accidents in the AP600*, Idaho National Engineering Laboratory, INEL-96/0395, (Proprietary), October 1996.

6-5. *Adequacy Evaluation of RELAP5/MOD3 for Simulating AP600 Small Break Loss-of-Coolant Accidents*, Idaho National Engineering Laboratory, INEL-96/0380, (Proprietary), October 1996.

6-6. *RELAP5/MOD3 Code Manual, Volume 2, User's Guide and Input Requirements*, Idaho National Engineering Laboratory, NUREG/CR-5535, INEL-95/0174, August 1995.

6-7. J. C. Determan, *ADS Valve Characteristics Sensitivity Study for the AP600 Design*, Idaho National Engineering Laboratory, letter from P. D. Bayless to F. Odar, PDB-9-95, April 11, 1995.

6-8. ANSI/ANS-5.1-1979, "American National Standard for Decay Heat Power in Light Water Reactors," American National Standards Institute/American Nuclear Society.

7 CONCLUSIONS

The RELAP5/MOD3, Version 3.2.1.2 code has been evaluated for the purpose of determining its adequacy for performing AP600 confirmatory SBLOCA analysis. This effort included review of code governing equations and numerics, evaluation of the applicability of code models and correlations, and assessment of integrated code performance for simulating AP600-related integral effects and separate effects experiments. Scaling analyses have been performed that indicate the experimental data base employed in the integral effects assessments is both sufficient and relevant for representing AP600. The assessments of code capabilities were performed using a standardized and consistent method that has been successfully applied in previous adequacy demonstrations of USNRC-sponsored codes. The assessments indicated that the code is capable of adequately predicting the SBLOCA phenomena of importance, as defined by the AP600 PIRT. This investigation demonstrates that the RELAP5/MOD3, Version 3.2.1.2, computer code, when used with the recommended modeling approach and guidance, is adequate for performing confirmatory AP600 SBLOCA analyses.